DESIGN OF NOVEL DELIVERY SYSTEMS TO PROBE ALTERNATIVE ROUTES OF ADMINISTRATION FOR A SELF-AMPLIFYING RNA-BASED RABIES VACCINE

Author:

Gustavo Lou Ramirez

Supervisors:

Prof. Yvonne Perrie

Prof. Craig W. Roberts

PhD in Pharmaceutical Sciences (Drug Delivery) at Strathclyde Institute of Pharmacy and Biomedical Sciences

This work was funded by PHA-ST-TRAIN-VAC (MSCA-ITN-EID)

Project ID: 675370

TABLE OF CONTENTS

DECLARATION OF AUTHENTICITY

ACKNOWLEDGEMENTS

The research projected was funded by the European Commission Project *Leveraging Pharmaceutical Sciences and Structural Biology Training to Develop 21st Century Vaccines* (H2020-MSCA-ITN-2015 grant agreement 675370). Gustavo Lou is a PhD candidate at the University of Strathclyde (Glasgow, UK) and participated in the project at GSK (Siena, Italy). This project was co-sponsored between the University of Strathclyde and GSK.

ABSTRACT

Current vaccine design aims to develop safer vaccines based on one or few selected antigens. RNA-based vaccines can be engineered to encode any antigen of interest and have the potential for rapid, inexpensive and scalable manufacturing and have an acceptable safety profile. Moreover, they enable *in situ* antigen expression, mimicking a real viral infection hence eliciting robust humoral and cellular-mediated immune responses. RNA vaccines therefore represent a versatile tool to fight infectious diseases and emerging pathogens effectively and rapidly. Furthermore, the antigen can be designed in a self-amplifying RNA (SAM) to enhance the immunogenicity and to reduce the therapeutic dose compared to conventional non-amplifying mRNA vaccines.

RNAs can be encapsulated in delivery systems to protect them against degradation upon injection and to facilitate their delivery in host cells. Among them, lipid-based delivery systems and, more specifically, lipid nanoparticles (LNPs) are efficient non-viral delivery systems for RNA and SAM vaccines. Within this thesis, a panel of cationic LNPs (cLNPs), based on existing cationic lipids (e.g. DOTAP and DDA), was designed to deliver a SAM vaccine. The rabies virus was used as a model, as there is an established correlate of protection (neutralising antibodies) and there exist efficacious vaccines in the market (e.g. Rabipur) to be used as comparators. To this end, a SAM vaccine encoding the rabies virus glycoprotein (RVG), the only target for neutralising antibodies, was used.

Microfluidics-based methods for producing cLNPs of desired physicochemical properties were developed and optimal operating parameters (e.g. total flow rate and flow rate ratio) were established. Most promising SAM-cLNP candidates were chosen according to their physicochemical attributes, their ability to protect SAM from enzymatic degradation and their capacity to associate with cells and to induce antigen expression. These formulations were well retained at the injection site when administered intramuscularly or intradermally, while they were rapidly cleared following intranasal administration. On the other hand, SAM-cLNPs induced protective levels of anti-RVG antibodies following intramuscular injection in mice and RVG-specific polyfunctional T cell responses even with a dose as low as 0.15 μg RVG-SAM. Remarkably, the immune responses elicited by SAM-cLNPs were comparable to Rabipur, a commercial vaccine

based on an inactivated rabies virus, and a cationic nanoemulsion, a safe and well-established SAM delivery system which is currently being investigated in a phase I clinical trial in humans (as of September 2019). Intradermal administration of SAM-cLNPs resulted in similar humoral and cell-mediated immune responses, while significantly weaker immune responses were achieved when administered intranasally.

LIST OF PUBLICATIONS

Scientific Publications

G. Lou, G. Anderluzzi, S. Woods, C.W. Roberts, Yonne Perrie. A novel microfluidic-based approach to formulate size-tuneable large unilamellar cationic liposomes: Formulation, cellular uptake and biodistribution investigations. European Journal of Pharmaceutics and Biopharmaceutics, 143 (**2019**) 51-60.

Efficient delivery of a self-amplifying RNA (SAM) rabies vaccine by cationic lipid nanoparticles (*in preparation*).

Design of novel delivery systems to probe alternative routes of administration for a self-amplifying RNA (SAM) vaccine (*in preparation*).

Oral presentations

G. Lou, B.C. Baudner, D. O'Hagan and Y. Perrie (**2018**). Design novel delivery systems to probe alternative routes of administration of a self-amplifying RNA rabies vaccine. *11th GSK PhD annual workshop*. Siena, Italy.

G. Lou and Y. Perrie (**2018**) Cationic liposomes as vaccine adjuvants: a comparison of DOTAP, DC-Chol and DDA containing liposomes biodistribution. *UK and Ireland Controlled Release Society (UKICRS) annual meeting*. Queen's University Belfast, UK.

Poster presentations

G. Lou, S. Gallorini, B. Brazzoli, B.C. Baudner, D. O'Hagan, Y. Perrie (**2019**). Design of lipid nanoparticles to deliver a self-amplifying RNA vaccine. *Control Release Society (CRS) annual meeting*. Valencia, Spain.

G. Lou, B.C. Baudner, D. O'Hagan and Y. Perrie (**2018**). Designing next generation vaccine adjuvants: Biodistribution of cationic liposomes to create a depot effect and target lymph nodes. *2018 AAPS PharmSci 360.* Washington DC, USA.

G. Lou and Y. Perrie (**2018**). Liposomes as vaccine adjuvants: An *in vitro* an *in vivo* comparison between DOTAP and DC-Chol liposomes. *Control Release Society (CRS) annual meeting*. New York, USA.

G. Lou, B.C. Baudner, D. O'Hagan and Y. Perrie (**2017**). Taking advantage of microfluidics to formulate neutral and cationic liposomes to carry a self-amplifying RNA vaccine. *10th GSK PhD annual workshop*. Siena, Italy.

G. Lou, B.C. Baudner, D. O'Hagan and Y. Perrie (**2017**). Design of cationic liposomal delivery systems to develop a self-amplifying RNA-based vaccine. *International Liposome Society*. Athens, Greece.

G. Lou, B.C. Baudner, D. O'Hagan and Y. Perrie (**2017**). Taking advantage of microfluidics to formulate neutral and cationic liposomes to carry a self-amplifying RNA vaccine. *8th APS international PharmSci*. University of Hertfordshire, UK.

G. Lou, B.C. Baudner, D. O'Hagan and Y. Perrie (**2017**). A novel size reduction technique for liposomal vaccine delivery formulations. *Control Release Society (CRS) annual meeting*. Boston, USA.

G. Lou, B.C. Baudner, D. O'Hagan and Y. Perrie (**2017**). High-throughput method to scale-up liposomal formulations for vaccine delivery. *UK and Ireland Controlled Release Society annual meeting*. University of Strathclyde, UK.

G. Lou, B.C. Baudner, D. O'Hagan and Y. Perrie (**2017**). A novel high-throughput technique to scale-up liposomal formulation for vaccine delivery. *5th Quality by Design Symposium*. De Montfort University, UK.

LIST OF ABBREVIATIONS

APC	Antigen presenting cell
ApoE	Apolipoprotein E
BCA	Bicinchoninic Acid assay
BFA	Brefeldin A
BHK	Baby hamster kidney
BMDC	Bone marrow-derived dendritic cell
BMDM	Bone marrow-derived macrophage
CD	Cluster of differentiation
cLNP	Cationic lipid nanoparticle
CNE	Cationic nanoemulsion
Cryo-TEM	Cryo transmission electron microscopy
CTL	Cytotoxic T lymphocyte
Chol	Cholesterol
DC	Dendritic cell
DC-Chol	3ß-[N-(N',N'-dimethylaminoethane)-carbamoyl]cholesterol
DDA	Dimethyldioctadecylammonium
DIL-C_{18}	1,1'-dioctadecyl-3,3,3',3'-tetramethylindocarbocyanine perchlorate
DLS	Dynamic light scattering
DLin-DMA	1,2-dilinoleyloxy-N,N-dimethyl-3-aminopropane
DLin-KC2-DMA	1,2-dilinoleyl-4-(2- dimethylaminoethyl)-[1,3]-dioxolane
DLin-MC3-DMA	Dilinoleylmethyl-4-dimethylaminobutyrate
DMPC	1,2-dimyristoyl-*sn*-glycero-3-phosphocholine
DMPG	1,2-Dimyristoyl-*sn*-glycero-3-phosphorylglycerol
DMTAP	Dimyristoyl-3-trimethylammonium-propane
DMG-PEG2000	1,2-dimyristoyl-sn-glycero-3-phosphoethanolamine-N-[methoxy(polyethylene glycol)-2000]

DOBAQ	N-(4-carboxybenzyl)-N,N-dimethyl-2,3-bis(oleoyloxy)propan-1-aminium
DODAC	N-N-dioleoyl-N,N-dimethylammonium chloride
DODAP	1,2-dioleoyl-*sn*-glycero-3-phosphocholine (DOPC); 1,2-dioleoyl-3-dimethylammonium-propane
DOPC	1,2-dioleoyl-*sn*-glycero-3-phosphocholine
DOPS	1,2-dioleoyl-*sn*-glycero-3-phospho-L-serine
DOPE	1,2-dioleoyl-sn-3-phosphoethanolamine
DOPG	1,2-dioleoyl-sn-glycero-3-phospho-(1'-rac-glycerol)
DOTAP	1,2-dioleoyl-3-trimethylammonium-propane
DOTMA	N-[1-(2,3-dioleyloxy)propyl]-N,N,N-trimethylammonium chloride
DPPC	1,2-dipalmitoyl-*sn*-glycero-3-phosphocholine
DSPC	1,2-dipalmitoyl-sn-glycero-3-phosphocholine
DSG-PEG2000	1,2-distearoyl-*sn*-glycero-3-phosphoethanolamine-N-[amino(polyethylene glycol)-2000]
dsRNA	Double-stranded RNA
DSTAP	Disteroyl-trimethylammonium-propane
DLVO	Derjaguin-Landau-Verweley-Overbeek
E.E.	Encapsulation efficiency
ELISA	Enzyme-linked immunosorbent assay
HI-FBS	Heat-inactivated foetal bovine serum
FAVN	Fluorescent antibody virus neutralisation assay
FRR	Flow rate ratio
GC	Gas chromatography
GFP	Green fluorescent protein
GUV	Giant unilamellar vesicle
HPLC	High-performance liquid chromatography
ID	Intradermal
IFN	Interferon

IFNAR	Interferon receptor
Ig	Immunoglobulin
IL	Interleukin
iLNP	Ionisable lipid nanoparticle
ILN	Inguinal lymph node
IM	Intramuscular
IN	Intranasal
IVP	*In vitro* potency
IVT	*In vitro* transcription
LAMP-1	Lysosomal-associated membrane protein 1
LDLR	Low-density lipoprotein receptor
LNP	Lipid nanoparticle
LOD	Limit of detection
LOQ	Limit of quantification
LUV	Large unilamellar vesicle
MHC	Major histocompatibility complex
MLV	Multilamellar vesicle
MHF	Micro hydrodynamic focusing
mPES	Modified polyethylene sulfone
MPL	Monophosphoryl lipid A
mRNA	Messenger RNA
NA	Neutralising antibody
NK	Natural killer
NMR	Nuclear magnetic resonance
OVA	Ovalbumin
PAMP	Pathogen-associated molecular pattern
PDI	Polydispersity index

PBS	Phosphate-buffered Saline
PC	Phosphatidylcholine
PE	Phosphoethanolamine
PEG	Polyethylene glycol
PLN	Popliteal lymph node
PLGA	Poly(lactic-co-glycolic acid)
Poly I:C	Polyinosinic:polycytidylic acid
PRR	Pattern recognition receptor
PS	Phosphatidylserine
RIG-I	Retinoic acid-inducible protein 1
RFFIT	rapid fluorescent focus inhibition assay
ROS	Reactive oxygen species
RVG	Rabies virus glycoprotein
SAM	Self-amplifying RNA
SAXS	Small-angle X-ray scattering
siRNA	Small interfering RNA
SHM	Staggered herringbone micromixer
SLN	Solid-lipid nanoparticle
ssRNA	Single-stranded RNA
SUV	Small unilamellar vesicle
TDB	Trehalose 6,6'-dibehenate
TEM	Transmission electron microscopy
T_H	T helper
T_M	Transition temperature
TFF	Tangential flow filtration
TFR	Total flow rate
TLR	Toll-like receptor

TMP	Transmembrane pressure
TNF	Tumour necrosis factor
TRIS	Tris(hydroxymethyl)aminomethane)

LIST OF FIGURES

Figure 2.3. The effect of aqueous:organic flow rate ratio (FRR) **(A – D)** and total flow rate (TFR) **(E – F)** on neutral DSPC:Chol liposomes **(A and E)** and cationic DOPE:DOTAP **(B and F)**, DOPE:DC-Chol **(C)** and DOPE:DDA liposomes **(D)**. Liposomes were formulated at 1:1 molar ratio in 10 mM TRIS buffer pH 7.5 and 4 mg/mL. 15 mL/min TFR and 1:1 FRR were used to investigate the effect of FRR and TFR respectively. Samples were dialysed and subsequently characterised by dynamic light scattering in terms of size (bars), PDI (dots) and zeta-potential (values). Results are represented as mean ± SD of 3 independent experiments.

Figure 2.4. The effect of initial lipid concentration on neutral PC:Chol (♦) and DSPC:Chol liposomes (●) liposomes and cationic DOPE:DOTAP (●), DOPE:DDA (■) and DOPE:DC-Chol liposomes (▲). Liposomes were formulated by microfluidics at 1:1 molar ratio in 10 mM TRIS buffer pH 7.4, at 4 mg/mL and 15 mL/min TFR. Neutral and cationic liposomes were prepared at 3:1 and 1:1 FRR respectively. Samples were dialysed and subsequently characterised by dynamic light scattering in terms of size **(A)**, PDI **(B)** and zeta-potential **(C)**. Results are represented as mean ± SD of 3 independent experiments.

Figure 2.5. Influence of sample concentration on dynamic light scattering (DLS) characterisation of DSPC:Chol liposomes. DSPC:Chol liposomes were formulated at 1:1 molar ratio in 10 mM TRIS buffer pH 7.4, at 4 mg/mL, 1:1 FRR and 15 mL/min TFR, dialysed, serially diluted and characterised by DLS. **A)** Hydrodynamic size (●) and PDI (■). **B)** Zeta-potential (▲). Range of sample concentration used in previous liposome sizing measurements (0.00625 – 0.5 mg/mL) is highlighted in pink. Results are represented as mean ± SD of three consecutive measurements.

Figure 2.6. Schematic representation of the microfluidic formulation of small **(A)** and large **(B)** unilamellar liposomes (SUVs and LUVs). Small (40 nm) and large (>500 nm) liposomes were formulated by microfluidics in the Nanoassemblr Platform at 4 mg/mL, 1:1 FRR and 15 mL/min TFR at either 10 or higher TRIS concentration. Solvent removal and buffer exchange was undertaken via dialysis against 10 mM TRIS (200 mL) for 1 hour under magnetic stirring to adjust buffer concentration. The concentration of buffer and lipid selection offer controlled production of large unilamellar liposomes.

Figure 2.7. The effect of aqueous buffer concentration on liposomes formulated by microfluidics I. DOPE:DOTAP (●), DOPE:DDA (■), DOPE:DC-Chol (▲), DOPE:DMTAP (■), DOPE:PS (♦) and DSPC:Chol (●) liposomes were formulated by microfluidics in the Nanoassemblr Platform at 1:1 molar ratio, 4 mg/mL, 1:1 FRR and 15 mL/min TFR at increasing concentrations of TRIS buffer pH 7.4, then dialysed and characterised by dynamic light scattering in terms of size **(A)**, PDI **(B)** and zeta-potential **(C)**. **D)** 3D structures of lipids. Results are represented as mean ± SD of three independent experiments.

Figure 2.8. The effect of aqueous buffer concentration on liposome size distribution of liposomes. DOPE:DOTAP **(A)**, DOPE:DC-Chol **(B)**, DOPE:DDA **(C)**, DOPE:DMTAP **(D)**, DOPE:PS **(E)** and DSPC:Chol **(F).** Liposomes were formulated by microfluidics in the Nanoassemblr Platform at 1:1 molar ratio, 4 mg/mL, 1:1 FRR and 15 mL/min TFR at increasing concentrations of TRIS buffer pH 7.4, then dialysed and characterised by dynamic light scattering in terms of size **(A)**, PDI **(B)** and zeta-potential **(C)**. Representative images of liposomes prepared at lowest (left) and highest (right) TRIS concentration are shown for each formulation.

Figure 2.9. Negative-staining electron microscopy images of small and large cationic liposomes formulated by microfluidics. Small DOPE:DOTAP **(A-C)**, small DOPE:DDA **(D-F)**, large DOPE:DOTAP **(G, H)** and DOPE:DDA liposomes **(I, J)**. Liposomes were formulated by microfluidics in the Nanoassemblr Platform at 4 mg/mL, 1:1 FRR and 15 mL/min TFR. Small cationic liposomes were prepared at 10 mM TRIS and large DOPE:DOTAP and large DOPE:DDA liposomes were produced at 1000 and 300 mM TRIS respectively.

Figure 2.10. Cryo-TEM micrographs of small **(A, B)** and large DOPE:DOTAP liposomes **(D , E)** formulated by microfluidics at 4 mg/mL, 1:1 FRR, 15 mL/min TFR and 10 and 1000 mM TRIS buffer pH 7.4. The dense black spheres are water crystals. Hydrodynamic size (bars) and PDI (values) **(F)** and size distribution plots of small and large liposomes **(G)** are shown. Results are represented as mean ± SD of three consecutive DLS measurements.

Figure 2.11. The effect of aqueous buffer concentration on liposomes formulated by microfluidics II: the effect of molar percentage of cationic lipid. DSPC:Chol liposomes (10:10 molar ratio) were prepared at increasing molar percentages of either DOTAP (0% - ●, 5% - ■, 13% - ▲, 23% - ♦) or DDA (13% - ■, 23% - ●). All DOTAP **(A-C)** and DDA liposome formulations **(D-F)** were prepared at 4 mg/mL, 1:1 FRR, 15 mL/min TFR, dialysed and characterised by DLS in terms of size **(A, D)**, PDI **(B, E)** and zeta-potential **(C, F)**. The effect of buffer choice on size **(G)** and PDI **(H)**. DSPC:Chol (10:10 molar ratio) and DSPC:Chol:DOTAP (5% DOTAP) liposomes were prepared at 4 mg/mL, 1:1 FRR and 15 mL/min at increasing concentrations of TRIS buffer pH 7.4 or citrate buffer pH 6.0, dialysed and characterised by DLS. Results are represented as mean ± SD of three independent experiments.

Figure 2.12. The effect of sterile filtration of neutral DSPC:Chol **(A)** and cationic DOPE:DOTAP liposomes **(B)** through 0.22 µm filters. Millipore's PES (▧), PVDF (▧) and MCE (▧) filters. Fisherbrand's PES filters (▧) were used as a comparison. Size (bars), PDI (dots) and zeta-potential (values) were compared to non-filtered liposome samples (▧). Results are represented as mean ± SD of three independent experiments. **Polyethersulfone (PES), polyvinylidene Fluoride (PVDF), mixed cellulose ester (MCE); Millipore (MP), Fisherbrand (FB).* Results are represented as mean ± SD of three independent experiments.

Figure 2.13. Effect of X-ray irradiation over physicochemical attributes **(A, C, E)** and stability of liposomes at 4˚C **(B, D, F)**. Liposomes were characterised by DLS in terms of size **(A)**, PDI **(C)** and zeta-potential **(E)** before (▧) and after X-ray irradiation (▧). The stability of DOPE:DOTAP (●), DOPE:DC-Chol (■), DOPE:DDA (▲) and DSPC:Chol liposomes (♦) was also evaluated by size **(B)**, PDI **(D)** and zeta-potential **(F)**. Results are represented as mean ± SD of three independent experiments.

Figure 2.14. Schematic representation of TFF. Sample is passed through a column thanks to a transmembrane pressure (TMP) in such a way that solvent and free drug (or antigen) is removed by size exclusion.

Figure 2.15. Example of shear-to-flow rate dependence in KR2i TFF (Lab Spectrum).

Figure 2.16. Characterisation of liposomes formulated by continuous manufacturing. Size distribution of DSPC:Chol liposomes formulated in Nanoassemblr at 1:1 molar ratio, 6 mg/mL, 3:1 TFR, 15 mL/min in 10 mM TRIS pH 7.4 before **(A)** and after concentration (6-fold) and washing (14-fold) **(B)**. Size distribution of DSPC:Chol liposomes prepared from MLVs and size-reduced in M-110P at 30 KPSI for 5 cycles before **(C)** and after TFF concentration (10-fold) **(D)**. Size distribution of DOPE:DOTAP liposomes formulated in Nanoassmblr at 1:1 molar ratio, 4 mg/mL, 15 mL/min TFR and 10 mM TRIS pH 7.4 before **(E)** and after TFF concentration (6-fold) and washing (14-fold) **(F)**. Samples were characterised both off-line (▬) and on-line (▬). Plots are represented as the average of three measurements.

Figure 2.17. Calibration curve for quantification of methanol by head-space gas chromatography. Limit of detection (LOD) and limit of quantification (LOQ) were 552 and 1672 ppm.

Figure 2.18. Physicochemical characterisation of liposomes after solvent removal. DSPC:Chol liposomes were formulated by microfluidics at 1:1 molar ratio, 4 mg/mL at 15 mL/min TFR in 10 mM TRIS pH 7.4 at 1:1, 3:1 and 5:1 FRR, purified by TFF (▧) or dialysis (▧), and characterised by DLS in terms of size **(A)** and

PDI **(B)** with respect to non-purified control liposomes (▧) Representative size distribution plots of non-purified (—), TFF-washed (—) and dialysed liposomes (—), formulated by microfluidics at 1:1 **(C)**, 3:1 **(D)** and 5:1 FRR **(E),** are shown. **F)** Validation of solvent removal from DSPC:Chol liposomes (1 mL) by TFF analysed by head-space gas chromatography (HS-GC). Results are represented as mean ± SD of three independent experiments. *Represents estimates of initial concentrations.

Figure 2.19. Protein removal from liposome formulations by tangential flow filtration (TFF). DSPC:Chol liposomes (2 mL), formulated at 1:1 molar ratio, 4 mg/mL, 3:1 FRR and 15 mL/min. Then, liposomes (1 mg/mL) were mixed with 0.9 (●), 0.45 (■), 0.25 (▲) and 0.125 mg/mL OVA (◆) and washed with PBS in TFF in a 750 KDa pore size mPES column at 27 mL/min rate. Results are represented as mean ± SD of three independent experiments.

Figure 3.1. Validation of the method used to differentiate murine bone marrow cells into macrophages **(A)** and dendritic cells **(B)**. The percentage of bone marrow-derived macrophages (BMDMs) and bone-marrow-derived dendritic cells (BMDCs) (black) was determined by flow cytometry as percentage of $F4/80^+$ and $CD11c^+$ cells from gates G1 and G2 (FSC – SSC) respectively with respect to unstained cells (shaded grey). The percentage of BMDMs and BMDCs was at least 95% and 70%.

Figure 3.2. *In vitro* cytotoxicity of liposomes in bone marrow-derived macrophages **(A)** and bone marrow-derived dendritic cells **(B)** after 24 hours. 40 nm DOPE:DOTAP (●), 40 nm DOPE:DDA (■), 90 nm DOPE:DC-Chol (▲) and 80 nm DSPC:Chol (◆) liposomes were formulated by microfluidics at 1:1 molar ratio, 4 mg/mL, 1:1 FRR, 15 mL/min TFR and 10 mM TRIS pH 7.4. Results are represented as mean ± SD of three independent experiments.

Figure 3.4. *In vitro* cellular uptake of DOPE:DOTAP **(A, B)** and DOPE:DC-Chol liposomes **(C, D)** in bone marrow- derived macrophages **(A, C)** and bone marrow-derived dendritic cells **(B, D)** at 37 ˚C (filled symbols) and 4 ˚C (empty symbols). **C)** Representative flow cytometry plots of cellular uptake of liposomes (DOPE:DOTAP – black, DOPE:DC-Chol – blue) with respect to control cells (shaded grey) at 37 ˚C. The percentage of cellular interaction (adsorption and uptake) was calculated thanks to the fluorescent lipophilic dye Dil-C_{18} anchored within the liposome bilayer.

Figure 3.4. Physicochemical characterisation of cationic liposomes for *in vitro* experiments. Small DOPE:DOTAP (▧, —), Large DOPE:DOTAP (▧, —), small DOPE:DDA (▧, —), large DOPE:DDA (▧, —) and small DOPE:DC-Chol liposomes (▧, —) were produced by microfluidics at 1:1 molar ratio, 4 mg/mL, 1:1 FRR, 15 mL/min TFR. Small DOPE:DOTAP and small DOPE:DDA were formulated at 10 mM TRIS pH 7.4, large DOPE:DDA was formulated at 300 mM TRIS pH 7.4 and large DOPE:DOTAP and DOPE:DC-Chol were formulated at 1000 mM TRIS. **A)** Liposomes were dialysed and characterised by DLS in terms of size (bars), PDI (dots) and zeta-potential (values, in mV). **B)** Representative size distribution plots of liposome formulations. Results are represented as mean ± SD of three independent experiments.

Figure 3.5. Effect of composition and size on the *in vitro* cellular uptake of cationic liposomes in BMDMs at 37 ˚C in DMEM + 10 % FBS **(A, B)** and serum-free DMEM **(C, D)**. Cellular uptake is represented in terms of percentage of Dil-C_{18}^+ cells (surface-bonded or internalised liposomes) **(A, C)** and Mean Fluorescence Intensity **(B, D)**. **(E)** Representative flow cytometry plots of liposome uptake (colored) with respect to control cells (shaded grey). Small DOPE:DOTAP (●), small DOPE:DDA (■), small DOPE:DC-Chol (▲), large DOPE:DOTAP (◆) and large DOPE:DDA liposomes (●). Results are represented as mean ± SD of 3 independent experiments. Statistical analysis was performed by one-way ANOVA followed by Tukey test. Statistical significance of DC-Chol liposomes with respect to small DOTAP and DDA liposomes: $p < 0.05$ (*).

Figure 3.6. Effect of composition and size on the *in vitro* cellular uptake of cationic liposomes in BMDMs at 37 ˚C in DMEM + 10 % FBS **(A, C, E)** and serum-free DMEM **(B, D, F)**. in terms of relative liposome surface area (SA_r) **(A, B)**, number of liposomes (N_r) **(C, D)** and internal liposome volume (V_r) **(E,F)**. Small DOPE:DOTAP (●), small DOPE:DDA (■), small DOPE:DC-Chol (▲), large DOPE:DOTAP (♦) and large DOPE:DDA liposomes (●). Results are represented as mean ± SD of 3 independent experiments. Statistical analysis was performed by one-way ANOVA followed by Tukey test. Statistical significance of small (DOTAP and DDA) liposomes with respect to large (DOTAP and DDA) liposomes: $p < 0.05$ (*).

Figure 3.7. Effect of cholesterol incorporation on liposome attributes. Small and large DOPE:DOTAP, small and large DOPE:DDA and DOPE:DC-Chol liposomes were prepared at 1:1 molar ratio at 4 mg/mL in presence (▨) or absence of 1 µg/mL Chol (▨), 1:1 FRR and 15 mL/min TFR. In this way, a 50 µL dose would contain 50 µg DOPE, 50 µg cationic lipid (DOTAP, DDA, DC-Chol) and 25 ng Chol. Liposomes were then dialysed and characterised by DLS in terms of size **(A)** and PDI **(B)**. Results are represented as mean ± SD of three independent experiments.

Figure 3.8. (A) Retention of the radioactive marker ^{3}H-Chol in liposome bilayer of small (●) and large (♦) DOPE:DOTAP liposomes. Liposomes were formulated by microfluidics and then were dialysed against TRIS:FBS (50:50 v/v) at 37 ˚C for 168 hours (7 days). **(B-D)** Stability of cationic liposomes in *in vivo* simulated conditions. Small DOPE:DOTAP (●), large DOPE:DOTAP (♦), small DOPE:DDA (■), large DOPE:DDA (●) and DOPE:DC-Chol (▲) were formulated by microfluidics, dialysed and incubated in TRIS/FBS (50:50 v/v) at 37 ˚C under shaking and characterised at relevant time points by DLS in terms of size **(C)**, PDI **(B)** and zeta-potential **(C)**. Results are represented as mean ± SD of three replicates.

Figure 3.9. Physicochemical characterisation of cationic liposomes for *in vivo* biodistribution experiments. Small DOPE:DOTAP (▨, —), Large DOPE:DOTAP (▨, —), small DOPE:DDA (▨, —), large DOPE:DDA (▨, —) and small DOPE:DC-Chol liposomes (▨, —) were formulated by microfluidics at 1:1 molar ratio, 4 mg/mL in presence of 1 µg/mL chol, 1:1 FRR, 15 mL/min TFR. Small DOPE:DOTAP and small DOPE:DDA were formulated at 10 mM TRIS pH 7.4, large DOPE:DDA was formulated at 300 mM TRIS pH 7.4 and large DOPE:DOTAP and DOPE:DC-Chol were formulated at 1000 mM TRIS. **(A)** Liposomes were dialysed and characterised by DLS in terms of size (bars), PDI (dots) and zeta-potential (values). **(B)** Representative size distribution plots of liposome formulations. Results are represented as mean ± SD of three consecutive DLS measurements.

Figure 3.10. Effect of composition and size on the *in vivo* biodistribution of cationic liposomes in mice. The percentage of injected dose of DOPE:DOTAP **(A, D, G)**, DOPE:DDA **(B, E, H)** and DOPE:DC-Chol liposomes **(C, E, I)** was analysed at the injection site **(A-C)**, popliteal lymph node **(D-F)** and inguinal lymph node **(G-I)**. Small DOPE:DOTAP (●), large DOPE:DOTAP (♦), small DOPE:DDA (■), large DOPE:DDA liposomes (●), small DOPE:DC-Chol (▲). Results are represented as mean ± SD of 4 ± 1 mice. **(J)** AUC for each of the sites.

Figure 4.1. Representative Ribo Green calibration curves in presence (●) and absence (●) of 1% triton-X100 for quantification SAM encapsulation efficiency of LNPs. Limit of detection (LOD) and limit of quantification (LOQ), calculated according to ICH guideline Q2 (R1): "*Validation of Analytical Procedures: Text and Methodology*" (2005), were below 200 ng/mL and 600 ng/mL respectively. Therefore, this method was sensitive enough to quantify SAM E.E. of LNPs.

Figure 4.2. Schematic representation of cationic liposomes and possible structure of cationic lipid nanoparticles (cLNPs) investigated in this thesis. Cationic liposomes were composed of the fusogenic lipid DOPE and a cationic lipid (e.g. DOTAP) at a 50:50 molar ratio. cLNPs were composed of DOPE, a cationic lipid and a PEGylated lipid at a 49:49:2 molar ratio.

Figure 4.3. Cationic lipids investigated to design cationic lipid nanoparticles. *1,2-dioleoyl-3-trimethylammonium-propane (DOTAP), 1,2-stearoyl-3-trimethylammonium-propane (DSTAP), 1,2-dimyristoyl-3-trimethylammonium-propane (DMTAP), dimethyldioctadecylammonium (DDA), 3ß-[N-(N',N'-dimethylaminoethane)-carbamoyl]cholesterol (DC-Chol), N-(4-carboxybenzyl)-N,N-dimethyl-2,3-bis(oleoyloxy)propan-1-aminium (DOBAQ).*

Figure 4.4. Physicochemical stability of GFP-SAM LNPs at 4 ˚C. DOPE:Cationic:PEG-lipid (49:49:2 mole %) SAM-LNPs were formulated by microfluidics at 4 mg/mL, 3:1 FRR, 5 mL/min TFR, 8:1 N:P in 100 mM citrate buffer pH 6.0, dialysed and characterised by DLS in terms of size **(A)**, PDI **(B)** and zeta-potential **(C)** at relevant time points. Cationic Lipid: DOTAP (●), DDA (■), DC-Chol (▲) DMTAP (◆), DOBAQ (●). Results are represented as mean ± SD of three replicates.

Fig. 4.5. RNase protection assay of DOPE:Cationic:PEG-lipid GFP-SAM LNPs.

Figure 4.6. *In vitro* cellular uptake of GFP-SAM LNPs in BMDMs in DMEM (10 % FBS) in terms of percentage of DiI-C_{18}^{+} cells (internalised and surface-associated LNPs) **(A, B)** and Mean Fluorescence Intensity (MFI) **(C, D)**. **(C)** Representative flow cytometry plots of LNP uptake (colored) with respect to control cells (shaded grey). DOPE:Cationic:PEG-C18 **(A, C)**, DSPC:Chol:Cationic:PEG-C14 **(B, D)**. Cationic lipid: DOTAP (●), DDA (■), DC-Chol (▲), DMTAP (◆), DOBAQ (●). Results are represented as mean ± SD of 4 independent experiments. Statistical significances of DOTAP, DDA with respect to DMTAP, DC-Chol and DOBAQ-cLNPs. $p < 0.05$ (*).

Figure 4.7. Effect of LNP formulation design on the *in vitro* cellular uptake **(A-D)**, endosomal escape of SAM and antigen expression **(E, F)** in BHK fibroblasts in presence (5 %) **(A, C, E)** and absence of serum **(B, D, F)** after 16 hours. Cells were treated with 200 ng SAM/well. Cellular uptake is represented in terms of LNP^{+} cells and mean fluorescence intensity (MFI). Endosomal escape and antigen expression are represented as percentage of $dsRNA^{+}$ and GFP^{+} cells respectively. Cationic lipid: DOTAP (▧), DDA (▧), DC-Chol (▧), DMTAP (▧), DOBAQ (▧) and Lipid K (▧). Results are represented as mean ± SD of 3 independent experiments.

Figure 4.8. *In vitro* potency of GFP-SAM cLNPs and iLNPs in BHK cells in presence **(A)** and absence **(B)** of serum (5 %). GFP-SAM cLNPs were composed of DOPE, a cationic lipid and PEG-C18 (49:49:2 mole %), where cationic lipid was DOTAP (●), DDA (■), DC-Chol (▲), DMTAP (◆), DOBAQ (▲). ILNPs were composed of DSPC, Chol, Ionisable lipid K and PEG-C14 (10:48:40:2 mole %) (●). Lipofectamine2000 (■) was used as a control. Results are represented as mean ± SD of 4 independent experiments. Statistical analysis was performed by one-way ANOVA followed by Tukey-test where appropriate. Statistical significances of DDA or DOTAP LNPs with respect to DC-Chol and DMTAP LNPs are shown in black, while those between DDA and DOTAP LNPs are represented in blue. $P < 0.05$ (*). *Please note that the representation of statistical significances with respect to DOBAQ-cLNPs, K-iLNPs and Lipofectamine2000 are not represented due to space limitations.*

Figure 4.9. *In vitro* potency of RVG-SAM cLNPs and iLNPs in BHK cells in presence **(A)** and absence **(B)** of serum (5 %). RVG-SAM cLNPs were composed of DOPE, a cationic lipid and PEG-C18 (49:49:2 mole %), where cationic lipid was DOTAP (●), DDA (■), DC-Chol (▲), DMTAP (◆). ILNPs were composed of DSPC, Chol, Lipid K and PEG-C14 (10:48:40:2 mole %) (●). Lipofectamine2000 (■) was used as a control. Results are represented as mean ± SD of 4 independent experiments. Statistical analysis was performed by one-way ANOVA followed by Tukey-test where appropriate. Statistical significances of DDA or DOTAP LNPs with respect to DC-Chol and DMTAP LNPs are shown in black, while those between DDA and DOTAP LNPs are represented in blue. $P < 0.05$ (*). *Please note that the representation of statistical significances with respect to K-iLNPs and Lipofectamine2000 are not represented due to space limitations*

Figure 4.10. Effect of the PEGylated on the *in vitro* potency of RVG-SAM cLNPs in presence **(A, C, E, G)** and absence **(B, D, F, G)** of serum (5 %). cLNPs were composed of DOPE, a cationic lipid and a PEGylated lipid (PEG-C18 or PEG-C14) at 49:49:2 mole %. DOTAP/PEG-C18 (●) vs DOTAP/PEG-C14 (○) **(A, B)**, DDA/PEG-C18 (■) vs DDA/PEG-C14 (■) **(C, D)**, DC-Chol/PEG-C18 (▲) vs DC-Chol/PEG-C14 (△) **(E, F)**, DMTAP/PEG-C18 (◆) vs DMTAP/PEG-C14 (◇) **(G, H)**. Lipofectamine2000 (■) was used as a control. Results are represented as mean ± SD of 4 independent experiments. Statistical analysis was performed by one-way ANOVA comparing PEG-C18 cLNPs vs PEG-C14 cLNPs. $P < 0.05$ (*).

Figure 5.1. *In vivo* biodistribution of RVG-SAM DOTAP-cLNPs (black), DDA-cLNPs (red) and K-iLNPs (blue) in mice following intramuscular injection. **A)** Acquired images. **B)** Biodistribution profiles. **C)** Area under de curve. Results are represented as mean ± SD of five animals. Statistical significance: (*) $p < 0.05$.

Figure 5.2. Total anti-RVG IgG titres in mice upon intramuscular injection of SAM formulations or Rabipur on days 0 and 28. Sera were collected after 14 **(A)**, 27 **(B)**, 42 **(C)** and 56 days **(D)** and total IgG titres were quantified using PLATELIA RABIES II KIT (Bio-Rad). Dots depict measurements from pools of 2 mice each. Solid lines represent the geometric mean of each group. Dotted lines at 0.5 and 0.125 EU/mL correspond to protection threshold and limit of quantification respectively. *HD (human dose*). Statistical significance: (*) $p < 0.05$.

Figure 5.3. Time course of total anti-RVGP IgG titers in mice upon intramuscular injection of SAM formulations or Rabipur on days 0 and 28 (denoted by arrows). **A)** DOTAP-cLNPs, **B)** DDA-cLNPs, **C)** K-iLNPs, **D)** CNE56. Sera were collected after 14, 27, 42 and 56 days and total IgG titers were quantified using PLATELIA RABIES II KIT (Bio-Rad). Dotted lines at 0.5 and 0.125 EU/mL correspond to protection threshold (according to manufacturer) and limit of quantification respectively. *HD (Human dose*).

Figure 5.4. Gating strategy used for the identification of antigen-specific T cells upon restimulation. **A)** Gating on CD4+ and CD8+ T cells. **B)** CD4+ T cell cytokines. **C**) CD8+ T cell cytokines and CD107a. TNF-α+, IL-2+ and IFN-γ+ cells were analysed in combination with Boolean gates. CD107a+ cells were analysed separately.

Figure 5.5. Frequencies of RVG Ag-specific T cells 2 after the second immunisation from splenocytes stimulated *in vitro* with a peptide pool spanning RVG. **A)** Cytokine-producing $CD8^+$ T cells **B)** $CD8^+$ $CD107^+$ T cells. **C)** Cytokine-producing $CD4^+$ Th0 and Th1 cells according to secreted cytokines. No IL-17^+ cells were detected. Results are represented as mean ± SD of three samples.

Figure 6.1. In vivo biodistribution of RVG-SAM DOTAP-cLNPs and K-iLNPs in mice following intramuscular, intradermal and intranasal administration.

Figure 6.2. Biodistribution of DOTAP-cLNPs (black) and K-iLNPs (red) after intramuscular **(A, B)**, intradermal **(C, D)** and intranasal administration **(E, F)**. Biodistribution pharmacokinetics **(A, C, E)** and area under the curve (AUC), represented as corrected flux · day) for each of the formulations and routes tested **(B, D, F)**. Results are represented as mean ± SD of five animals per experimental group. The biodistribution data of the IM groups is the same as that represented in Fig. 5.1.

Figure 6.3. Comparison of total IgG titres of bridged groups from current Chapter (2^{nd}) with the previous *in vivo* study shown in Chapter 5 (1^{st}) two weeks after prime (*2wp1*), four weeks after prime (*4wp1*) and two weeks after boost (*2wp2*) 1/20 HD Rabipur or 0.15 µg SAM formulated in either K-iLNPs (*iLNPs*) or DOTAP-cLNPs (*cLNPs*).

Figure 6.4. Total anti-RVG IgG titres in BALB/c mice upon intramuscular, intradermal or intranasal injection of DOTAP-cLNPs, K-iLNPs and Rabipur on days 0 and 28. Sera were collected after 14 **(A)**, 27 **(B)** and 42 **(C)** and total IgG titres were quantified using PLATELIA RABIES II KIT (Bio-Rad). Dots depict measurements

from pools of 2 mice each. Solid lines represent the geometric mean of each group. Dotted lines at 0.5 and 0.125 EU/mL correspond to protection threshold and limit of quantification respectively. *HD (human dose*). Statistical significance: $p < 0.05$ (*).

Figure 6.5. Gating strategy used for the identification of antigen-specific T cells upon restimulation as previously described (Goswami et al., 2019). **A)** Gating on $CD4^+$ and $CD8^+$ T cells. **B)** $CD4^+$ T cell cytokines. **C)** $CD8^+$ T cell cytokines and CD107a. TNF-α^+, IL-2^+ and IFN-γ^+ cells were analysed in combination with Boolean gates. $CD107a^+$ cells were analysed separately.

Figure 6.6. Frequencies of RVG Ag-specific T cells two weeks second vaccination from splenocytes stimulated *in vitro* with a peptide pool spanning RVG. **A)** Cytokine-producing $CD8^+$ T cells. **B)** $CD8^+$ $CD107a^+$ T cells. **C)** Cytokine-producing $CD4^+$ Th0 and Th1 cells according to secreted cytokines. No IL-17^+ cells were detected. Results are represented as mean ± SD of three samples.

Figure 6.5. Frequencies of RVG Ag-specific T cells two weeks after second vaccinations from lung cells stimulated *in vitro* with a peptide pool spanning RVG. **A)** Cytokine-producing $CD8^+$ T cells. **B)** $CD8^+$ $CD107a^+$ T cells. **C)** Cytokine-producing $CD4^+$ Th0 and Th1 cells according to secreted cytokines. No IL-17^+ cells were detected. Results are represented as mean ± SD of three samples.

LIST OF TABLES

Table 4.1. Physicochemical properties of SAM-LNPs formulated by microfluidics. Lipid compositions – DOPE:Cationic:DSG-PEG2000 49:49:2 mole % (**†**), DOPE:Cationic:DSG-PEG2000 49:49:2 mole % (**‡**), DSPC:Chol:Cationic:DMG-PEG2000 10:48:40:2 mole % (*****). Abbreviations: SAM E.E. (encapsulation efficiency), ZP (zeta-potential). Results are represented as mean ± SD of 3 independent experiments.

Table 5.1. Physicochemical properties of SAM-nanoformulations used for immunisation studies in mice. *SAM encapsulation efficiency (E.E.); zeta-potential (ZP)*. Size, PDI and zeta-potential values are represented as mean ± SD of three consecutive measurements. cLNPs were composed of DOPE, a cationic lipid (DOTAP or DDA) and DMG-PEG2000 at 49:49:2 mole %. K-iLNPs were composed of DSPC, Chol, lipid K and DMG-PEG2000 at 10.48:40:2 mole %.

Table 6.1. Physicochemical properties of SAM-nanoformulations used for immunisation studies in mice. *SAM encapsulation efficiency (E.E.); zeta-potential (ZP)*. Size, PDI and zeta-potential values are represented as mean ± SD of three consecutive measurements. DOTAP-cLNPs were composed of DOPE, DOTAP and DMG-PEG2000 at 49:49:2 mole %. K-iLNPs were composed of DSPC, Chol, lipid K and DMG-PEG2000 at 10.48:40:2 mole %.

CHAPTER 1: INTRODUCTION

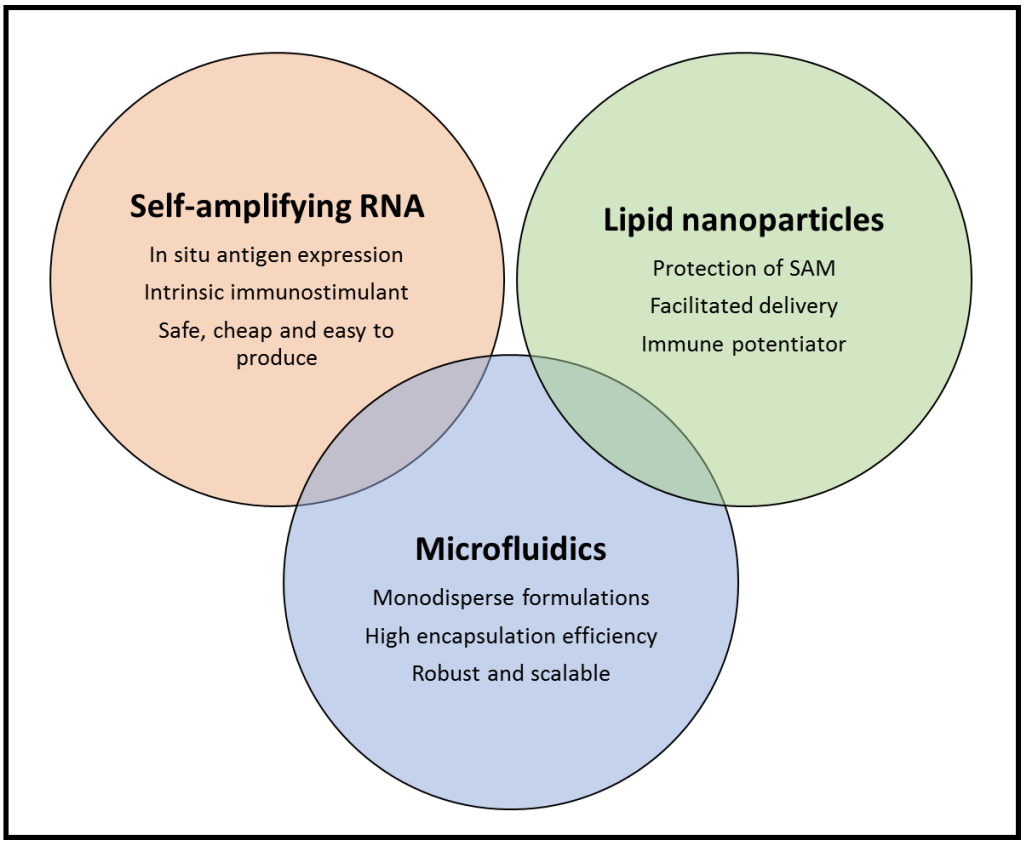

1.1. THE RABIES VIRUS

The Rabies virus belongs to the *Lyssavirus* genus, zoonotic pathogens within the family *Rhaboviridae*. It has a negative sense single-stranded ribonucleic acid (-ssRNA) genome encoding a nucleoprotein (N), a phosphoprotein (P), a matrix protein (M), a glycoprotein (G) and a RNA polymerase (L) (Tordo et al., 1988). The rabies virus glycoprotein (RVG) is the only surface-exposed protein on the virion and is therefore the only target for neutralising antibodies (NAs), which confer full protection against virus challenge (Xiang et al., 1995). Standardised assays for measuring NAs to rabies have been developed (Smith et al., 1973). NA titres above 0.5 international units (IU), quantified against an infectious reduction assay against a World Health Organisation (WHO) reference serum, are considered protective in mammals (Ertl, 2009). Furthermore, although cell-mediated immunity does not prevent initial viral infection, it plays a key role in virus clearance in mice (Wiktor, 1978).

The rabies virus causes over 50,000 human deaths annually, most of which occur in developing countries of Africa and Asia (Sudarshan et al., 2007). Infection occurs following a transcutaneous or mucosal exposure to saliva of rabid animals, which represent a reservoir for the virus. Following infection, the virus travels along the peripheral nerves to reach the central nervous system (CNS). Virus replication within the brain results in presentation of clinical symptoms and fatal encephalitis. Indeed, there is still no treatment to prevent death once the virus has reached the CNS (Hicks et al., 2012).

Marketed vaccines such as Imovax (Sanofi) or Rabipur/RabAvert (GSK Biologicals) are based on an inactivated cell culture-derived rabies virus. Although they are efficacious, they must be administered several times for both pre- (days 0, 7, 21 and 28) and post-exposure prophylaxis (days 0, 3, 7, 14 and 30). In case of severe exposure, rabies virus-specific immunoglobulin (RIG) is also administered. Moreover, boosting is also recommended at 2-5-year intervals for pre-exposure prophylaxis, hence limiting patience compliance. Adjuvantation with aluminium salts allow to reduce the dose while increasing immunogenicity (e.g. Rabivax). Nevertheless, the high cost of these vaccines represents great barrier for the developing countries (Hicks et al., 2012). Therefore, there is an unmet need of cheap vaccines to confer long-term and sustained protection, ideally after a single vaccination. Some novel rabies vaccines are in preclinical

development and include live-attenuated vaccines, recombinant viral vector vaccines, protein subunit vaccines and DNA vaccines (Brito et al., 2015). However, before describing these types of vaccines, it is essential to understand what the immune system is and how it works.

1.2. A GENERAL OVERVIEW OF THE IMMUNE SYSTEM

1.2.1. Innate immunity

Innate immunity, together with external physical (skin, epithelium, mucous membranes) and chemical barriers (enzymes, stomach acids), represents the first line of host defence against pathogens. Although innate immune responses are triggered rapidly (within hours), they lack memory. The innate immune system is comprised by phagocytic cells (neutrophils, dendritic cells and macrophages), leucocytes (natural killer [NK] cells, mast cells, eosinophils, basophils) and the complement system.

Tissue damage caused by an invading pathogen induces a complex series of events collectively known as the inflammatory response, characterised by the release of chemokines (McDonald et al., 2010). Chemokines are “danger signals” which lead to the recruitment of phagocytic cells at the site of infection to eradicate the pathogen. The activity of neutrophils is mainly anti-pathogenic. They exert a combination of cytotoxic mechanisms that include the production of reactive oxygen species (ROS), release of microbial peptides, and neutrophil extracellular traps (NETs) (Mayadas et al., 2014). Macrophages and dendritic cells (DCs) are able to process intracellularly the phagocyted pathogens to subsequently expose their antigens on their surface in a process known as antigen presentation. In general, peptides derived from exogenous antigens are presented by the major histocompatibility complex (MHC) class II (MHC-II), while those derived from endogenous antigens are exposed in association with the MHC class I (MHC-I). Some exogenous antigens, however, can be presented by the MHC-I in a process known as cross-presentation (Rock and Clark, 1996).

Recognition of pathogens by the cells of the innate immune system occurs through a series of surface receptors, named pattern recognition receptors (PPRs). PRRs are able to detect conserved molecular structures expressed by pathogens, often referred to as pathogen-

associated molecular patterns (PAMPs). Lipopolysaccharide (LPS) and lipoteichoic acid, expressed in gram-negative and gram-positive bacteria respectively, are examples of PAMPs (Tang et al., 2012).

Toll-like receptors (TLRs) are a likely the most important family of PPRs. TLRs 1, 2, 4, 5 and 6 are expressed on the cell surface and recognize bacterial products, while TLRs 3, 7, 8 and 9 are expressed in the endoplasmic reticulum. Recognition of PAMPs by TLR triggers a series of signalling cascades that eventually induce the production of cytokines necessary to activate the adaptive immunity. (Muzio et al., 2000). Nucleotide-binding and oligomerisation domain (NOD)-like receptors (NLRs) and retinoic acid-inducible gene-I (RIG-I)-like receptors (RLRs) represent another type of PPRs able to detect PAMPs in the cytosol (Kawai and Akira, 2009). Type-I interferons (IFNs) and tumour necrosis factors (TNFs) are important cytokines secreted by antigen presenting cells (APCs). For instance, IFN-α produced by macrophages and dendritic cells enhances antigen presentation and chemokine production in innate cells, and effector B and T cell responses (Ivashkiv and Donlin, 2014).

1.2.2. Adaptive immunity

Adaptive immunity represents the second line of host defence. Although they take several days or weeks to develop, adaptive immune responses are, however, antigen-specific and able to recognize and eliminate virtually any known pathogen. More importantly, adaptive immunity establishes memory, so that the host is protected more efficiently and rapidly from re-exposure. Memory is the hallmark of adaptive immunity and can be induced by natural infection or vaccination. Adaptive immune responses are divided in humoral and cellular immune responses, which are responsible for protection against extracellular and intracellular pathogens respectively.

1.2.2.1. Main effector mechanisms of the adaptive immune response

1.2.2.1.1. B cells and antibodies

B cells are subset of antigen presenting cells characterised by the surface expression of the so-called B cell receptor (BCR), a membrane-bound immunoglobulin (Ig). B cells usually remain in

the lymphoid tissue (lymph nodes), where they are able to recognise antigens through the BCR. Importantly, each B cell expresses a unique and randomly determined antigen-specific BCR. Antigen encounter results in stimulation, differentiation and clonal expansion of B cells in plasma cells – and memory B cells – with the subsequent release antigen-specific antibodies to the blood. Except for some antigens (e.g. cell wall products or polymers with repeating epitopes), B cells require from co-stimulatory signals provided by T cells. This co-stimulation, provided by the engagement between the cluster of differentiation (CD) 40 (CD40) on B cells and CD40L on activated T cells, is essential for B cell survival and generation of memory B cells.

Antibodies flag pathogens or infected cells such that they are recognised and neutralised by effector immune cells, including macrophages and killer cells (cytotoxic T lymphocytes and NK cells), by mechanisms known as antibody-dependent cell phagocytosis (ADCP) and antibody-dependent cell cytotoxicity (ADCC) respectively (Gül and van Egmond, 2015). Alternatively, antibodies can promote pathogen lysis by activating the complement system (Daha et al., 2011). Neutralising antibodies (NAs) constitute a type of antibodies able to neutralise pathogens and their toxins by themselves (Corti and Lanzavecchia, 2013).

1.2.2.1.2. T cells

T cells are phenotypically characterised by the expression of a surface complex composed of the T cell receptor (TCR) and CD3. This latter contains intracellular tails with conserved motifs known as immunoreceptor tyrosine-based activation motif (ITAM), which are responsible for the TCR signal transduction and therefore essential for effective T cell activation. Contrary to the BCR, the TCR is only able to recognise antigens when presented by MHC-I or MHC-II. T cells can be divided in $CD8^+$ and $CD4^+$ T cells. The activation of T cells requires three signals from APCs: 1) antigen presentation to the T cells via MHC, 2) the interaction of adhesion and costimulatory molecules (CD80 and CD86 expressed on ACPs with CD28 on T cells and CD40 with CD40L) and 3) secretion of cytokines by APCs. The panel of cytokines secreted by APCs directs the differentiation of antigen-specific T cells into effector T cells and ultimately dictates the type of immune response elicited (cell-mediated vs humoral) (Gutcher and Becher, 2007).

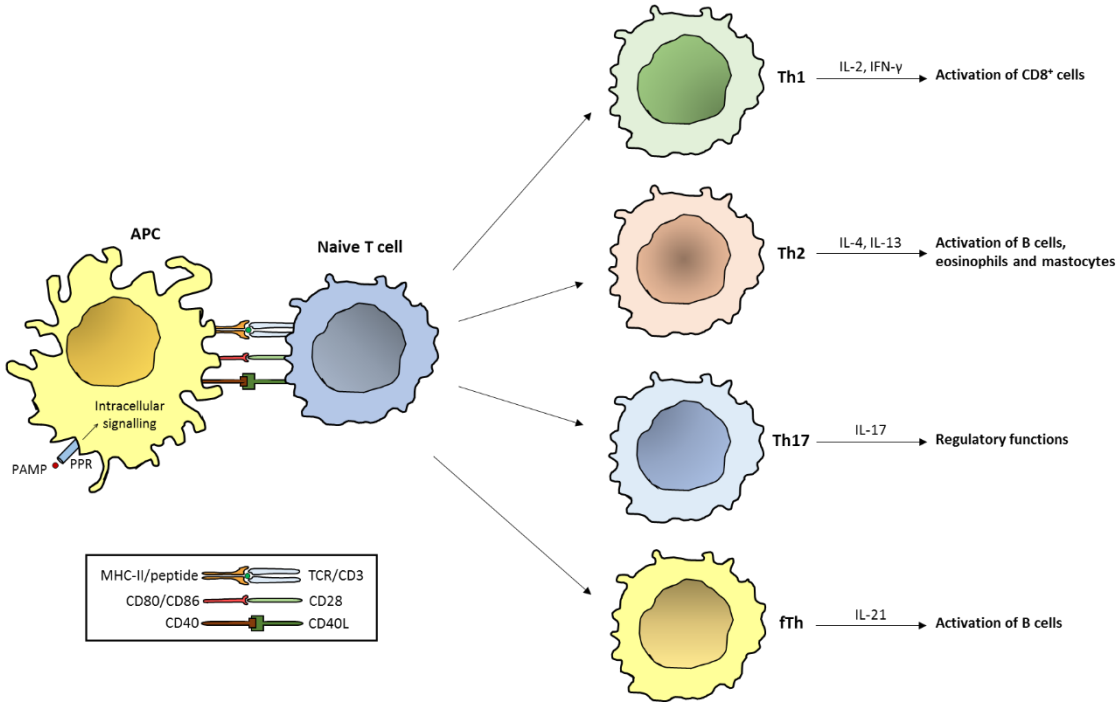

Figure 1.1. Schematic representation of $CD4^+$ T cell activation. Adapted and redrawn from (Moser and Leo, 2010).

Activated $CD8^+$ T cells, known as cytotoxic T lymphocytes (CTLs) are capable of inducing death (apoptosis) of infected or damaged/dysfunctional (e.g. tumour) cells expressing a specific MHC-I/antigen complex. CTLs exert their cytotoxic activity through either the release of cytolytic proteins (perforin and granzyme B) or binding via death receptors (FAS and TRAIL) (Squier and John Cohen, 1994). Furthermore, CTLs also secrete IFNs and TNFs, both of which inhibit the intracellular replication of the pathogen. Indeed, the depletion of TNFs and IFNs results in impaired cytotoxic activity of $CD8^+$ T cells (Ghanekar et al., 2001; Murthy et al., 2011). Notably, the expression of the lysosomal-associated membrane protein 1 (LAMP-1), also known as CD107a, correlates with the cytotoxic activity of $CD8^+$ T cells *in vivo* (Aktas et al., 2009).

On the other hand, $CD4^+$ T cells, commonly known as T helper (Th) cells, regulate other immune cells through the secretion of cytokines. Th cells can be divided in several groups. Th1 cells mainly promote immune responses against intracellular pathogens by activating $CD8^+$ T cells and macrophages via secretion of interleukin-2 (IL-2) and IFN-γ respectively. Th2 cells secrete IL-4, which induces the upregulation of co-stimulatory molecules on B cells and, consequently,

promote the production of antibodies. Th2 cells also produce IL-5 and IL-13 which, in combination with IL-4, activate other cells of the immune system (eosinophils and mastocytes) involved in elimination of large extracellular pathogens (Moser and Leo, 2010). Follicular helper T cells (fTh) are a subset of Th cells able to promote the production of high-levels of antibodies by antigen-specific B cells independently of Th1 and Th2 cytokines. Follicular Th cells are characterised by the production of IL-21 (Mackay, 2000). Finally, Th17 cells are a class of Th cells that produce IL-17, a cytokine involved in several models of autoimmune inflammation (Tesmer et al., 2008). Importantly, Th1 and Th2 cytokines antagonize each other and block Th17 responses (Fig. 1.1).

1.3. FROM CLASSICAL TO NEXT-GENERATION VACCINES

1.3.1. Classical vaccines

In 1796, Edward Jenner discovered that inoculation with cowpox could protect against smallpox infection. Since then, vaccines have become a successful tool to fight infectious diseases (Plotkin and Plotkin, 2008). To date, vaccines are the most cost-effective and powerful healthcare intervention to save lives. Historically, they have been prepared by empirical methods with little or no immunological insight.

Live-attenuated vaccines are potent vaccines produced by serially passing the pathogen in tissue, animals or a cell culture to reduce their virulence almost completely. For instance, the Bacillus Calmette-Guerin (BCG) vaccine for tuberculosis was first used in 1921 and is still being used nowadays. These vaccines, which mimic a real infection, induce strong humoral and cellular-mediated immune responses, which can last for several decades even after a single dose. However, they present potential risks such as reversion of attenuation and pathogenicity in susceptible (e.g. immunocompromised) patients.

An example of live-attenuated rabies vaccines is based on a mutation in the amino acid 333 of the glycoprotein, which generally attenuates the virus (Dietzschold et al., 1983). Due to the rapidly mutating nature of rabies virus, a single site-directed mutation is not enough to ensure a long-lasting non-pathogenic phenotype. Indeed, serial passages of the virus resulted in reversal

of attenuation (Faber et al., 2005). Advances in genetic engineering are paving the way on the development of safer live-attenuated vaccines to rabies. For example, deletion of virus phosphoprotein (P) or matrix protein (M) abolished rabies virulence while maintaining immunogenicity (Ertl, 2009).

Inactivated (killed) whole-cell vaccines constitute another type of classical vaccines prepared by inactivation of the pathogen with chemicals (e.g. formaldehyde), heat or radiation. Because they do not contain live pathogens, they have a safe profile (Giesen et al., 2015). However, they induce weaker immune responses compared to live-attenuated vaccines so that they require from boost shots every few years to ensure protection over time unless co-formulated with adjuvants.

As already discussed, inactivated tissue-culture vaccines to rabies (e.g. Imovax or Rabipur) are efficacious but require from 4-5 injections and boosting every 2-5 years. The immunogenicity of these rabies vaccines can be enhanced by co-administering adjuvants (DiStefano et al., 2013). In a recent study, the ability of a range of adjuvants to enhance the immunogenicity of Rabipur was investigated. Alum (especially nanometre-sized alum) induced earlier and more vigorous production of NAs and conferred improved protection in mice against rabies challenge compared to other adjuvants such as bacterial-like particles, AS02, AS03, MF59 and Poly I:C. (Shi et al., 2018).

Protein-based vaccines are composed of the antigenic parts of the pathogen (e.g. recombinant hepatitis B vaccine). Although they have a safe profile, subunit antigens elicit weaker immune responses than live-attenuated vaccines. This is partially attributed to the fast clearance from the body upon injection and low cellular uptake by APCs. However, adsorption of antigens on a particulate delivery system (a category of adjuvant), enhances the immunogenicity to the antigen and allows to polarize the immune responses. For example, cationic liposomes have been widely used to deliver negatively charged subunit antigens thus increasing the immunogenicity to the antigens by a combination of depot effect and immune potentiation (Christensen et al., 2007). Several research groups have investigated vaccines based on recombinant RVG expressed in different systems, such as insects, yeast cultures and plants, mostly with negative results (Ertl, 2009).

1.3.2. DNA vaccines

Since the discovery that plasmid DNA induced antibody responses to viral and non-viral antigens when delivered into the skin or muscle (Tang et al., 1992), DNA vaccines gained a great deal of attention. These combine the advantages of live-attenuated vaccines and subunit vaccines. Indeed, they are able to induce antigen-specific humoral and cellular-mediated immunity while having a great safety profile. The main barriers for DNA vaccines are poor delivery of DNA to the immune cells and inadequate stimulation of the human immune system. Indeed, despite they showed promising results in small animal models, DNA vaccines lacked efficiency in humans, with high doses (in the order of milligrams) being required to induce acceptable immune responses (Ferraro et al., 2011).

A series of approaches have been explored to overcome these barriers, including electroporation (Sardesai and Weiner, 2011), immune potentiators (Grunwald and Ulbert, 2015) and particulate delivery systems (Christensen et al., 2007). These technologies have allowed to develop a second generation of DNA vaccines able to induce robust immune responses in non-human primates and humans in phase I and II clinical trials (Danko et al., 2018; Gaudinski et al., 2018). Similarly, these novel DNA-based vaccines have been efficacious in eliciting NAs to rabies in a number of animal models, such as mice (Lodmell et al., 1998), cats, dogs (Osorio et al., 1999) and non-human primates (Lodmell et al., 2002). A clear limitation of DNA vaccines to rabies is the slow onset of the immune responses elicited, which restrain their use for post-exposure immunisations, where quick immune responses to prevent infiltration of rabies in the central nervous system are a milestone. To date, no DNA vaccines to rabies are being investigated in human clinical trials.

1.3.3. Viral vector vaccines

Viral vector vaccines are based on viruses, usually with a DNA genome, which have been genetically engineered to be safe and to encode the gene(s) of interest. Their ability to promote gene expression was first reported with an engineered vaccinia virus in 1982 (Mackett et al., 1982). The natural invasiveness of the viral particles allows to effectively deliver the payload in the appropriate subcellular compartment.

Viral vector vaccines elicit robust and potent cellular-mediated immune responses with no need of adjuvants. An important limitation of viral vector vaccines could be the potential induction of antiviral immunity. However, thorough investigations have demonstrated the safety of viral vector vaccines. Moreover, pre-existing anti-vector immunity, generated by the viral antigens, impairs the ability of viral vector vaccines to induced antigen expression and consequently limits the potency of the immune responses. This could be circumvented by using different vectors for prime and boost doses respectively (Ulmer et al., 2012).

1.3.4. mRNA vaccines

1.3.4.1. Basic Pharmacology of mRNA vaccines

The first report of successful use of messenger RNA (mRNA) in animals was published in 1990, when intramuscular injection of mRNA was shown to induce local production of encoded reporter genes (Wolff et al., 1990). A subsequent study reported immune responses to the influenza nucleoprotein encoded in a mRNA vaccine (Martinon et al., 1993). These promising results did not lead to substantial efforts to develop mRNA therapeutics, mostly owing to the poor stability of RNA compared to DNA (Lesnik and Freier, 1995). Despite this limitation, RNA vaccines have clear advantages over DNA and viral vector vaccines. RNA vaccines do not generate infectious particles or integrate in the genome of host cells. They can be delivered in the cytosol to directly induce *in situ* antigen expression, with no need of nuclear import. Furthermore, RNA vaccines can be rapidly produced by means of synthetic manufacturing processes and hence are an ideal platform to fight newly emerging pathogens (Maruggi et al., 2019).

RNA vaccines can be divided in 1) conventional small non-amplifying mRNA and 2) self-amplifying mRNA (SAM). Both types of RNA molecules are composed of a coding region flanked by noncoding regions named untranslated regions (UTRs) at both 5' and 3' ends, a cap and a poly adenosine (A) tail. All four elements are essential to guarantee the proper stability and translation of mRNA (Wu and Brewer, 2012). A schematic representation of mRNA and SAM vaccines is shown in Fig. 1.2.

Each of them have own advantages and limitations. mRNA molecules are relatively smaller compared to SAM (2-3 Kb vs 9-10 Kb) and do not encode other proteins that could elicit

undesired immune responses (Schlake et al., 2012). However, due to the short half-life of mRNA, only weak and transient antigen expression can be achieved. In contrast, SAM transfection results in higher levels of antigen expression due to self-amplification in host cells.

SAM vaccines are based on engineered alphavirus replicons, including Sindbis, Semliki Forest and Venezuelan equine encephalitis viruses. They have a positive sense single-stranded RNA (+ssRNA) genome with two open reading frames (ORFs) encoding non-structural (NSP1, 2, 3 and 4) and structural proteins respectively. In SAM vaccines, the genes encoding the structural proteins are substituted for the gene of interest such that the viral replicon is unable to produce infectious virions. However, NSP genes, which encode for the proteins responsible for replication, allow SAM to self-replicate over time.

The whole mechanism of action of SAM vaccines, from replication to antigen expression, can be divided in four phases. First, an RNA-dependent-RNA-polymerase (RDRP) complex is produced from the ORF encoding the NSP genes. Then, the RDRP transcripts a genomic negative RNA molecule, from which a positive RNA and the sub-genomic RNA are generated. Finally, the sub-genomic RNA is translated into the antigen (Iavarone et al., 2017) (Fig. 1.3).

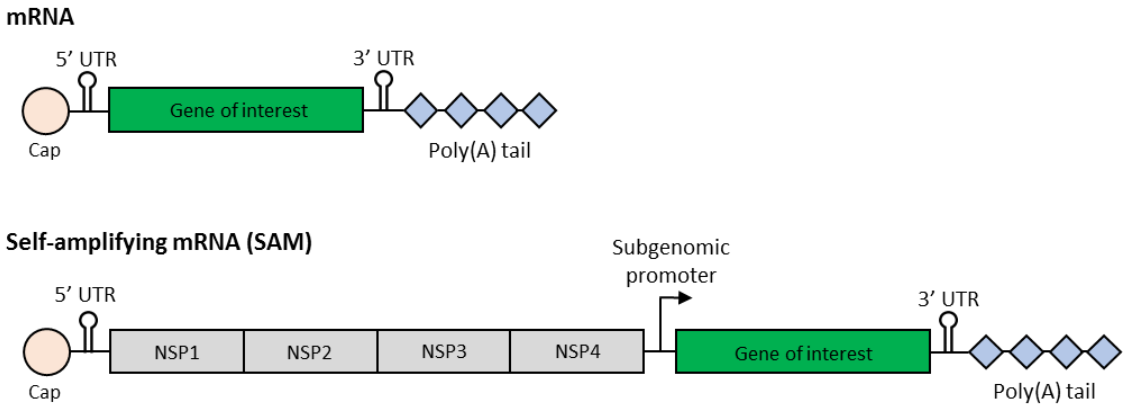

Figure 1.2. Schematic representation of mRNA and self-amplifying mRNA (SAM) vaccines. SAM vaccines are derived from an alphavirus genome in which the genes encoding the structural proteins have been substituted by the gene of interest (GOI). The genes encoding the non-structural proteins (NSP1-4) produce the proteins responsible for the self-replication of SAM.

SAM self-replicates over time and, consequently, leads to higher levels of expression compared to non-amplifying mRNA vaccines. The intramuscular injection of a naked SAM encoding a firefly luciferase, a nonimmunogenic reporter protein, induced expression for over one week, with levels 5-fold higher compared to luciferase-mRNA. Higher antigen expression levels also result in enhanced immune responses compared non-amplifying mRNA vaccines. In the same study, a SAM vaccine encoding the influenza virus hemagglutinin induced equivalent levels of protection than its mRNA counterpart with a dose 64-fold lower (1.25 µg vs 80 µg) (Vogel et al., 2018). Such a decrease in the dose required to confer protection represent an outstanding achievement for the translation of RNA-based vaccines from bench to the clinics, as a significant increase in the dose is required for equivalence in human studies. Another important feature of SAM vaccines that accounts for improved immunogenicity compared to conventional mRNA vaccines is the formation of a double-stranded RNA (dsRNA) intermediate generated during SAM amplification. These dsRNA macromolecules are known to be potent stimulators of innate immunity. A limitation of SAM vaccines is the induction of immune responses against the other genes expressed in the replicon potentially limiting the repeated use of SAM vaccines.

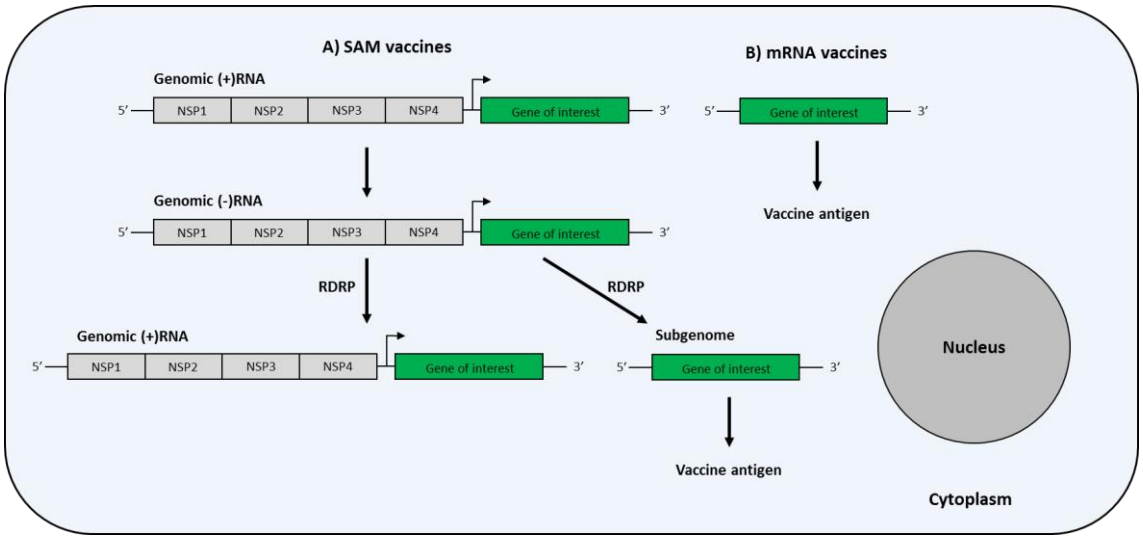

Figure 1.3. Schematic illustration of replication and expression processes of mRNA and SAM after delivery to target mammalian cells. Redrawn from (Brito et al., 2015).

Intramuscular injection of SAM vaccines results in transfection of myocytes (Lazzaro et al., 2015). Myocytes act as a source of antigen for dendritic cells to cross-prime $CD8^+$ T cells. It was

hypothesised that myocytes undergo apoptosis during SAM amplification such that apoptotic bodies are subsequently phagocytosed by dendritic cells. Whether this apoptotic bodies contain functional SAM molecules or myocyte-derived antigens still needs to be elucidated. Indeed, the authors were unable to directly transfect dendritic cells neither *in vitro* nor *in vivo*. Therefore, it seems that direct targeting of dendritic cells does not seem to be a pre-requisite to elicit potent immune responses. However, the functionalisation of lipid nanoparticles (LNPs) with mannose, a targeting ligand of C-type lectin receptors expressed by dendritic cells, resulted in a more rapid onset and enhanced humoral immune responses of a SAM influenza vaccine compared to non-glycosylated LNPs, both after intramuscular and intradermal administration (Goswami et al., 2019). These recent findings suggest that targeted delivery of SAM vaccines could improve their immunogenicity.

1.3.4.2. Modulation of mRNA immunogenicity

Macrophages and dendritic cells can sense ssRNA and dsRNA via TLR7/8 and TLR3 respectively (Takeda and Akira, 2005). The engagement of TLRs results in the activation of these cells thereby increasing antigen presentation, promoting cytokine secretion, isotype switching and memory B cell survival (Iavarone et al., 2017). In addition, nonimmune cells can sense dsRNA via cytoplasmic RIG-I-like receptors (RLRs) (Loo and Gale, 2011).

Although TLR signalling pathways lead to the activation of innate immune cells, they can potentially induce the production of proinflammatory cytokines and chemokines and type-I interferons. These immunostimulatory properties of mRNA could be beneficial or detrimental depending on the therapeutic application and hence should be modulated accordingly. For instance, activation of innate immunity should be avoided in other applications such as gene silencing (e.g. siRNA) or tissue regeneration (Kaczmarek et al., 2017).

Type-I interferons trigger intracellular antimicrobial activities and influence the development of innate and adaptive immune responses. Indeed, the lack of interferon-mediated immune responses resulted impaired immunogenicity (McNab et al., 2015). However, type I interferon also upregulates protein kinase R (PKR) and 2’-5’-oligoadenylate synthetase (OAS) consequently inhibiting translation and promoting the degradation of mRNA and ribosomal RNA respectively

(Pardi et al., 2018). This antiviral activity also results in blockade of B cell responses and production of immunosuppressive cytokines such as IL-10 (Maes et al., 1999).

In the context of SAM vaccines, determinants within the NSP1/NSP2 cleavage domain in the alphavirus genome play a key role in the modulation of type I interferon immune responses. The directed mutagenesis in the position 538 in NSP1 alphavirus genome resulted in enhanced type I interferon compared to the wild type virus both *in vitro* and *in vivo* (Cruz et al., 2010). A single mutation in the NSP1 gene of a Venezuelan equine encephalitis-Sindbis virus-based SAM vaccine potentiated the production of type I interferon but reduced both antigen expression and vaccine immunogenicity. In contrast, mutations in the 5'-UTR had no significant impact on vaccine immunogenicity (Maruggi et al., 2013).

An example of the detrimental effect of type I interferon on vaccine potency was reported by Pollard and colleagues (Pollard et al., 2013). The subcutaneous injection of a mRNA encoding the HIV-1 antigen Gag complexed with cationic DOPE:DOTAP liposomes resulted in the induction of both T and B cell responses. The authors demonstrated that type I interferon inhibited antigen expression and antigen-specific immune responses. The negative effect of type I interferon on SAM vaccines was further evidenced by Pepini and co-workers (Pepini et al., 2017). Vaccination with a SAM vaccine elicited early and robust production of type I interferon responses and reduced the immunogenicity. However, the potency of the SAM vaccine significantly increased in an interferon receptor (IFNAR) knockout mouse model. These findings evidence the antagonist roles of type I interferon and suggest that these responses could be modulated to achieve desired immune responses.

The immunostimulatory properties of RNA can be shaped by the purification of *in vitro* transcribed (IVT) RNA. Indeed, enzymatically synthesised mRNA contain dsRNA contaminants generated in the IVT reaction. Notably, elimination of dsRNA contaminants from IVT mRNA resulted in 1000-fold increase in antigen expression in primary human dendritic cells (Karikó et al., 2011). Despite dsRNA traces are removed, ssRNA molecules have intrinsic PAMP activity. In order to reduce their ability to engage innate immune sensors, the use of naturally occurring chemically modified nucleosides such pseudourine or 1-methylpseudourine has been extensively investigated (Pardi et al., 2018).

Another strategy consists on using small molecule modulators, such as glucocorticoids (Iavarone et al., 2017). Conversely, these properties can be enhanced by incorporating an adjuvant such as particulate delivery system or a mRNA encoding immune modulators. For instance, Manara and co-workers (Manara et al., 2019) recently described that the co-administration of granulocyte-macrophage colony-stimulating factor (GM-CSF)-SAM boosted the potency of an influenza SAM vaccine and improved the protection against lethal challenge. In particular, the authors demonstrated that such enhancement was related to the increased recruitment of antigen presenting cells to the injection site. Another effective approach consists on Trimix, a mix of mRNAs encoding CD70, CD40L and a constitutively active TLR4. TriMix has been successfully used to enhance the potency of tumour-associated (TTA)-based mRNA cancer vaccines by enhancing the maturation of dendritic cells, priming of TAA-specific T cells and CTL responses (Van Lint et al., 2012).

1.3.4.3. Optimisation of stability and translation capacity of mRNA vaccines

The backbone of mRNA vaccines can be optimised to improve the pharmacological properties of mRNA vaccines. For instance, methylation of cap reduces the recognition of RNA by innate immune cells and accounts for enhanced immunogenicity *in vivo*. On the other hand, modification of 5' and 3' UTRs has also been explored to increase the stability and translation capacity of mRNA vaccines. Another approach consists on modifying the codon usage. Indeed, substitution of adenine and thymine nucleosides for guanine or cytosine has been shown to increase *in vivo* antigen expression and immunogenicity of mRNA vaccines. However, it is important to consider that these modifications could also result in modified secondary structures of mRNA and consequently the shape of the immune responses elicited (Iavarone et al., 2017).

1.4. DELIVERY OF mRNA VACCINES

mRNA molecules are labile and can be de degraded within seconds in presence of extracellular RNases (Probst et al., 2006). Moreover, the cellular internalisation of naked mRNA is impaired by its hydrophilic and anionic nature. Furthermore, mRNA can be rapidly degraded in the lysosomes upon cellular internalisation. A key challenge in RNA delivery is therefore the efficient

delivery in the cytoplasm of target cells. This can be accomplished by physical methods such as electroporation or gene gun, by means of non-viral delivery systems (e.g. lipid nanoparticles) or viral delivery systems. Non-viral delivery systems not only enhance the uptake of mRNA but also to facilitate endosomal escape and cargo release into the cytosol. The use of viral particles to deliver mRNA has also been extensively investigated, considering the ability of viruses to traffic within host cells and effectively deliver their genome in the appropriate subcellular compartment.

1.4.1. Viral delivery systems

Viral delivery systems consist on genetically engineered viral RNA replicons (e.g. alphavirus) in which the genes encoding the structural proteins are substituted by the gene of interest (vaccine antigen). Helper cells expressing the genes encoding the viral structural proteins are transfected with the RNA replicons, such that RNA replicons are packed in viral particles (VRPs) lacking the structural protein genes. Accordingly, VRPs can infect cells without producing virions. VRP-based vaccines elicit strong $CD4^+$ and $CD8^+$ T cell responses in small animal models and non-human primates. A VRP vaccine candidate to cytomegalovirus (CMV) was found to be safe and potent in humans (Reap et al., 2007).

1.4.2. Non-viral delivery systems

1.4.2.1. Electroporation and particle-mediated epidermal delivery (gene gun)

Electroporation represents an efficient method to improve the delivery of nucleic acids and has been thoroughly investigated with plasmid DNA (pDNA). Electroporation consists on applying a pulsed electrical field to open hydrophilic pores in the cell membrane thereby enabling the delivery of nucleic acids directly to the cytosol. When DNA is delivered by electroporation either intramuscularly or intradermally, antigen expression and humoral and cellular-mediated immune responses are induced. In a study conducted by Geall et al., electroporated DNA induced antigen expression over a longer period of time compared to a SAM delivered by lipid nanoparticles. However, both systems elicited similar levels of IgG titres, suggesting that there are other factors that have an impact on the immunogenicity (Geall et al., 2012).

Particle-mediated epidermal delivery (PMED), commonly known as gene gun is another efficient physical method to deliver nucleic acids. Nucleic acids are adsorbed on gold/tungsten microparticles, loaded on cartridges and then delivered by the gene gun device at high pressure directly to the cells. As for electroporation, PMED delivery of DNA has been extensively reported in the literature. Although efficient PMED-based SAM delivery has been demonstrated, lipid-based delivery systems such as lipid nanoparticles (LNPs) elicit more potent immune responses.

1.4.2.2. Lipid nanoparticles

1.4.2.2.1. General attributes of lipid nanoparticles

Liposomes, and more recently denoted as lipid nanoparticles (LNPs), generally consist on vesicles composed of single or multiple concentric bilayers enclosing an aqueous core. Although there are other lipid-based delivery systems such as solid-lipid nanoparticles (SLNs) and emulsions, they will not be regarded as LNPs in this thesis. Since they were first described by Bangham in 1964 (Bangham and Horne, 1964) and their potential as drug delivery systems was demonstrated by Gregoriadis et al. (Gregoriadis et al., 1971), LNPs have become a hot topic in research (mathematics, theoretical physics, biophysics, chemistry, colloid science, biochemistry, biology) (Akbarzadeh et al., 2013), food industry (Mozafari et al., 2008) and clinical applications (Immordino et al., 2006; Weiner et al., 1994). LNPs are composed of phospholipids, amphiphilic molecules with a hydrophilic head group and two aliphatic hydrophobic chains (10 – 18 carbon length) which are usually linked by a glycerol backbone. When dispersed in aqueous solutions, at a concentration above a threshold level known as the critical micelle concentration (CMC), they self-assemble in a reversible and thermodynamically favourable process (Lasic, 1993), enhanced by hydrogen bonding and electrostatic interactions of polar heads with water molecules, as well as hydrophobic and Van der Waals forces among hydrocarbon tails (Israelachvili et al., 1980).

Phospholipids with acyl chains of up to 16 carbons are saturated, while 18-carbon chains can have from one to three unsaturated cis-double bonds. Both the length of acyl chain and degree of unsaturation determine the phase transition temperature (T_M) of the phospholipids. T_M is defined as the temperature required to induce a change in the physical phase of the lipid from ordered gel phase, where the hydrocarbon chains are fully extended and packed, to the

disordered liquid crystalline phase, where the hydrocarbon chains are randomly oriented and fluid. Thus, the longer the acyl chain and/or lower the degree of unsaturation, the higher the T_M will be. As the fluid state of lipids is more permeable to water and, it can be exploited to encapsulate drugs during liposome production.

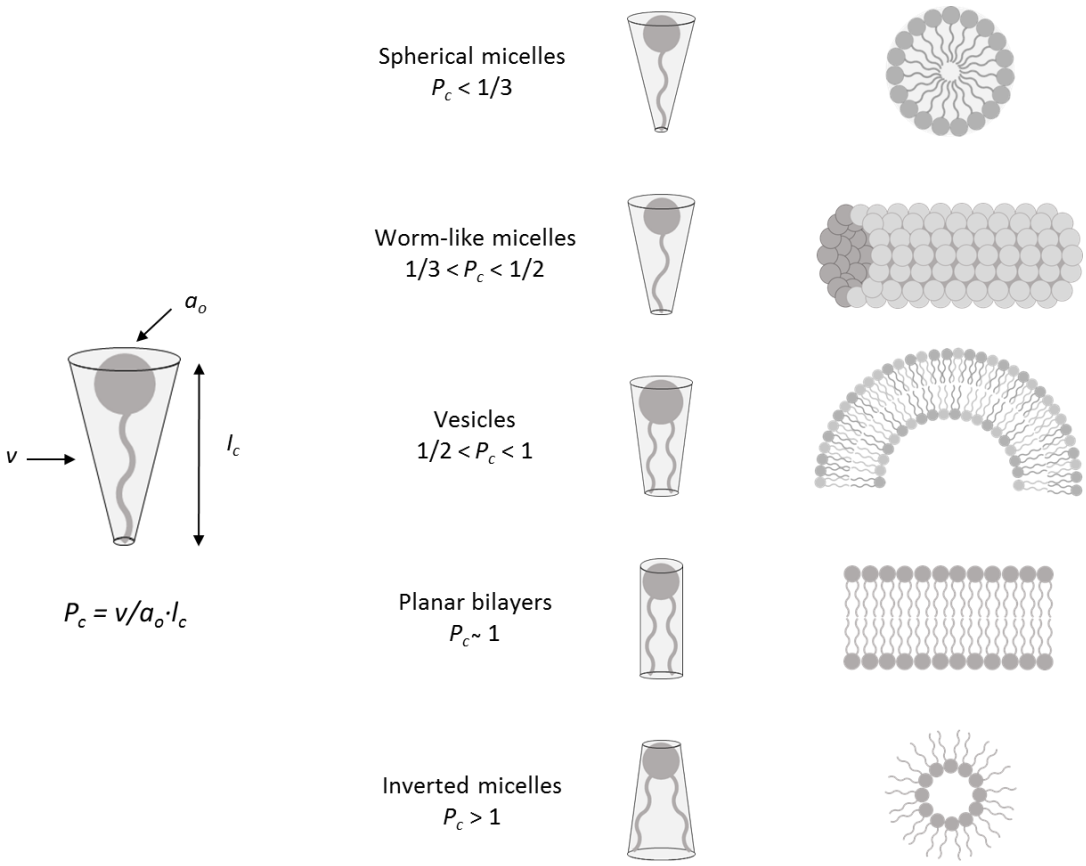

Figure 1.4. Lipid structures predicted by the critical packing parameter (P_c).

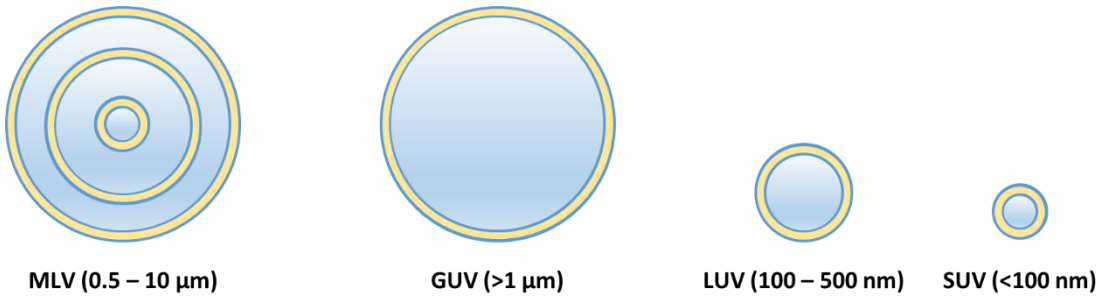

Figure 1.5. Schematic representation of LNPs and different structures they can adopt.

Self-aggregation of polar lipids is not limited to conventional bilayer structures. As first described by Israelachvili (Israelachvili et al., 1980), the geometry in which lipids self-assemble is given by their critical packing parameter (P_C) and therefore it can be predicted. P_C is defined as $v/a_o \cdot l_c$, where a_o is the effective area of the headgroup, l_c is the length of the alkyl chain and v is the alky chain volume (Israelachvili, 1992). For $P_C \leq 1$, lamellar (L_α) phases are formed, including spherical micelles ($P_C < 0.3$), worm-like micelles ($P_C = 1/3 – 1/2$), vesicles ($P_C = 1/2 – 1$) and planar bilayers ($P_C \sim 1$). For $P_C > 1$, inverted hexagonal (H_{II}) and cubic phases (Q_{II}) appear (Fig. 1.4).

From a morphological perspective, LNPs can be classified in multilamellar (MLVs) and unilamellar vesicles (ULVs). MLVs are typically large (0.5 – 10 µm) and exhibit an onion-like structure in which unilamellar vesicles enclose others of smaller size, thereby giving rise to a multilamellar structure of concentric spheres separated by layers of aqueous solvent. ULVs are divided in small (SUV, < 100 nm), large (LUV, 100 – 500 nm) and giant (GUV, > 1 µm) (Fig. 1.5). The size of LNPs for medical applications range from 50 to 200 nm (Etheridge et al., 2013). Both size and degree of lamellarity affect the encapsulation efficiency of drugs and their release profile. For instance, unilamellar LNPs of 130 nm showed much faster release kinetics than MLVs of 250 nm (Betageri and Parsons, 1992).

Ambisome, an amphotericin B-encapsulated liposomal formulation for the treatment of fungal infections, was the first liposomal drug product to be approved. Since then, other liposomal drug products have been approved. For instance, Doxil (doxorubicin-loaded liposomes) was approved by the Food and Drug Administration (FDA) of the United States of America (USA) in 1995 for the treatment of refractory acquired immune deficiency syndrome (AIDS)-related Kaposi's sarcomas (Allen and Cullis, 2013).

Cationic lipids can electrostatically interact with negatively charged nucleic acids, to form DNA-lipid complexes named lipoplexes. The use of cationic lipids to deliver nucleic acids was first described over 3 decades ago, when Felgner et al. demonstrated that the transfection efficiency of a DNA could be enhanced up to 100-fold when delivered by cationic lipid nanoparticles (cLNPs) based on the cationic lipid DOTMA (Felgner et al., 1987). Owing the effectivity of cationic lipids to deliver nucleic acids, a wide range of synthetic cationic lipids (DOTAP, DDA, DC-Chol, DODAC, etc.) and lipofection reagents (e.g. Lipofectamine) were developed in the following years.

Cationic LNPs allow to protect mRNA from RNase degradation, to delay mRNA clearance upon injection (depot effect) and to facilitate their delivery to host cells (Fig. 1.6). Encapsulation or surface adsorption of SAM on DOTAP and DDA-based cLNPs has been shown to prevent degradation against RNase challenge (Blakney et al., 2019b). Cellular internalisation of cLNPs occurs mainly through clathrin-dependent and caveolae-dependent endocytosis. To avoid degradation of mRNA in the endo-lysosomal compartments, cLNPs can be designed to promote endosomal escape and mRNA release into the cytosol where it can exert its therapeutic effect (gene silencing, antigen expression, etc.). This is achieved by the incorporation of pH-sensitive lipids (e.g. DOPE) with the ability to fuse with the endosomal membranes at mildly acidic pH (5.5-6.5) and to induce endosomal escape. DOPE is a cone-shaped lipid with an ethanolamine head group that undergoes a lamellar-to-hexagonal ($L\alpha$-H_{II}) phase transition at acidic pH thereby destabilising the endosomal membrane (Farhood et al., 1995; Mochizuki et al., 2013) consequently increasing the transfection efficiency (Kim et al., 2015; Zhang et al., 2010). The ratio between cationic lipid and helper lipid has shown to have a great impact on the capacity of cLNPs to transfect cells (Kim et al., 2015). In general, cLNPs are formulated at a molar ratio of 1:1 (cationic:helper lipid). Enhanced potency of cLNPs can also be achieved by the incorporation of cholesterol. Cholesterol reduces the transition temperature and facilitates lamellar-to-hexagonal phase transition in the endosomal compartment thus improving the transfection efficiency. At the same time, cholesterol confers improved stability *in vivo* (Pozzi et al., 2012).

Achieving efficient endosomal escape and cargo release is likely the hallmark in RNA delivery. The therapeutic dose highly determines the use of therapeutic mRNA in humans. Continued efforts at screening novel lipids and formulations have led to the development of efficient novel lipid-based delivery systems. Among them, the so-called stable nucleic acid lipid nanoparticles

(SNALPs), also known as ionisable lipid nanoparticles (iLNPs), represent the most effective nonviral delivery system to date (Cullis and Hope, 2017). iLNPs were originally designed to deliver small interfering RNA (siRNA) intravenously to knockdown hepatocytes. However, iLNPs are also very effective in delivering mRNA (Richner et al., 2017) and SAM vaccines (Hekele et al., 2013). As for cLNPs, iLNPs confer full protection against RNase challenge (Geall et al., 2012).

iLNPs are composed of a cationic-ionisable lipid, a PEGylated lipid, DSPC and cholesterol. The headgroup of the ionisable lipid contains a tertiary amine with a pKa<7 which allows to efficiently enclose nucleic acids at pH<pKa and to maintain a low surface charge density at physiological pH. In the acidic environment of endosomes, ionisable lipids become positively charged and interact with the negatively charged lipids of the endosomal membranes leading to the formation of ion pairs, the adoption of a hexagonal H_{II} phase and eventually the fusion and membrane disruption (Semple et al., 2010). The pKa of the ionisable lipid is the most important parameter affecting the potency of iLNPs. This correlation was confirmed in a the murine FVII model by mixing ionisable lipids with different apparent pKa values to achieve net pKa values ranging from 5.5 to 6.9 as to find that optimal LNP activity was achieved with a pKa of 6.44 (Cullis and Hope, 2017). Remarkably, the initial effective dose 50 (ED50) achieved with first generation iLNPs, based on DLinDAP, was 40-50 mg/kg, while the ED50 of iLNPs containing DLin-MC3-DMA (commonly known as MC3) was as low as 0.005 mg/kg. Hasset et al. conducted a systematic study with a panel of 30 ionisable lipids to deliver a mRNA vaccine intramuscularly as to find that optimal pKa for intramuscular delivery of mRNA was 6.6-6.8 (Hassett et al., 2019).

SNALPs are prepared by bottom-up approaches (e.g. microfluidics) where the rapid mixing conditions allow the particles to enclose the nucleic acid as they self-assemble. The incorporation of a PEGylated confers improved stability. More importantly, it avoids uncontrolled growth of lipid particles and aggregation during the production process. Because the PEGylated lipid can only be incorporated on the LNP surface, it dictates the size of LNPs. Indeed, higher content of PEG-lipid imposes higher surface-to-volume ratios and consequently smaller LNPs to be formed. For instance, increasing the percentage of PEGylated lipid from 0.25% to 5% gradually reduced the size of siRNA-iLNPs from 120 to 25 nm (Belliveau et al., 2012). In another study, non-PEGylated SAM-LNPs had a size of over 500, while incorporation of 2% PEG-lipid resulted in LNPs of 130 nm (Goswami et al., 2019).

PEG moieties also create a steric barrier to plasma opsonins thus inhibiting recognition and clearance by the mononuclear phagocytic system (MPS). The potency of LNPs is highly dependent on the type of PEGylated lipid. Indeed, PEG-lipids have been widely reported to transfer from lipid vesicles in a process known as de-PEGylation. Therefore, longer acyl chains are expected to provide stronger hydrophobic interactions within the lipid conformer and slower transfer rates. The use of PEGylated lipids with long acyl chains (PEG-C18) limits the ability of LNPs to interact with endosomal membranes and therefore results in reduced endosomal escape compared to PEGylated lipids having shorter acyl chains (PEG-C14), termed diffusive PEGylated lipids (Pozzi et al., 2014). The type of PEGylated lipid also dictates the desorption rate and the pharmacokinetics of iLNPs following intravenous administration. For instance, MC3-iLNPs containing 1.5% (mole %) of either PEG-C14, PEG-C16 or PEG-C18 had blood half-lives of approximately 0.6, 2.2 and 4.0 hours. Conversely, PEG-C14 LNPs accumulated in a greater extent in the liver and consequently allowed higher knock down activity (Mui et al., 2013).

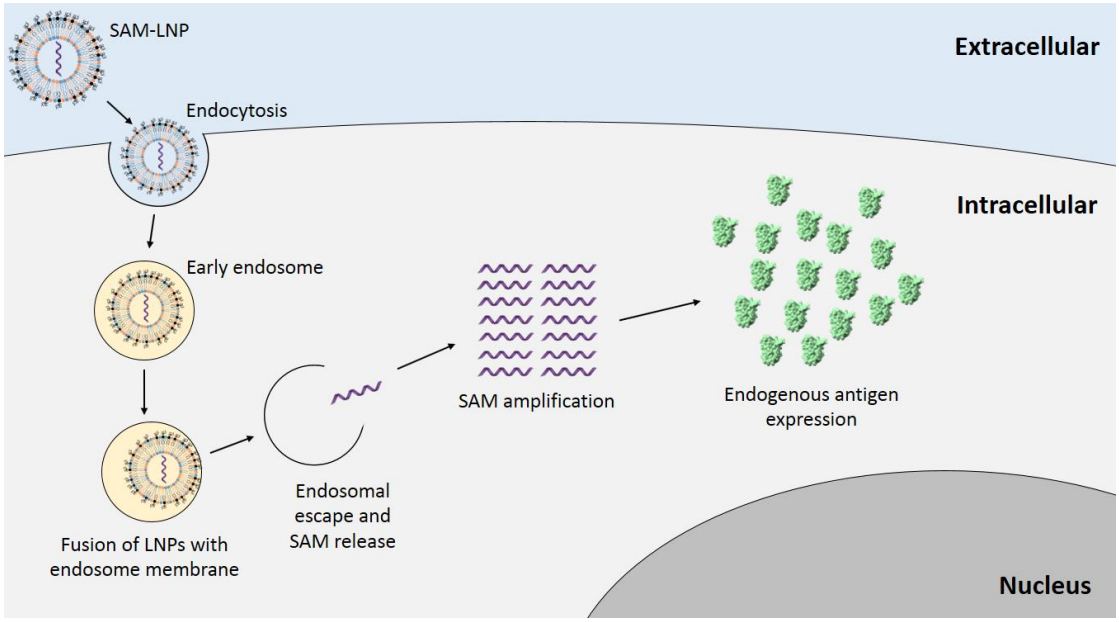

Figure 1.6. Possible mechanism of action of SAM-LNPs.

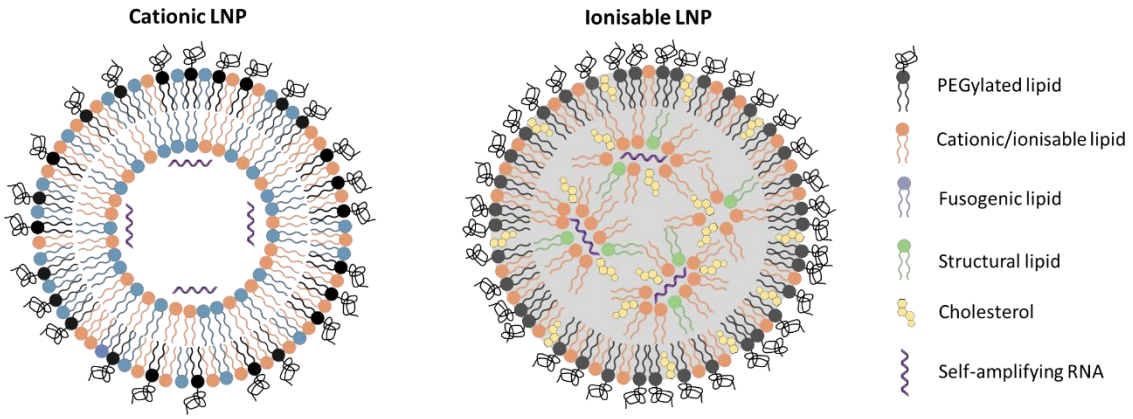

Figure 1.7. Schematic representation of cationic LNPs and ionisable LNPs enclosing a self-amplifying RNA.

Finally, DSPC and cholesterol confer integrity and improve the stability of the particles *in vivo*. For instance, cholesterol has been shown to inhibit the transfer of phospholipids from the lipid bilayer to high-density lipoprotein (HDL) and low-density lipoprotein (LDL) (Esnault-Dupuy et al., 1987). Optimised iLNPs are composed of DSPC, cholesterol, MC3 and the diffusible DMG-PEG2000 (PEG-C14), usually at a molar ratio of 10:48:40:2. This MC3-iLNP formulation was tested in humans to deliver a therapeutic siRNA (Patisiran) for the treatment of hereditary transthyretin-mediated amyloidosis (hATTR). This siRNA-iLNP drug product (trademark Onpattro, owned by Alnylam Pharmaceuticals) was approved by the FDA in 2018 and became the first siRNA-based drug product to be licenced. To date, MC3-iLNPs are the gold standard in LNP-facilitated RNA delivery.

iLNPs display a characteristic electron-dense core structure whereby the RNA is packed by inverted micelles mainly composed of the ionisable lipid. In contrast, cLNPs tend to display bilayer-like structures (Kulkarni et al., 2018b) (Fig. 1.7). On the other hand, cellular internalisation of iLNPs occurs in an apolipoprotein E (ApoE)-dependent manner by the low-density lipoprotein (LDL) receptor (LDLR) through a clathrin-mediated endocytosis process, while cLNPs can directly associate with cells due to their cationic nature at physiological pH. Indeed, the activity of iLNPs to knock down hepatocytes was almost abolished in apoE -/- and LDLR -/- knockout mouse models (Akinc et al., 2010).

1.4.2.2.2. Adjuvant properties of lipid nanoparticles: the importance of physicochemical attributes

Adjuvants are molecules, compounds or macromolecular complexes that boost the potency and longevity of antigen-specific immune responses. Alum salts were the first compounds reported to enhance the immune response of vaccines when administered with killed or attenuated pathogens. Adjuvants are mainly divided in immunostimulants and delivery systems. Immunostimulants boost the immune responses by inducing activation and maturation of APCs, by up-regulating the production of cytokines and chemokines and activation of inflammasomes. Cationic/ionisable lipids engage and activate TLR-4 and enhance the expression of MHC and the co-stimulatory molecules CD80 and CD86 in APCs thus leading to activation, antigen presentation and cytokine release. The adjuvant properties of cationic lipids are tightly related to their physicochemical properties. For instance, Vangasseri et al. reported that cationic lipids having quaternary amine head groups stimulated the expression of CD80 and CD86 in dendritic cells in a greater extent than those having tertiary amine head groups. Similarly, unsaturated cationic lipids were more potent than their saturated counterparts (Vangasseri et al., 2006).

Delivery systems potentiate the immune responses by enhancing cellular uptake and the formation of a depot at the injection site. Because cationic/ionisable lipids can stimulate the innate immune system, cLNPs and iLNPs benefit from both mechanisms. Again, the capacity of LNPs to induce these effects is heavily dependent on their physicochemical properties, including surface charge (Henriksen-Lacey et al., 2010c), size (Allen and Everest, 1983; Brewer et al., 1998), hydrophobicity/hydrophilicity (Kaur et al., 2012b) and lamellarity (Betageri and Parsons, 1992). For example, a relationship between *in vitro* cellular uptake and liposome surface charge was shown, with charged (anionic and cationic) liposome being better internalised than neutral ones (Epstein-Barash et al., 2010; Johnstone et al., 2001). Additionally, increasing percentages of charged lipid within the formulation enhances cellular uptake (Dabbas et al., 2008; Takano et al., 2003).

The injection of cLNPs and iLNPs induces a broad but transient influx of immune cells including neutrophils and innate immune cells such as monocytes and skin-resident dendritic cells (Henriksen-Lacey et al., 2010b; Lutz et al., 2017), which are relevant to mount adaptive immune responses. The intramuscular injection of a LNP-formulated unmodified mRNA encoding the

rabies virus glycoprotein induced the up-regulation of the chemokines MCP-1, MIP-1α, MIP-1β, CXCL-1 and CXCL-9, which are pivotal in the recruitment of immune cells. In addition, a pronounced but transient release of the pro-inflammatory cytokines TNF and IL-6 at the injection site and draining lymph nodes was elicited. In contrast, only low concentrations of cytokines and chemokines where detected for non-formulated mRNA. Moreover, this LNP-formulated mRNA vaccine resulted in a 10-fold increase in the number of monocytes found in the draining lymph nodes compared to the non-formulated mRNA (Lutz et al., 2017). The intramuscular injection of mRNA-iLNP vaccines has also been reported to promote the influx of neutrophils and dendritic cells (Liang et al., 2017). The infiltration of immune cells to the injection site and trafficking to the local lymph nodes has been also been reported crucial for the mechanism of action of other lipid-based vaccine adjuvants such as MF59 (Calabro et al., 2011).

cLNPs and iLNPs aggregate in presence of proteins from the extracellular matrix found at the injection site leading to the formation of a depot. The two most important parameters that influence the pharmacokinetics of LNPs (clearance from the injection site and accumulation in the lymph nodes) are size and surface charge. For instance, cLNPs are retained longer at the injection site compared to neutral formulations when administered intramuscularly (Henriksen-Lacey et al., 2011b; Kaur et al., 2012a) or subcutaneously (Carstens et al., 2011; Henriksen-Lacey et al., 2010c). These electrostatic interactions at the injection site can be avoided by masking the cationic nature of the liposomes via PEGylation. In the case of liposomes composed of dimethyldioctadecylammonium bromide (DDA) and trehalose 6,6'-dibehenate (TDB) incorporation of 25 mole% PEG was required to block the depot effect and promote drainage to the local lymph node irrespective of the size of the liposomes (120 nm up to 500 nm) (Kaur et al., 2012a) and resulted in different immune response profiles to a subunit antigen (Kaur et al., 2012b).

LNP size has been shown to play a major role in the intracellular trafficking, processing and presentation of antigens by antigen presenting cells (Brewer et al., 2004) and to polarize the type of immune responses. For instance, in a study conducted by Brewer et al., LNPs above 225 nm generated IgG2a titers and high production of IFN-γ, characteristic pattern of a Th1 response. In contrast, smaller LNPs (<155 nm) induced a Th2 response, as evidenced by production of IgG1 and IL-5 (Brewer et al., 1998). However, improved accumulation in the lymphatics does not

necessarily translate into more potent immune responses. Roces et al. recently explored the use biotinylated DDA:TDB liposomes in avidin-pretreated mice to increase the retention of antigen in the local lymph nodes. Despite this strategy allowed to accumulate significantly higher doses of antigen in the local lymph nodes compared to bare DDA:TDB liposomes, no enhancement in the immune responses were observed (Roces et al., 2019).

Further systematic studies conducted on the vaccine adjuvant DDA:TDB and its associated subunit antigen unveiled the influence of lipid bilayer fluidity on the *in vivo* fate of lipid-based nanoparticles. DDA:TDB liposomes display a solid-ordered phase. However, the substitution of DDA by DODAC, an unsaturated analogue of DDA, resulted in liposomes having a fluid-disorder phase. While DDA:TDB formed a strong depot at the injection site, as previously described, DODAC:TDB were drained to the local lymph nodes significantly faster, thus resulting in weaker immune responses (Christensen et al., 2012). Blakney and colleagues recently investigated the use of cationic adjuvant formulations (CAFs) based on combinations of a cationic lipid (DDA or DODAC) and a immunostimulatory molecule (TDB or MMG) to deliver a surface-adsorbed SAM vaccine intramuscularly. Although the biodistribution of these formulations was not reported, solid-phase (DDA) and fluid-phase (DODAC) CAFs induced similar levels of local antigen expression after intramuscular administration (Blakney et al., 2019a).

As they are injected in the body, LNPs are gradually cleared from the injection site by immune cells and eventually transported to the liver, where they are degraded and excreted. Accumulation of cationic lipids could potentially induce hepatic side-effects owing the cytotoxicity of cationic lipids, for instance, through the production of reactive oxygen species (ROS). Some researchers have aimed to develop biodegradable ionisable lipids while maintaining the potency. For instance, in the studies performed by Hassett et al. on the intramuscular delivery mRNA-iLNP vaccines, the amount of DLin-MC3-DMA at the injection site only decreased by 50% 24 hours post injection and was detected in the liver. In contrast, the percentage of injected dose of 5 “biodegradable LNPs” found at the injection site and liver after 24 hours was significantly lower and even undetected for 2 formulations. Despite being cleared off the injection site and inducing a weak depot effect, all 5 “biodegradable LNPs” induced significantly higher IgG titres compared to MC3-iLNPs (Hassett et al., 2019). Similarly, DOPE:DOTAP liposomes of 140 nm exhibited significantly faster clearance rates compared to 500 nm DOPE:DOTAP

liposomes but not translated in enhanced performance of a DNA vaccine after subcutaneous administration (Carstens et al., 2011). These studies suggest that, while the depot effect is beneficial for subunit vaccines it may be detrimental for nucleic acid vaccines and demonstrate the tight relationship between adjuvant pharmacokinetics and the quality of the immune response.

1.4.2.2.3. Immunogenicity of mRNA-LNP vaccines

Early investigations conducted by Gregoriadis and Perrie demonstrated that antigen-specific humoral and cellular-mediated immune responses elicited by a DNA vaccine where enhanced when delivered by cLNPs based on DOTAP (Gregoriadis et al., 2002; Perrie et al., 2001). Since then, cLNPs have been extensively explored to deliver DNA and mRNA vaccines. For instance, a mRNA encoding the HIV-1 gag protein generated strong and multifunctional $CD4^+$ and $CD8^+$ T cell responses after subcutaneous injection in mice when delivered by DOTAP-based cLNPs (Pollard et al., 2013). Recently, DDA-based cLNPs were explored to deliver a surface-adsorbed SAM vaccine encoding the major outer membrane protein (MOMP) of *Chlamydia trachomatis*. The intramuscular administration of this vaccine resulted in robust production of antibodies and IFN-γ in re-stimulated splenocytes (Blakney et al., 2019a).

As already discussed, cLNPs and iLNPs can enhance the immunogenicity to mRNA and SAM vaccines through a combination of improved protection against RNA degradation in biological media and enhanced cellular uptake in target cells. Protection against RNase degradation can be achieved by encapsulating the mRNA in both cLNPs (Blakney et al., 2019b) and iLNPs (Geall et al., 2012). mRNA protection can be accomplished by electrostatic adsorption on cLNPs. Because iLNPs display neutral or low cationic surface charge, adsorption of SAM on iLNP does not confer protection. Accordingly, the ability of iLNPs to deliver surface-adsorbed SAM is reduced (Blakney et al., 2019b). The combined effect of protection and enhanced cellular uptake translates in long-lasting local antigen expression upon injection. Improved local antigen expression has been found to reflect in enhanced immunogenicity *in vivo* (Geall et al., 2012). However, in the systematic study performed by Hassett and co-workers with a panel of 30 iLNPs, only a correlation of 0.55 was found, suggesting that expression alone is insufficient to identify ideal mRNA vaccine formulations (Hassett et al., 2019).

mRNA and SAM-LNP vaccines have shown promising results in small animal models and non-human primates for a range of infectious diseases such respiratory syncytial virus, influenza, human cytomegalovirus, zika virus and rabies virus (Brito et al., 2015). Owing the versatility of mRNA and SAM-LNP platforms to elicit broad, robust, potent and long-lasting humoral and cellular-mediated immune responses to virtually any infectious disease has been reflected in several clinical trials in humans. A dose of 0.5 μg of an unmodified mRNA vaccine encoding the rabies virus glycoprotein (RVG) formulated in iLNPs elicited protective levels of neutralising antibodies (NAs) after 1 single injection when administered intramuscularly in mice, while an 80-fold higher dose of unformulated mRNA required a boost dose. The enhanced potency of iLNP-formulated mRNA was also reflected in significantly higher frequencies of multifunctional $CD4^+$ and $CD8^+$ T cells. This mRNA-iLNP vaccine candidate, developed by CureVac AG, induced long-lived humoral responses in non-human primates after a prime-boost strategy with a mRNA dose as low as 1 μg. Moreover, a third dose given 5 months after complete vaccination further enhanced the production of virus NAs 10-fold, thus demonstrating the existence of B cell memory (Lutz et al., 2017). A phase I clinical trial is currently recruiting to explore the safety, reactogenicity and immune response in healthy adults as of September 2019 (NCT03713086). In other investigations with a mouse model, an iLNP-formulated RVG-SAM vaccine elicited significantly more potent NA titres than the commercial vaccine Rabipur 180 days after the boost dose (Brito et al., 2015).

Another mRNA-iLNP vaccine candidate to zika virus was capable of protecting mice against virus challenge. Furthermore, the mRNA vaccine was also modified to prevent the risk of sensitising individuals to re-exposure to dengue virus (Richner et al., 2017). A phase I clinical trial in humans is currently recruiting to explore the safety and immunogenicity of this mRNA-iLNP vaccine candidate (Moderna Therapeutics Inc.) in seropositive and seronegative adults as of September 2019 (NCT04064905). A LNP-formulated mRNA vaccine candidate to influenza, encoding hemagglutinin (HA) protein of N7N9 or H10N8 (Moderna Therapeutics Inc.) also generated rapid and robust immune responses in mice, ferrets and non-human primates. Indeed, a single dose of mRNA-LNP vaccine protected mice from lethal challenge and reduced lung viral titres in ferrets. Moreover, vaccination resulted in high levels of seroconversion in humans with

acceptable tolerability profiles (Bahl et al., 2017). This vaccine candidate is currently being investigated in a phase I study in humans (NCT03345043).

1.4.2.3. Nanoemulsions

Emulsions are colloidal lipid-based formulations which, contrary to LNPs, display a dense oily core. The emulsion vaccine adjuvant MF59, composed of squalene tween and span, was the first-ever approved emulsion adjuvant for human (Fluad vaccine). Owing the excellent safety profile of MF59, other emulsion adjuvants have been approved since then (e.g. Prepandrix, Aflunov). A MF59-like cationic nanoemulsion (CNE), composed of squalene, tween, span and DOTAP, was used to deliver SAM vaccines. The electrostatic surface adsorption of SAM onto the CNE allows to protect the nucleic acid against RNase challenge. A clear advantage of using CNE is the possibility of manufacturing and storing CNE separately, so that SAM-CNE complexation can be performed immediately before use. This DOTAP-based CNE, designed and developed by GSK Biologicals, have been demonstrated to be effective in delivering SAM vaccines in mice, rats, rabbis and non-human primates for various infectious diseases including respiratory syncytial virus, cytomegalovirus, HIV and rabies (Brito et al., 2014). The intramuscular injection of 1.5 µg of a CNE-formulated RVG-SAM vaccine in a prime-boost strategy, elicited protective levels of NAs for a period of 5 months. This RVG-SAM CNE vaccine candidate to rabies is currently being investigated in a phase I clinical trial in humans (NCT04062669).

1.4.2.2.4. Routes of administration

The route of administration can highly influence the quality of the immune responses. Intramuscular (IM) injection is the most practiced route of administration for most vaccines. IM injection of mRNA-LNP vaccines effectively induces Th1 type immune responses and cell-mediated immune responses (Brito et al., 2015; Geall et al., 2012; Hassett et al., 2019; Lutz et al., 2017; Richner et al., 2017). The skin is densely populated with Langerhans cells in the epidermis and dendritic cells in the dermis. Considering that dendritic cells are pivotal in the mechanism of action of mRNA vaccines, intradermal (ID) injection is an attractive route of administration for mRNA and SAM vaccines to directly target dendritic cells. Dendritic cells express a wide variety of surface receptors like the mannose receptor, DC-SIGN, DEC-205 and Langerin such that

mannose glycans could potentially be used for dendritic cell targeting. However, the binding affinity of these saccharides is very weak and high percentages of glycosylation are required to efficiently target dendritic cells. For instance, 11 mole% of mannosylated lipids was required to see a targeting effect (Reichmuth et al., 2016). In a recent study, mannosylated iLNPs (15 mole% mannose-lipid) exhibited enhanced immunogenicity for a SAM vaccine to influenza compared to bare iLNPs both after intramuscular and intradermal administration (Goswami et al., 2019). The targeting efficiency could be enhanced by decorating LNPs with multivalent targeting ligands such by means of scaffolds or multibranched saccharides.

The subcutaneous (SC) injection of mRNA-LNP vaccines has also been demonstrated to elicit antigen-specific immune responses (Pollard et al., 2013). This route would offer the possibility of transfecting plasmacytoid dendritic cells, a subpopulation naturally occurring in the local lymph nodes. Intravenous (IV) administration of mRNA-LNP vaccines has been less explored, as it can potentially lead to uncontrolled production of cytokines ("cytokine storm") leading to shock and death. In addition, LNPs could be accumulated in the lungs thereby inducing inflammation and tissue damage (Reichmuth et al., 2016).

Some studies have aimed to investigate the influence of the route of administration on the local antigen expression induced by mRNA-LNPs. For instance, Pardi et al. quantified the local antigen expression of a iLNP-formulated mRNA encoding firefly luciferase after IM, ID, SC and IV injection in mice. The duration of antigen expression in mice was ranked as ID > IM > SC > IV (Pardi et al., 2015). Opposing observations have been reported with respect to the immunogenicity of mRNA-LNP vaccines upon injection by these routes of administration. 100% of mice responded to an iLNP formulated HIV-gp140 SAM vaccine two weeks after IM immunization, while only 40% responded when the same vaccine was given ID. 2 weeks after the boost dose, IM vaccination resulted in significantly higher antibody titres and frequencies of antigen-specific cytokine-producing $CD4^+$ and $CD8^+$ T cells than the ID administration. However, IM was not superior than ID (Geall et al., 2012). In contrast, Liang et al. observed a more rapid onset in the production of antibodies elicited by a mRNA-iLNP vaccine when administered ID in rhesus macaques, while no titres where observed in animals immunised IM. Two weeks after a second dose, antibody titres were significantly higher in the ID group compared to IM but similar at later time points (Liang et al., 2017).

Intranasal delivery (IN) of vaccines offers some advantages over the aforementioned routes of administrations. The mucosa is the first barrier that many pathogens must interact with in order to initiate the infection. Indeed, mucosal immunity plays a key role in preventing pathogen invasion through the secretion of IgA, the most abundant Ig isotype produced in mucosal tissues. Accordingly, intranasal delivery benefits from the induction of local immunity in the mucosal associated lymphoid tissue (MALT). B and T cells activated in mucosal tissues are able to migrate through the common mucosal immune system (CMIS), thanks to the chemokines produced in the local microenvironment via mucosal tissue-specific receptors (e.g. integrins) on vascular endothelial cells. In addition, mucosal vaccination induces systemic production of IgGs such that it can be used for protecting against pathogens which infect the host through non-mucosal tissues. Finally, because IN vaccination is a needle-free and noninvasive approach it can improve patient compliance and mitigate potential issues related to needle re-use.

Several studies have shown enhanced production of IgG and IgA after IN immunisation with LNP vaccines. For instance, a single dose of a DDA-based cLNP formulation entrapping a DNA-hsp65 vaccine (25 μg) elicited robust cellular-mediated immune responses when given IN and was significantly more potent than the IM group (Rosada et al., 2008). In other studies, mice immunised with liposomal-adjuvanted subunit antigens showed high rates of survival when challenged with pathogens such as influenza and *Mycobacterium tuberculosis*. However, other researchers have observed weaker immune responses compared to other routes of administration (Csaba et al., 2009). Only few investigations have explored the IN administration of mRNA-LNP vaccines. A mRNA vaccine complexed with nanoparticles composed of a polymer and a DOPC:DOTAP:DSG-PEG shell resulted in antigen-specific CTL responses against a lymphoma, delayed tumour onset and increased survival rates in prophylactic and therapeutic mouse models (Phua et al., 2014). To date, IN delivery of SAM-cLNPs and SAM-iLNPs has not been explored.

Tailoring the composition of LNPs for IN delivery is also crucial to elicit potent immune responses. For instance, muco-adhesive compounds, such as chitosan or polylactic acid (PLA) are used to improve the association to the epithelial tissue upon administration. The density of PEG-coating, on the other hand, can highly influence the efficiency of LNP delivery systems. High PEG density

facilitates the interaction with the tissue and results in improved mucosal immunogenicity (Csaba et al., 2009).

1.5. PREPARATION OF LIPID NANOPARTICLES

1.5.1. Bulk methods

The usefulness of LNPs for biomedical applications requires from robust and scalable techniques to produce LNPs of defined size, size distribution and lamellarity. There is a multitude of approaches to prepare LNPs, each one of which influences their size, polydispersity (Stepto, 2010), lamellarity and encapsulation efficiency of the therapeutic compounds. The most widely used bulk method (Carugo et al., 2016) for LNPs preparation is the thin lipid film hydration method, also known as the Bangham method (Bangham et al., 1965). It consists on creating a lipid thin film in a round bottom flask by evaporating the organic solvent containing the lipids, typically by evaporation, spray draying or lyophilisation. The thin lipid film is subsequently hydrated in an aqueous buffer, which may contain the nucleic acid (or the drug) to be encapsulated, and mechanically shaken for the MLVs to form (Gregoriadis et al., 1990) (Fig. 1.8). MLVs are used as lipid reservoirs in nanotube-vesicle network fabrication (Karlsson et al., 2004), though their use as drug delivery systems is hampered by their large size, heterogeneous size distribution and uncontrolled degree of lamellarity, so that size reduction techniques such as extrusion or sonication are often applied following MLV preparation.

Extrusion consists on passing the MLVs through double-stacked polycarbonate membranes of defined size with subsequently smaller pore sizes (down to 50 nm) at high pressure (Olson et al., 1979). Because lipid bilayers are disrupted and resealed as they are passed through the filters, nucleic acids are released, in such a way that encapsulation efficiency decreases along with size and lamellarity (Berger et al., 2001; Hope et al., 1985; Mui et al., 2003). For instance, the encapsulation efficiency of PC:DOPE:DOTAP cLNPs entrapping a pDNA vaccine dropped from 100% to 47% as their size was reduced from 560 nm to 140 nm (Carstens et al., 2011).

Probe sonication is a well-characterised and rapid method in which a titanium probe is used under a passive atmosphere to reduce LNP size (Papahadjopoulos and Miller, 1967). The main

disadvantages of this method are the low encapsulation efficiency, possible degradation of lipids and compounds to be encapsulated due to exposure to high and uncontrolled temperature and presence of MLVs along with SUVs (Akbarzadeh et al., 2013). Furthermore, samples may be contaminated from metal particles sheared off the probe thus requiring from their elimination upon sonication and hampering its use in sterile conditions. Bath sonication does not cause sample degradation and can be conducted in a sterile environment (Khadke et al., 2018). Although they are simple and well-established techniques, sonication and extrusion are challenging (although not impossible) techniques to scale-up (Charcosset et al., 2015). Extrusion, for instance, is used in the preparation of Doxil (doxorubicin-loaded LNPs) to reduce the size of LNPs from several hundreds of nanometres (MLVs) to 100 nm (LUVs) (Abraham et al., 2005).

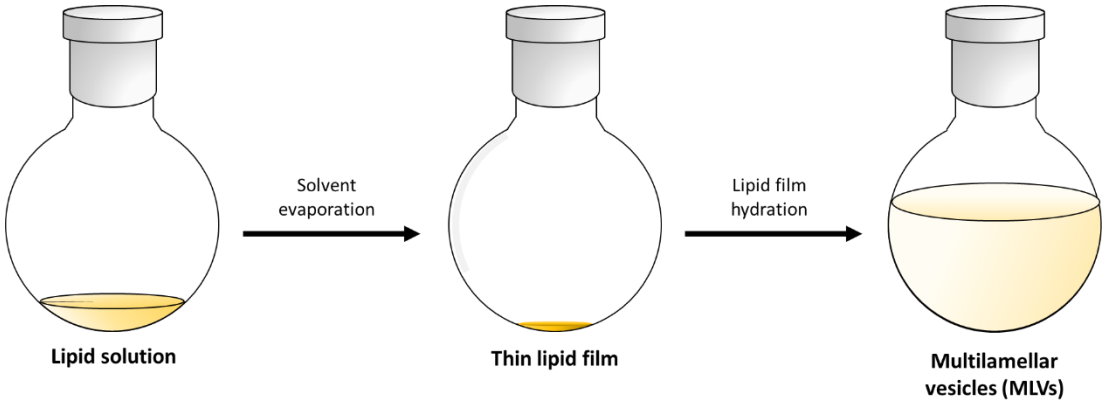

Figure 1.8. Schematic representation of the thin lipid film hydration method. An organic phase containing the lipids is removed, usually rotary evaporation, and subsequently hydrated in buffer for the MLV to form.

Microfluidization is an alternative size reduction technique that converts high fluid pressure into shear forces. In brief, the suspension of MLVs is transferred to a reservoir and pumped at high pressure through the interaction chamber, where the suspension is divided into two streams which then collide at high velocity to produce smaller vesicles (Yu et al., 1990). The main advantage of microfluidization over extrusion and sonication is that microfludizers can be designed to process from millilitres to hundreds of litres per hour and, hence, not only are suitable for lab-scale production but also for industrial applications. A microfluidizer processor from Microfluidics, for instance, is used to prepare the vaccine adjuvant MF59, a water-in-oil emulsion (Kommareddy et al., 2017). Homogenisation is another method in which the

suspension of MLVs is pressed through an orifice at high pressure and then hit against a stainless-steel wall (Bachmann et al., 1990). One homogenisation/microfluidization cycle may not be enough to reduce LNP size below 100-200 nm, so that several passes are often required (Barnadas-Rodríguez and Sabés, 2001; Özer et al., 1989). By using this size-reduction approach, DNA encapsulation efficiencies of 65-70% were obtained with PC:DOPE:DOTAP cLNPs (Pupo et al., 2005)

Other macroscale bulk methods include methods involving the use of 1) co-solvent in which lipids are soluble, 2) an additional non-bilayer forming co-amphiphile, or 3) specific ion species that influence the supramolecular aggregation of the lipids. Some of these are the reverse-phase evaporation (Cortesi, 1999; Szoka and Papahadjopoulos, 1978), ethanol injection (Batzri and Korn, 1973; Pons et al., 1993), solvent exchange (Buboltz and Feigenson, 1999), LNP electroformation (Angelova and Dimitrov, 1986) double emulsion templating (Pautot et al., 2003).

1.5.2. Microfluidic techniques

Bulk LNP production methods, relying on macroscopic mixing, often display poor batch-to-batch reproducibility. Over the past 15 years, microfluidic-based technologies, either based on bulk methods or as new technologies, have been recently developed to address these issues (van Swaay and deMello, 2013). Some of these are pulsed jetting (Stachowiak et al., 2008), double emulsion templating (Chu et al., 2007), ice droplet hydration (Sugiura et al., 2008), transient membrane ejection (Ota et al., 2009), electroformation (Kuribayashi et al., 2006), double emulsion templating (Hamada et al., 2008; Tan et al., 2006) and extrusion (Dittrich et al., 2006). LNPs produced with these techniques, reviewed elsewhere (van Swaay and deMello, 2013), are generally large (LUVs and GUVs).

Hydrodynamic flow focusing (Jahn et al., 2004) and other microfluidic mixing techniques (Ushikubo et al., 2014) based on the flash nanoprecipitation of single lipids at the nanolitre scale enable an excellent control over size and lamellarity and are regarded as the most efficient methods for producing sub-100 nm LNPs. As channel dimensions are reduced, fluid properties such as surface tension, energy dissipation or fluidic resistance, become increasingly controlled

by viscous forces rather than inertial forces, as predicted by the Reynolds number (Rapp, 2017), in such a way that the flow becomes lamellar instead of turbulent. Hence, mixing within microfluidic systems occurs through diffusion rather than through convective processes. Some advantages of microfluidics over bulk methods are the precise control physical and chemical parameters (concentration, pH, temperature, shear force, channel width, channel length, stream ratios, etc.) which ensure more uniform reaction conditions and higher grade production in single and multi-step reactions (DeMello, 2006). Furthermore, microfluidic mixing enables *in situ* monitoring of LNP production and characterisation, continuous manufacturing and scaling-up via parallelisation (Capretto et al., 2013; Jeong et al., 2016). Because diffusion is an inherently slow process, microfluidic mixers aim to enhance mixing efficiencies. These can be divided in active or passive. In active mixing schemes, diffusion mixing and, consequently mixing performance, are enhanced by applying external forces by acoustic/ultrasonic, dielectrophoretic, electro kinetic time-pulse, pressure perturbation, electro-hydrodynamic, magnetic or thermal techniques (Lee et al., 2011).

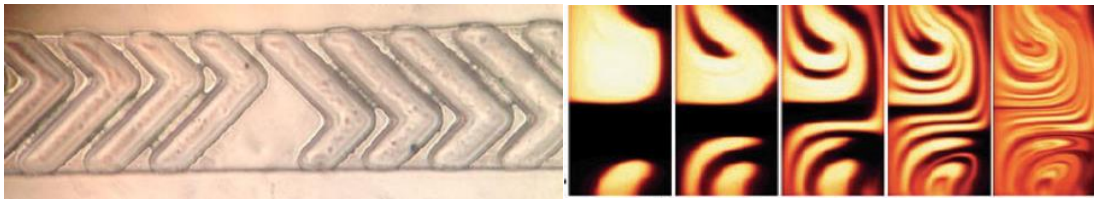

Figure 1.9. Microfluidic channel modified with grooves **(left)** designed to induce chaotic advection at low Reynolds numbers **(right)** (Stroock et al., 2002).

Passive mixers take advantage of the geometry of the channels to maximize the diffusion area, either by designing microchannel configurations where the reagents are folded multiple times or by increasing the time of contact. Contrary to active mixers, passive schemes are inefficient at generating high degrees of mixing within short times. Rapid mixing can be achieved, however, with chaotic advection by introducing obstacles within channels or by modifying channel geometries thereby enhancing stretching folding and breaking of the flow (DeMello, 2006). For instance, Stroock et al. made use of a micromixer with a pattern of grooves in the channel floor, to which they referred as staggered herringbone micromixer (SHM), to induce chaotic mixing at

Reynolds numbers up to 100 thus inducing stretching and folding of fluid thus accelerating mass transfer by increasing the interfacial area (Fig. 1.9) (Stroock et al., 2002).

Microfluidic hydrodynamic focusing (MHF), described by Jahn et al., was the first microfluidic mixing technique described for formulating LNPs (Jahn et al., 2004). In MHF, an organic phase containing phospholipids is intersected and sheathed by two streams of water phase. The alcohol stream then diffuses into the water stream as they merge. As alcohol concentration decreases below a critical level, lipids at the alcohol/water interface precipitate in intermediate structures (oblate micelles) which bend to reduce contact of the hydrophobic acyl chains of the lipids with the water phase, and eventually close into spherical vesicles (Fig 1.10) (Jahn et al., 2007).

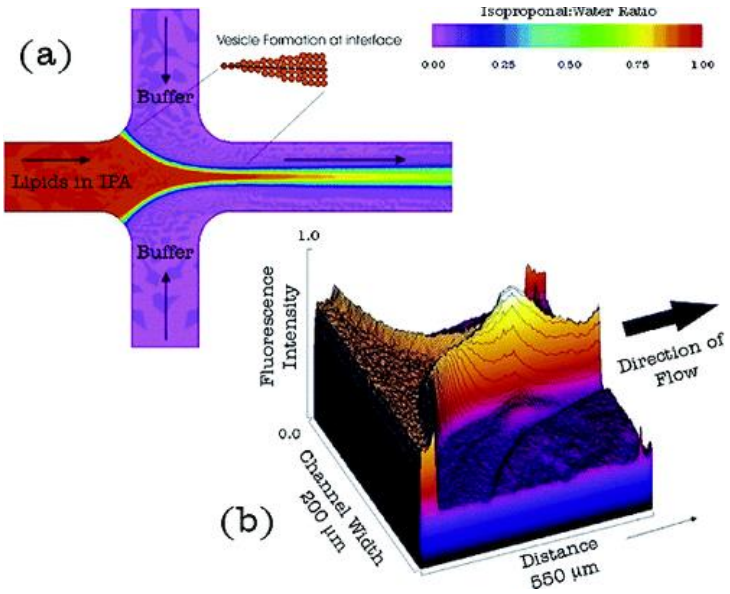

Figure 1.10. (A) LNP production by microfluidic hydrodynamic focusing (MHF). Colour contours correspond to concentration of isopropanol (IPA) and aqueous buffer. **(B)** 3D contour map of Dil-C_{18} fluorescence intensity at focused region during LNP formation (Jahn et al., 2004).

The molecular dynamics behind the self-assembly of iLNPs (also known as stable nucleic acid lipid nanoparticles [SNALPs]) differ to those of conventional LNP formulations. As the acidic aqueous buffer diffuses into the stream, the solvent polarity increases such that the ionisable lipids protonate and form inverted micelles around the nucleic acid. These inverted micelles serve as nucleating structures for the rest of the lipids to assemble into a solid core particle. Finally, the PEGylated lipid, due to its hydrophilic nature, would be the last to be recruited in the nascent

lipid conformer (Kulkarni et al., 2018a). This results in particles displaying a characteristic electron-dese core. It is important to point out that this mechanism has been described for siRNA-LNPs (Fig. 1.11) (Kulkarni et al., 2018b; Leung et al., 2012). Micromixers can also be designed with other configurations such as T-junction or Y-junction (Ushikubo et al., 2014). The principle of LNP formation, however, is based on nanoprecipitation of lipids at the nanolitre scale regardless of micromixer design. Notably, microfluidic mixing allows to directly control LNP size by adjusting parameters such as the aqueous-to-organic phase flow rate ratio (FRR), total flow rate (TFR) and phospholipid concentration (van Swaay and deMello, 2013). Indeed, a range of studies has been performed to understand how these operating parameters affect LNP attributes, especially size and size distribution.

Based on current research, FRR is one of the most important parameters to consider when formulating liposomes and LNPs by microfluidics (Forbes et al., 2019). As explained above, LNP formation is promoted by the reciprocal diffusion of organic and aqueous phase. From this point of view, the higher the aqueous:organic FRR, the more rapidly the concentration of alcohol will decrease and the less the time for lipids discs to stabilize. Therefore, smaller LNPs are expected at increasing FRR (Zook and Vreeland, 2010). Indeed, this is what was found in previous studies (Forbes et al., 2019). The same trend was observed by Jahn et al. in their studies (Jahn et al., 2010; Jahn et al., 2007). TFR has been reported to have little to no effect on liposome/LNP size (Carugo et al., 2016; Guimaraes Sa Correia et al., 2017; Joshi et al., 2016; Kastner et al., 2015). Several studies have highlighted that liposome/LNP size increases with lipid concentration (Balbino et al., 2013; Mijajlovic et al., 2013), while others have reported the opposite trend (Joshi et al., 2016).

It should be noted that the effect of these parameters on LNP size could be potentially influenced by other variables such as micromixer design (geometry, microchannel size, orientation of inlet channels) and LNP composition and, therefore, results should be carefully interpreted. MHF cartridges of 10 and 65 µm width were used by Jahn et al. to show that the combinational effect of microfluidic device geometry and hydrodynamic flow focusing had an impact on LNP size. In the 10 µm channel device, lower (half) FRR were required to obtain LNP of comparable size (Jahn et al., 2010). Similarly, Carugo et al. investigated the effect of FRR on LNP size in three microfluidic devices with significantly different design parameters (material, geometry, channel dimensions

and side channel angle). For the chip#1, LNP size dropped from 80 nm to 40 nm by increasing FRR from 10 to 50. When prepared in chip#2, LNPs were 120 nm in size regardless of the FRR. Finally, LNP size decreased from 120 nm to 80 nm when produced in the chip#3 (Carugo et al., 2016).

Remarkably, micromixer-based technologies have been used to efficiently encapsulate nucleic acids, including pDNA (Kulkarni et al., 2017), siRNA (Belliveau et al., 2012), mRNA (Hassett et al., 2019) and SAM (Geall et al., 2012). To ensure efficient packing of nucleic acids in LNPs, ratios of nitrogen (in the cationic/ionisable lipid) to phosphate (in the nucleotides/nucleosides) above 4:1 should be used. The versatility of microfluidics has been demonstrated with a wide range of therapeutic compounds, including hydrophobic drugs (Kastner et al., 2015), combinations of hydrophobic and hydrophilic drugs (Joshi et al., 2016) and proteins (Forbes et al., 2019) with, in most cases, significantly higher encapsulation efficiencies compared to bulk methods.

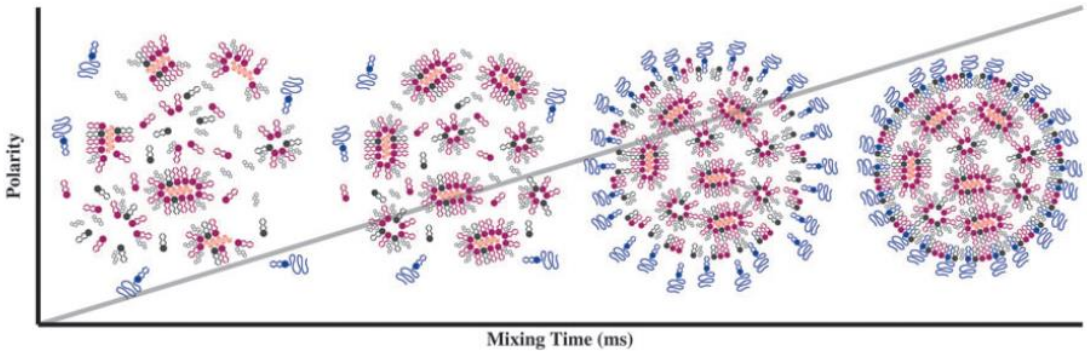

Figure 1.11. Proposed mechanism of formation of siRNA-iLNPs (Kulkarni et al., 2018a).

1.6. GENERAL AIM AND OBJECTIVES OF THE THESIS

Owing the versatility and potency of SAM vaccines, the advantages of LNPs to deliver nucleic acid-based vaccines (DNA, mRNA and SAM) and the efficiency of microfluidics to formulate monodisperse and size-tuneable LNPs enclosing nucleic acids with high degree of encapsulation, this thesis aimed to combine all these technologies to develop a SAM-LNP vaccine to Rabies. To this end, the objectives of the thesis were the following:

- To develop methods to produce LNPs and to optimize operating parameters to obtain LNPs of desired physicochemical properties (Chapter 2)
- To understand the effect of LNP attributes (e.g. composition) on cellular uptake *in vitro* and on their biodistribution pharmacokinetics *in vivo* (Chapter 3).
- To design cationic LNPs to deliver a SAM vaccine to rabies and to select most promising candidates given their physicochemical attributes (size, polydispersity and SAM encapsulation), their ability to protect SAM from degradation and their capacity to induce antigen expression *in vitro* (Chapter 4).
- To investigate the humoral and cellular-mediated immune responses of selected SAM-cLNP candidates and compare them to the commercial vaccine Rabipur (Chapter 5)
- To probe alternative routes of administration (IM, ID, IN) of a SAM-cLNP vaccine (Chapter 6)

CHAPTER 2:

DEVELOPMENT OF METHODS FOR THE FORMULATION OF LIPOSOMES

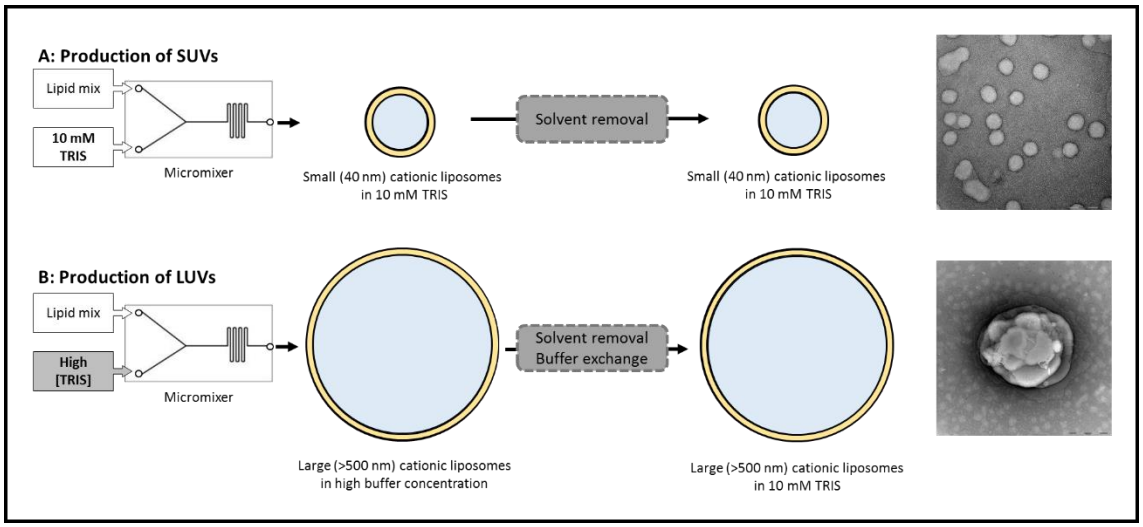

2.1. INTRODUCTION

Since they were first described in the 1960s (Bangham et al., 1965) and their potential as a drug delivery system was demonstrated in the early 1970s by Gregoriadis (Gregoriadis, 1976a, b), the liposome field has become a hot topic in research and healthcare applications, cosmetics (Weiner et al., 1994) and food industry (Mozafari et al., 2008). However, the successful use of liposomes in clinical applications relies on the development of robust and reliable manufacturing techniques. There is a multitude of methods to prepare liposomes, each one of which influences the size, size distribution and lamellarity of liposomes, as well as encapsulation efficiency of drugs or antigens. The first method to prepare liposomes was described by Bangham (Bangham et al., 1965). It consists on creating a thin lipid film that is then hydrated to form multilamellar vesicles (MLVs). Because MLVs exhibit a large size, broad size distribution and uncontrolled degree of lamellarity, they are often further processed by size-reduction techniques such as extrusion and sonication. However, liposomes prepared by extrusion or sonication exhibit poor batch-to-batch reproducibility, inconsistent encapsulation efficiency, contact of cargo with organic phases and variable size distributions. Furthermore, scale-up of extrusion and sonication processes can be challenging thereby limiting their use for industrial applications. Novel size-reduction techniques, such as high-shear homogenisation, however, allow to process large sample volumes very rapidly and therefore can be exploited in high-throughput manufacturing of liposomal drug or vaccine products.

Microfluidics is novel bottom-up liposome formulation approach that takes advantage of controlled mixing of lipids with an aqueous solvent in the microscale. More importantly, microfluidics allows to control physical (shear force, channel width, channel length) and chemical parameters (pH, temperature, concentration, total flow rate, flow rate ratio) to obtain liposomes of desired physicochemical properties (size, size distribution, surface charge). Furthermore, microfluidic production can be scaled-up in parallel thus maintaining the structure of the micromixer and, consequently, obtaining comparable results to those obtained at small scale.

2.2. AIM AND OBJECTIVES

The aim of the work covered within this chapter was to develop and optimise methods for producing liposome formulations by top-down and bottom-up approaches. To achieve this, the objectives were:

- To characterize liposomes prepared by lipid film hydration followed by size reduction in a M-110P microfluidizer (Microfluidics) (top-down) and to investigate the effect of operating parameters (temperature, pressure, number of passes) on their physicochemical properties.
- To characterise liposomes produced by microfluidics (bottom-up) and to investigate the effect of operating parameters (lipid concentration, flow rate ratio, total flow rate, buffer concentration) on their physicochemical properties.
- To establish appropriate methods for liposome sterilisation, including X-ray irradiation and filtration.
- To set up a platform for the continuous manufacturing of liposomes where formulations can be formulated, concentrated, washed and characterised in a single step.
- To validate methods for solvent and protein removal from liposome formulations

2.3. MATERIALS & METHODS

2.3.1. Materials

1,2-distearoyl-sn-glycero-3-phosphocholine (DSPC), phosphathydilcholine (PC), 1,2-dioleoyl-sn-3-phosphoethanolamine (DOPE), dimethyldioctadecylammonium (DDA), 1,2-dioleoyl-3-trimethylammonium-propane (DOTAP), 3ß-[N-(N',N'-dimethylaminoethane)-carbamoyl]cholesterol (DC-Chol), 1,2-dimyristoyl-3-trimethylammonium-propane (DMTAP), 1,2-stearoyl-3-trimethylammonium-propane (DSTAP) and phosphatidylserine (PS) were purchased from Avanti Polar Lipids. Cholesterol was purchased from Sigma. 1,1'-dioctadecyl-3,3,3',3'-tetramethylindocarbocyanine perchlorate (Dil-C_{18}) and the Pierce BCA protein assay was obtained from Thermo Scientific. Ovalbumin (OVA) was purchased from Calbiochem. 750 KDa modified polyethersulfone (mPES) membranes were obtained from Lab Spectrum.

2.3.2. Top-down formulation of liposomes

Lipid solutions (10 mg/mL) of PC:Chol and DSPC:Chol (1:1 molar ratio) were prepared in a chloroform:methanol solution (9:1 v/v). The organic solvent was subsequently removed by rotary-evaporation (200 rpm, 15 min). The resulting PC:Chol and DSPC:Chol thin films were then hydrated in phosphate-buffered saline (PBS) at a 60 ˚C and vigorously vortexed for the multilamellar vesicles (MLVs) to form. Liposomes were diluted to a final volume of 50 mL (0.5 mg/mL) before size reduction. Finally, MLVs were processed by the high-shear M-100P microfluidiser (Microfluidics, Corp, Westwood, MA) for up to 5 cycles at a pressure ranging from 20 to 30 KPSI.

2.3.4. Bottom-up formulation of liposomes by microfluidics

Liposomes were prepared in the Nanoassemblr Platform (Precision Nanosystems Inc.) in a Y-shaped staggered herringbone micromixer of 300 µm width and 130 µm height. Briefly, lipid mixtures in methanol and an aqueous phase (PBS or TRIS buffer pH 7.4) were injected simultaneously in the micromixer. Initial lipid concentration ranged from 0.25 to 10 mg/mL, the aqueous:organic flow rate ratio (FRR) was varied from 1:1 to 5:1 and total flow rate (TFR) was modified from 5 to 20 mL/min to obtain optimal formulations. In addition, TRIS buffer concentration was varied from 10 to 1000 mM to prepare size-tuneable liposomes. Newly formed liposomes (1 mL) were then dialysed against 10 mM TRIS pH 7.4 (200 mL) for 1 hour under magnetic stirring.

2.3.5. Tangential flow filtration (TFF)

Methanol traces of some liposome formulations were removed in a KR2i TFF (Lab spectrum) in a modified polyethersulfone (mPES) column of 750 KDa (40 nm) pore size. In brief, liposome sample was recirculated for 1 min and then TFF was run at 27 mL/min ($3000s^{-1}$ shear). TFF was also used to remove protein from liposome formulations. In brief, OVA (0.125 – 0.9 mg/mL) was added to 2 mL of DSPC:Chol liposomes (1 mg/mL). Liposomes (2 mL) were then washed with PBS (24 mL) and aliquots (1 mL) were collected in the permeate. Finally, concentration of OVA was quantified by Pierce BCA assay at 562 nm wavelength in a SpectroMax190 (Molecular Devices).

2.3.6. Liposome characterisation

All formulations were characterised after solvent removal in terms of hydrodynamic size (Z-average), polydispersity index (PDI) and surface charge (zeta-potential) by dynamic light scattering (DLS) in a Zetasizer Nano ZS (Malvern, UK) at 25 ˚C. Liposomes were diluted 1:10. Some formulations were also sized on-line right in a Malvern's Zetasizer AT at 0.5 mL/min flow rate.

2.3.7. Lipid recovery

To determine lipid recovery, liposomes were co-formulated with the fluorescent dye DiI-C_{18} (0.2 mole %). Fluorescence was measured at 490 nm in a POLARStar OMEGA fluorimeter (BMG Labtech).

2.3.8. Negative staining transmission electron microscopy (NS-EM)

5 µL of liposome samples (200 µg/mL) were deposited onto a glow discharged copper 300-square mesh grid. After 30 seconds, excess of samples was blotted and the grid was negatively stained with a NanoW for 30 second. Samples were observed in a Tecnai G2 Spirit and images were acquired in a Veleta CCD.

2.3.9. Cryogenic transmission Electron microscopy (cryo-TEM)

Liposome samples (3 µL) were deposited on a pre-cleaned lacey carbon-coated grid and flashed frozen by plunging into liquid ethane cooled by liquid nitrogen. Samples were then observed in a cryo-holder in electron microscope Tecnai 12 G2 (FEI, Eindhoven) at liquid nitrogen temperature and 80 KV with magnifications ranging from 40,000X to 135,000X.

2.3.10. Liposome sterilisation

The effect of sterilisation over the physicochemical attributes of liposomes was studied. Sterilisation by X-ray radiation was carried out for 10 min at 10 Gy in a X-RAD 225 Biological Irradiator (Precision X-Ray). Liposomes were also sterilised by filtration (0.22 µm). In brief, liposomes (1 mL) were passed through Millipore filters of different nature, including polyethersulfone (PES), polyvinylidene Fluoride (PVDF) and mixed cellulose ester (MCE). Liposomes were also filtered through Fisherbrand PES filters.

2.4. RESULTS & DISCUSSION

2.4.1. Top-down formulation of liposomes

The transition temperature of a lipid (T_M) is defined as the temperature required to induce a change in the physical phase of the lipid from ordered gel phase, where the hydrocarbon chains are fully extended and packed, to the disordered liquid crystalline phase, where the hydrocarbon chains are randomly oriented and fluid. Incorporation of cholesterol increases the fluidity of high transition temperature phospholipid bilayers and, consequently, reduces the overall T_M (Liu et al., 2000). So as to determine whether working above the T_M was a prerequisite to obtain small unilamellar liposomes (SUVs) from multilamellar vesicles (MLVs) in a microfluidizer M-110P, liposomes composed of cholesterol (Chol) and phosphatidylcholine (PC), whose T_M is close to zero, or 1,2-distearoyl-sn-glycero-3-phosphocholine (DSPC; T_M of 55°C) were used.

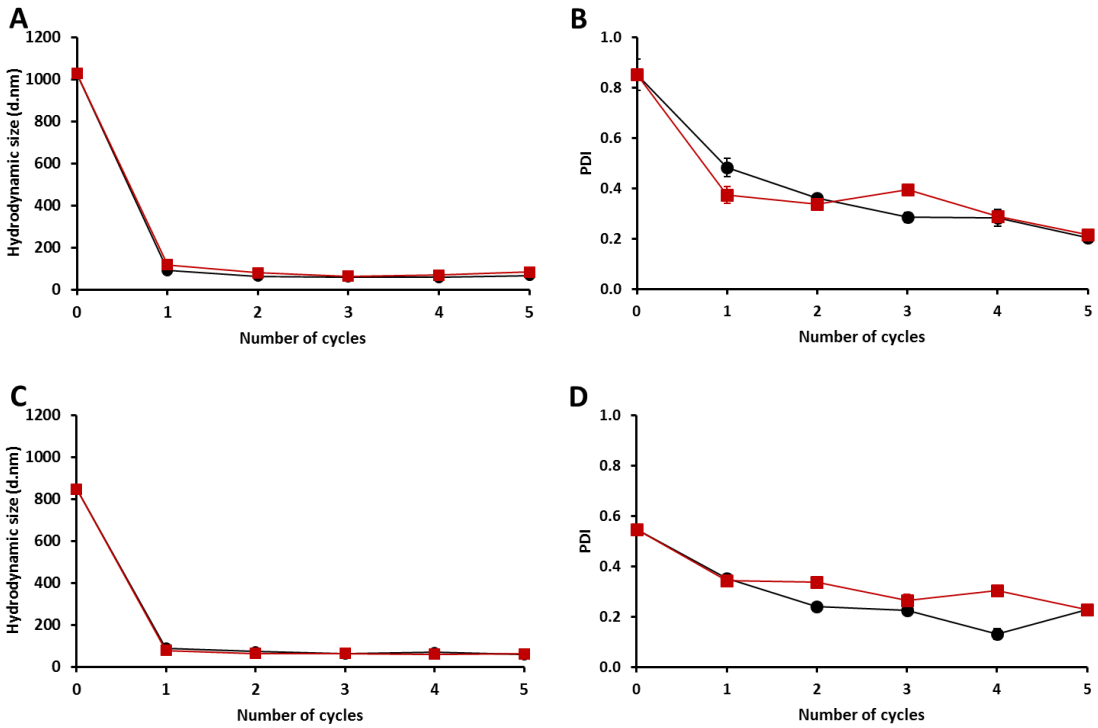

Figure 2.1. The effect of working temperature on liposomes processed by the M-110P microfluidizer. Hydrodynamic size **(A, C)** and PDI **(B, D)** of PD:Chol **(A, B)** and DSPC:Chol liposomes **(C, D)** prepared below (●) and above (■) transition temperature (T_M) of the phospholipid (0 and 55 °C for PC and DSPC respectively). Results are represented as mean ± SD of three consecutive measurements.

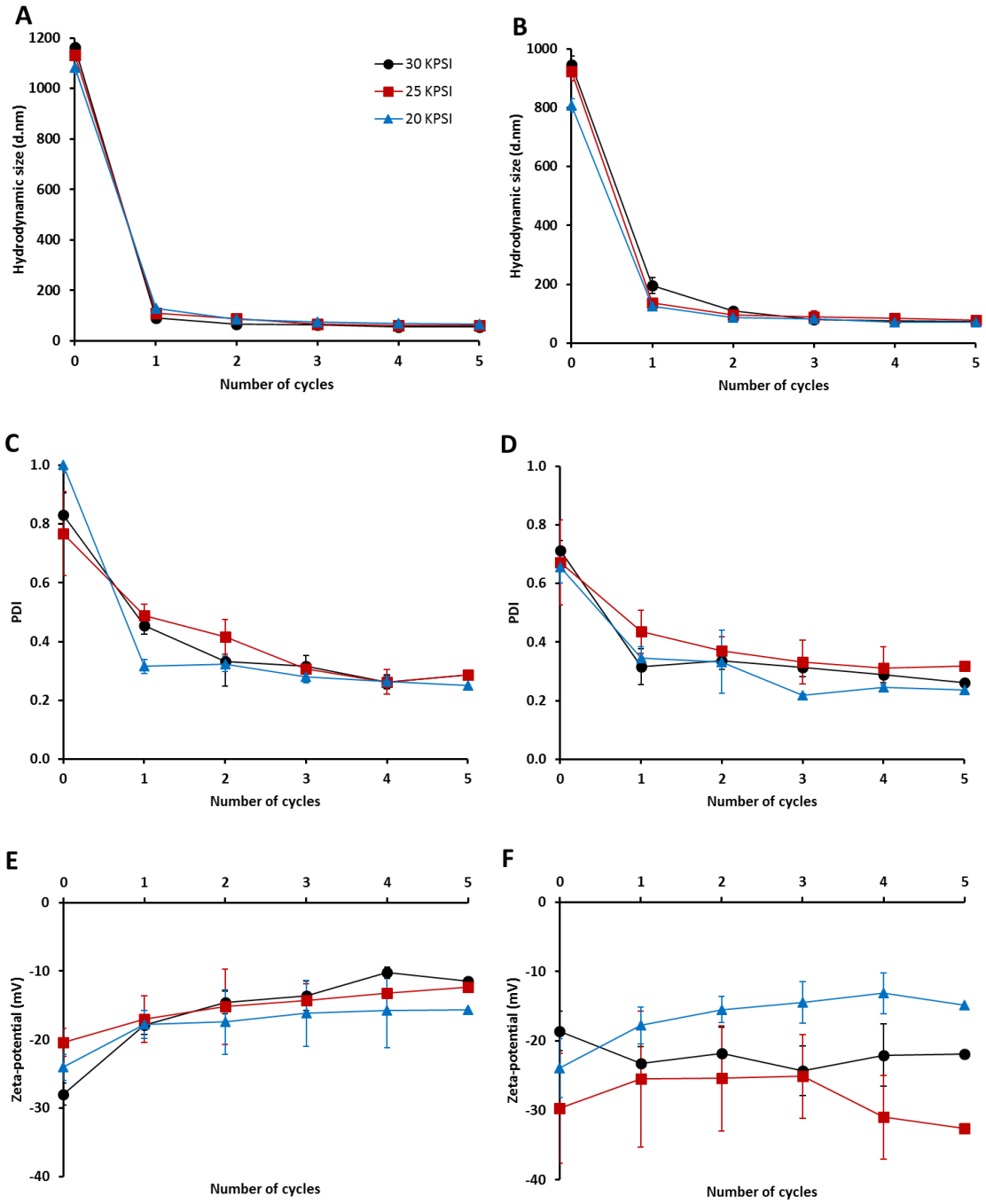

Figure 2.2. The effect of pressure on the physicochemical properties of neutral liposomes processed in the M-110P microfluidizer. Neutral liposomes were treated at 20 (●), 25, (■) and 30 KPSI (▲) and characterised by dynamic light scattering in terms of hydrodynamic size (PC:Chol – **A**, DSPC:Chol – **B**), PDI (PC:Chol – **C**, DSPC:Chol – **D**) and zeta-potential (PC:Chol – **E**, DSPC:Chol – **F**). Results are represented as mean ± SD of three different experiments.

PC:Chol and DSPC:Chol MLVs (1:1 molar ratio) were prepared by lipid thin film hydration and subsequently processed in the microfluidizer M-110P for up to 5 cycles below and above the T_M of PC (0 °C) and DSPC (55 °C) (Fig. 2.1). In this way, PC:Chol MLVs were processed at 0 °C and room temperature, while DSPC:Chol liposomes were processed at 55 °C and room temperature. The hydrodynamic size and PDI of PC:Chol and DSPC:Chol MLVs was 800-1000 nm and 0.6-1.0 respectively. A single pass was enough to reduce the size and PDI below 120 nm and 0.4. After 5 passes, size and PDI further dropped to approximately 60 nm and 0.25 respectively with no differences observed between samples processed below and above the T_M. Therefore, following experiments were performed at room temperature.

Pressures ranging from 20 to 30 KSPI were then explored. At the lipid concentration used (0.5 mg/mL), the pressure had no impact on liposome size and PDI (Fig. 2.2). Again, size and PDI of PC:Chol and DSPC:Chol liposomes dramatically dropped to 100-200 nm and 0.3-0.5 respectively after one pass. Above 4 cycles, the resulting liposomes had a size and a PDI below 100 nm and 0.3 respectively. The zeta-potential of all samples remained slightly negative (Fig. 2.2) as expected for neutral liposomes. These results are in agreement with previous published work with microfluidizer technology: the first cycle drastically decrease in liposome size, while subsequent three passes result in samples under 100 nm with a low polydispersity index (Lajunen et al., 2014).

Classical size reduction techniques, such as sonication and extrusion, are well established within the literature. However, these approaches do not scale-up effectively. Extrusion is a time- and energy-consuming process that requires multiple cycles to obtain SUVs. Moreover, sample and drug recovery decrease with increasing number of cycles (Cho et al., 2013). Similarly, although easy and simple, sonication displays several issues such as the contamination due to erosion of the probe tip as well as degradation of liposomes under high amplitude conditions (Akbarzadeh et al., 2013). In contrast, the M-110P microfluidizer provides a high-throughput approach (100 – 120 mL/min) that easily reduces the size of preformed MLVs from several hundreds of nm to sub-100 nm liposomes and hence represents an attractive alternative for sonication and extrusion.

2.4.2. Bottom-up formulation of liposomes by microfluidics

Microfluidic production of liposomes was performed in the Nanoassemblr platform (Precision Nanosystems Inc.) in a Y-shaped staggered herringbone micromixer of 300 µm width and 130 µm height. In general, the operating parameters were optimised in the following order: 1) aqueous:organic flow rate ratio (FRR), 2) initial lipid concentration, 3) total flow rate (TFR), 4) aqueous buffer concentration.

Based on current research, FRR is the most important parameter to consider when formulating liposomes by microfluidics (Forbes et al., 2019). Indeed, liposome formation in the micromixer is promoted by the mixing between organic and aqueous phase; which makes the lipids nanoprecipitate and self-assemble into planar lipid bilayers, which bend to reduce contact of the hydrophobic acyl chains of the lipids with the water phase, and eventually close into spherical vesicles. The higher the FRR, the more rapidly the concentration of alcohol will decrease and the less the time for lipids discs to stabilize. Therefore, smaller liposomes are expected at increasing FRR (Forbes et al., 2019). The same trend was observed by Jahn et al. in their studies (Jahn et al., 2010; Jahn et al., 2007).

The hydrodynamic size of neutral DSPC:Chol liposomes was 67 ± 7 nm when formulated at 1:1 FRR and dropped to 53 ± 6 and 44 ± 15 nm when produced at 3:1 and 5:1 FRR (Fig. 2.3A). In contrast, the PDI increased from 0.05 to 0.12 with higher (3:1 and 5:1) FRRs. The zeta-potential, however, did not vary with FRR (Fig. 2.3A). Notably, size and size distribution of cationic liposomes were highly influenced by the FRR. DOPE:DOTAP, DOPE:DC-Chol and DOPE:DDA liposomes prepared at 3:1 and 5:1 FRR had high PDI (>0.4) and poor batch-to-batch reproducibility, as evidenced by high standard deviations. When prepared at 1:1 FRR, liposomes had an average size diameter of 40 nm and a PDI below 0.2. All cationic formulations had a zeta-potential above 45 mV (Fig. 2.3 B-D).

A Y-shape micromixer was used elsewhere to evaluate the effect of FRR on neutral and cationic liposomes. The size of neutral PC:Chol liposomes dropped from 450 to 50-60 nm by increasing the FRR from 1:1 to 5:1 (Kastner et al., 2015).. Similarly, the size of cationic DOPE:DOTAP liposomes dropped from 200 to 100 nm. However, reducing liposome size came along with higher PDI values (>0.4) (Kastner et al., 2014).

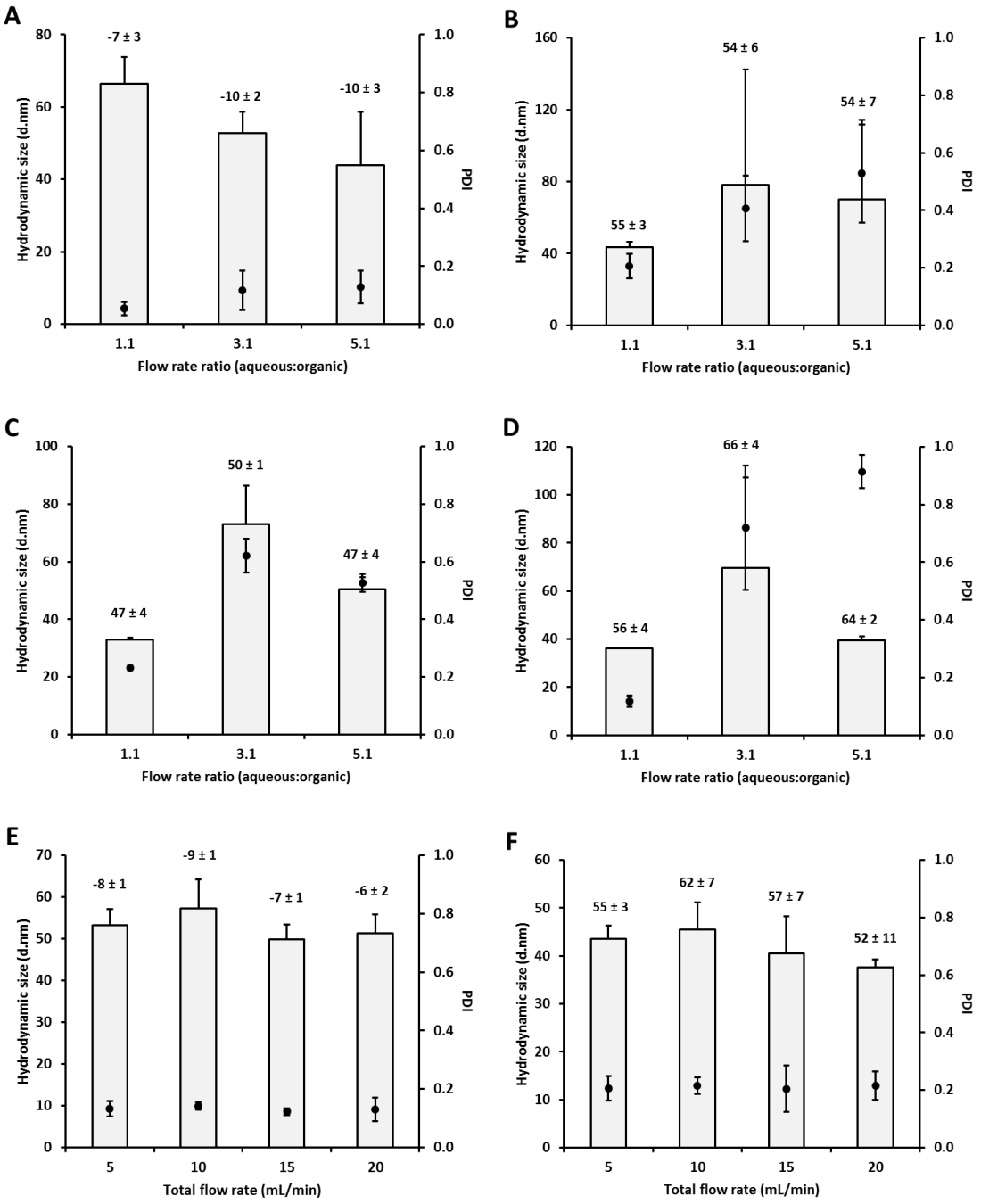

Figure 2.3. The effect of aqueous:organic flow rate ratio (FRR) **(A – D)** and total flow rate (TFR) **(E – F)** on neutral DSPC:Chol liposomes **(A and E)** and cationic DOPE:DOTAP **(B and F)**, DOPE:DC-Chol **(C)** and DOPE:DDA liposomes **(D)**. Liposomes were formulated at 1:1 molar ratio in 10 mM TRIS buffer pH 7.5 and 4 mg/mL. 15 mL/min TFR and 1:1 FRR were used to investigate the effect of FRR and TFR respectively. Samples were dialysed and subsequently characterised by dynamic light scattering in terms of size (bars), PDI (dots) and zeta-potential (values). Results are represented as mean ± SD of 3 independent experiments.

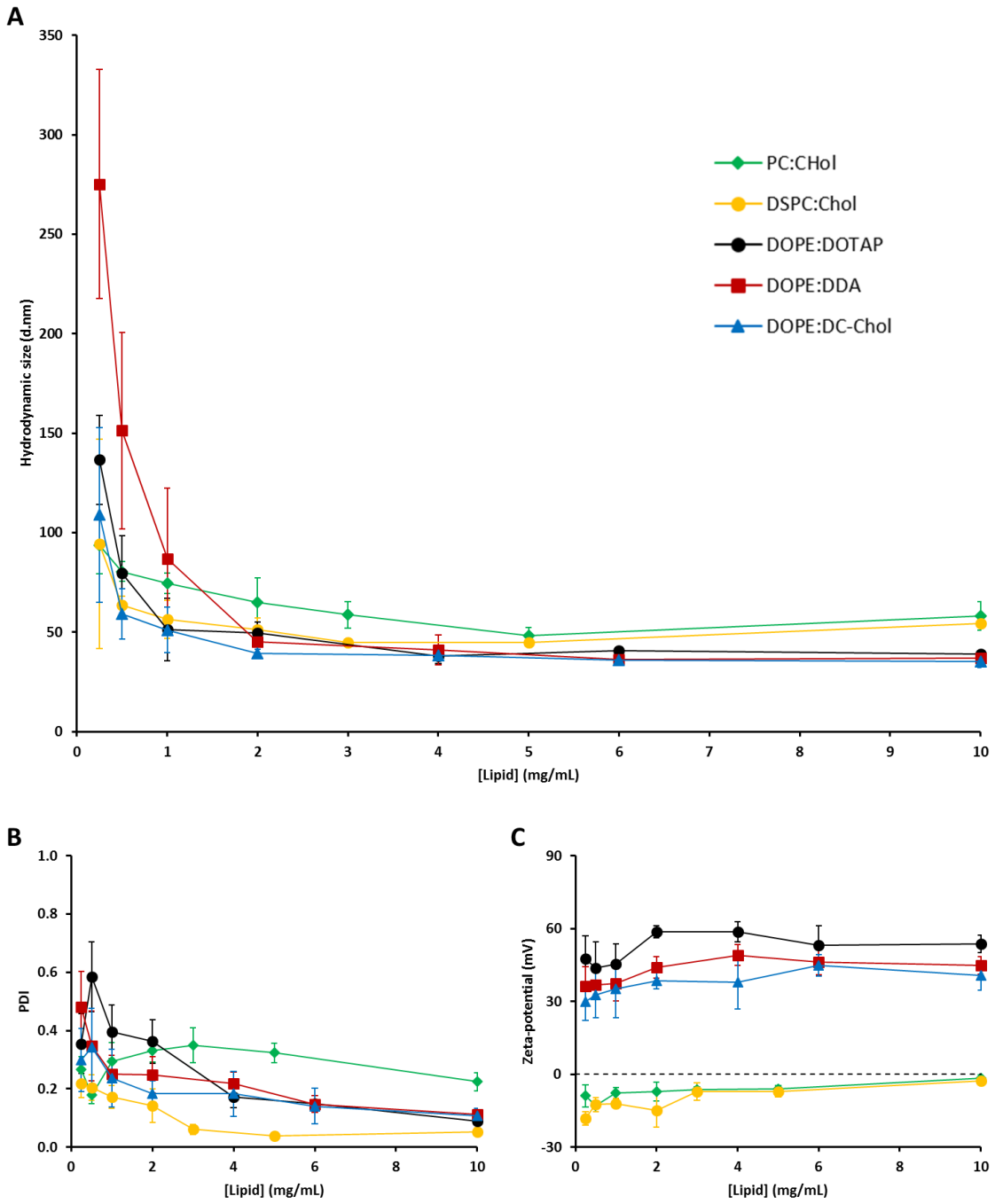

Figure 2.4. The effect of initial lipid concentration on neutral PC:Chol (♦) and DSPC:Chol liposomes (●) liposomes and cationic DOPE:DOTAP (●), DOPE:DDA (■) and DOPE:DC-Chol liposomes (▲). Liposomes were formulated by microfluidics at 1:1 molar ratio in 10 mM TRIS buffer pH 7.4, at 4 mg/mL and 15 mL/min TFR. Neutral and cationic liposomes were prepared at 3:1 and 1:1 FRR respectively. Samples were dialysed and subsequently characterised by dynamic light scattering in terms of size **(A)**, PDI **(B)** and zeta-potential **(C)**. Results are represented as mean ± SD of 3 independent experiments.

TFR had no impact on the size of DSPC:Chol (50-60 nm) and DOPE:DOTAP liposomes (40-45 nm) in the range of 5-20 mL/min. Both formulations exhibited narrow size distribution and low PDI (<0.2) regardless of the TFR (Fig 2.3E and F). Indeed, TFR has been reported to have little to no effect on liposome size in a range of studies (Carugo et al., 2016; Guimaraes Sa Correia et al., 2017; Joshi et al., 2016; Kastner et al., 2015).

The effect of initial lipid concentration was then evaluated in the range of 0.25-10 mg/mL on neutral and cationic liposomes. The hydrodynamic size and PDI of liposomes dropped with increasing lipid concentration; with no further size reduction observed at concentrations above 4 mg/mL. Indeed, liposomes produced at higher lipid concentrations had an average size diameter of 40-50 nm and low (<0.2) PDI (Fig. 2.4). However, the PDI of PC:Chol liposomes was not influenced by lipid concentration (Fig. 2.4A and B). The zeta-potential varied ±10 mV with lipid concentration, with neutral and cationic liposomes becoming more neutral and cationic respectively (Fig. 2.4C).

The size of liposomes prepared in the Nanoassemblr Platform was reported elsewhere to decrease with increasing lipid concentration (Joshi et al., 2016). In contrast, other studies have reported that size of liposomes prepared by microfluidics increases with concentration. Indeed, at higher concentrations, more lipid molecules are available at the mixing interface and hence larger liposomes are expected (Balbino et al., 2013; Carugo et al., 2016; Mijajlovic et al., 2013; Pradhan et al., 2008). In a study conducted by Mijajlovic et al., for instance, the size of 1-palmitoyl-2-oleoylsn-glycero-3-phosphocholine (POPC) liposomes augmented from 60 nm to 180 nm by increasing the lipid concentration from 2.5 to 20 mM (3.5 and 14 mg/mL respectively).

Nevertheless, other variables should be taken into consideration, including micromixer design (geometry, microchannel size, orientation of inlet channels) and liposome composition. For example, Jahn et al. used a microfluidic hydrodynamic focusing (MHF) cartridges of 10 and 65 µm width to demonstrate that the combination of micromixer geometry and hydrodynamic flow focusing regime had an impact on liposome size (Jahn et al., 2010). In another study, Carugo et al. reported that liposome size and size distribution depend on microfluidic device and architecture. In particular, the size of liposomes formulated in one chip dropped from 80 to 30 nm by increasing the FRR from 10 to 50; while the size of those prepared in a different chip was 120 nm regardless of FRR used (Carugo et al., 2016).

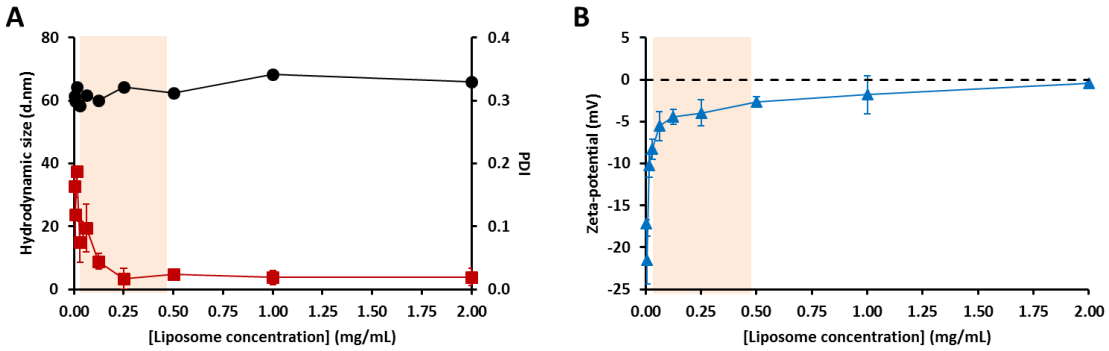

Figure 2.5. The influence of sample concentration on dynamic light scattering (DLS) characterisation of DSPC:Chol liposomes. DSPC:Chol liposomes were formulated at 1:1 molar ratio in 10 mM TRIS buffer pH 7.4, at 4 mg/mL, 1:1 FRR and 15 mL/min TFR, dialysed, serially diluted and characterised by DLS. **A)** Hydrodynamic size (●) and PDI (■). **B)** Zeta-potential (▲). Range of sample concentration used in previous liposome sizing measurements (0.00625 – 0.5 mg/mL) is highlighted in beige. Results are represented as mean ± SD of three consecutive measurements.

Size and zeta-potential DLS measurements have been reported to be dependent on nanoparticle (NP) concentration. Higher concentration of NPs results in cross-interaction among light scattered from single NPs thus resulting in artificially smaller sizes, while measuring highly diluted samples results in insufficient scattered light and hence their DLS size tends to be higher. The relationship between zeta-potential and particle concentration is complex. The zeta-potential of a particle is related to its surface charge, electrolyte concentration and valency of the buffer it is are suspended in (Attwood, 1998). In order to consider the effect of sample concentration, DSPC:Chol liposomes were serially diluted, from 2 mg/mL up to 0.004 mg/mL, and subsequently characterised by DLS. As seen in Fig. 2.5, liposome size did not vary with sample concentration while PDI was slightly reduced from by increasing sample concentration. Although zeta-potential showed an asymptotic dependence, with negative values becoming more neutral at increasing concentrations; its variations were subtle in the range of concentrations reported in Fig. 2.4. These results therefore demonstrate that size of liposomes prepared by microfluidics in the Nanoassemblr platform is not affected by sample concentration in the range of concentrations considered, while zeta-potential is slightly affected.

As first described by Israelachvili (Israelachvili et al., 1980), the geometry in which lipids self-assemble is given by the critical packing parameter of the lipid (P_C). P_C is defined as $v/a_0 \cdot l_c$, where

a_0 is the effective area of the head group, l_c is the length of the alkyl chain and v is the alky chain volume. Therefore, P_C can be used to predict what structural aggregates the lipids will form (Israelachvili, 1992). For $P_C \leq 1$, lamellar (L_α) phases are formed, including spherical micelles ($P_C <$ 0.3), worm-like micelles ($P_C = 1/3 – 1/2$), vesicles ($P_C = 1/2 – 1$) and planar bilayers ($P_C \sim 1$), For P_C > 1, inverted hexagonal (H_{II}) and cubic phases (Q_{II}) appear. For charged lipids, the presence of electrolytes can potentially reduce the repulsion among lipid head groups, reducing a_0 and consequently increasing P_C. From this point of view, we investigated the use of microfluidics to produce liposomes in a range of sizes (40-750 nm) and can be hypothesised that increasing the ionic strength of the aqueous phase (i.e. buffer concentration) injected in the micromixer could increase lipid P_C enough to form large unilamellar liposomes but not enough to induce a negative curvature and the consequent formation of non-liposomal self-assemblies such as cubosomes (Muir et al., 2012).

Previous studies have suggested that salt concentration can control liposome formation. For example, Meyuhas et al. reported that lipid vesicles composed of phosphatidylcholine (PC) and sodium cholate, prepared in 10 mM TRIS (pH 7.4), increased in size from 40 to 100 nm by adding increasing NaCl concentration up to 500 mM (Meyuhas et al., 1997). Similarly, Edwards and co-workers prepared vesicles composed of PC and cetyltrimethylammonium chloride and observed a vesicle-to-micelle transition and an increase in vesicle size over time in presence of 100 mM NaCl which did not occur in absence of salt (Edwards et al., 1993). Electrolytes (NaCl, Ca^{2+}) have also been reported to induce lamellar-to-cubic phase transitions in lipid membranes composed of monoolein and other lipid, such as dioleoylphosphatidylglycerol (Awad et al., 2005), dioleoylphosphatidylserine (Alam et al., 2011; Oka et al., 2017), and also in pre-formed liposomes composed of phytantriol and DDA (Muir et al., 2012).

This concept was explored in the context of microfluidic production of liposomes and buffer ionic strength (TRIS buffer), where liposomes were prepared with varying buffer concentrations and then the buffer concentration was re-set to 10 mM Tris (Fig. 2.6). Results shown in Fig. 2.7 demonstrate that the size of cationic liposomes can be controlled with electrolyte content using in the initial preparation, whilst neutral formulations were not sensitive to changes in the range considered.

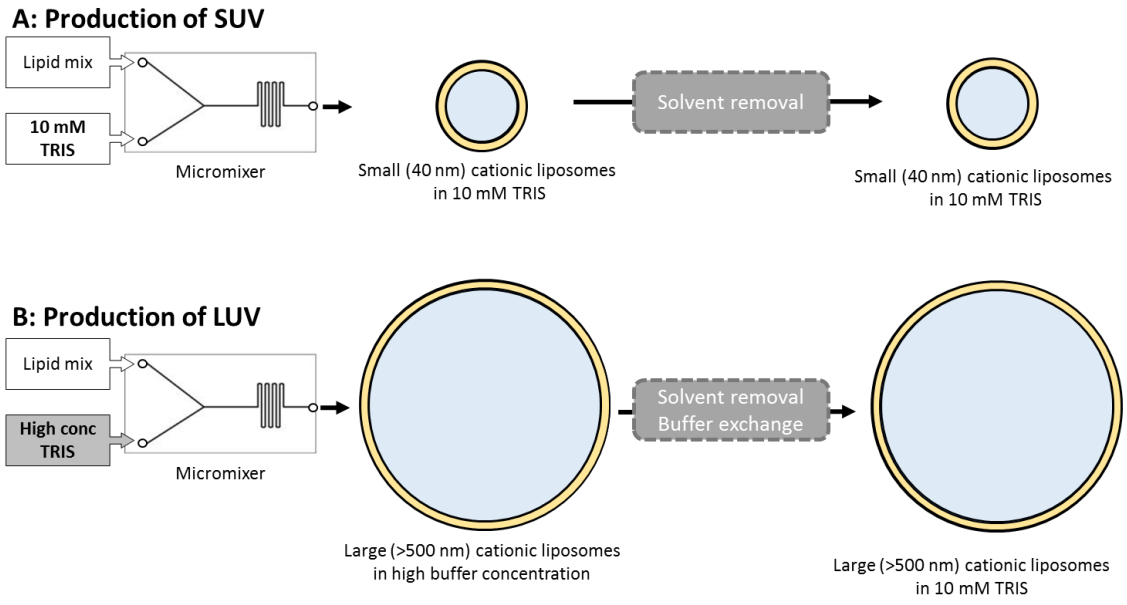

Figure 2.6. Schematic representation of the microfluidic formulation of small **(A)** and large **(B)** unilamellar liposomes (SUVs and LUVs). Small (40 nm) and large (>500 nm) liposomes were formulated by microfluidics in the Nanoassemblr Platform at 4 mg/mL, 1:1 FRR and 15 mL/min TFR at either 10 or higher TRIS concentration. Solvent removal and buffer exchange was undertaken via dialysis against 10 mM TRIS (200 mL) for 1 hour under magnetic stirring to adjust buffer concentration. The concentration of buffer and lipid selection offer controlled production of large unilamellar liposomes.

Neutral liposomes, composed of DSPC:Chol, remained at approximately 80 nm in size over TRIS buffer concentrations of 0 to 1000 mM. In contrast, the size of cationic liposomes increased stepwise at increasing buffer concentrations. For instance, DOPE:DOTAP increased in size from 40 to over 600 nm over the same TRIS concentration range. This increase in size with increasing buffer concentration was even more notable with DOPE:DDA, with 350 mM TRIS being sufficient to produce vesicles of 600 nm in size. Interestingly, DOPE:DDA liposomes did not form at higher ionic strengths, and resulted in macroscopic lipid aggregation; probably due to an excessive increase of P_C (Fig. 2.7A).

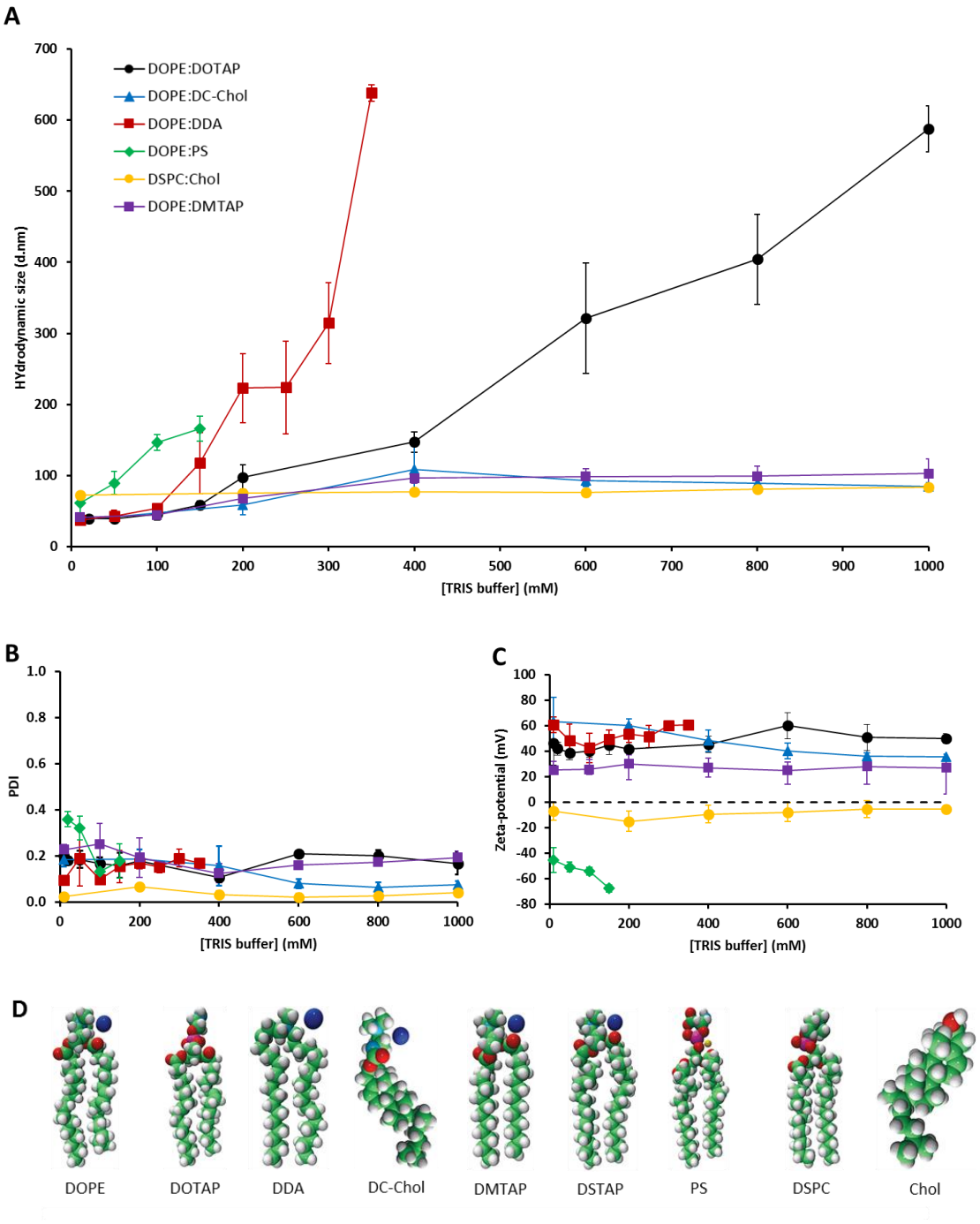

Figure 2.7. The effect of aqueous buffer concentration on liposomes formulated by microfluidics I. DOPE:DOTAP (●), DOPE:DDA (■), DOPE:DC-Chol (▲), DOPE:DMTAP (■), DOPE:PS (◆) and DSPC:Chol (●) liposomes were formulated by microfluidics in the Nanoassemblr Platform at 1:1 molar ratio, 4 mg/mL, 1:1 FRR and 15 mL/min TFR at increasing concentrations of TRIS buffer pH 7.4, then dialysed and characterised by dynamic light scattering in terms of size **(A)**, PDI **(B)** and zeta-potential **(C)**. **D)** 3D structures of lipids. Results are represented as mean ± SD of three independent experiments.

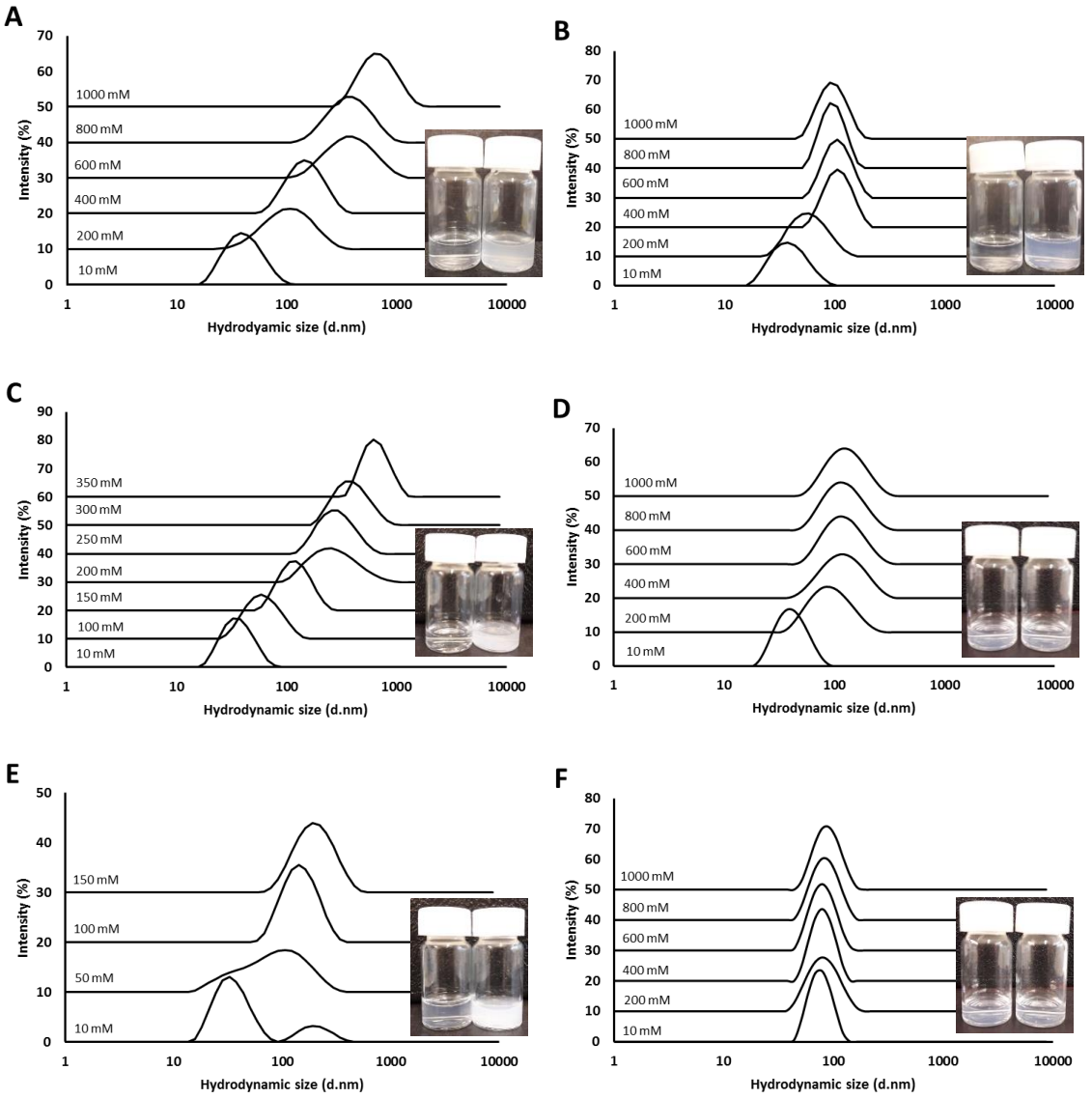

Figure 2.8. The effect of aqueous buffer concentration on liposome size distribution of liposomes. DOPE:DOTAP **(A)**, DOPE:DC-Chol **(B)**, DOPE:DDA **(C)**, DOPE:DMTAP **(D)**, DOPE:PS **(E)** and DSPC:Chol **(F).** Liposomes were formulated by microfluidics in the Nanoassemblr Platform at 1:1 molar ratio, 4 mg/mL, 1:1 FRR and 15 mL/min TFR at increasing concentrations of TRIS buffer pH 7.4, then dialysed and characterised by dynamic light scattering in terms of size **(A)**, PDI **(B)** and zeta-potential **(C)**. Representative images of liposomes prepared at lowest (left) and highest (right) TRIS concentration are shown for each formulation.

It has been generally assumed that P_c is given only by a_o because the ratio $a_o \cdot l_c$ is independent of the alkyl chain length and thus the effect of chain length has been often underestimated. However, it was demonstrated that the chain length plays a role in determining the size and

shape of self-assemblies in equilibrium (Nagarajan, 2002). At the same time, the 3D structure of a lipid, and consequently the volume of the alkyl chains (*v*), is influenced by the degree of unsaturation. We attempted to investigate to what extent both length and degree of unsaturation of the acyl chain had an impact on the size of liposomes produced at different buffer concentrations. To this end, liposomes composed of DOPE and either DMTAP (14:0 TAP) or DSTAP (18:0 TAP), which have the same headgroup as DOTAP (also known as 18:1 TAP), were explored. The hydrodynamic size of DOPE:DMTAP liposomes increased from 40 nm to 100 nm by increasing buffer concentration to 400 mM TRIS, but did not further increase at higher (up to 1000 mM) TRIS concentrations (Fig. 2.7A). Unfortunately, DOPE:DSTAP liposomes prepared at 10 mM TRIS exhibited inconsistent size and size distributions and high PDI (>0.4). Furthermore, samples aggregated when higher TRIS concentrations were used (data not shown). Nevertheless, these results are in agreement with Nagarajan findings and suggest that the effect of buffer concentration on liposome size not only depends on the lipid headgroup but also in the length and/or degree of unsaturation of the alkyl chain. Similarly, only an increase from 40 to 100 nm was observed on DOPE:DC-Chol liposomes (Fig. 2.7A).

Finally, the effect of buffer concentration was also investigated in anionic DOPE:PS liposomes, whose size increased from 60 to 165 nm in the range of 10-150 mM TRIS. At higher TRIS concentrations liposomes did not form, as observed on DOPE:DDA liposomes (Fig. 2.7A). Notably, all formulations except DOPE:PS liposomes prepared at <50 mM TRIS concentration, exhibited low PDI (0.05-0.25) regardless of liposome size (Fig. 2.7B). Charged liposomes had high a zeta-potential (40-60 mV), either positive or negative across the buffer concentration range tested, while the zeta-potential of DSPC:Chol liposomes was slightly negative (Fig. 2.7C). All formulations, except DOPE:PS liposomes prepared at <50 mM TRIS concentration, exhibited narrow unimodal size distribution irrespective of the size and buffer concentration they were initially prepared in (Fig. 2.8) and the effect of initial buffer concentration on liposome size could also be easily observed visually with large liposomes showing notable increases in turbidity, (Fig. 2.8).

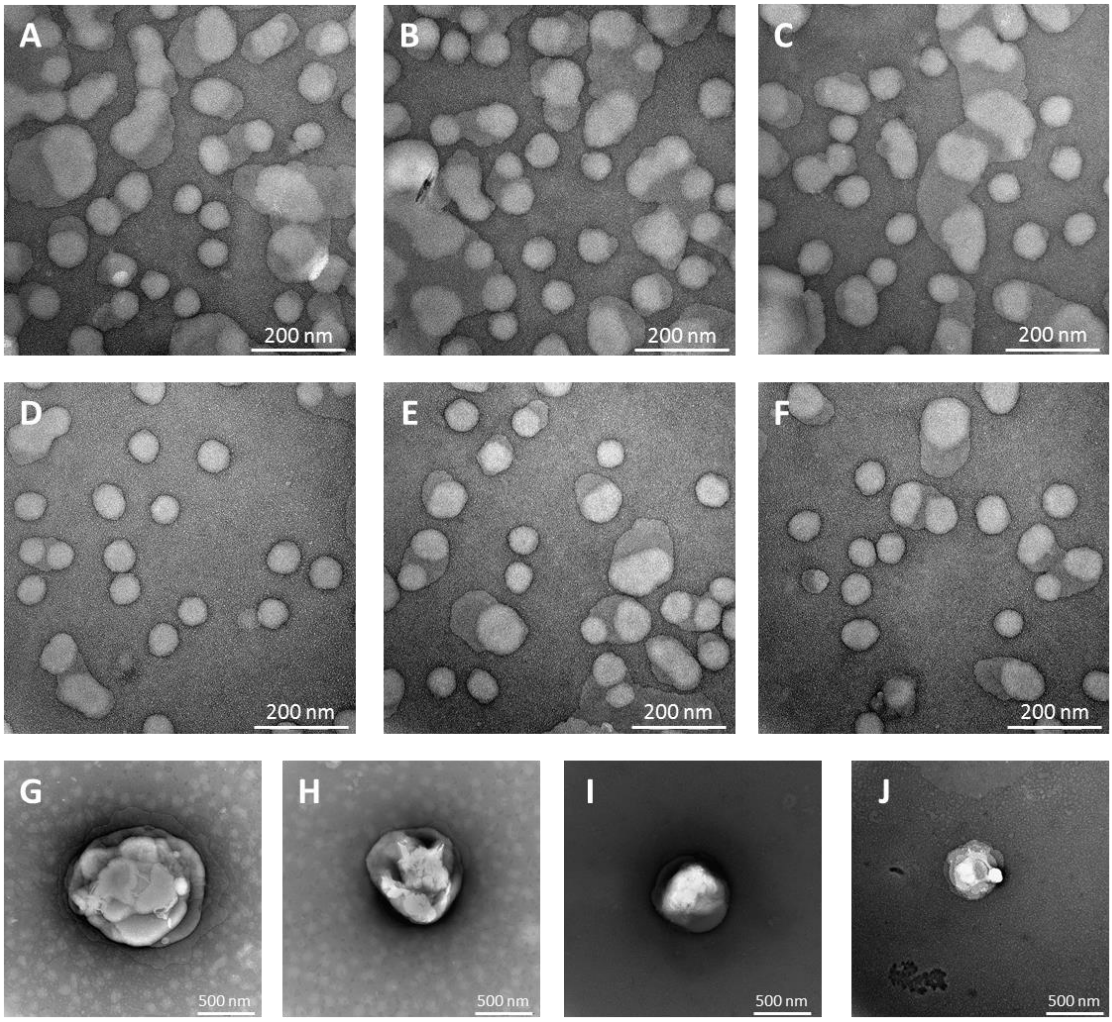

Figure 2.9. Negative-staining electron microscopy images of small and large cationic liposomes formulated by microfluidics. Small DOPE:DOTAP **(A-C)**, small DOPE:DDA **(D-F)**, large DOPE:DOTAP **(G, H)** and DOPE:DDA liposomes **(I, J)**. Liposomes were formulated by microfluidics in the Nanoassemblr Platform at 4 mg/mL, 1:1 FRR and 15 mL/min TFR. Small cationic liposomes were prepared at 10 mM TRIS and large DOPE:DOTAP and large DOPE:DDA liposomes were produced at 1000 and 300 mM TRIS respectively.

Small and large DOPE:DOTAP (50 and 750 nm) and DOPE:DDA (>500 nm) liposomes were further characterised by negative-stain electron microscopy (NS-EM) (Fig. 2.9). In NS-EM, particles are compressed and fixed onto a grid. Because liposomes are flexible structures, they are squeezed when deposited, so that they do not maintain their three-dimensional structure and particle sizes are slightly overestimated. Nevertheless, small and large liposomes had a EM size that matched their DLS size. However, small liposomes exhibited subtle degree of aggregation.

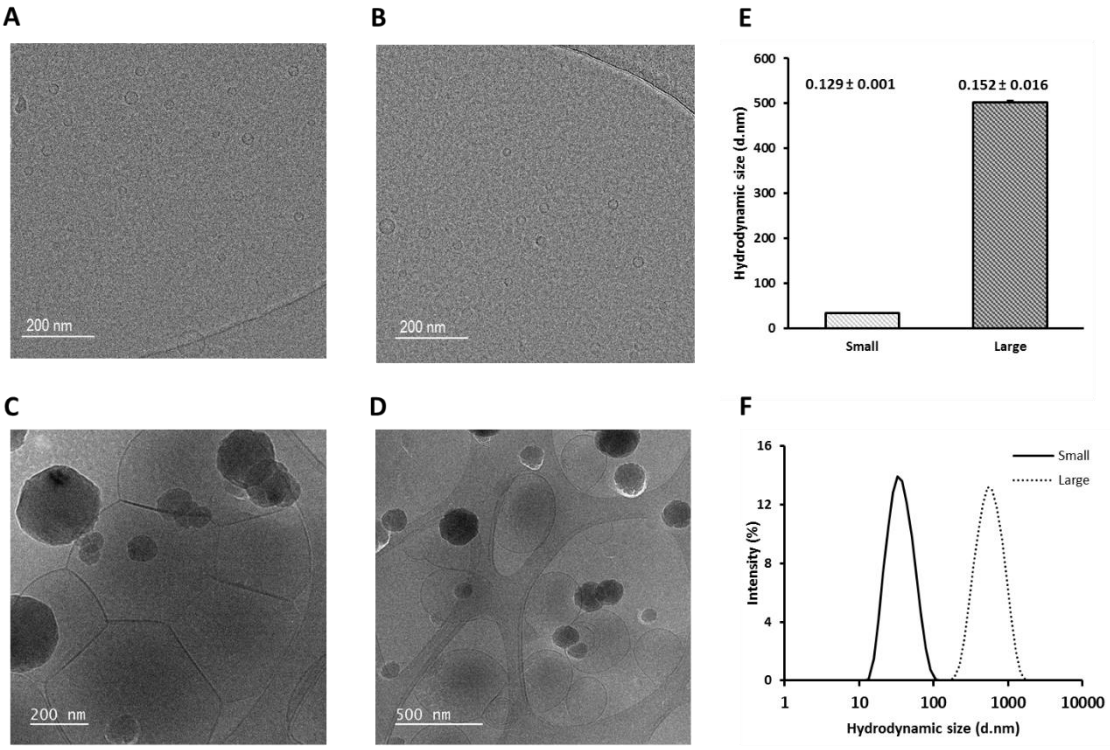

Figure 2.10. Cryo-TEM micrographs of small **(A, B)** and large DOPE:DOTAP liposomes **(D , E)** formulated by microfluidics at 4 mg/mL, 1:1 FRR, 15 mL/min TFR and 10 and 1000 mM TRIS buffer pH 7.4. The dense black spheres are water crystals. Hydrodynamic size (bars) and PDI (values) **(F)** and size distribution plots of small and large liposomes **(G)** are shown. Results are represented as mean ± SD of three consecutive DLS measurements.

Small and large DOPE:DOTAP were also characterised by cryo-TEM, a microscopy technique that not only allows to preserve the three-dimensional structure of liposomes but also permits to analyse the degree of lamellarity. Results shown in Fig. 2.10 demonstrate that this approach allows to obtain cationic unilamellar liposomes in the range of 35 to 750 nm. Again, liposomes had a size and a size distribution that matched with DLS measurements (Fig. 2.10E and F).

To investigate to what extent the charged lipid concentration was responsible for the increase in liposome size, DSPC:Chol liposomes were formulated with increasing molar percentages of DOTAP (0, 5, 13 and 23%) (Fig. 2.11) and DDA (13 and 23%). With the DOTAP formulations, the impact of buffer concentration on particle size increased with cationic lipid content (Fig. 2.11). The size of formulations containing low DOTAP levels increased up to 112 nm whilst formulations containing 5 and 13% DOTAP increased to 140 nm and 175 nm respectively. However, increasing

the molar percentage of DOTAP to 23% did not result in larger liposomes (Fig. 2.11A). In general, all PDI values were low (<0.2) with the exception of the 23% DOTAP formulation prepared at 1000 mM TRIS, whose PDI rose to 0.3 (Fig. 2.11B). In terms of their zeta-potential, DSPC:Chol liposomes were slightly negative (approximately -15 mV) and increasing the cationic lipid content increased the zeta-potential as would be expected (Fig. 2.11C). When considering the addition of DDA (13% and 23%) to the DSPC:Chol formulations, liposomes did not change in size and remained at 120 – 140 nm, PDI < 0.2 and 40 mV zeta-potential (Fig 2.11D to F).

Both shape and size of lipid aggregates can be predicted by the packing parameter. For lipid mixtures, a mean packing parameter between those of the individual lipids may be considered if only if the different molecules mix ideally and do not phase-separate, such that vesicle size can be tuned by adding a lipid with a higher (or lower) packing parameter (Carnie et al., 1979; Israelachvili, 1992). From this point of view, the combination of DDA with DSPC and Chol may result in an asymmetrical distribution of lipids throughout the lipid bilayer thereby inhibiting the effect of ionic strength. These results suggest that different buffer-dependent liposome sizes are expected for specific combinations of cationic and structural lipids.

To consider if this size-controlling effect was achievable with other buffers, the effect of ionic strength was also investigated on citrate buffer pH 6. Citrate buffer is often used in the preparation of RNA lipid nanoparticles (LNPs) containing ionisable/cationic lipids. DOPE:DOTAP and DOPE:DDA liposomes were prepared in citrate buffer, but all formulations aggregated regardless of citrate concentration. Therefore only DSPC:Chol and DSPC:Chol:DOTAP (5% DOTAP) formulations were tested. Interestingly, when DSPC:Chol liposomes were formulated in citrate buffer pH 6.0, a small but significant ($p < 0.05$) increase in vesicle size from 80 to 120 nm was noted , while size did not increase when formulated at same concentrations of TRIS pH 7.4 (Fig. 2.11G). The 9% DOTAP liposome formulation also displayed a trend of increasing size (from 98 to 166 nm) with increasing citrate buffer concentration, and only 400 mM was required to obtain liposomes of same size achievable with 1000 mM TRIS buffer (Fig. 2.11AçG). As with the TRIS formulations, the PDI of all formulations tested remained low (<0.25) (Fig. 2.11H). Finally, the effect of buffer pH was tested as to find that the size of DSPC:Chol liposomes prepared in citrate buffer pH 4.0 or 6.0 increased in a similar extent (data not shown).

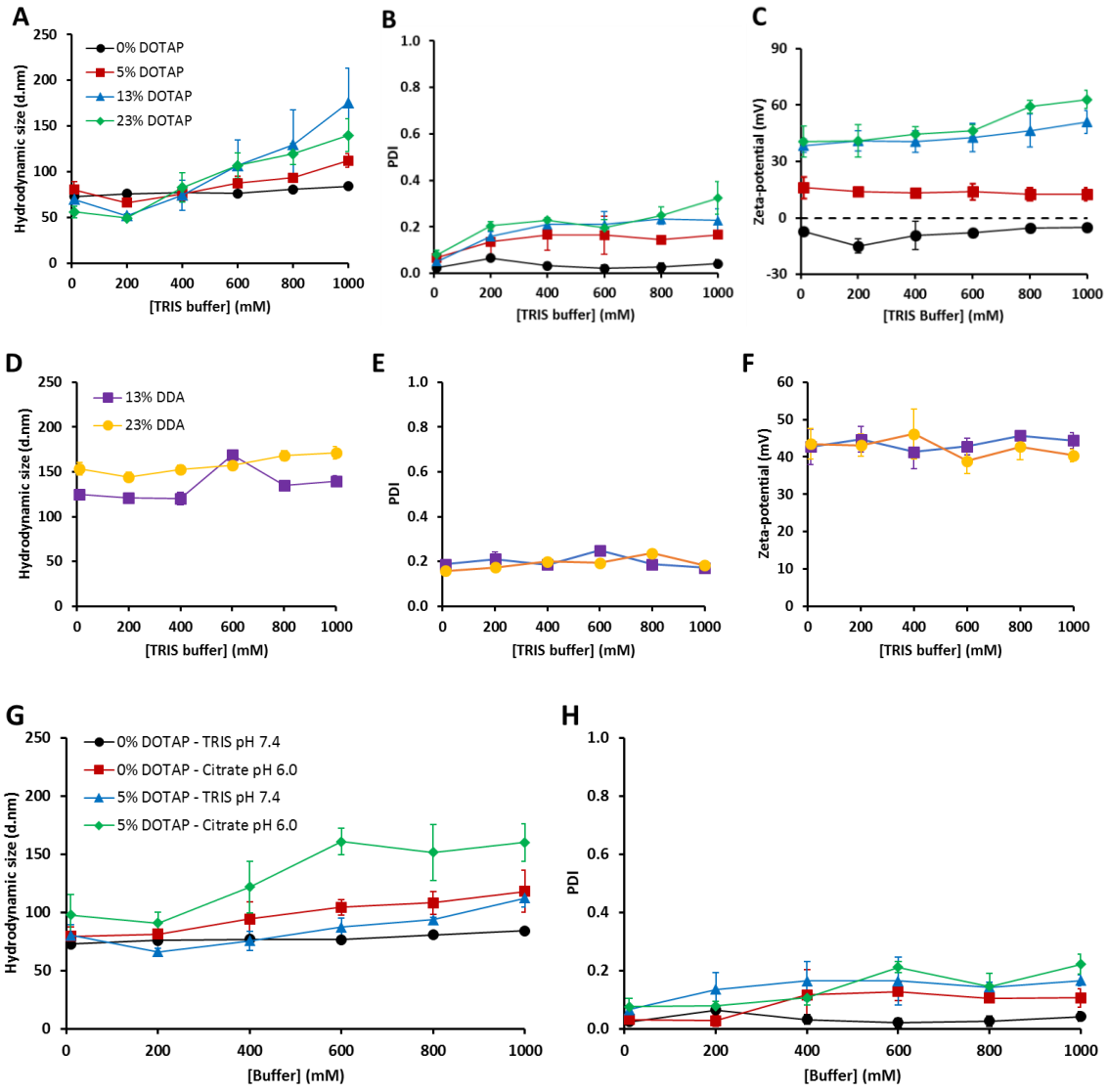

Figure 2.11. The effect of aqueous buffer concentration on liposomes formulated by microfluidics II: the effect of molar percentage of cationic lipid. DSPC:Chol liposomes (10:10 molar ratio) were prepared at increasing molar percentages of either DOTAP (0% - ●, 5% - ■, 13% - ▲, 23% - ◆) or DDA (13% - ■, 23% - ●). All DOTAP **(A-C)** and DDA liposome formulations **(D-F)** were prepared at 4 mg/mL, 1:1 FRR, 15 mL/min TFR, dialysed and characterised by DLS in terms of size **(A, D)**, PDI **(B, E)** and zeta-potential **(C, F)**. The effect of buffer choice on size **(G)** and PDI **(H)**. DSPC:Chol (10:10 molar ratio) and DSPC:Chol:DOTAP (5% DOTAP) liposomes were prepared at 4 mg/mL, 1:1 FRR and 15 mL/min at increasing concentrations of TRIS buffer pH 7.4 or citrate buffer pH 6.0, dialysed and characterised by DLS. Results are represented as mean ± SD of three independent experiments.

2.4.3. Sterilisation of liposomes

Development of sterile formulations is an important requirement for drug and vaccine products. Herein, filtration (0.22 μm) and X-ray irradiation as methods for the sterilisation of neutral and cationic liposomes were investigated. Membranes composed of polyethersulfone (PES), polyvinylidene Fluoride (PVDF), mixed cellulose ester (MCE) from Millipore (MP) were used. PES filters from Fisherbrand (FB) were also used for a comparison between manufacturers.

Non-filtered neutral DSPC:Chol liposomes were approximately 100 nm in size, with low PDI (0.10) and neutral zeta-potential (-3 mV). Filtration through PES (either MP or FB) or PDVF filters did not alter their physicochemical properties and allowed high lipid recovery (70-80%). However, DSPC:Chol liposomes aggregated when filtered through MCE membranes, as evidenced by low lipid recovery (<1 %, data not shown) (Fig. 2.12A). Cationic DOPE:DOTAP liposomes had a size of 40 nm, a PDI of 0.20 and a zeta-potential of +47 mV. Their size and PDI did not change upon filtration through PES (MP) and MCE filters but unexpectedly increased to 129 nm after filtration through PES (FB) filter (Fig. 2.12). The zeta-potential of DOPE:DOTAP liposomes (47 mV) dropped at least 10 mV after filtration through PES filters, but was not affected by MCE filters. The lipid recovery of DOPE:DOTAP was lower compared to DSPC:Chol liposomes. The percentage of lipid recovery was 55-60 % for PES (MP) and MCE filters and only 21 % for PES (FB) filters. The lower lipid recovery by PES (FB) compared to PES (MP) could be attributed to a higher filter surface area of FB filters given by their larger membrane diameter. When filtered through PVDF, DOPE:DOTAP liposomes aggregated (<10% lipid recovery, Fig. 2.12B).

Sterilisation of liposomes by X-ray radiation did not alter the physicochemical properties of liposomes. Cationic DOPE:DOTAP, DOPE:DC-Chol and DOPE:DDA liposomes were 30-40 nm in size with 0.2-0.3 PDI and 30-45 mV zeta-potential. Neutral DSPC:Chol liposomes were 84 nm in size, with a PDI of 0.09 and neutral zeta-potential (1 mV; Fig 2.13). Gamma-irradiated DSPC:Chol liposomes were stable for 14 days at 4 ˚C, while signs of aggregation were observed after 7 days on cationic liposomes (Fig. 2.13).

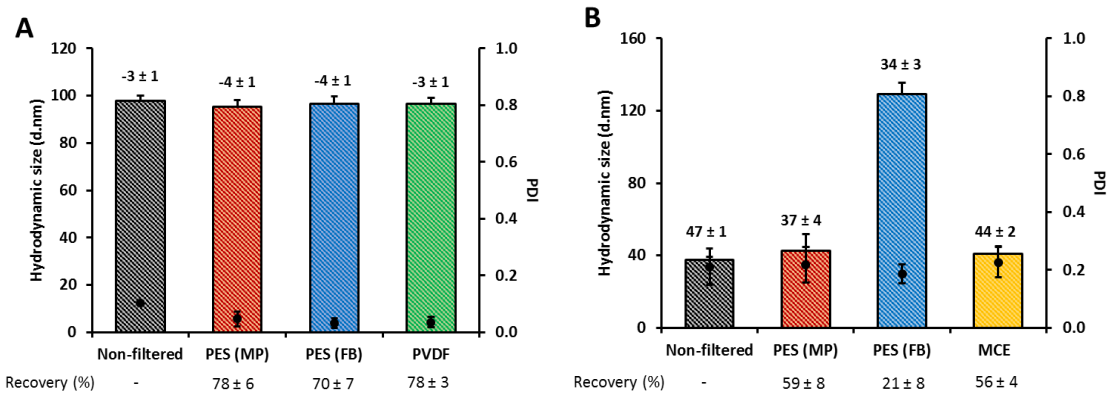

Figure 2.12. The effect of sterile filtration of neutral DSPC:Chol **(A)** and cationic DOPE:DOTAP liposomes **(B)** through 0.22 µm filters. Millipore's PES (▨), PVDF (▨) and MCE (▨) filters. Fisherbrand's PES filters (▨) were used as a comparison. Size (bars), PDI (dots) and zeta-potential (values) were compared to non-filtered liposome samples (▨). Results are represented as mean ± SD of three independent experiments. **Polyethersulfone (PES), polyvinylidene Fluoride (PVDF), mixed cellulose ester (MCE); Millipore (MP), Fisherbrand (FB).* Results are represented as mean ± SD of three independent experiments.

The size of DOPE:DOTAP, DOPE:DC-Chol and DOPE:DDA liposomes increased to 66, 87 and 55 nm after 7 days and further increased to 71, 95 and 77 nm at day 14. Similarly, the PDI exponentially augmented after two weeks up to 0.57, 0.86 and 0.43 for DOPE:DOTAP, DOPE:DC-Chol and DOPE:DDA liposomes respectively. The zeta-potential of all formulations remained constant in the time frame studied (Fig. 2.13).

Although simple, sterile filtration is relatively time consuming and not efficient for removal of sub-200 nm viruses. Moreover, it requires to work under high pressure conditions (up to 25 Kg/cm^2) (Toh and Chiu, 2013). Although commercial liposomal drug products are commonly sterilised by filtration, it was discarded because of low lipid recovery. Gamma-irradiation, on the other hand, is a highly efficient method to sterilise certain health care products. However, high doses of radiation (>10 KGy) can potentially induce the formation free radicals, consequently leading to peroxidation of unsaturated lipids and fragmentation of phospholipids (Toh and Chiu, 2013). Herein, a modest dose of radiation (10 Gy) did not change liposome attributes (size and PDI) right after sterilisation. However, gamma-irradiated cationic (DOPE:DOTAP, DOPE:DDA and DOPE:DC-Chol) liposomes were not stable over time (Fig. 2.13). Cationic liposomes are relatively unstable *per se* and, therefore, it is not possible to attribute such instability to potential oxidation of the unstaturated lipids by gamma-irradiation.

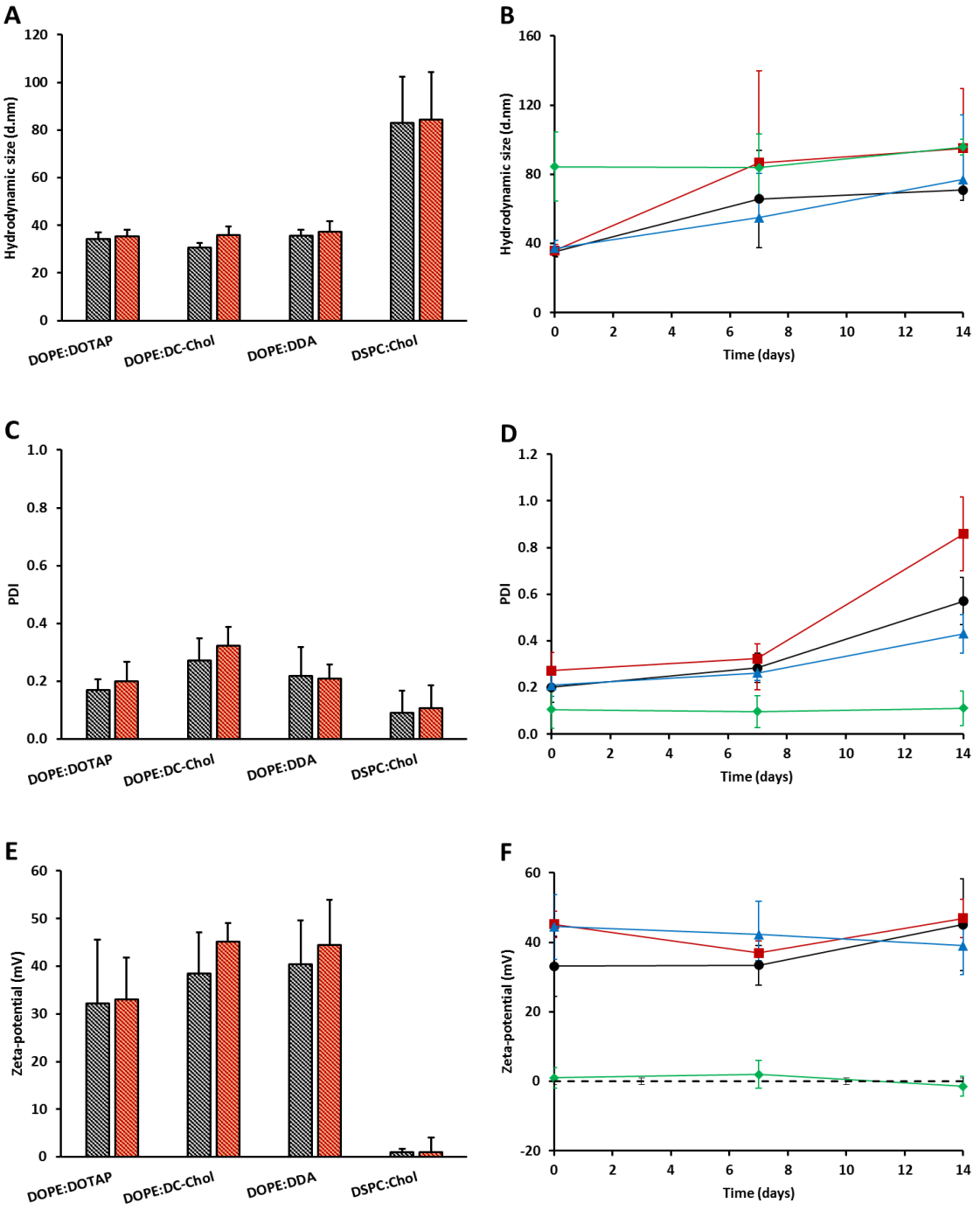

Figure 2.13. Effect of X-ray irradiation over physicochemical attributes **(A, C, E)** and stability of liposomes at 4˚C **(B, D, F)**. Liposomes were characterised by DLS in terms of size **(A)**, PDI **(C)** and zeta-potential **(E)** before (▨) and after X-ray irradiation (▨). The stability of DOPE:DOTAP (●), DOPE:DC-Chol (■), DOPE:DDA (▲) and DSPC:Chol liposomes (◆) was also evaluated by size **(B)**, PDI **(D)** and zeta-potential **(F)**. Results are represented as mean ± SD of three independent experiments.

2.4.4. Continuous manufacturing

Establishing continuous and cost-effective manufacturing processes is key to scale-up the production of liposome formulations. Although microfluidic formulation of liposomes allows to produce large volumes of liposomes in parallel, traces of organic solvent (up to 50%) have to be removed from sample after production. From this point of view, dialysis is not suitable for high-throughput approaches.

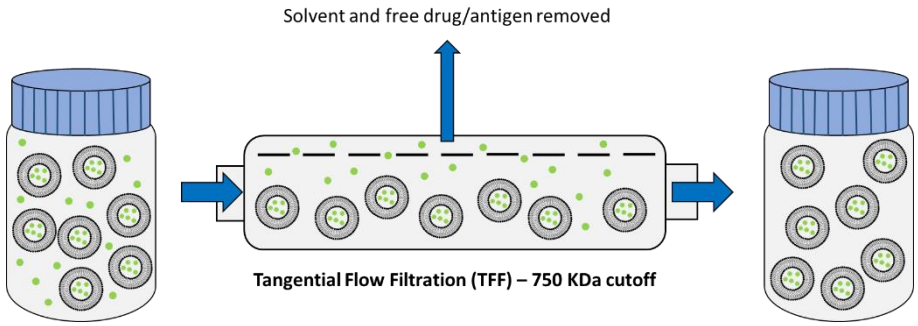

Figure 2.14. Schematic representation of TFF. Sample is passed through a column thanks to a transmembrane pressure (TMP) in such a way that solvent and free drug (or antigen) is removed by size exclusion.

Tangential Flow Filtration (TFF) is a process that makes use of pore-sized membranes to remove undesired compounds from particulate solutions based on size exclusion. Briefly, the solution is passed parallel to the membrane surface in such a way that compounds having a size below the cut-off will be removed ("permeate"), while those having a larger size will be circulated back to the reservoir ("retentate"), where they are re-circulated again through the membrane inside the column as many times as desired. Therefore, samples can be purified, buffer-exchanged and concentrated down to the desired concentration (Fig. 2.14). The rate of the process is mainly governed by the transmembrane pressure (TMP) which is given by the difference between the pressure at the feed compared to the permeate end, and the flow rate, which eventually dictates the shear. The advantage of TFF over direct flow filtration is the reduced chance of membrane fouling as the parallel flow does not form a direct layer over the surface of the membrane. The main disadvantage of TFF systems is that the sample is subjected to shear and thus liposomes

could be destabilised. As the shear rate is directly proportional to the flow rate (Fig. 2.15) this latter can be adjusted according to the characteristics of the sample.

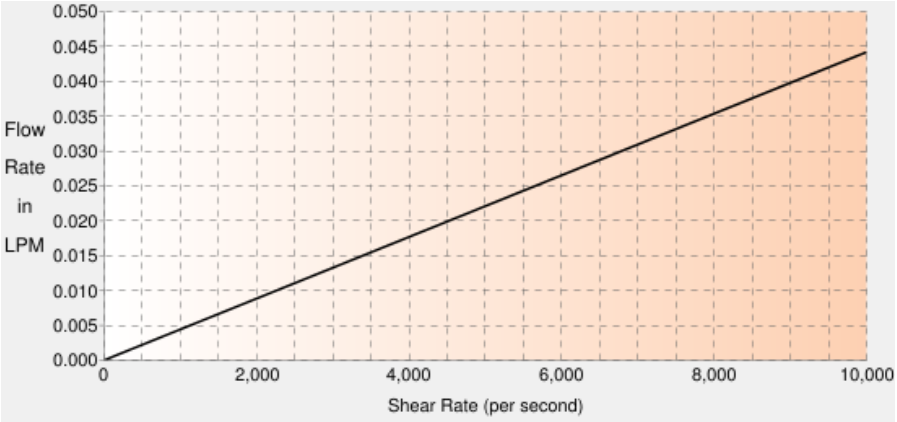

Figure 2.15. Example of shear-to-flow rate dependence in KR2i TFF (Lab Spectrum).

A setup for the continuous manufacturing of liposomes was proposed as follows. A bottom-up (Nanoassemblr) or top-down (M-110P microfluidizer) liposome formulation platform was coupled to an in-line purification system (TFF) and to an on-line Zetasizer AT (Malvern, UK) which allows to characterise samples as they are produced. In this way, liposomes could be produced, purified, concentrated and characterised in a single-step process. Values obtained from on-line measurements were compared to those obtained in a conventional off line Zetasizer Nano ZS (Malvern, UK). Furthermore, the liposome formulation prepared by microfluidics were co-formulated with the fluorescent lipophilic dye Dil-C_{18} so lipid recovery after TFF could be calculated.

DSPC:Chol liposomes prepared by microfluidics had a size and a PDI of 54.3 ± 0.1 nm and 0.06 ± 0.01 when measured off-line and 54.2 ± .10 nm and 0.07 ± 0.01 when sized on-line. After 6-fold concentration by TFF, size and PDI slightly increased and a subtle variation between both equipment was showed. Whereas the off-line sizer measured a size and a PDI of 63.0 ± 1.0 nm and 0.21 ± 0.01, the on-line sizing measured 66 ± 1 nm and 0.27 ± 0.01 (Fig. 2.16).

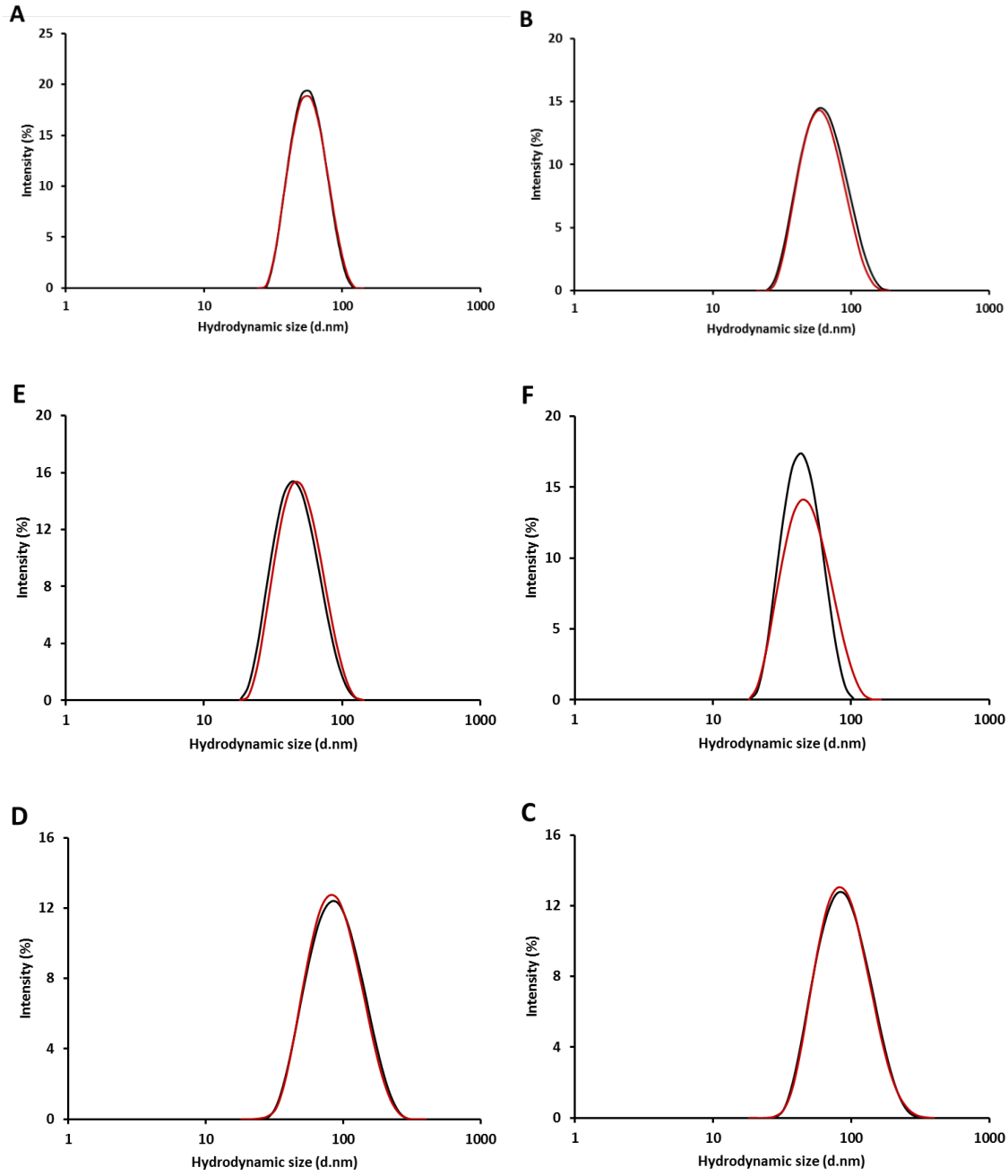

Figure 2.16. Characterisation of liposomes formulated by continuous manufacturing. Size distribution of DSPC:Chol liposomes formulated in Nanoassemblr at 1:1 molar ratio, 6 mg/mL, 3:1 TFR, 15 mL/min in 10 mM TRIS pH 7.4 before **(A)** and after concentration (6-fold) and washing (14-fold) **(B)**. Size distribution of DSPC:Chol liposomes prepared from MLVs and size-reduced in M-110P at 30 KPSI for 5 cycles before **(C)** and after TFF concentration (10-fold) **(D)**. Size distribution of DOPE:DOTAP liposomes formulated in Nanoassmblr at 1:1 molar ratio, 4 mg/mL, 15 mL/min TFR and 10 mM TRIS pH 7.4 before **(E)** and after TFF concentration (6-fold) and washing (14-fold) **(F)**. Samples were characterised both off-line (—) and on-line (—). Plots are represented as the average of three measurements.

DSPC:Chol liposomes prepared by thin lipid film hydration and subsequently processed in the M-110P microfluidizer were 82 ± 1 nm in size with a PDI of 0.19 ± 0.01. When characterised on-line, they had a size and a PDI of 82 ± 1 nm and 0.19 ± 0.01 respectively. Upon TFF concentration, the hydrodynamic size obtained off-line and on-line was 82 ± 1 and 81 ± 1, whereas the PDI was 0.19 ± 0.01 and 0.19 ± 0.02. After TFF concentration, the lipid recovery of DSPC:Chol liposomes by microfluidics and M-110P was 93.2 and 95.4% respectively. The same setup was employed to formulate cationic DOPE:DOTAP liposomes. Liposome size and PDI was 43 ± 1 nm and 0.14 ± 0.01 when measured off-line and 47 ± 0 nm and 0.15 ± 0.01 when measured on-line. After TFF, size and PDI obtained on-line were 42 ± 1 nm and 0.085, while those obtained on-line were 47 ± 1 and 0.21 ± 0.02 respectively. Lipid recovery was 93.3% (Fig. 2.16). Such a design was recently utilised for the rapid and scale-independent manufacture of protein-loaded liposomes and the translation of liposome manufacturing from bench to the clinic (Forbes et al., 2019).

2.4.5. Solvent and protein removal

Microfluidic formulation of liposomes is based on the mixing between an organic (ethanol, methanol) and an aqueous (PBS, TRIS buffer, citrate buffer) phase. Liposomes will then be dispersed in a mixture of organic and aqueous solvent. Traces of organic solvent (up to 50%) must be completely removed, or at least reduced below 0.3% (3000 ppm), as stated by the ICH guidelines, before further *in vitro* or *in vivo* applications. We investigated the ability of dialysis and tangential flow filtration (TFF) to remove traces of organic solvent.

A calibration curve of different methanol concentrations was prepared (Fig. 2.17). Limit of detection (LOD) and limit of quantification (LOQ), calculated according to ICH guideline Q2 (R1): "*Validation of Analytical Procedures: Text and Methodology*" (2005), were 552 and 1672 ppm and therefore was sensitive enough to verify that the samples had less than 3000 pm, as stated by the ICH guidelines.

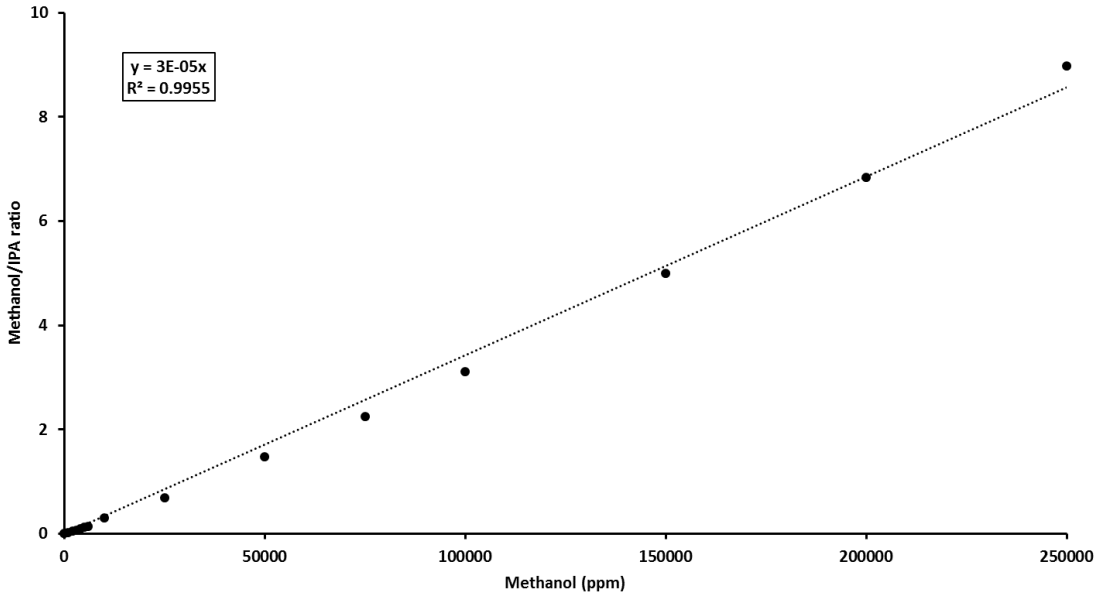

Figure 2.17. Calibration curve for quantification of methanol by head-space gas chromatography. Limit of detection (LOD) and limit of quantification (LOQ) were 552 and 1672 ppm.

TFF allowed to remove methanol below the LOD. As can be seen in Fig. 2.18, the number of washes required to remove methanol concentration below the required ICH guidelines from liposome samples depended on the initial methanol concentration. In contrast to TFF, where the solvent is actively removed by washing, dialysis is based on the passive diffusion of molecules between sample and solvent that stops when an osmotic equilibrium between both systems is reached. Considering that 1 mL sample was dialysed against 200 mL buffer, the 1:1, 3:1 and 5:1 FRR formulations would have a percentage of residual methanol of 0.25, 0.125 and 0.085% respectively. When analysed by head-space gas chromatography, the residual methanol percentage was 0.21 ± 0.04, 0.16 ± 0.06 and 0.10 ± 0.06%, in agreement with theoretical calculations. The hydrodynamic size of non-purified DSPC:Chol liposomes prepared at 1:1, 3:1 and 5:1 FRR was 81, 52 and 48 nm respectively. While after dialysis size was similar (73, 54 and 55 nm), it increased to 89, 85 and 89 nm after TFF. In the same way, the PDI of TFF-purified liposomes augmented from 0.02, 0.10 and 0.13 to 0.17, 0.21 and 0.25 respectively (Fig. 2.18). Increments in size and PDI can be clearly seen in the size distribution plots. Indeed, TFF-purified liposomes exhibited broader size distributions compared to non-purified or dialysed liposomes. Lipid recovery was above 90% for both TFF and dialysis.

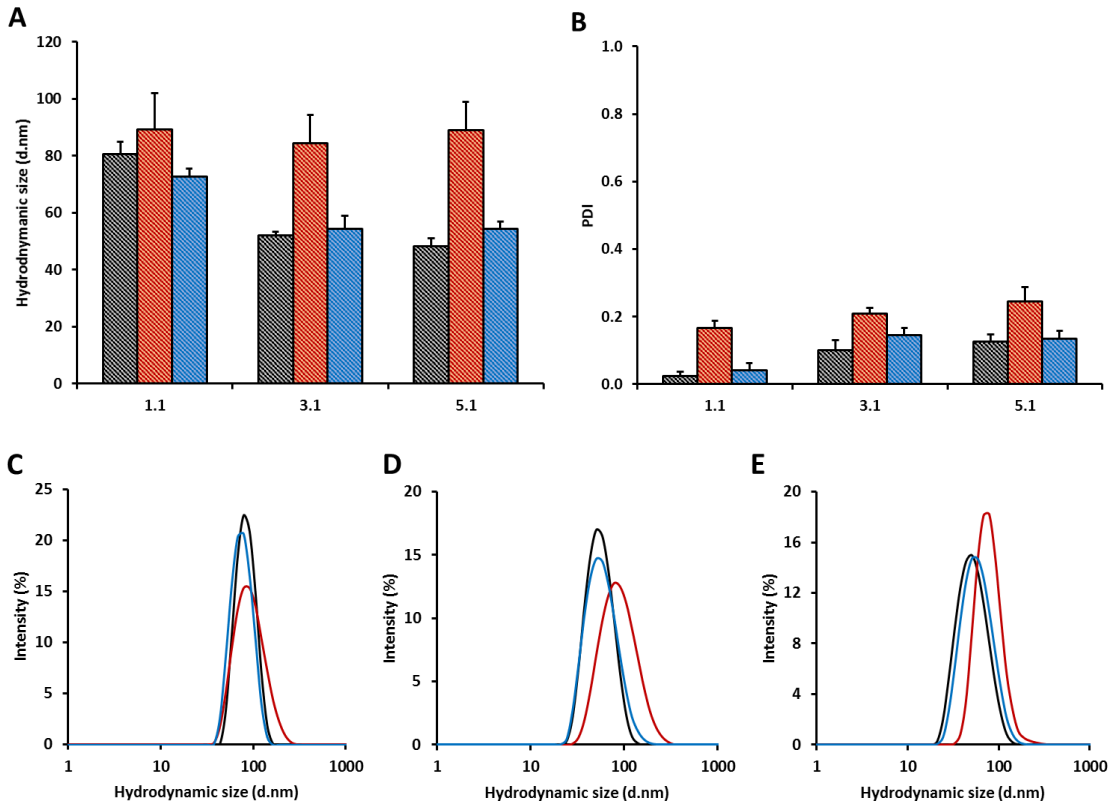

F

Wash (mL)	1:1 FRR (ppm)	3:1 FRR (ppm)	5:1 FRR (ppm)
0	500000*	250000*	170000*
4	122522 ± 23262	89549 ± 4418	49968 ± 4209
8	20334 ± 7436	19578 ± 1931	6990 ± 1801
12	5258 ± 1591	3291 ± 463	378 ± 330 (<LOD)
16	790 ± 1121	275 ± 89 (<LOD)	0 ± 0 (<LOD)
20	0 ± 0 (<LOD)	0 ± 0 (<LOD)	0 ± 0 (<LOD)

Figure 2.18. Physicochemical characterisation of liposomes after solvent removal. DSPC:Chol liposomes were formulated by microfluidics at 1:1 molar ratio, 4 mg/mL at 15 mL/min TFR in 10 mM TRIS pH 7.4 at 1:1, 3:1 and 5:1 FRR, purified by TFF (▨) or dialysis (▨), and characterised by DLS in terms of size **(A)** and PDI **(B)** with respect to non-purified control liposomes (▨) Representative size distribution plots of non-purified (—), TFF-washed (—) and dialysed liposomes (—), formulated by microfluidics at 1:1 **(C)**, 3:1 **(D)** and 5:1 FRR **(E),** are shown. **F)** Validation of solvent removal from DSPC:Chol liposomes (1 mL) by TFF analysed by head-space gas chromatography (HS-GC). Results are represented as mean ± SD of three independent experiments. *Represents estimates of initial concentrations.

Finally, the capacity of TFF to remove protein (ovalbumin, OVA) from liposomes was tested. As expected, the number of washes (1 mL) required to completely remove protein from liposome samples was correlated to the initial protein concentration in the preparation. The number of washes needed to wash 0.9, 0.45, 0.25 and 0.125 mg/mL OVA from liposomes (1 mg/mL) was 15, 10, 8 and 6 (Fig. 2.19). Altogether, these results show the potential use of TFF to remove solvent and protein with minor variation in the physicochemical properties of liposomes and how to implement it in a continuous manufacturing process. These results on AT-line sizing and TFF-purification of liposomes to remove solvent and free-protein are in agreement with those described elsewhere (Forbes et al., 2019).

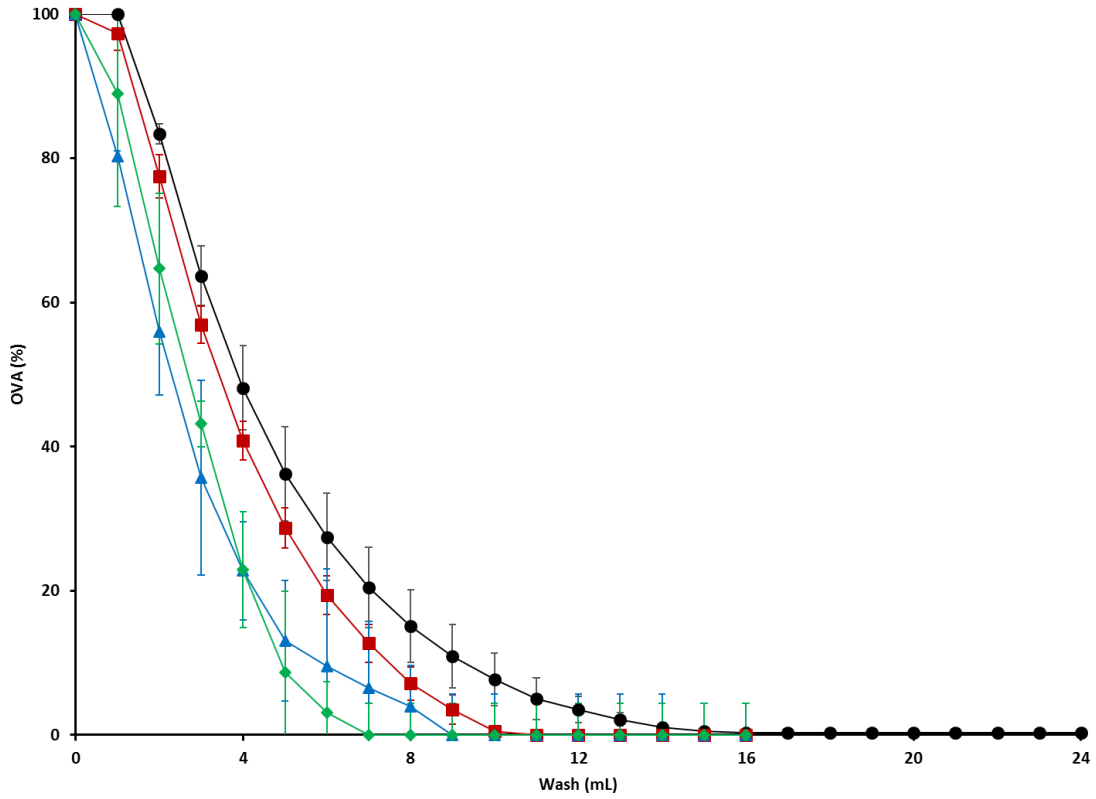

Figure 2.19. Protein removal from liposome formulations by tangential flow filtration (TFF). DSPC:Chol liposomes (2 mL), formulated at 1:1 molar ratio, 4 mg/mL, 3:1 FRR and 15 mL/min. Then, liposomes (1 mg/mL) were mixed with 0.9 (●), 0.45 (■), 0.25 (▲) and 0.125 mg/mL OVA (◆) and washed with PBS in TFF in a 750 KDa pore size mPES column at 27 mL/min rate. Results are represented as mean ± SD of three independent experiments.

2.5. CONCLUSIONS

Herein, a top-down (M-110P microfluidizer) and a bottom-up approach (microfluidic Nanoassemblr Platform) were used to produce liposomes, and a range of operating parameters was evaluated to obtain desired physicochemical attributes. While size and PDI of neutral multilamellar vesicles (MLVs) decreased with increasing number of microfluidisation cycles, neither working temperature nor working pressure had an impact on liposome attributes. Conventional operating parameters, including lipid concentration, total flow rate (TFR) and aqueous:organic flow rate ratio (FRR) were investigated for the microfluidic formulation of liposomes. In general, liposome size and PDI decreased with increasing lipid concentration, while TFR had little to no effect. In contrast, the effect of FRR on liposome attributes were highly dependent on liposome composition. While size of neutral liposomes decreased with increasing FRRs, cationic liposomes could only be formulated at low FRR (1:1).

More importantly, a novel approach to formulate size-tuneable cationic unilamellar liposomes was described. This approach consisted on increasing the ionic strength of the aqueous buffer to be injected in the micromixer. In contrast to the aforementioned operating parameters, which usually allow to obtain liposomes within 30 to 300 nm (depending on the formulation), increasing buffer concentration allowed to obtain liposomes up 750 nm while being homogeneous (PDI < 0.25) and unilamellar, as demonstrated by electron microscopy imaging. Finally, methods for sterilising (filtration and X-rays) and purifying liposomes were validated.

In summary, these techniques were evaluated, validated and optimised to produce liposomes of desired physicochemical attributes, which would then be *tested in vitro* and *in vivo*.

CHAPTER 3: THE EFFECT OF LIPOSOME COMPOSITION AND SIZE: *IN VITRO* AND *IN VIVO* INVESTIGATIONS

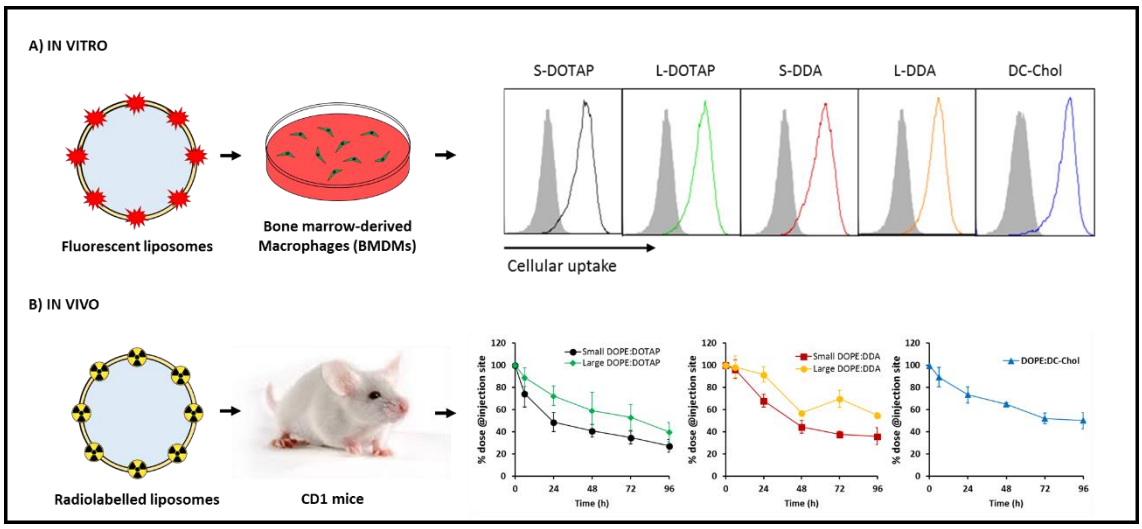

3.1. INTRODUCTION

Both liposome size and surface charge are recognised as important parameters that can influence their cellular uptake. However, there remains a lack of clarity when considering the role of size coupled with charge in relation to the function of liposomal systems, and current manufacturing methods have limited our ability to effectively explore this issue. For example, a relationship between *in vitro* cellular uptake and liposome surface charge has been shown, with charged (anionic and cationic) liposomes being better internalised than neutral ones (Epstein-Barash et al., 2010; Johnstone et al., 2001). Additionally, increasing percentages of charged lipid within the formulation enhances cellular uptake (Dabbas et al., 2008; Takano et al., 2003).

It has been also reported that increasing the size of anionic liposomes from 80 nm up to 600 nm initially increases cellular uptake but by 48 h uptake was similar across all size ranges (Epstein-Barash et al., 2010). In contrast, studies using neutral liposomes have shown the opposite effect. Andar et al. (Andar et al., 2014) explored the cellular uptake mechanisms of neutral liposomes prepared by microfluidics. In their studies, the authors investigated size ranges of 40 to 275 nm and showed that liposome uptake is strongly size dependent, with smaller liposomes having higher uptake and that the uptake mechanisms also varying with size (Andar et al., 2014). In further contrast to this, with cationic formulations it has been previously shown the vesicle size has no impact on cellular uptake (Henriksen-Lacey et al., 2011b).

When considering the effect of surface charge and size on the *in vivo* fate of liposomes, we see the two factors must be considered in combination. For example, cationic liposomes are retained longer at the injection site compared to neutral formulations when administered intramuscularly (Henriksen-Lacey et al., 2011b; Kaur et al., 2012a) or subcutaneously (Carstens et al., 2011; Henriksen-Lacey et al., 2010c). Furthermore, clearance of the cationic liposomes from the injection site was not influenced by particle size when considering particle size ranges from approximately 200 to 3000 nm (Henriksen-Lacey et al., 2011b). Indeed, cationic vesicles aggregate in presence of proteins found within the extracellular matrix at the injection site. These electrostatic interactions resulting from the cationic nature of the liposomes were shown to be more important than the size of the vesicles in terms of clearance from the injection site (Kaur et al., 2012a, b). These electrostatic interactions at the injection site can be avoided by

masking the cationic nature of the liposomes via PEGylation. In the case of liposomes composed of dimethyldioctadecylammonium bromide (DDA) and trehalose 6,6'-dibehenate (TDB) incorporation of 25 mole% PEG was required to block the depot effect and promote drainage to the local lymph node irrespective of the size of the liposomes (120 nm up to 500 nm) (Kaur et al., 2012a) and resulted in difference immune response profiles (Kaur et al., 2012b).

In contrast, with anionic vesicles, the particle size has been shown to play a major role in the intracellular trafficking, processing and presentation of antigens by antigen presenting cells (Brewer et al., 2004) and dictates the type of immune responses. For instance, in a study conducted by Brewer et al., vaccination with liposomes above 225 nm induced IgG2a titres and high production of IFN-γ, characteristic pattern of a Th1 response. In contrast, smaller liposomes (<155 nm) induced a Th2 immune response, as evidenced by the production of IgG1 and IL-5 (Brewer et al., 1998). In another study, 100 nm liposomes induced a Th2 response, while 400 and 1000 nm liposomes induced a Th1 type immune response (Badiee et al., 2012). However, in many of these studies size reduction techniques were used to produce the different particle size populations and thus lamellarity cannot easily be controlled or standardised; with larger vesicles being multilamellar in nature compared to the lower size ranges unilamellar vesicles.

3.2. AIM AND OBJECTIVES

The aim of the work covered within this chapter was to take advantage of the effect of buffer concentration to formulate small (<50 nm) and large (>500 nm) cationic liposomes to investigate the effect of liposome size and composition *in vitro* and *in vivo*. To achieve this, the objectives were the following:

- To make a comparison on the *in vitro* liposome uptake in BMDMs and BMDCs.
- To investigate the effect of liposome composition and size on the *in vitro* cellular uptake in BMDMs.
- To study the *in vivo* biodistribution of cationic liposomes.
- To investigate the effect of liposome composition and size on the *in vivo* biodistribution of liposomes.

3.3. MATERIALS AND METHODS

3.3.1. Materials

1,2-dioleoyl-sn-3-phosphoethanolamine (DOPE) and 1,2-dioleoyl-3-trimethylammonium-propane (DOTAP), dimethyldioctadecylammonium (DDA), and 3ß-[N-(N',N'-dimethylaminoethane)-carbamoyl]cholesterol (DC-Chol) were purchased from Avanti Polar Lipids. 1,1'-dioctadecyl-3,3,3',3'-tetramethylindocarbocyanine perchlorate (Dil-C_{18}) and Alamar Blue were obtained from Thermo Scientific. Dulbecco's Modified Eagle Medium (DMEM), Roswell Park Memorial Institute 1640 medium (RPMI-1640) and foetal bovine serum (FBS) were obtained from Gibco. FITC-labelled anti-F4/80 (clone BM8) and FITC-labelled anti-CD11c (clone N418) monoclonal antibodies were obtained from Biolegend. Cholesterol, [1,2-3H(N)]-, 1 mCi (37 MBq) and Ultima Gold were obtained from Perkin Elmer. Trehalose and hydrogen peroxide 30% v/w were purchased from Acros Organics. Penicillin-streptomycin, L-glutamine, cholesterol (Chol) and pontamine blue was purchased from Sigma.

3.3.2. Formulation of liposomes by microfluidics

Liposomes were prepared in the Nanoassemblr Platform (Precision Nanosystems Inc.) in a Y-shaped staggered herringbone micromixer of 300 µm width and 130 µm height. Briefly, DOPE:DOTAP, DOPE:DDA and DOPE:DC-Chol lipid mixtures were prepared in methanol at 1:1 molar ratio. Then, the lipids and an aqueous phase (TRIS buffer pH 7.4) were injected simultaneously in the micromixer. All formulations were prepared at 4 mg/mL initial lipid concentration, 1:1 aqueous:organic flow rate ratio (FRR) and 15 mL/min total flow rate (TFR). Small DOPE:DOTAP and small DOPE:DDA liposomes were prepared at 10 mM TRIS pH 7.4, large DOPE:DDA liposomes were formulated at 300 mM TRIS pH 7.4 and DOPE:DC-Chol and large DOPE:DOTAP were prepared at 1000 mM TRIS pH 7.4. Newly formed liposomes (1mL) were dialysed against 10 mM TRIS pH 7.4 (200 mL) for 1 hour under magnetic stirring.

3.3.3. Liposome characterisation

Liposomes were characterised in terms of hydrodynamic size (Z-average), polydispersity index (PDI) and surface charge (zeta-potential) by dynamic light scattering (DLS) in a Zetasizer Nano ZS (Malvern, UK) at 0.1-0.2 mg/mL in 10 mM TRIS pH 7.4. Three consecutive measurements were performed at 25 °C.

3.3.4. Bone marrow-derived macrophages (BMDMs)

Bone marrow cells, obtained from femur and tibiae of 6–8-week-old male BALB/c mice, were incubated in petri dishes in macrophage medium: DMEM supplemented with 20% heat inactivated foetal bovine serum (HI-FBS), 0.1 mg/mL penicillin-streptomycin, 4 mM L-glutamine and 20% L-Cell conditioned medium (supernatant obtained from confluent L929 fibroblast cell line) at 37 °C, 95 % humidity and 5% CO_2 in a cell incubator (Panasonic). A total of 4 petri dishes (10 mL) were obtained per mice. At day 2, fresh macrophage medium (10 mL) was added to each petri dish. At day 7, 15 mL of media were removed from each petri dish and were replaced for 15 mL fresh macrophage medium. At day 10, the cells were scraped, washed and cultured in 24-well plates in DMEM supplemented with 10 % HI-FBS, 0.1 mg/mL penicillin-streptomycin and 4 mM L-glutamine (complete DMEM, or cDMEM) at $2 \cdot 10^5$ cells/well and were allowed to adhere for 24 hours at 37 °C and 5% CO_2. The percentage of BMDMs was determined as percentage of $F4/80^+$ cells. F4/80 is a membrane glycoprotein that has been widely used as specific cell marker for murine macrophages (Austyn and Gordon, 1981). Briefly, a total of $2 \cdot 10^5$ cells were incubated with a FITC-labelled anti-$F4/80^+$ monoclonal antibody (1/200 dilution) in FACS buffer (PBS supplemented with 5% FBS) for 30 min at 4 °C and analysed by flow cytometry (FACSCanto, BD Biosciences).

3.3.5. Bone marrow-derived dendritic cells (BMDCs)

Bone marrow cells, obtained from femur and tibiae of 6-8-week-old male BALB/c mice, were incubated in petri dishes in dendritic cell medium: RPMI-1640 supplemented with 10 % heat inactivated foetal bovine serum (HI-FBS), 0.1 mg/mL penicillin-streptomycin, 4 mM L-glutamine and 10% granulocyte-macrophage colony-stimulating factor (GM-CSF, supernatant obtained from confluent geneticin-selected X63 murine mammary tumor cell line) at 37 °C, 95% humidity and 5% CO_2 in a cell incubator (Panasonic). A total of 4 petri dishes (10 mL) were obtained per mice. At day 2, fresh dendritic cell medium (10 mL) was added to each petri dish. At day 5, 10 mL of media were removed from each petri dish and were replaced for 10 mL fresh dendritic cell medium. At day 7, the cells were scraped and cultured in 24-well plates in cDMEM at $2 \cdot 10^5$ cells/well and were allowed to adhere for 24 hours at 37 °C and 5% CO_2. The percentage of BMDCs was determined as percentage of $CD11c^+$ cells. CD11c is the preferred marker for BMDCs

(Inaba et al., 1992). Briefly, a total of $2 \cdot 10^5$ cells were incubated with a FITC-labelled anti-$CD11c^+$ monoclonal antibody (1/200 dilution) for 30 min at 4 °C and analysed by flow cytometry.

3.3.6. *In vitro* cytotoxicity

Cell viability was determined by Alamar Blue assay. Alamar Blue contains a blue-coloured molecule resazurin, which turns into the red-coloured resorufin when chemically reduce and hence can be correlated to metabolic (mitochondrial) activity of cells and, consequently, cell viability (Nakayama et al., 1997). A total of $5 \cdot 10^4$ BMDMs and 10^5 BMDCs were cultured per well in a flat bottom 96-well plate and allowed to adhere for 24 hours at 37 °C and 5% CO_2. Liposomes were then added at concentrations ranging from 0.06 to 1000 µg/mL. Subsequently, Alamar Blue was added to a final concentration of 10% v/v. Cells were incubated for 6 hours at 37 °C and 5% CO_2. Then, the absorbance was measured at 570 and 600 nm in a SpectroMax190 (Molecular Devices). Cell viability (%) was determined as follows:

$$\text{Cell viability (\%)} = \frac{\left[\left(\varepsilon_{\text{OX(600 nm)}}\right) \cdot \left(\text{Abs}_{\text{570 nm}}\right) - \left[\left(\varepsilon_{\text{OX(570 nm)}}\right) \cdot \left(\text{Abs}_{\text{600 nm}}\right)\right.\right.}{\left[\left(\varepsilon_{\text{RED(570 nm)}}\right) \cdot \left(\text{Control Abs}_{\text{600 nm}}\right) - \left[\left(\varepsilon_{\text{RED(600 nm)}}\right) \cdot \left(\text{Abs}_{\text{570 nm}}\right)\right.\right.} \text{ x } 100$$

Where the extinction coefficient of Alamar Blue oxidation (ε_{OX}) and reduction (ε_{RED}) at 570 and 600 nm are: $\varepsilon_{OX(570\ nm)}$ = 80586; $\varepsilon_{OX(600\ nm)}$ = 117216; $\varepsilon_{RED(570\ nm)}$ = 155677; $\varepsilon_{OX(600\ nm)}$ = 14672. TRIS 10 mM pH 7.4 and Triton X-100 (10% w/v) were used as negative and positive controls.

3.3.7. *In vitro* liposome uptake by BMDCs and BMDMs

Liposomes were co-formulated with the lipophilic fluorescent dye Dil-C_{18} (0.2 mol%) to track their cellular uptake. BMDMs and BMDCs were incubated with cationic liposomes (10 µg/mL) for 1, 4 and 24 hours at 37 °C and analysed by flow cytometry. The lipophilic dye Dil-C_{18} can be only incorporated within the lipid bilayer and, therefore, its concentration is constant for unilamellar liposomes regardless of liposome size. Therefore, the liposome fluorescence can be expressed as:

$$\text{Liposome fluorescence} \equiv \text{F}_\text{m} \cdot [\text{Dil} - \text{C}_{18}] \cdot \frac{4}{3} \Pi [\text{r}^3 - (\text{r} - 5)^3] \quad (equation\ 3.1)$$

Where F_m is the fluorescence of Dil-C_{18}, *r* is the liposome radius (estimated by DLS) and *5* is the lipid bilayer thickness (in nm) estimated from cryo-TEM images of unilamellar 40 nm DOPE:DOTAP liposomes. The mean fluorescence intensity quantified by flow cytometry is

proportional to the amount of dye taken up by the macrophages, which is directly proportional to the product of the number of liposomes by liposome fluorescence. Therefore, the relative number of liposomes (N_r), liposome surface (SA_r) area and liposome internal volume (V_r) can be deducted:

$$\text{Relative number of liposomes } (N_r) \equiv \frac{\text{Mean Fluorescence Intensity}}{\frac{4}{3}\Pi[r^3 - (r-5)^3]} \quad (equation\ 3.2)$$

$$\text{Relative liposome surface area } (SA_r) \equiv N_r \cdot 4\Pi r^2 \ (equation\ 3.3)$$

$$\text{Relative liposome internal volume } (V_r) \equiv N_r \cdot \frac{4}{3}\Pi(r-5)^3 \quad (equation\ 3.4)$$

Although no absolute values are obtained with these equations, direct comparisons can be made among liposomes of different size.

3.3.8. Stability studies

Cationic liposomes (small and large DOPE:DOTAP, small and large DOPE:DDA and DOPE:DC-Chol), prepared as described above, were incubated in TRIS/FBS 50:50 v/v in a shaking bath at 37 ˚C. Liposomes were characterised by dynamic light scattering (DLS) at relevant time points.

3.3.9. Quantification of radiolabelling retention

To measure ^{3}H-Chol retention in the liposome bilayer, small and large DOPE:DOTAP liposomes (1 mL), prepared as described above, were placed in a 14 KDa cut off cellulose membrane and dialysed against TRIS/FBS (50:50 v/v, 200 mL). 1 mL aliquots were removed from the dialysis buffer at relevant time points and replaced with 1 mL buffer to maintain sink conditions. 10 mL of Ultima Gold scintillation fluid were added to each sample and radiation was subsequently quantified in a Liquid Scintillation Analyser Tri-Carb 2810 TR (Perkin Elmer).

3.3.10. Biodistribution studies

All *in vivo* studies were conducted under the regulations of the Directive 2010/63/EU. All protocols were subjected to ethical review and were carried out in a designated establishment. The *in vivo* biodistribution of cationic liposomes was studied in 4-5 weeks-old female CD1 mice (20-25 g). Liposomes were radiolabeled with ^{3}H-cholesterol. In brief, ^{3}H-cholesterol was incorporated to the lipid mixture and liposomes were formulated by microfluidics and dialysed

against 10 mM TRIS pH 7.4. Finally, trehalose was added to a final concentration of 10% w/v to maintain isotonicity. Each dose (50 µL) contained 50 µg of DOPE, 50 µg of cationic lipid (DOTAP, DDA or DC-Chol) and 25 ng of ^{3}H-cholesterol (200 KBq/dose). The concentration of cholesterol was low enough not to change the size of liposomes. 3-4 days before injection, mice were injected with 200 µL of Chicago Blue (0.5% w/v) subcutaneously (S.C.) into the neck scruff as a marker for lymph nodes. Formulations were injected (50 µL) intramuscularly (I.M.) in the right quadriceps muscle. Mice were terminated at relevant time points (6, 24, 48, 72 and 96 h) post injection and tissue from the injection site and draining lymph nodes on the side of the injection site were collected for analysis. Samples were solubilised completely in 10 M NaOH (2 mL) at 60 °C overnight and then bleached with 30% w/v H_2O_2 (200 µL) for 2 h at 60 °C. Then, 10 mL of Ultima Gold Scintillation fluid were added and radiation was quantified in a Liquid Scintillation Analyser Tri-Carb 2810 TR (Perkin Elmer). The percentage of injected dose was calculated as:

$$\%\ \text{injected dose} = \frac{\text{counts (cpm) in organ}}{\text{counts (cpm) in original dose}}\ \text{x}\ 100$$

3.3.11. Statistical analysis

Statistical analysis of cellular uptake experiments was performed on the mean of at three replicates by one-way analysis of variance (ANOVA) followed Tukey's honest significance test in GraphPad Prism version 7 (GraphPad Software Inc., La Jolla, CA). To compare the biodistribution of the liposomes, the area under the curve for biodistribution was calculated for each mouse, and the mean calculated. These were then compared using the t-test (Excel) to consider significance ($p<0.05$).

3.4. RESULTS AND DISCUSSION

3.4.1. *In vitro* studies

3.4.1.1. Differentiation of murine bone marrow cells in macrophages and dendritic cells

Antigen presenting cells (APCs), such as macrophages and dendritic cells (DCs), are pivotal in the innate-to-adaptive immune response transition and therefore are perfect candidates to target in vaccine design. Accordingly, we investigated how the composition and size of liposomes influenced the *in vitro* cellular uptake in murine bone marrow-derived macrophages (BMDMs) and dendritic cells (BMDCs).

A method for obtaining BMDMs and BMDCs was implemented as described in materials and methods. Incubation of bone marrow cells in a medium enriched with granulocyte-macrophage colony-stimulating factor (GM-CSF) and macrophage colony-stimulating factor (M-CSF) resulted in differentiation into macrophages; at least 95% of cells were F4/80$^+$ (Fig. 3.1A), a specific cell marker for murine macrophages (Austyn and Gordon, 1981). Differentiation of bone marrow cells into BMDCs upon culture in a GM-CSF enriched medium was less efficient. Only 70-80% of cells were CD11c$^+$ (Fig. 3.1B), the preferred marker for BMDCs (Inaba et al., 1992). This method was therefore used in following *in vitro* experiments.

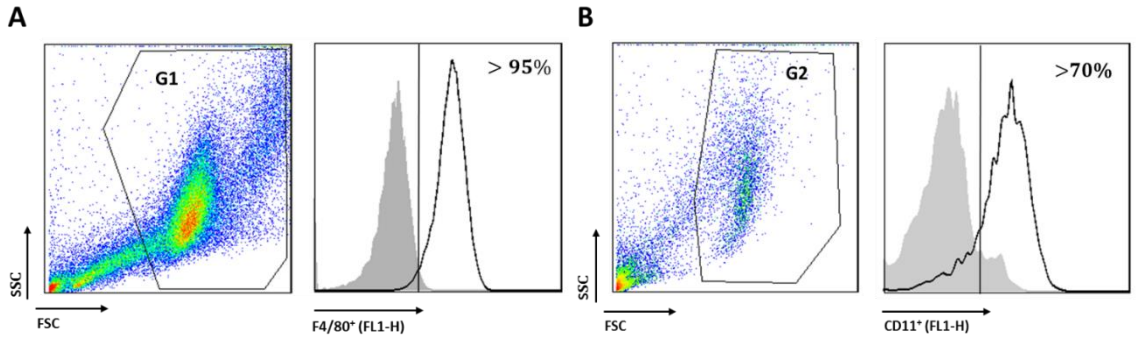

Figure 3.1. Validation of the method used to differentiate murine bone marrow cells into macrophages **(A)** and dendritic cells **(B)**. The percentage of bone marrow-derived macrophages (BMDMs) and bone-marrow-derived dendritic cells (BMDCs) (black) was determined by flow cytometry as percentage of F4/80$^+$ and CD11c$^+$ cells from gates G1 and G2 (FSC – SSC) respectively with respect to unstained cells (shaded grey). The percentage of BMDMs and BMDCs was at least 95% and 70%.

3.4.1.2. Cytotoxicity of cationic liposomes in bone marrow-derived macrophages and dendritic cells

Appropriate (i.e. subtoxic) liposome concentrations for studying the *in vitro* cellular uptake were selected. Cell viability of BMDMs and BMDCs after 24-hour exposure to different concentrations of neutral DSPC:Chol (90 nm) and cationic DOPE:DOTAP (40 nm), DOPE:DDA (40 nm) and DOPE:DC-Chol liposomes (90 nm) is shown in Fig. 3.2. DSPC:Chol liposomes were not toxic to BMDMs or BMDCs at concentrations up to 1000 µg/mL (1500 µM).

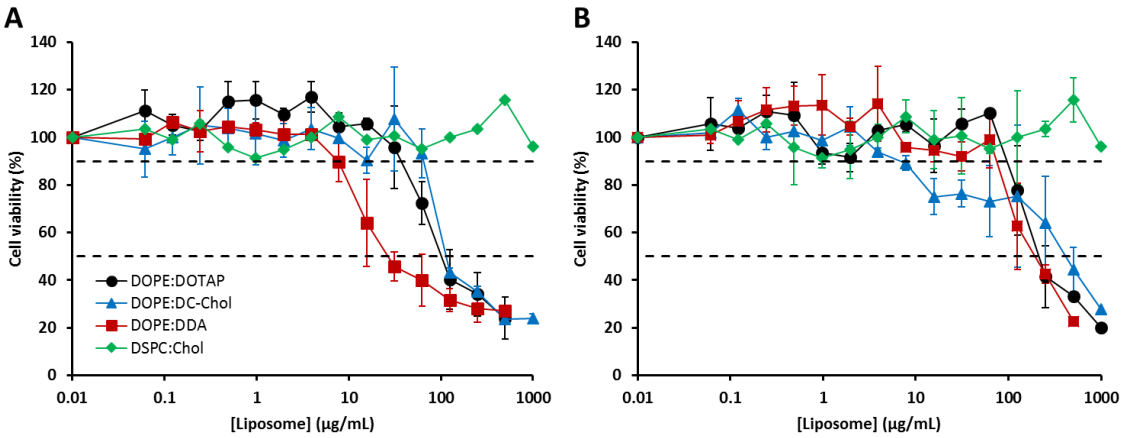

Figure 3.2. *In vitro* cytotoxicity of liposomes in bone marrow-derived macrophages **(A)** and bone marrow-derived dendritic cells **(B)** after 24 hours. 40 nm DOPE:DOTAP (●), 40 nm DOPE:DDA (■), 90 nm DOPE:DC-Chol (▲) and 80 nm DSPC:Chol (◆) liposomes were formulated by microfluidics at 1:1 molar ratio, 4 mg/mL, 1:1 FRR, 15 mL/min TFR and 10 mM TRIS pH 7.4. Results are represented as mean ± SD of three independent experiments.

Cationic liposomes, and cationic nanoparticles in general, strongly interact with negatively charged cellular membranes and hence they are taken up and accumulated in cells and tissues in a greater extent, thus causing increased cytotoxicity *in vitro* and *in vivo* compared to their neutral and anionic counterparts (Kedmi et al., 2010). Moreover, cationic lipids also disrupt the cellular membrane and subcellular compartments causing toxicity (Xu and Szoka, 1996). DOPE is a fusogenic lipid that undergoes a lamellar-to-hexagonal phase transition at acidic pH and leads to destabilisation of lysosomal membrane and, therefore, may also contribute to liposome toxicity. Indeed, the progressive replacement of DOPE with pH-insensitive

dipalmitoylphosphatidycholine (DPPC) in liposomes containing DOTAP did not change the zeta-potential but resulted in reduced toxicity in macrophages (Filion and Phillips, 1997).

Cytotoxicity of cationic lipids strongly depends on liposome size, cationic lipid nature and concentration but also on cell type (Lonez et al., 2012). The cytotoxicity of cationic DOPE:DOTAP, DOPE:DDA and DOPE:DC-Chol liposomes increased with liposome concentration. DOPE:DOTAP and DOPE:DC-Chol liposomes had a calculated half inhibitory concentration 50 (IC50) of approximately 100 μg/mL (150 μM) on BMDMs. DOPE:DDA liposomes were more toxic on BMDMs, with an IC50 of 50 μg/mL (75 μM). Cationic liposomes were less toxic on BMDCs with an IC50 ranging from 200 to 250 μg/mL (280-380 μM) regardless of cationic lipid. A liposome concentration of 10 μg/mL was chosen for cellular uptake experiment (Fig. 3.2).

3.4.1.3. Effect of composition and size on the liposome-cell interactions with antigen presenting cells

In initial studies, the *in vitro* cellular uptake of DOPE:DOTAP (40 nm) and DOPE:DC-Chol liposomes (90 nm) was investigated in BMDMs and BMDCs by flow cytometry. To distinguish between surface-associated and internalised liposomes, experiments were carried out at 4 and 37 °C. At 4 °C, temperature at which endocytosis is inhibited (Goldenthal et al., 1984; Harding et al., 1983), the percentage of DiI-C_{18}^{+} cells (i.e. liposome^{+} cells) was 10-20% after 1 hour and did not increase over time (Fig. 3.3). Therefore, it seems that at 4 °C cationic liposomes were interacting with BMDCs and BMDMs without further internalisation.

Similar percentages of positive cells were observed at 37 °C after 1 hour for both BMDCs (34-42%) and BMDMs (20-30%) thus suggesting that a significant amount of cationic liposomes could be surface-associated rather than internalised. At 37 °C, the percentage of positive BMDCs and BMDMs increased over 65% and 75% respectively after 24 hours (Fig. 3.3), with both formulations showing similar kinetics. The contribution of surface-associated liposomes (given at 4 °C) could be considered negligible after 4 hours and therefore results shown in Fig. 3.3 could be attributed to cellular uptake rather than a combination of surface-associated and internalised liposomes. These findings were in line with other studies showing high cellular uptake of charged (cationic and anionic) liposomes (Epstein-Barash et al., 2010; Johnstone et al., 2001).

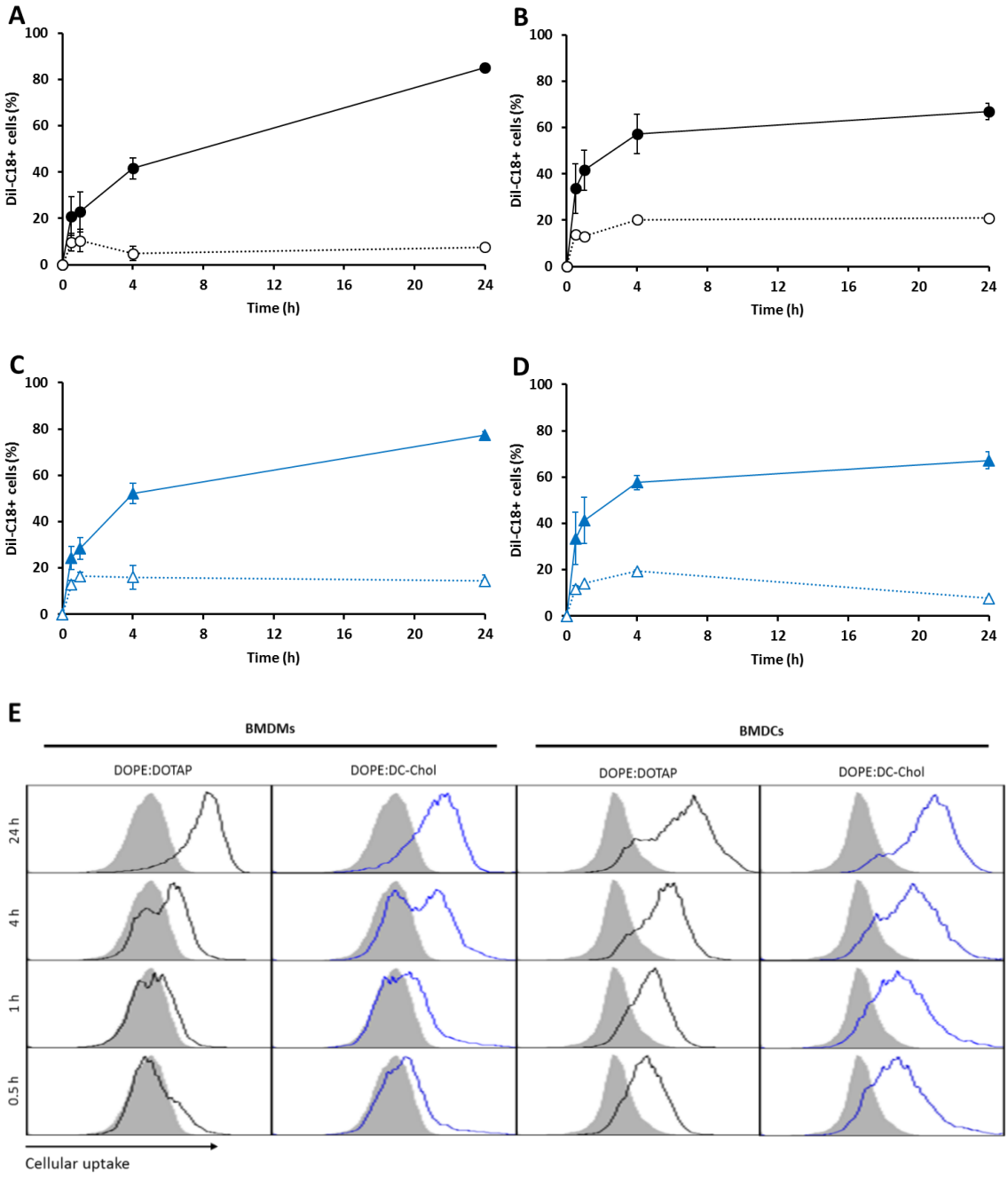

Figure 3.3. *In vitro* cellular uptake of DOPE:DOTAP **(A, B)** and DOPE:DC-Chol liposomes **(C, D)** in bone marrow- derived macrophages **(A, C)** and bone marrow-derived dendritic cells **(B, D)** at 37 ˚C (filled symbols) and 4 ˚C (empty symbols). **C)** Representative flow cytometry plots of cellular uptake of liposomes (DOPE:DOTAP – black, DOPE:DC-Chol – blue) with respect to control cells (shaded grey) at 37 ˚C. The percentage of cellular interaction (adsorption and uptake) was calculated thanks to the fluorescent lipophilic dye Dil-C_{18} anchored within the liposome bilayer.

The higher percentage of positive cells observed on BMDMs after 24 hours could be attributed to an improved differentiation of bone marrow cells into BMDMs (>95%) compared to BMDCs (>70%), as described in Fig. 3.1. Indeed, the *in vitro* differentiation of bone marrow cells with GM-CSF gives rise to a heterogeneous cell population, comprised not only by dendritic cells but also by macrophages and granulocytes (Helft et al., 2015). Granulocytes are less phagocytic than monocytes (Maitz et al., 2017), in such a way that uptake by BMDCs may be underestimated. This was further supported by the shape of the flow cytometry plots in BMDC samples after 24 hours, where a shoulder at lower fluorescence intensity values, potentially attributed to the presence of less phagocytic cells, can be observed (Fig. 3.3E). BMDMs were chosen for subsequent *in vitro* experiments.

To investigate the effect of liposome composition and size on the internalisation in murine bone marrow-derived macrophages (BMDMs), small (<50 nm) and large (>500 nm) cationic unilamellar DOPE:DOTAP and DOPE:DDA liposomes were prepared by microfluidics, as described in Chapter 2. Small DOPE:DOTAP and small DOPE:DDA liposomes had a size of 40-45 nm, while their larger counterparts were 750 and 500 nm in size. 90 nm DOPE:DC-Chol liposomes were also used. All formulations had low PDI (<0.2), high zeta-potential (36-61 mV) and exhibited narrow and unimodal size distribution (Fig. 3.4).

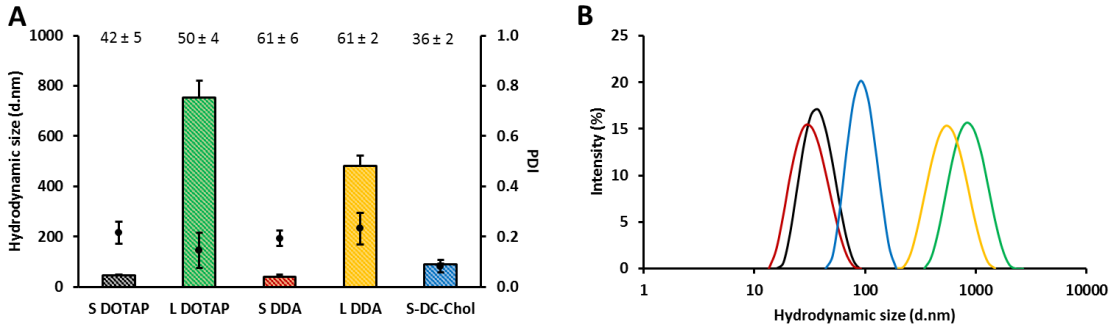

Figure 3.4. Physicochemical characterisation of cationic liposomes for *in vitro* experiments. Small DOPE:DOTAP (▧, —), Large DOPE:DOTAP (▧, —), small DOPE:DDA (▧, —), large DOPE:DDA (▧, —) and small DOPE:DC-Chol liposomes (▧, —) were produced by microfluidics at 1:1 molar ratio, 4 mg/mL, 1:1 FRR, 15 mL/min TFR. Small DOPE:DOTAP and small DOPE:DDA were formulated at 10 mM TRIS pH 7.4, large DOPE:DDA was formulated at 300 mM TRIS pH 7.4 and large DOPE:DOTAP and DOPE:DC-Chol were formulated at 1000 mM TRIS. **A)** Liposomes were dialysed and characterised by DLS in terms of size (bars), PDI (dots) and zeta-potential (values, in mV). **B)** Representative size distribution plots of liposome formulations. Results are represented as mean ± SD of three independent experiments.

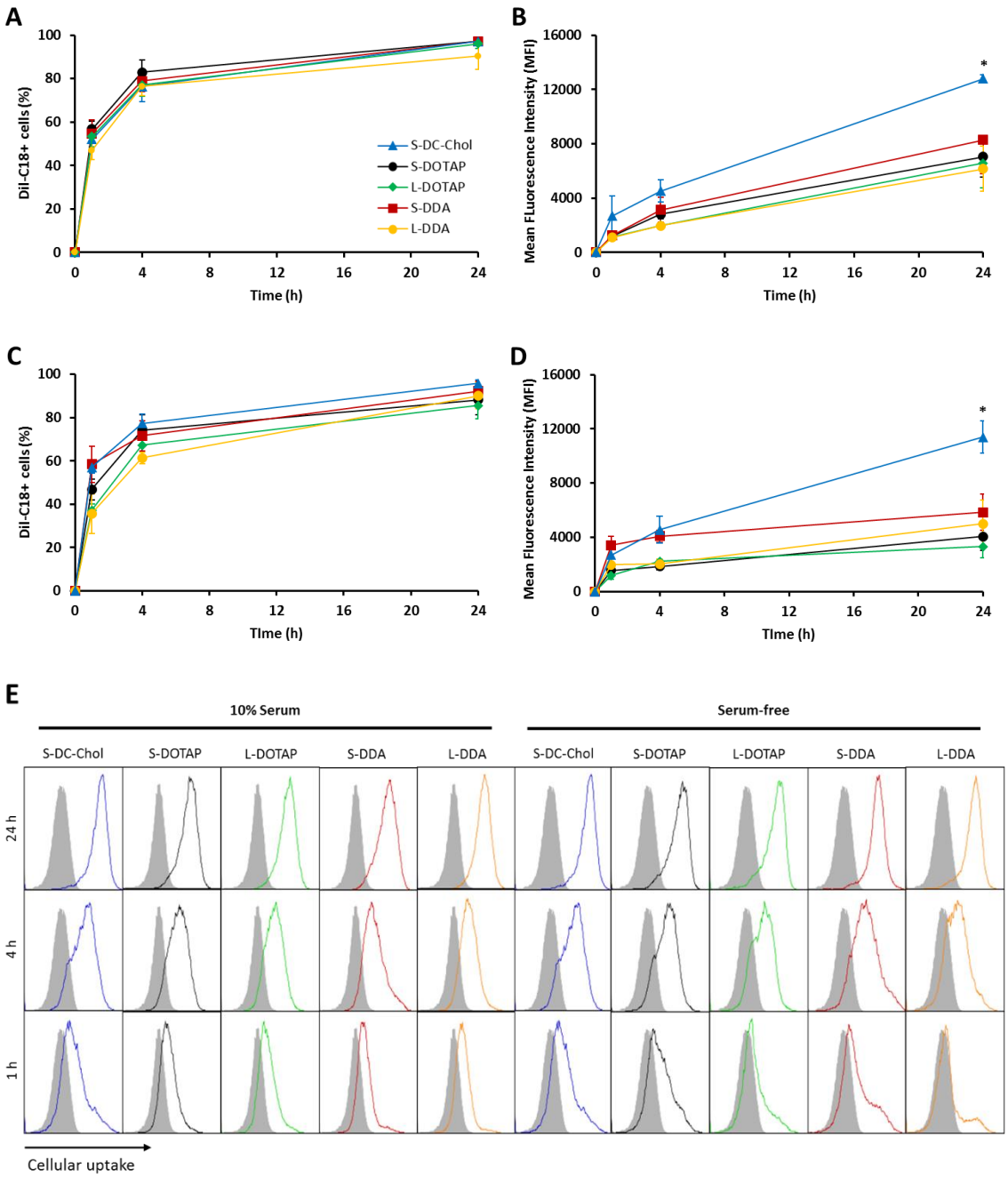

Figure 3.5. The effect of composition and size on the *in vitro* cellular uptake of cationic liposomes in BMDMs at 37 ˚C in DMEM + 10 % FBS **(A, B)** and serum-free DMEM **(C, D)**. Cellular uptake is represented in terms of percentage of Dil-C_{18}^{+} cells (surface-bonded or internalised liposomes) **(A, C)** and Mean Fluorescence Intensity **(B, D)**. **(E)** Representative flow cytometry plots of liposome uptake (colored) with respect to control cells (shaded grey). Small DOPE:DOTAP (●), small DOPE:DDA (■), small DOPE:DC-Chol (▲), large DOPE:DOTAP (◆) and large DOPE:DDA liposomes (●). Results are represented as mean ± SD of 3 independent experiments. Statistical analysis was performed by one-way ANOVA followed by Tukey test. Statistical significance of DC-Chol liposomes with respect to small DOTAP and DDA liposomes: $p < 0.05$ (*).

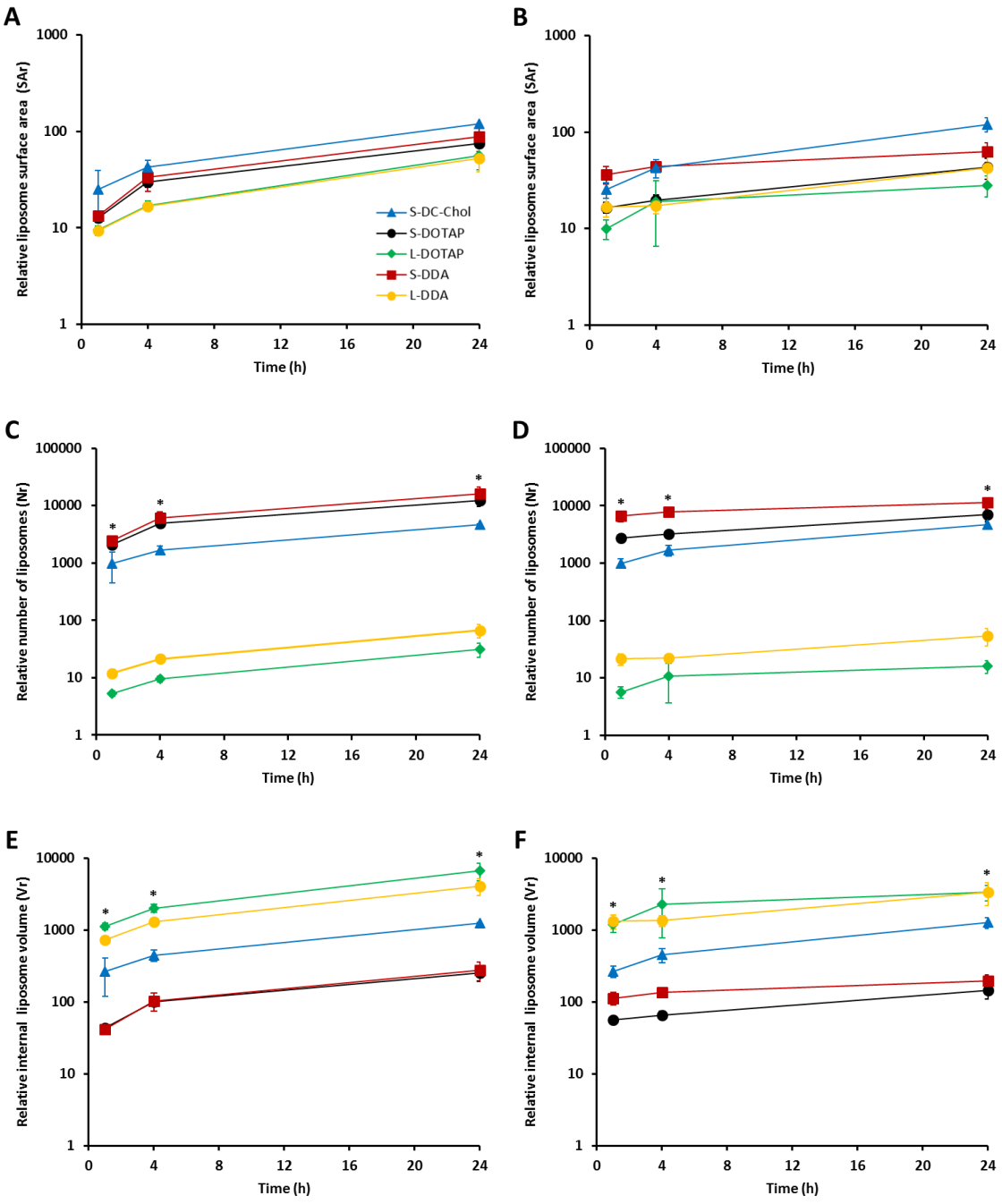

Figure 3.6. Effect of composition and size on the *in vitro* cellular uptake of cationic liposomes in BMDMs at 37 ˚C in DMEM + 10 % FBS **(A, C, E)** and serum-free DMEM **(B, D, F)**. in terms of relative liposome surface area (SA_r) **(A, B)**, number of liposomes (N_r) **(C, D)** and internal liposome volume (V_r) **(E,F)**. Small DOPE:DOTAP (●), small DOPE:DDA (■), small DOPE:DC-Chol (▲), large DOPE:DOTAP (◆) and large DOPE:DDA liposomes (●). Results are represented as mean ± SD of 3 independent experiments. Statistical analysis was performed by one-way ANOVA followed by Tukey test. Statistical significance of small (DOTAP and DDA) liposomes with respect to large (DOTAP and DDA) liposomes: $p < 0.05$ (*).

In presence of serum (10 %), cationic liposomes were readily taken up by BMDMs, with approximately 50 % liposome$^+$ cells after 1 hour. The percentage of liposome$^+$ cells increased in a similar manner over time regardless of liposome composition and size (Fig. 3.5A). The mean fluorescence intensity (MFI), which is proportional to the liposome dose, also increased over time, with no differences observed among small (<50 nm) and large (>500 nm) DOPE:DOTAP and DOPE:DDA liposomes. However, the MFI of DOPE:DC-Chol liposomes (90 nm) was significantly higher ($p<0.05$) compared to DOPE:DOTAP and DOPE:DDA liposomes of comparable (40-45 nm) size (Fig. 3.5B). In absence of serum, similar internalisation kinetics were observed on both the percentage of positive cells (Fig 3.5C) and MFI (Fig 3.5D), as observed elsewhere (Johnstone et al., 2001). Again, DC-Chol liposomes showed improved uptake compared to DOTAP and DDA liposomes, while increasing liposome size had no effect.

Several studies have highlighted a relationship between liposome composition and cellular uptake. For example, in a recent study conducted on triple negative breast cancer cells, Abumanhal-Masarweh and co-workers reported an improved liposome internalisation with increasing acyl chain length and unsaturation of lipids. Furthermore, cellular uptake was also modulated by the head group of the lipids, with phosphatidylethanolamine (PE) and phosphatidic acid (PA) resulting in highest cellular uptake. Finally, incorporation of cholesterol resulted in enhanced uptake of DMPC liposomes but restrained uptake of HSPC liposomes (Abumanhal-Masarweh et al., 2019). In another study, silencing RNA (siRNA)-based ionisable lipid nanoparticles (LNPs) containing the lipid 1,2-dilinoleyloxy-3-dimethylaminopropane (DLin-DMA) were taken up in a greater extent compared to other siRNA-LNPs composed of other ionisable lipids such as heptatriaconta-6,9,28,31-tetraen-19-yl 4-(dimethylamino) butanoate (DLin-MC3-DMA), and 2,2-dilinoleyl-4-(2-dimethylaminoethyl)-[1,3]-dioxolane (DLin-KC2-DMA). Moreover, substitution of phosphatidylcholine for DOPE resulted in reduced cellular uptake. (Kulkarni et al., 2017).

Regarding liposome size, these results are opposite to previous investigations, where cellular uptake was reported to increase with increasing liposome size (Chono et al., 2006a; Chono et al., 2010; Chono et al., 2006b; Hsu and Juliano, 1982). However, it should be considered that in those studies liposomes were prepared by lipid film hydration followed by extrusion and therefore the degree of lamellarity was not controlled. Furthermore, in some cases liposome uptake was

quantified by radio-counting a radiolabelled non-exchangeable lipid and hence the cellular uptake of large liposomes may have been overestimated because of liposome lamellarity. For instance, the amount of 1000 nm liposomes taken up by peritoneal macrophages *in vitro* (ng lipid per µg protein) was shown to be 2-fold lower compared to MLVs of comparable size (Hsu and Juliano, 1982).

BMDM uptake was also analysed in terms of relative number of liposomes (N_r), relative liposome surface area (SA_r) and relative liposome internal volume (V_r) (Fig. 3.6). Differences in SA_r among formulations were similar to those observed in the MFI, as already expected (Fig. 3.6A and B). Indeed, SA_r would be directly proportional to MFI if bilayer thickness (5 nm) had been neglected. However, it was considered in the model as bilayer thickness constitutes at least 20% of the total diameter of small DOPE:DOTAP and DOPE:DDA liposomes (having an hydrodynamic radius below 25 nm). The effect of liposome size on BMDM uptake became more evident when looking at N_r and V_r, which decreased (>200-fold) and increased (>10-fold) respectively by increasing liposome size from 40 to >500 nm (Fig. 3.6 C to F). N_r and V_r of 90 nm DOPE:DC-Chol liposomes were in between those of <50 nm and >500 nm DOPE:DOTAP and DOPE:DDA liposomes. As already observed in Fig. 3.5, no differences were observed in presence or absence of serum.

A microfluidic-based approach was also used elsewhere to show that the cellular uptake of uniform (PDI < 0.05) unilamellar liposomes, ranging from 40 to 275 nm, improved (in terms of number of internalised liposomes) with reducing liposome size in the Caco-2 cell line (Andar et al., 2014). Similar results were observed in mouse peritoneal macrophages by Hsu and Juliano (Hsu and Juliano, 1982) and Schwendener et al. (Schwendener et al., 1984). In the first study, uptake of small unilamellar liposomes (35 nm) was 100-fold higher, in terms of liposome number, compared to 1000 nm liposomes, but 100-fold lower when represented as internal volume. In the second study, reducing liposome size from 180 to 25 nm resulted in 100-fold increase of cell-associated vesicles but 10-fold reduction in trapped volume.

3.4.2. *In vivo* studies

3.4.2.1. Development of methods for studying liposome biodistribution

So as to follow the movement of liposomes *in vivo*, a non-exchangeable radioactive tracer (^{3}H-Chol) was incorporated within the liposome bilayer. Liposomes were formulated at 4 mg/mLDOPE:Cationic Lipid (DOTAP, DDA, DC-Chol) in presence of 1 µg/mL ^{3}H-Chol in such a way that each 50 µL dose would contain 50 µg DOPE, 50 µg cationic lipid (DOTAP, DDA, DC-Chol) and 25 ng ^{3}H-Chol (200 KBq). Such amount of radiation (25 ng, 200 KBq) per dose was selected, based on previous studies (Henriksen-Lacey et al., 2010a), would be high enough to allow effective radio-counting but low enough not to change the physicochemical properties of liposomes. As shown in Fig. 3.7, neither size nor PDI of small/large cationic liposomes was influenced by the incorporation of Chol at this level and the molar ratio adopted was below what would be expected to modify any bilayer properties.

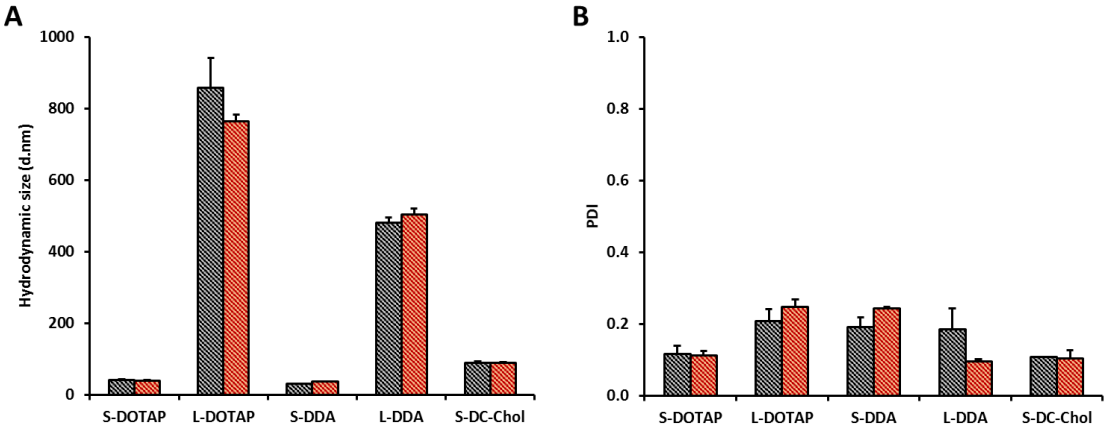

Figure 3.7. The effect of cholesterol incorporation on liposome attributes. Small and large DOPE:DOTAP, small and large DOPE:DDA and DOPE:DC-Chol liposomes were prepared at 1:1 molar ratio at 4 mg/mL in presence (▨) or absence of 1 µg/mL Chol (▧), 1:1 FRR and 15 mL/min TFR. In this way, a 50 µL dose would contain 50 µg DOPE, 50 µg cationic lipid (DOTAP, DDA, DC-Chol) and 25 ng Chol. Liposomes were then dialysed and characterised by DLS in terms of size **(A)** and PDI **(B)**. Results are represented as mean ± SD of three independent experiments.

The ability of ^{3}H-Chol to remain in the liposome bilayer was investigated so as to investigate whether quantification of the radioisotope could directly be correlated to liposome dose rather than to free radioisotope. For this purpose, a release study of ^{3}H-Chol was carried out in *in vivo*

simulated conditions (TRIS:FBS 50:50% v/v, 37 ˚C). Liposomes were placed in a cellulose membrane and dialysed for 168 hours (7 days). The pore size of the membrane was 14 KDa (approximately 2 nm), thus allowing the movement of free ^{3}H-Chol while retaining liposomes (>40 nm). The percentage of cumulative radiation loss was below 1% after 7 days for both small and large DOPE:DOTAP liposomes (Fig. 3.8A). Release of ^{3}H-DPPC in the same experimental conditions from DDA:TDB liposomes was below 10% over 96 hours (Henriksen-Lacey et al., 2010a).

Upon administration *in vivo*, liposomes, and nanoparticles in general, readily interact with biological components such as proteins and cells. These interactions are governed by the physicochemical properties of the nanoparticles (i.e. size, shape, hydrophobicity/hydrophilicity, surface charge, surface functionalisation, etc.) and therefore ultimately dictate the fate and the activity of the nanoparticles (Masoud Rahman, 2013). Most serum proteins have low isoelectric point (IEP) and hence are negatively charged at physiological pH (Latner, 1977); so that interaction with cationic liposomes is expected.

The stability of cationic liposomes in *in vivo* simulated conditions (50 % FBS, 37 ˚C) was investigated over 168 hours (7 days) (Fig. 3.8B to D). The zeta-potential of all liposome formulations (>30 mV) readily turned negative (-15 mV) in presence of serum proteins. The size of small DOTAP and DDA liposomes increased from 40 to 70-100 nm respectively after 1 hour and further increased above 200 nm after 72 hours. Their PDI (<0.25) increased above 0.5 after 24 and 72 hours respectively.

The hydrodynamic size of large DOTAP and DDA liposomes (>500 nm) remained unchanged over the first 48 hours but increased at later time points, while their PDI rapidly increased above 0.5 after 1 hour. Indeed, secondary peaks were observed in the DLS size distribution plots of large liposomes at lower intensity-weighted values (<100 nm), and could be attributed to free serum proteins or protein aggregates, potentially overestimating aggregation of large liposomes when measured by DLS. For small DOTAP and DDA liposomes these proteins would not account for increased PDI because they would scatter light in a similar extent. Finally, the size and PDI of DOPE:DC-Chol liposomes exponentially increased from 80 and 0.1 to over 800 nm and 0.5 readily after exposure to serum proteins.

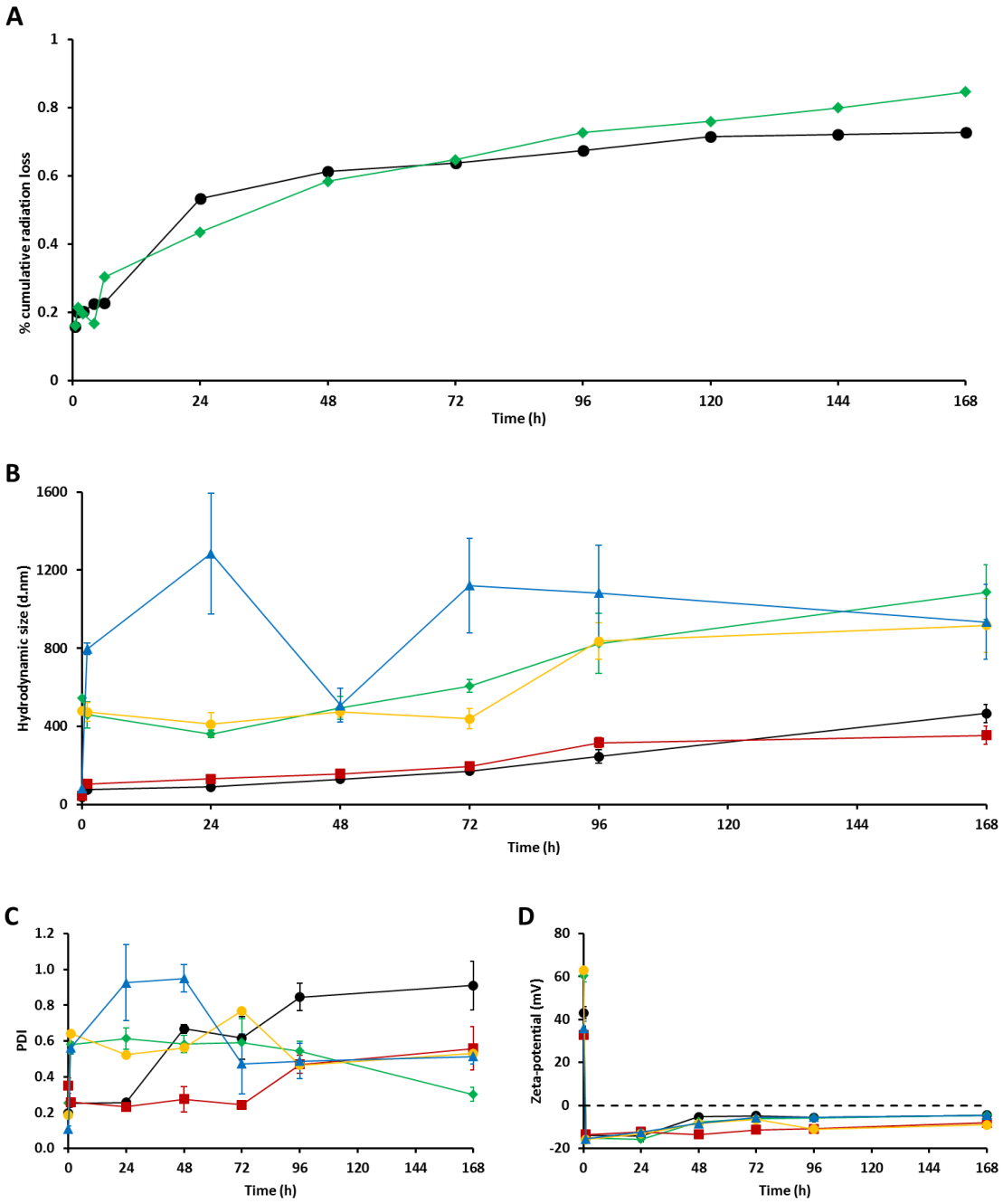

Figure 3.8. (A) Retention of the radioactive marker ^{3}H-Chol in liposome bilayer of small (●) and large (♦) DOPE:DOTAP liposomes. Liposomes were formulated by microfluidics and then were dialysed against TRIS:FBS (50:50 v/v) at 37 ˚C for 168 hours (7 days). **(B-D)** Stability of cationic liposomes in *in vivo* simulated conditions. Small DOPE:DOTAP (●), large DOPE:DOTAP (♦), small DOPE:DDA (■), large DOPE:DDA (●) and DOPE:DC-Chol (▲) were formulated by microfluidics, dialysed and incubated in TRIS/FBS (50:50 v/v) at 37 ˚C under shaking and characterised at relevant time points by DLS in terms of size **(C)**, PDI **(B)** and zeta-potential **(C)**. Results are represented as mean ± SD of three replicates.

Similar findings were reported on DOTAP:Chol lipoplexes by Xu et al. The exposure of these liposomes to FBS resulted in an increase in size from 195 to 235 nm and reduced zeta-potential from +46 mV to -16 mV due to the association of negatively charged serum proteins with the cationic lipids. Moreover, lipoplex PEGylation with DSG-PEG2000 (0.4 mole%) did not inhibit the formation of the protein corona around the lipoplexes (Xu et al., 2011), probably due to uncomplete lipoplex PEG coating. These interactions result in aggregation of cationic liposomes upon administration *in vivo* leading to the formation of a depot effect at the injection site (Henriksen-Lacey et al., 2011a).

3.4.2.3. The effect of composition and particle size on liposome pharmacokinetics

The local injection of liposome-based vaccines (in muscle, skin, etc.) triggers a series of events, including inflammation and recruitment of cells from the innate immune system. Either by a cell-free or cell-mediated mechanism, liposomes are eventually cleared from the injection site and transported to the secondary lymphoid tissues (lymph nodes), with clearance rates depending on surface charge (Henriksen-Lacey et al., 2010c), size (Allen and Everest, 1983; Brewer et al., 1998), hydrophilicity/hydrophobicity (Kaur et al., 2012b) and lamellarity (Betageri and Parsons, 1992). There, activated antigen presenting cells (either resident or not) can present the antigen epitopes to B and T cells and activate them. Consequently, it is essential to activate cells from the immune system (macrophages and dendritic cells) and to deliver the antigen to the lymph nodes. Indeed, a direct correlation between liposome biodistribution and immunogenicity has been reported. (Schmidt et al., 2016). Therefore, liposome biodistribution investigations are crucial in vaccine deign.

The ability of the cationic liposome formulations to move *in vivo* was therefore investigated. The biodistribution of small DOPE:DOTAP and DOPE:DDA (<50 nm), DOPE:DC-Chol (<100 nm) and large DOPE:DOTAP and DOPE:DDA (>500 nm) upon intramuscular injection was monitored in CD1 mice over a period of 96 hours. The physicochemical properties of liposomal formulations used for *in vivo* investigations were in line with those of the cationic liposomes investigated *in vitro* (Fig. 3.4). As can be seen in Fig. 3.9, small DOPE:DOTAP and DOPE:DDA liposomes were 35-40 nm in size, while their larger counterparts were 750 and 500 nm respectively. DOPE:DC-Chol liposomes were 83 nm in size. All formulations had low PDI (<0.25) and highly positive zeta-

potential (34-61 mV) with narrow and unimodal size distribution. To compare biodistribution profiles, the area under the curve (AUC) was calculated and the mean AUCs were compared.

Sub-50 nm DOPE:DOTAP and DOPE:DDA liposomes were cleared from the injection site more rapidly than their larger counterparts. For example, with the DDA formulation, 92% of large liposomes were retained at the injection site after 24 h compared to 68% with the small liposomes. This difference continues over 96 h with 54% and 36% of large and small vesicles respectively remaining at the injection site (Fig. 10B).

These differences were significant ($p<0.05$) when comparing the AUC for both the cationic lipids, with the smaller liposome formulations having a significantly lower AUC than their larger formulation counterparts (3847 vs 5462 %Dose·h for small and large DOTAP liposomes and 4689 vs 6402 %Dose·h for small and large DDA). Similarly, when comparing the distribution of these liposomes to the local draining lymph nodes, we see the smaller liposomes showing an increased accumulation at both the popliteal LN (Fig. D and E) and inguinal LN (Fig. G and H) with significantly higher ($p<0.05$) AUC for smaller liposomes (irrespective of the lipid choice) at both lymph nodes. However, across all formulations, only low levels (<0.6%) of the dose injected was measured at both the popliteal and inguinal LN irrespective of liposome composition and size.

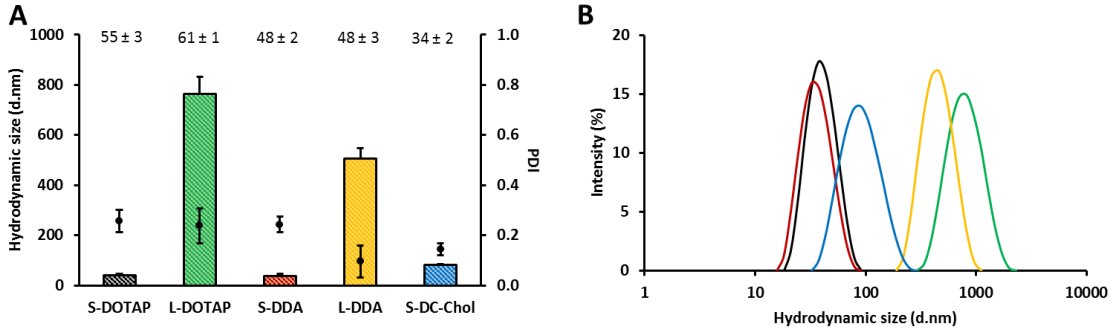

Figure 3.9. Physicochemical characterisation of cationic liposomes for *in vivo* biodistribution experiments. Small DOPE:DOTAP (▧, —), Large DOPE:DOTAP (▧, —), small DOPE:DDA (▧, —), large DOPE:DDA (▧, —) and small DOPE:DC-Chol liposomes (▧, —) were formulated by microfluidics at 1:1 molar ratio, 4 mg/mL in presence of 1 µg/mL chol, 1:1 FRR, 15 mL/min TFR. Small DOPE:DOTAP and small DOPE:DDA were formulated at 10 mM TRIS pH 7.4, large DOPE:DDA was formulated at 300 mM TRIS pH 7.4 and large DOPE:DOTAP and DOPE:DC-Chol were formulated at 1000 mM TRIS. **(A)** Liposomes were dialysed and characterised by DLS in terms of size (bars), PDI (dots) and zeta-potential (values). **(B)** Representative size distribution plots of liposome formulations. Results are represented as mean ± SD of three consecutive DLS measurements.

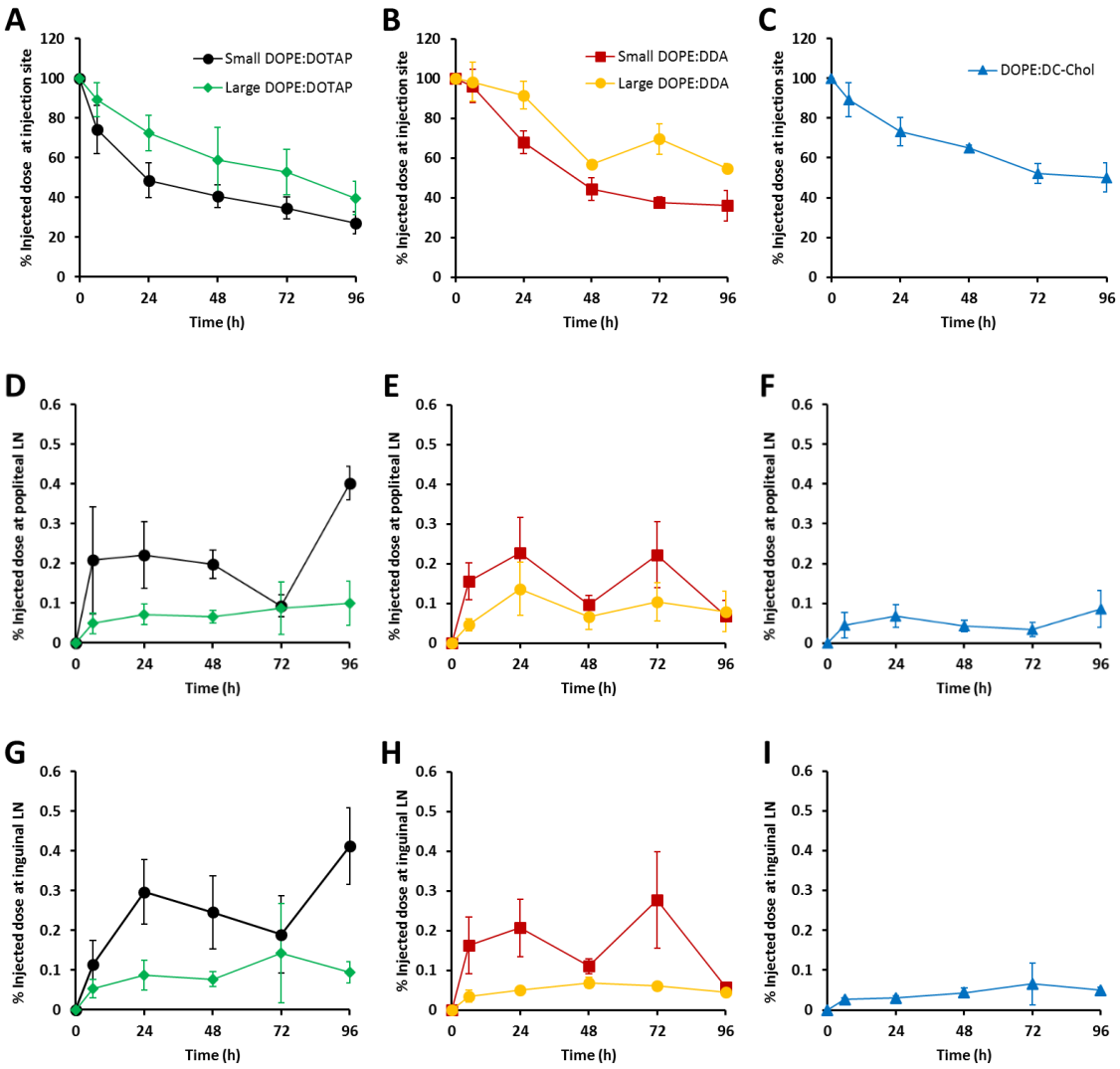

J

AUC (%Dose·h)			
Formulation	**Injection site**	**Popliteal LN**	**Inguinal LN**
Small DOTAP (●)	3847 ± 279	19 ± 2	24 ± 5
Large DOTAP (◆)	5462 ± 972	7 ± 2	10 ± 4
Small DDA (■)	4689 ± 307	13 ± 2	15 ± 4
Large DDA (●)	6402 ± 399	8 ± 2	5 ± 0
Small DC-Chol (▲)	5753 ± 233	5 ± 1	4 ± 2

Figure 3.10. Effect of composition and size on the *in vivo* biodistribution of cationic liposomes in mice. The percentage of injected dose of DOPE:DOTAP **(A, D, G)**, DOPE:DDA **(B, E, H)** and DOPE:DC-Chol liposomes **(C, E, I)** was analysed at the injection site **(A-C)**, popliteal lymph node **(D-F)** and inguinal lymph node **(G-I)**. Small DOPE:DOTAP (●), large DOPE:DOTAP (◆), small DOPE:DDA (■), large DOPE:DDA liposomes (●), small DOPE:DC-Chol (▲). Results are represented as mean ± SD of 4 ± 1 mice. **(J)** AUC for each of the sites.

Studies performed with the vaccine adjuvant CAF01, composed of DDA and trehalose 6,6'-dibehenate (TDB), and its associated antigen (Ag85B-ESAT-6) revealed that cationic liposomes from 200 to >2000 nm exhibited similar clearance rates from the injection site upon intramuscular injection (Henriksen-Lacey et al., 2011b; Kaur et al., 2012a). Furthermore, to promote clearance from the injection site of this formulation, both size reduction and PEGylation was required (Kaur et al., 2012a). However, it has previously been difficult to achieve the production of cationic liposomes in the size ranges achieved within this chapter and these results suggest that by formulating these highly cationic liposomes down to 40 nm allows to modify their pharmacokinetic profile after intramuscular injection. Recent studies looking at the biodistribution of cationic chitosan nanocapsules after sub-cutaneous administration, reported that 100 nm particles were drained more rapidly to the lymph nodes than those of 200 nm and this size reduction also improved interaction with both migratory and resident antigen presenting cells in the lymph nodes, suggesting a combination of free- and cell-mediated transport to the lymph nodes (Cordeiro et al., 2019). This could explain why similar pharmacokinetic profiles were observed for CAF01 formulated at different sizes, since none of the formulations were below 100 nm. Indeed, depletion of dendritic cells *in vivo* completely abolished trafficking of 500 nm polystyrene particles to the LN but not affected drainage of 20 nm particles (Manolova et al., 2008) (Bachmann and Jennings, 2010).

When comparing biodistribution profiles of liposomes of comparable size, similar clearance kinetics from the injection site and lymphatic drainage are observed for large (>500 nm) DOPE:DOTAP and DOPE:DDA. However, significant differences are observed among sub-100 nm cationic liposomes. 90 nm DOPE:DC-Chol liposomes exhibited significantly improved retention ($p<0.05$) at the injection site compared to 40 nm DOPE:DDA liposomes, which, at the same were better retained than 40 nm DOPE:DOTAP liposomes (5753 vs 4689 vs 3847 %Dose·h for DC-Chol, DDA and DOTAP liposomes). In contrast, the opposite trend was observed in the kinetics of lymphatic drainage. Accumulation in the popliteal and inguinal lymph nodes followed the order DOPE:DOTAP > DOPE:DDA > DOPE:DC-Chol. Indeed, 90 nm DOPE:DC-Chol liposomes exhibited similar biodistribution profiles than >500 nm DOPE:DOTAP and DOPE:DDA liposomes.

3.5. CONCLUSIONS

The suitability of liposomes as vaccine adjuvants is governed by their physicochemical properties, as they modulate their ability to interact with antigen presenting cells and to deliver the antigen to the secondary lymphoid tissue. Herein, a panel of formulations of different composition lipids (DOPE:DOTAP, DOPE:DDA and DOPE:DC-Chol) and size (<100 nm and >500 nm) were investigated *in vitro* and *in vivo*. All cationic liposome formulations were avidly taken up by $F4/80^+$ bone marrow-derived macrophages (BMDMs) and $CD11c^+$ bone marrow-derived dendritic cells (BMDCs). In BMDMs, DOPE:DC-Chol liposomes were internalised at significantly greater extent compared to sub-100 nm DOPE:DOTAP and DOPE:DDA liposomes. A size-dependent trend was also observed in the cellular uptake when represented in terms of liposome number, liposome surface area and liposome internal volume; with less number of particles but higher internal volume being delivered by >500 nm liposomes.

Both composition and size had important consequences on the biodistribution after intramuscular injection. All liposome formulations were well retained at the injection site, with over 50% of the injected dose after 2 days. However, small DOPE:DOTAP and DOPE:DDA liposomes were cleared faster from the injection site compared to their larger counterparts but showing improved drainage to the local lymph nodes over 96 hours. Despite their reduced size, DOPE:DC-Chol liposomes (90 nm) exhibited a great depot effect and slow clearance from the injection site and low drainage to the local lymph nodes. This biodistribution pharmacokinetics could highly influence the quality of the immune response, as has been previously reported with other lipid-based adjuvants (e.g. MF59 and CAF01).

In summary, these experiments allowed to better understand the interaction between cationic liposomes and antigen presenting cells *in vitro* and mice *in vivo*. Following chapters will be focused on the design and development of cationic lipid nanoparticles, based on these cationic lipid formulations, to deliver a self-amplifying RNA (SAM) vaccine.

CHAPTER 4: DESIGN OF CATIONIC LIPID NANOPARTICLES TO DELIVER A SELF-AMPLIFYING RNA VACCINE

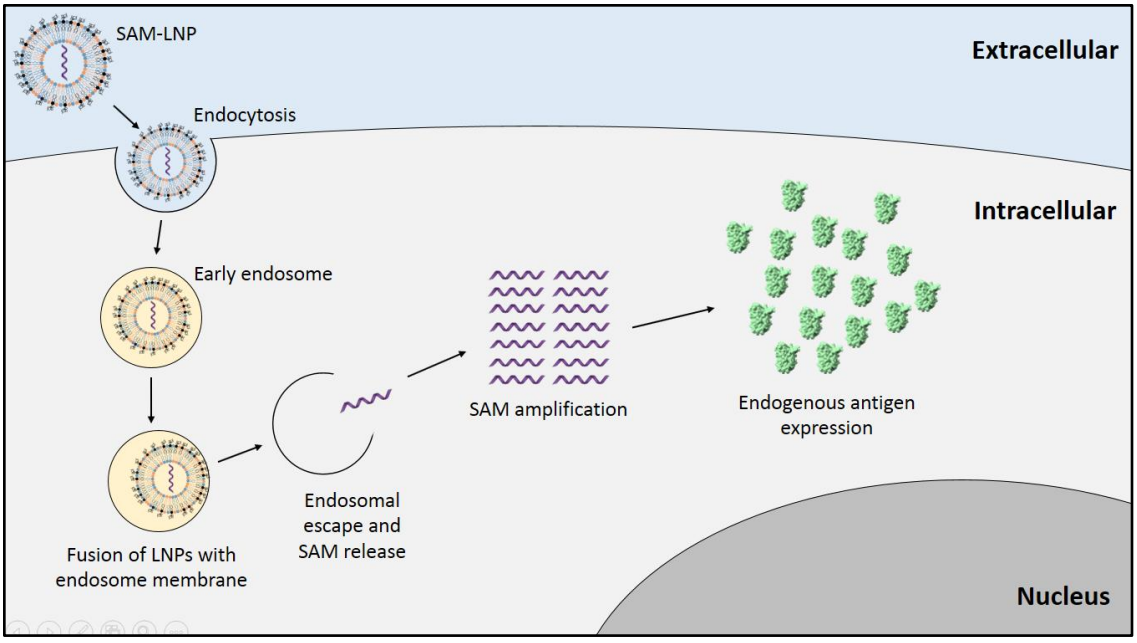

4.1. INTRODUCTION

Current vaccine design aims to develop safer vaccines based on one or few selected antigens. A novel vaccine development approach includes the use of nucleic acids, as they exhibit the advantage of both live attenuated and subunit vaccines: They are safe and enable *in situ* antigen expression, mimicking a real infection thus eliciting both humoral and cellular-mediated immune responses. The use of DNA or viral vector vaccines has been hampered by safety issues such as genomic integration. In contrast, RNA-based vaccines do not require nucleus importation and hence also enable transfection of senescent cells (e.g. dendritic cells).

Because poor stability of mRNA in biological environment, high concentrations of mRNA are necessary. However, the antigen can be designed in a self-amplifying RNA (SAM) to enhance the response and to reduce the effective dose. SAM vaccines are based on an engineered positive single stranded RNA (ssRNA+) virus, usually an alphavirus genome, in which the genes encoding for the viral structural proteins are substituted by the gene of interest. Stability of SAM vaccines, and RNA in general, can be improved by incorporating them in delivery systems.

Lipid-based delivery systems have been extensively utilised to deliver RNA (Xue et al., 2015) and DNA vaccines (Schwendener, 2014). Historically, these have been designed as complexes of nucleic acid and cationic lipids/liposomes called lipoplexes (Balazs and Godbey, 2011). Continued efforts at screening novel lipids and formulations have led to the development of efficient novel lipid based delivery systems. Among them, the so-called stable nucleic acid lipid nanoparticles (SNALPs), also known as ionisable lipid nanoparticles (iLNPs), represent the most effective nonviral delivery system to date (Cullis and Hope, 2017). Optimised iLNPs are composed of DSPC, Chol, the ionisable lipid DLin-MC3-DMA and the diffusible PEGylated lipid DMG-PEG2000 at 10:48:40:2 molar ratio. The head group of the ionisable lipid contains a tertiary amine with a pKa of 6.44 which enables iLNPs to maintain neutral or low cationic surface charge density at physiological pH and thus are less immunoreactive and have improved stability *in vivo*. At acidic pH (i.e. in the endosomes), the ionisable lipids become positively charged and interact with endogenous anionic lipids to form non-bilayer structures thus promoting endosomal escape (Semple et al., 2010). The PEGylated lipid avoids aggregation during the formulation process and to helps to maintain the particle size and stability before administration (Kulkarni et al., 2018a).

Finally, DSPC and cholesterol confer integrity and improve the stability of the particles *in vivo*. This formulation was originally designed to deliver Patisiran, a therapeutic small interfering RNA (siRNA), systemically for the treatment of hereditary transthyretin-mediated amyloidosis (hATTR). This siRNA-LNP drug product (trade name Onpattro) was approved by the FDA in 2018 and became the first siRNA-based product to be licenced. However, LNPs are also very effective in delivering mRNA (Richner et al., 2017) and SAM vaccines (Hekele et al., 2013). Indeed, they are currently being investigated in clinical trials for the treatment of infectious diseases such as rabies (NCT03713086), zika (NCT04064905) and influenza virus (NCT03345043).

Proof of concept of LNP-facilitated SAM delivery was first reported in 2012. DLin-DMA iLNPs enclosing a SAM encoding the respiratory syncytial virus fusion protein (RSV-F) elicited both humoral and cellular immune responses comparable to viral particles in a mouse model (Geall et al., 2012). Notably, optimal physicochemical properties of LNPs depend on the application. For instance, the optimal lipid pKa for systemic delivery of siRNA-LNPs for hepatocyte knockdown is 6.2-6.5. In contrast, the optimal lipid pKa for intramuscular administration of mRNA vaccines seem to be 6.6-6.8 (Hassett et al., 2019). While LNPs are the most studied formulations, other delivery systems (e.g. a cationic nanoemulsion) are able to efficiently deliver SAM. (Brito et al., 2014).

4.2. AIM AND OBJECTIVES

Since the potential of ionisable LNPs (iLNPs) to deliver nucleic acids was first described, iLNPs have attracted a great deal of attention. The composition of iLNPs, in particular the pKa of the ionisable lipid, has been deeply optimised over the past decade: From the development of first generation iLNPs based on the ionisable lipids DODAP or DODMA to the rational design of novel lipids such as DLin-DMA. An intense program of lipid synthesis led to the identification of DLin-MC3-DMA (abbreviated to MC3), which is currently the gold standard for non-viral RNA delivery (Cullis and Hope, 2017; Kulkarni et al., 2018a; Tam et al., 2013) and well-established relationships between chemical structure and potency have been defined for iLNP formulations.

The aim of this chapter was to design and investigate cationic lipid nanoparticles (cLNPs) based on existing cationic lipids (e.g. DOTAP or DDA) to deliver a self-amplifying RNA vaccine encoding for the rabies virus glycoprotein (RVG). To achieve this, the objectives were the following:

- To formulate and to characterise a panel of SAM-cLNPs of different composition.
- To investigate the ability of cLNPs to protect SAM from RNase degradation.
- To investigate the effect of cLNP composition on cellular uptake and antigen expression *in vitro.*
- To select most promising cLNP candidates for *in vivo* studies.

4.3. MATERIALS AND METHODS

4.3.1. Materials

1,2-distearoyl-sn-glycero-3-phosphocholine (DSPC), 1,2-dioleoyl-sn-3-phosphoethanolamine (DOPE), 3ß-[N-(N',N'-dimethylaminoethane)-carbamoyl]cholesterol (DC-Chol), dimethyldioctadecylammonium (DDA), 1,2-dioleoyl-3-trimethylammonium-propane (DOTAP), 1,2-dimyristoyl-3-trimethylammonium-propane (DMTAP), 1,2-stearoyl-3-trimethylammonium-propane (DSTAP), N-(4-carboxybenzyl)-N,N-dimethyl-2,3-bis(oleoyloxy)propan-1-aminium (DOBAQ), 1,2-distearoyl-sn-glycero-3-phosphoethanolamine-N-[amino(polyethylene glycol)-2000] (DSG-PEG2000) and 1,2-dimyristoyl-sn-glycero-3-phosphoethanolamine-N-[methoxy(polyethylene glycol)-2000] (DMG-PEG2000) were obtained from Avanti Polar Lipids. Cholesterol, [1,2-3H(N)]-, 1 mCi (37 MBq) and Ultima Gold were obtained from Perkin Elmer. Trehalose and hydrogen peroxide 30% v/w were purchased from Acros Organics. Penicillin-streptomycin, L-glutamine, cholesterol (Chol) and pontamine blue were purchased from Sigma. RNase A, proteinase K, Northern Max formaldehyde load dye, Northern Max running 10X buffer, Ambion millennium RNA, SYBR gold nucleic acid stain marker (10,000X in DMSO), 3 M sodium acetate buffer pH 5.2, Ribo Green RNA assay kit, 1,1'-dioctadecyl-3,3,3',3'-tetramethylindocarbocyanine perchlorate (DiI-C_{18}), Lipofectamine2000, opti-MEM, Alexa Fluor 488-labeled goat anti-mouse IgG2a Cross-Adsorbed secondary antibody and allophycocyanin (APC) Zenon antibody labelling kit for mouse IgG2a were purchased from Thermo Fisher. Dulbecco's Modified Eagle Medium (DMEM), Roswell Park Memorial Institute 1640 medium

(RPMI-1640), trypsin-EDTA (0.25%) and foetal bovine serum (FBS) were obtained from Gibco. Mini ReadyAgarose precast gels 1% TAE were obtained from Bio-Rad. 100 mM citrate buffer pH 6.0 was purchased from Teknova. Mouse anti-rabies glycoprotein antibody (clone 24-3F-10) was obtained from Merck. 10X Perm/Wash buffer and Cytofix/Cytoperm were obtained from BD Biosciences. The ionisable lipid K was kindly provided by GSK (Rockville, US).

4.3.2. Self-amplifying RNA (SAM)

DNA plasmids encoding the self-amplifying RNAs were constructed using standard molecular techniques. Plasmids were amplified in Escherichia coli and purified using Qiagen Plasmid Maxi kits (Qiagen). DNA was linearized immediately following the 3' end of the self-amplifying RNA sequence by restriction digest. Linearized DNA templates were transcribed into RNA using the MEGAscript T7 kit (Life Technologies) and purified by LiCl precipitation. RNA was then capped using the Vaccinia Capping system (New England BioLabs) and purified by LiCl precipitation before formulation (Quoted from (Geall et al., 2012)). SAM encoded for either a green fluorescent protein (GFP) or rabies glycoprotein (RVG). SAM constructs were kindly provided by GSK (Rockville, US).

4.3.3. Formulation of SAM lipid nanoparticles (SAM-LNPs)

SAM-LNPs were produced in the Nanoassemblr Platform (Precision Nanosystems Inc.) in a Y-shaped staggered herringbone micromixer of 300 µm width and 130 µm height. LNPs were composed of 1) DOPE, a cationic lipid and a PEGylated lipid at 49:49:2 molar ratio or 2) DSPC, Chol, a cationic/ionisable lipid and a PEGylated lipid at 10:48:40:2 molar ratio. Lipids dissolved in methanol an aqueous phase containing SAM were injected simultaneously in the micromixer. SAM-LNPs were produced at 4 mg/mL lipid concentration, 3:1 aqueous:organic flow rate ratio (FRR), 5 mL/min total flow rate (TFR). SAM was injected in 100 mM citrate buffer pH 6.0 at a 8:1 N:P mole ratio (N in the cationic/ionisable lipid and P in SAM). Newly formed SAM-LNPs (1 mL) were dialysed against 10 mM TRIS pH 7.4 (200 mL) for 1 hour under magnetic stirring.

4.3.4. Physicochemical characterisation of SAM-LNPs

SAM-LNPs were characterised in terms of hydrodynamic size (Z-average), polydispersity index (PDI) and surface charge (zeta-potential) by dynamic light scattering (DLS) in a Zetasizer Nano ZS (Malvern, UK) at 0.1-0.2 mg/mL at 25 ˚C.

4.3.5. SAM encapsulation efficiency (SAM E.E.)

SAM E.E. was quantified by Ribo Green assay following manufacturer instructions. Because Ribo Green fluorescent dye is unable to penetrate the lipid membrane, samples were treated with 1 % triton X-100 to release SAM from LNPs. Due to the interference of triton X-100 with Ribo Green quantification, calibration curves in presence and absence of 1 % triton X-100 were used. Fluorescence was measured at excitation and emission wavelength of 485 and 528 nm in either a POLARStar OMEGA fluorimeter (BMG Labtech) or a Synergy H1 microplate Reader (BioTek). Due to the inability of Ribo Green to penetrate the lipid membrane, SAM encapsulation efficiency was calculated as $(F_T - F_0)/F_T$ were F_T and F_0 are the amount of SAM quantified in presence and absence of 1 % triton X-100 (Fig. 4.1)

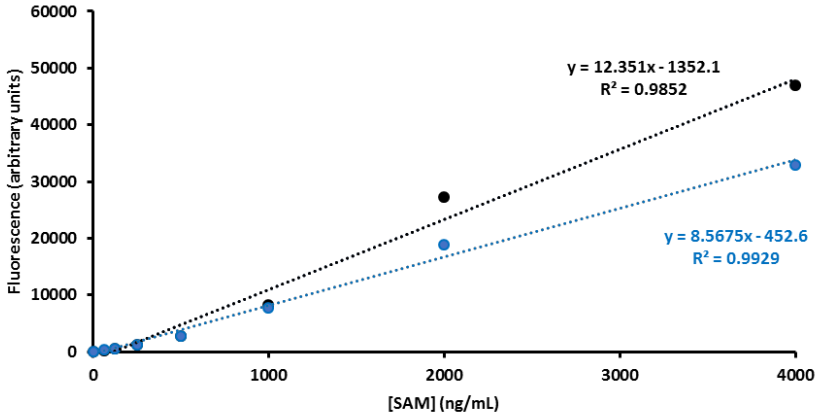

Figure 4.1. Representative Ribo Green calibration curves in presence (●) and absence (●) of 1% triton-X100 for quantification SAM encapsulation efficiency of LNPs. Limit of detection (LOD) and limit of quantification (LOQ), calculated according to ICH guideline Q2 (R1): "*Validation of Analytical Procedures: Text and Methodology*" (2005), were below 200 ng/mL and 600 ng/mL respectively. Therefore, this method was sensitive enough to quantify SAM E.E. of LNPs.

4.3.6. RNase protection assays

A total of 2.8 µg SAM (200 µL), either in solution or encapsulated in lipid nanoparticles (LNPs), were challenged with 0.028 µg RNase A (20 µL) for 30 min at room temperature, followed by an

incubation with 140 µg of recombinant proteinase K for 10 min at 55 °C. Subsequently, 750 µL of ethanol and 25 µL of 3 M sodium acetate pH 5.2 were added to each sample, which were then centrifuged at 14,000 rpm for 20 min. Ethanol precipitation and centrifugation was repeated twice. SAM pellets were resuspended in 35 µL of DEPC-treated water, mixed with formaldehyde load dye (1:3 v/v) and heated at 65 °C for 10 min and then cooled to room temperature. The equivalent of 200 ng of SAM (10 µL) were loaded in a denatured 1% agarose gel in Northern Max 3-(N-morpholino)propanesulfonic acid (MOPS) running buffer, containing 0.1 % of SYBR gold stain, and run at 90 V. Ambion Millennium marker was used as the molecular weight standard. Gel images were acquired in a Gel Doc EZ imager (BIO RAD).

4.3.7. Stability studies

SAM-LNPs were incubated in TRIS/FBS 50:50 v/v in a shaking bath at 37 ˚C. All formulations were characterised by dynamic light scattering (DLS) at relevant time points. The stability of SAM-LNPs was also studied at 4 ˚C.

4.3.8. Bone marrow-derived macrophages (BMDMs)

Bone marrow cells, obtained from femur and tibiae of 6-8-week-old male BALB/c mice, were incubated in petri dishes in macrophage medium: DMEM supplemented with 20 % heat inactivated foetal bovine serum (HI-FBS), 0.1 mg/mL penicillin-streptomycin, 4 mM L-glutamine and 20% L-Cell conditioned medium (supernatant obtained from confluent L929 fibroblast cell line) at 37 °C, 95% humidity and 5% CO_2 in a cell incubator (Panasonic). A total of 4 petri dishes (10 mL) were obtained per mice. At day 2, fresh macrophage medium (10 mL) was added to each petri dish. At day 7, 15 mL of media were removed from each petri dish and were replaced for 15 mL fresh macrophage medium. At day 10, the cells were scraped, washed and cultured in 24-well plates in DMEM supplemented with 10% HI-FBS, 0.1 mg/mL penicillin-streptomycin and 4 mM L-glutamine (complete DMEM, or cDMEM) at $2 \cdot 10^5$ cells/well and were allowed to adhere for 24 hours at 37 °C and 5% CO_2. The percentage of BMDM was determined as percentage of $F4/80^+$ cells. F4/80 is a membrane glycoprotein that has been widely used as a specific cell marker for murine macrophages (Austyn and Gordon, 1981). Briefly, a total of $2 \cdot 10^5$ cells were incubated with a FITC-labelled anti-$F4/80^+$ monoclonal antibody (1/200 dilution) in FACS buffer (PBS supplemented with 5% FBS) for 30 min at 4 °C, washed twice and analysed by flow cytometry (FACSCanto, BD Biosciences).

4.3.9. *In vitro* cellular uptake and antigen expression in BMDMs upon transfection with GFP-SAM-LNPs

LNPs were co-formulated with the lipophilic fluorescent dye Dil-C_{18} (0.2% mole %) to track their cellular internalisation as previously described (Kaur et al., 2014). BMDMs were incubated with GFP-SAM LNPs (200 ng SAM/well) for 1, 4 and 24 hours at 37 °C. Cells were then scraped and washed twice with PBS. Subsequently, cellular uptake and antigen expression was analysed by flow cytometry.

4.3.10. Immortalised immortal cell lines

Baby hamster kidney (BHK) cells were cultured in RPMI-1640 supplemented with 5% HI-FBS, L-glutamine and antibiotics in 75 cm^2 flasks at 50-80% confluence at 37 °C, 95% humidity and 5% CO_2 in a cell incubator (Heraeus).

4.3.11. Cellular uptake of LNPs, endosomal escape of SAM and antigen expression in BHK fibroblasts

A total of 50,000 BHK cells were cultured per well in 24-well plates in RPMI in presence (5%) or absence of HI-FBS and allowed to adhere for 8 hours at 37 °C and 5% CO_2. BHK cells were then incubated with GFP-SAM LNPs (200 ng SAM/well) for 16 hours. BHK cells were then trypsinised, washed twice with PBS and transferred to a conical 96-well plate. They were then incubated for 1 hour with an anti-dsRNA antibody (1 µg/well), which had previously labelled with an allophycocyanin (APC) Zenon antibody labelling kit following manufacturer instructions.

4.3.12. *In vitro* potency of GFP-SAM LNPs in BHK fibroblasts

A total of 50,000 BHK cells were cultured per well in a 24-well plate and allowed to adhere for 8 hours at 37 °C and 5% CO_2. Cells were then incubated with GFP-SAM LNPs in presence (5%) or absence of HI-FBS. As a control, cells were also treated with Lipofectamine2000-transfected SAM following manufacturer instructions. In brief, 2.5 µL of Lipofectamine2000 were diluted in opti-MEM (30 µL), mixed with 30 µL of opti-MEM containing GFP-SAM and left for 5 minutes at room temperature to allow complexation to occur. Then, 50 µL of the Lipofectamine-SAM complex were added BHK cells. After 16 hours, cells were washed twice with PBS supplemented with 5%

HI-FBS (FACS buffer), trypsinised and transferred to a conical 96-well plate. Subsequently, cells were washed twice with FACS buffer and resuspended in PBS (200 µL). The percentage of transfected cells (GFP^+ cells) was analysed by flow cytometry with respect to untreated cells.

4.3.13. *In vitro* potency of RVG-SAM LNPs in BHK fibroblasts

A total of 50,000 BHK cells were cultured per well in a 24-well plate and allowed to adhere for 8 hours at 37 °C and 5% CO_2. Cells were then incubated with RVG-SAM LNPs in presence (5%) or absence of HI-FBS. As a control, cells were also treated with Lipofectamine2000-transfected SAM following manufacturer instructions. After 16 hours, cells were washed twice with FACS buffer, trypsinised and transferred to a conical 96-well plate. BHK cells were washed twice again and incubated with Cytofix/Cytoperm (100 µL/well) for 15 minutes at 4 °C. Following 2 washing with 1X Perm/Wash buffer, BHK cells were incubated with a mouse anti-RVG monoclonal antibody (1:1000) for 1 hour at room temperature. Then, they were washed twice with 1X Perm/wash buffer and incubated with an Alexa Fluor 488-labelled goat anti-mouse IgG2a antibody (1:1000) for 1 hour at room temperature. Finally, cells were washed twice 1X Perm/wash buffer and resuspended in FACS buffer. The percentage of transfected BHK cells (RVG^+ cells) was then analysed by flow cytometry with respect to untreated cells.

4.3.14. Statistical analysis

Statistical analysis was performed by one-way analysis of variance (ANOVA) followed by Tukey's honest significance test in GraphPad Prism version 7 (GraphPad Software Inc., La Jolla, CA). P-values below 0.05 were considered significant.

4.4. RESULTS AND DISCUSSION

4.4.1. Formulation, characterisation and stability of SAM-LNPs

The concept of a lipid nanoparticle (LNP) is broad and encloses a range of different formulations with characteristic physicochemical properties, including formulations such as liposomes (Bangham and Horne, 1964), solid-lipid nanoparticles (Lobovkina et al., 2011) and the recently described stable nucleic acid lipid nanoparticles (SNALPs), also known as ionisable LNPs (iLNPs)

(Semple et al., 2010). Within this thesis, LNPs containing cationic lipids (e.g. DOTAP) will be referred to as cationic LNPs (cLNPs).

cLNPs were composed of a cationic lipid, DOPE and a PEGylated lipid (persistent DSG-PEG2000 or diffusible DMG-PEG2000) in a 49:49:2 molar ratio. Cationic lipids have limited capacity to promote endosomal escape by themselves so that they are often co-formulated with the helper lipid DOPE. DOPE is a cone-shaped lipid with an ethanolamine head group with a strong tendency to form inverted hexagonal phases at acidic pH and to destabilize endosomal membranes (Farhood et al., 1995; Mochizuki et al., 2013) consequently increasing the transfection efficiency of cationic liposomes (Kim et al., 2015; Zhang et al., 2010). An important difference between iLNPs and cLNPs is their structure. While iLNPs display an electron-dense core, LNPs containing cationic lipids tend to display bilayer-like structures (Kulkarni et al., 2018b) (Fig. 4.2). As for iLNPs, a PEGylated lipid was incorporated to control LNP size and avoid aggregation in the manufacturing process. In some experiments, cLNPs composed of DSPC, Chol, a cationic lipid and a PEGylated lipid were prepared for a direct comparison with iLNPs. Benchmark iLNPs, containing the cationic-ionisable lipid K, were used as gold standard for a comparison with cLNPs.

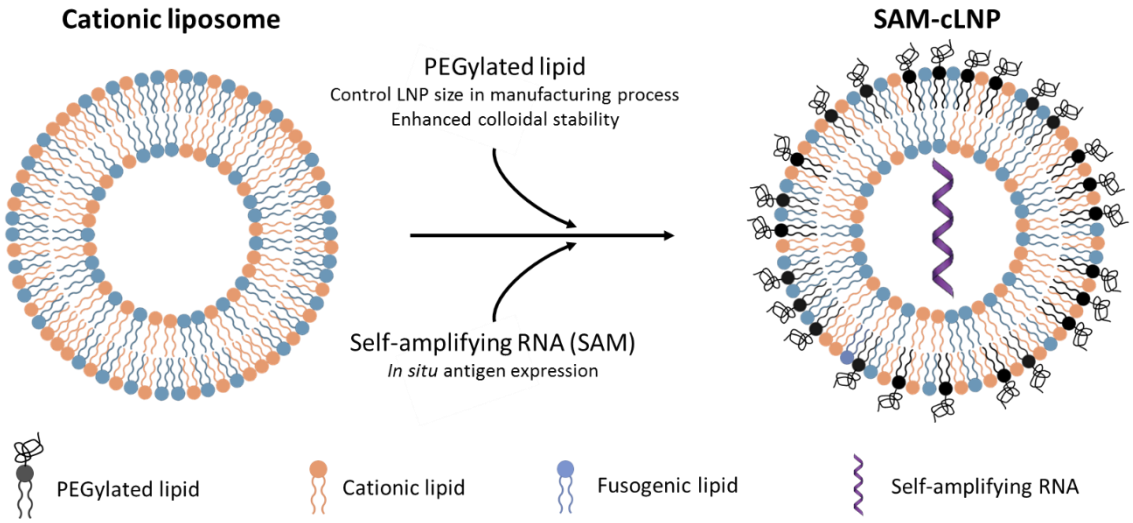

Figure 4.2. Schematic representation of cationic liposomes and possible structure of cationic lipid nanoparticles (cLNPs) investigated in this thesis. Cationic liposomes were composed of the fusogenic lipid DOPE and a cationic lipid (e.g. DOTAP) at a 50:50 molar ratio. cLNPs were composed of DOPE, a cationic lipid and a PEGylated lipid at a 49:49:2 molar ratio.

cLNPs were based on a panel of cationic lipids (DOTAP, DSTAP, DMTAP, DDA, DC-Chol and DOBAQ) of different physicochemical properties including head group, alkyl chain length and degree of unsaturation (Fig. 4.3A). All lipids but DC-Chol contain a quaternary amine group. DOTAP and DOBAQ have an unsaturated 18-carbon acyl chain, while DDA and DSTAP have a saturated 18-carbon chain length. In contrast, DMTAP and DC-Chol have a saturated 14-carbon acyl chain and a tetracyclic ring respectively. Importantly, DOTAP, DSTAP and DMTAP contain the same trimethylammonium-propane (TAP) head group. This would allow to investigate the effect of unsaturation and acyl chain length. DOBAQ contains a quaternary amine and a carboxybenzyl group and hence could be defined as a zwitterionic lipid. Regardless, DOBAQ will be considered a conventional cationic lipid. Finally, the lipid K contains a tertiary amine head group with an apparent pKa <7.0 (structure not shown). SAM encoding for either a green fluorescent protein (GFP) or the rabies virus glycoprotein (RVG) were used.

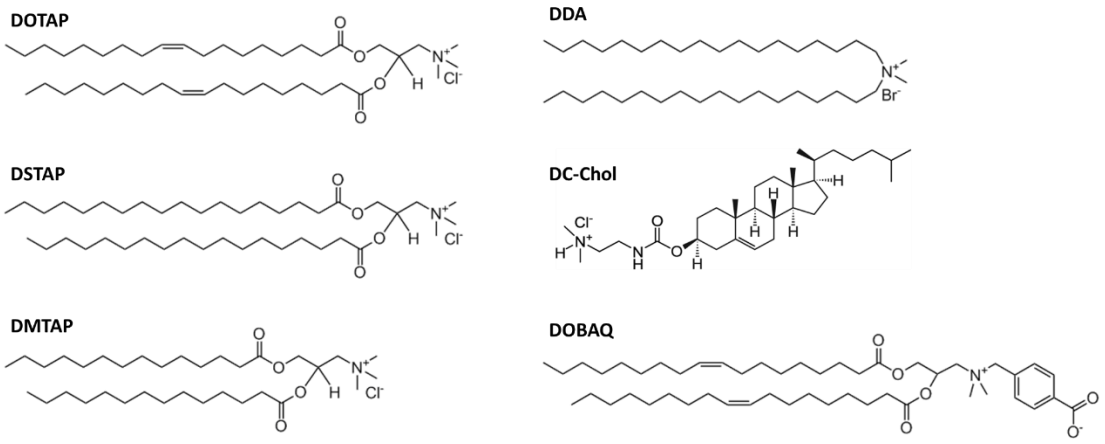

Figure 4.3. Cationic lipids investigated to design cationic lipid nanoparticles*1,2-dioleoyl-3-trimethylammonium-propane (DOTAP), 1,2-stearoyl-3-trimethylammonium-propane (DSTAP), 1,2-dimyristoyl-3-trimethylammonium-propane (DMTAP), dimethyldioctadecylammonium (DDA), 3ß-[N-(N',N'-dimethylaminoethane)-carbamoyl]cholesterol (DC-Chol), N-(4-carboxybenzyl)-N,N-dimethyl-2,3-bis(oleoyloxy)propan-1-aminium (DOBAQ).*

cLNPs and iLNPs were prepared by flash precipitation in a microfluidic mixing chamber (Nanoassemblr) by simultaneously injecting an organic phase containing the lipids and an aqueous phase containing SAM. For doing so, the method for producing sub-100 nm cationic liposomes, described in Chapters 2 and 3, was adapted. Empty cationic liposomes composed of

DOPE and a cationic lipid were prepared at 1:1 FRR, the only FRR that allowed to produce monodisperse liposomes, in TRIS pH 7.4 as aqueous phase. In contrast, LNPs were prepared at 3:1 FRR, not to jeopardize SAM stability, in citrate buffer pH 6.0 as the aqueous phase.

The physicochemical properties of cLNPs and iLNPs is summarised in Table 4.1. All formulations had a hydrodynamic size between 65 and 150 nm and low PDI (<0.25), with DOPE:Cationic:PEG-C18 SAM-LNPs having a slightly more positive zeta-potential (5-15 mV) compared to DOPE:Cationic:PEG-C14 and DSPC:Chol:Cationic:PEG-C14 (<5 mV). High (80-100%) SAM encapsulation efficiencies (E.E.) were achieved, with no significant differences between GFP-SAM and RVG-SAM. DC-Chol and DOBAQ-LNPs had lower encapsulation efficiencies compared to their DOTAP, DDA or DMTAP-based formulation counteparts. For instance, the GFP-SAM and RVG-SAM E.E. of DOPE:DC-Chol:PEG-C14 was 80% and 90%, while DDA-cLNPs encapsulated 92% and 97% respectively (Table 4.1).

In a recent study, the use of iLNPs and cLNPs to deliver mRNA to the back of the eye was reported. iLNPs exhibited low PDI (<0.18) and high mRNA E.E. (<95%), while for cLNPs both particle size and mRNA E.E. highly depended on the choice of cationic lipid. cLNPs containing unsaturated cationic lipids such as DOTAP or 1,2-distearoyl-sn-glycero-3-ethylphosphocholine (18:1 EPC) were approximately 100 nm in size with over 99% mRNA E.E. However, cLNPs based on their saturated counterparts (DSTAP and 18:0 EPC) had lower mRNA E.E. (48.1% and 81.5%) and higher sizes (>1000 nm). The lipid DDA allowed to encapsulate over 95% mRNA, as also observed in Table 4.1, while DOBAQ-cLNPs only encapsulated 67.5% mRNA (Patel et al., 2019).

The lower E.E. of DOBAQ-LNPs reported both in Table 1 and in the above study could be attributed to the working pH utilised during the manufacturing process. At pH 6.0, the surface charge density of DOBAQ (pKa=5) is reduced and, consequently, its ability to pack negatively charged nucleic acids is partially impaired. Indeed, increasing the pH of the working buffer from 3 to 5 reduced the E.E. of siRNA in DOBAQ-LNPs from 85% to 39% (Nguyen et al., 2012).

Table 4.1. Physicochemical properties of SAM-LNPs formulated by microfluidics. Lipid compositions – DOPE:Cationic:DSG-PEG2000 49:49:2 mole % (**†**), DOPE:Cationic:DSG-PEG2000 49:49:2 mole % (**‡**), DSPC:Chol:Cationic:DMG-PEG2000 10:48:40:2 mole % (*****). Abbreviations: SAM E.E. (encapsulation efficiency), ZP (zeta-potential). Results are represented as mean ± SD of 3 independent experiments.

Encoded antigen		**Green Fluorescent Protein (GFP)**				**Rabies Glycoprotein (RVG)**			
Cationic lipid	**Composition**	**Size (d.nm)**	**PDI**	**ZP (mV)**	**SAM E.E. (%)**	**Size (d.nm)**	**PDI**	**ZP (mV)**	**SAM E.E. (%)**
DOTAP	†	89 ± 11	0.15 ± 0.04	9 ± 3	94 ± 1	73 ± 6	0.15 ± 0.02	8 ± 1	96 ± 3
	‡	80 ± 2	0.17 ± 0.04	2 ± 1	94 ± 2	79 ± 9	0.17 ± 0.04	3 ± 1	97 ± 2
	*	92 ± 19	0.24 ± 0.02	3 ± 0	99 ± 1	-	-	-	-
DDA	†	110 ± 26	0.19 ± 0.05	13 ± 3	95 ± 3	80 ± 12	0.15 ± 0.03	9 ± 1	97 ± 2
	‡	75 ± 1	0.10 ± 0.01	1 ± 1	94 ± 2	80 ± 8	0.12 ± 0.02	3 ± 1	98 ± 2
	*	99 ± 15	0.16 ± 0.02	2 ± 0	99 ± 1	-	-	-	-
DC-Chol	†	95 ± 7	0.17 ± 0.03	12 ± 2	80 ± 1	77 ± 8	0.19 ± 0.04	8 ± 1	90 ± 5
	‡	87 ± 1	0.17 ± 0.03	3 ± 1	80 ± 2	88 ± 5	0.16 ± 0.03	2 ± 2	91 ± 6
	*	82 ± 12	0.17 ± 0.03	1 ± 1	96 ± 1	-	-	-	-
DMTAP	†	85 ± 6	0.18 ± 0.03	12 ± 2	95 ± 1	77 ± 8	0.21 ± 0.03	8 ± 2	95 ± 3
	‡	78 ± 3	0.17 ± 0.02	2 ± 1	90 ± 1	84 ± 8	0.16 ± 0.02	2 ± 2	96 ± 3
	*	77 ± 8	0.14 ± 0.04	2 ± 1	99 ± 0	-	-	-	-
DOBAQ	†	74 ± 1	0.14 ± 0.01	7 ± 2	83 ± 2	-	-	-	-
	‡	73 ± 1	0.17 ± 0.01	2 ± 2	85 ± 1	-	-	-	-
	*	66 ± 2	0.21 ± 0.02	2 ± 1	86 ± 1	-	-	-	-
Lipid K	*	101 ± 14	0.10 ± 0.04	2 ± 1	98 ± 1	122 ± 14	0.11 ± 0.02	3 ± 1	98 ± 1

DOPE:DSTAP:PEG-lipid LNPs had sizes above 250 nm, high PDI (>0.8) and multimodal size distribution and significantly lower SAM E.E. (<75 %) compared to the other formulations, as also observed by Patel et al. (Patel et al., 2019). Therefore, DSTAP-LNPs were not considered for further investigations. K-iLNPs were 100-120 nm in size, with low PDI (<0.12), neutral zeta-potential (<3 mV) and almost complete SAM. E.E. (>98%) (table 4.1). The physicochemical properties of all SAM-LNPs investigated *in vitro* within this Chapter exhibited physicochemical properties within those ranges shown in Table 4.1.

The physicochemical stability of DOPE:Cationic:PEG-lipid GFP-SAM LNPs at 4 °C was investigated over a period of 8 weeks. DOTAP (78 nm) and DMTAP-LNPs (68 nm) increased in size to over 100 nm after 8 weeks, while DDA (150 nm) and DC-Chol (80 nm) did not change in size over the same period of time (Fig. 4.4A). On the other hand, the PDI of SAM-LNPs increased stepwise but remained below 0.3, with the exception of DOTAP-LNPs (Fig. 4.4B). Finally, the zeta-potential of DOTAP-LNPs dropped below -15 mV after 8 weeks, while the that of DDA, DC-Chol and DMTAP-LNPs remained close to the neutrality (Fig 4.4C).

The stability of SAM-LNPs in *in vivo* simulated conditions was then explored. For doing so, cLNPs were incubated in 50% FBS at 37 ˚C. Interaction of cLNPs with serum proteins rapidly resulted in an exponential increase in size and macroscopic aggregation and the presence of 2% PEG-lipid did not block particle aggregation. Indeed, cation lipid particles aggregate in presence of extracellular proteins and require high degree of PEGylation (>20%) to block aggregation (Kaur et al., 2012a, b).

The next step was to quantify the ability of cLNPs to protect SAM from degradation. The chemical nature of SAM, as any other RNA molecule, is labile. The role of LNPs is to facilitate delivery by promoting endosomal escape upon uptake in target cells while protecting it from RNA degradation in physiological environment (e.g. RNases). Unformulated SAM was completely degraded when exposed to RNase A, while it was protected when enclosed in DLin-DMA iLNPs (Geall et al., 2012). In addition, the surface adsorption of a SAM vaccine on a DOTAP-based cationic nanoemulsion was sufficient to confer protection from RNAse degradation (Brito et al., 2014).

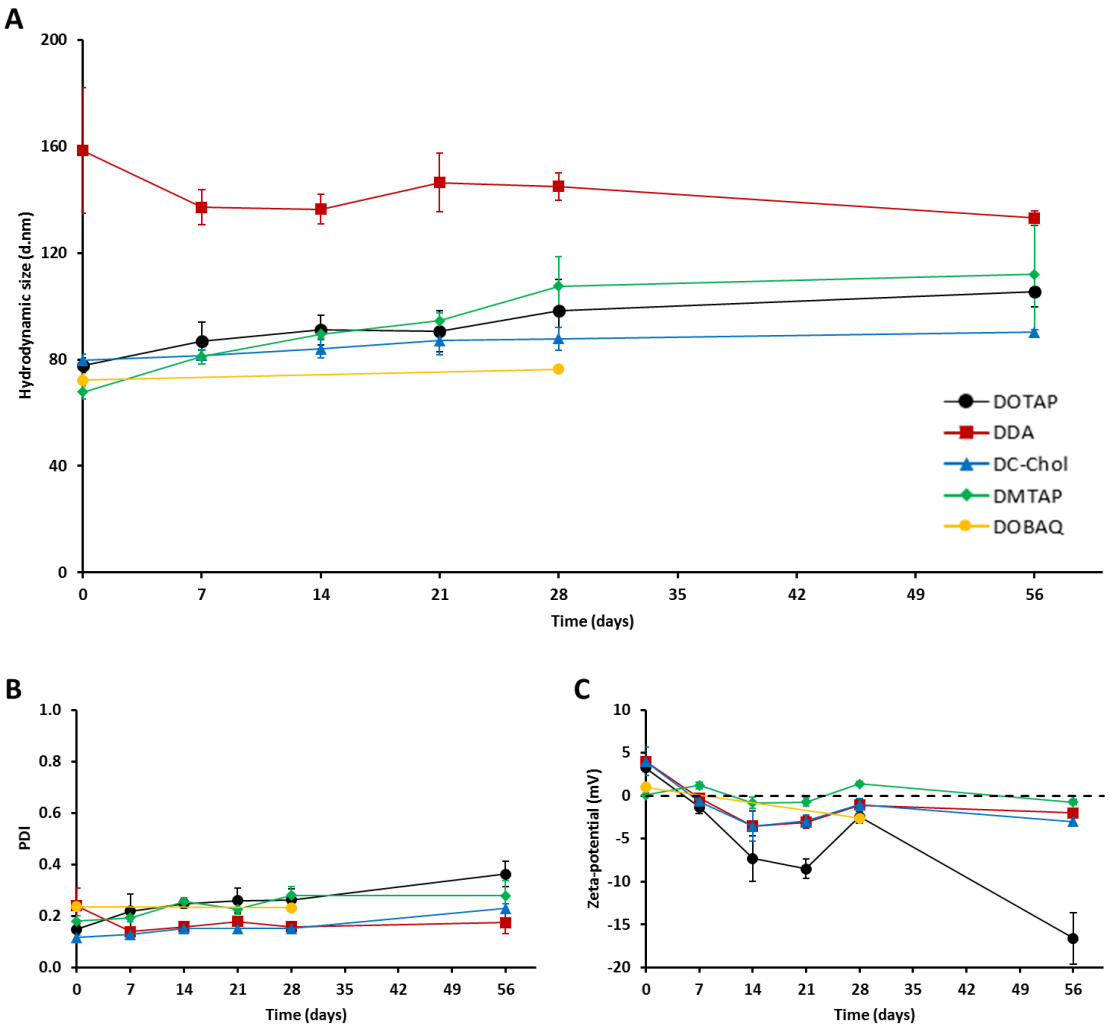

Figure 4.4. Physicochemical stability of GFP-SAM LNPs at 4 ˚C. DOPE:Cationic:PEG-lipid (49:49:2 mole %) SAM-LNPs were formulated by microfluidics at 4 mg/mL, 3:1 FRR, 5 mL/min TFR, 8:1 N:P in 100 mM citrate buffer pH 6.0, dialysed and characterised by DLS in terms of size **(A)**, PDI **(B)** and zeta-potential **(C)** at relevant time points. Cationic Lipid: DOTAP (●), DDA (■), DC-Chol (▲) DMTAP (◆), DOBAQ (●). Results are represented as mean ± SD of three replicates.

Notably, at the RNase concentration tested, the ability to protect SAM depended on the cationic lipid choice (Fig. 4.5). In the conditions investigated, DOPE:DDA:PEG-lipid LNPs conferred full protection against RNase challenge, while DOTAP-LNPs and DMTAP-LNPs only protected SAM partially. In contrast, DC-Chol LNPs did not protect SAM from degradation. Approximately, the percentage of protection estimated by visual analysis was ranked in the following order: DDA > DOTAP = DMTAP > DC-Chol.

DDA and DOTAP contain saturated and unsaturated 18-C alkyl chain respectively, while DMTAP has a saturated 14-C alkyl chain. In contrast, DC-Chol is based on a tetracyclic ring. Both shortening of the lipid alkyl chain length and increasing degree of unsaturation result in reduced hydrophobic interactions between alkyl chains of neighbour lipids and therefore the capacity to form rigid structures. At the same time, DC-Chol has a tertiary amine group, while DDA, DOTAP and DMTAP have a quaternary amine group that facilitates SAM complexation. A systematic study conducted on the biophysical properties of lipoplexes containing DOTAP analogues showed that DOTAP-containing lipoplexes (determined by anisotropy measurements) were more stable compared to DMTAP and DSTAP-containing lipoplexes (Regelin et al., 2000). Similar results were reported on siRNA lipoplexes where the inclusion of DSPC (T_M = 55 °C) enhanced the stability of DOTAP lipoplexes in presence of serum (Khatri et al., 2014). Protection of SAM against RNase degradation can be also accomplished by electrostatic adsorption on cationic formulations like a cationic nanoemulsion (Brito et al., 2014).

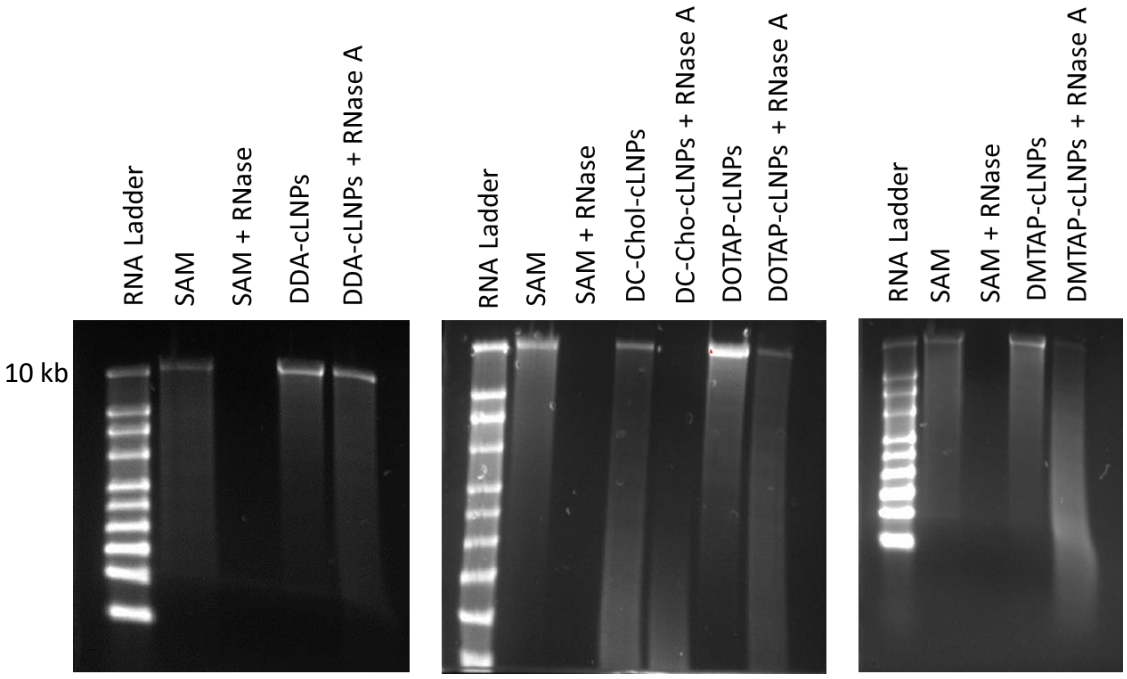

Fig. 4.5. RNase protection assay of DOPE:Cationic:PEG-lipid GFP-SAM LNPs.

4.4.2. *In vitro* cellular uptake and transfection efficiency of LNPs

4.4.2.1. Bone marrow-derived macrophages

Antigen presenting cells (APCs) play a key role in the transition of innate to adaptive immune responses. The ability of DOPE:Cationic:PEG-C18 and DSPC:Chol:Cationic:PEG-C14 cLNPs to associate with bone marrow-derived macrophages (BMBMs) and to induce antigen expression was investigated *in vitro*. To do this, fluorescent LNPs, labelled with DiI-C_{18} dye, were used. Before conducting experiments with the SAM vaccine encoding for the rabies virus glycoprotein (RVG), a GFP-SAM was used as a model.

Despite being avidly taken up by macrophages (>95% DiI-C_{18}^{+} cells, Fig. 4.5), no GFP expression was observed in a 24-hour frame despite SAM concentrations as high as 1000 ng/well were used. Lipofectamine2000, a well-known and widely used nucleic acid-transfection agent (Dalby et al., 2004), also failed to induce GFP expression. The lack of expression was likely attributed to the sensing of RNA molecules by pattern recognition receptors such as the endosomal toll-like receptors (TLR) 7 and 8 expressed in macrophages, thereby resulting in SAM degradation and inhibition of antigen expression (Tatematsu et al., 2018).

LNP composition played an important role on cellular uptake kinetics. When considering the effect of the cationic lipid, DOTAP, DDA and DMTAP-cLNPs exhibited significantly greater uptake compared to DC-Chol and DOBAQ-cLNPs (Fig. 4.6). For instance, the percentage of DiI-C_{18}^{+} cells treated with DOPE:Cationic:PEG-C18 was 30, 60-80 and 90-100% after 1, 4 and 24 hours for the cationic lipids DOTAP, DDA and DMTAP. Interaction of DOPE:DOBAQ:PEG-C18 LNPs with BMDMs was slower, with only 7, 12 and 61 positive cells after 1, 4 and 24 hours. Only 30% DiI-C_{18}^{+} cells were quantified when treated with DOPE:DC-Chol:PEG-C18. Such percentage did not further increase at further time points (Fig. 4.6A), suggesting that DOPE:DC-Chol:PEG-C18 LNPs would be interacting with BMDMs without further internalisation.

DOTAP and DDA-cLNPs had significantly higher MFI values ($p<0.05$) compared to DMTAP, DOBAQ and DC-Chol-cLNPs after 24 hours. The MFI increased over time for all formulations with the exception of DOPE:DC-Chol-cLNPs. These results further support the lack of internalisation of DC-Chol-LNPs (Fig. 4.6C). Such finding was surprising, considering that DOPE:DC-Chol liposomes showed comparable uptake to empty DOPE:DOTAP and DOPE:DDA liposomes in BMDMs

(Chapter 3). The internalisation of DOPE:DOTAP:PEG-C18 and DOPE:DDA:PEG-C18 cLNPs was comparable to DOPE:DOTAP and DOPE:DDA liposomes. Indeed, higher percentages of PEG-lipid are required to inhibit LNP-cell interactions and subsequent cellular uptake (Allen et al., 1991; Li et al., 2011; Takano et al., 2003).

The combination of structural and PEGylated lipids (DOPE/PEG-C18 vs DSPC/Chol/PEG-C14) also played a role in cellular uptake kinetics. Notably, the percentage of positive BMDMs treated with DC-Chol LNPs increased over time up to 75% after 24 hours when co-formulated with DSPC, Chol and PEG-C14. Moreover, substitution of DOPE/PEG-C18 for DSPC/Chol/PEG-C14 resulted in quicker association of DOTAP and DDA-cLNPs with BMBMs (65-70% vs 35-40% positive cells after 1 hour) (Fig 4.6B). Again, the MFI of DOTAP and DDA-cLNPs was significantly higher compared to DMTAP and DC-Chol cLNPs (Fig. 4.6D).

These results suggest that both the cationic lipid and the combination of structural/PEGylated lipids are important parameters to consider in the cellular internalisation of cLNPs in BMDCs. For instance, PC-containing iLNPs were taken up in a significantly higher extent than DOPE-iLNPs (Kulkarni et al., 2017). In a another study, the incorporation of cholesterol enhanced the uptake of DMPC liposomes but had a negative effect on HSPC liposomes in a breast cancer cell line. Liposomes composed of DMPC (T_M = 24 °C) tend to form soft rounder liposomes displaying a liquid disordered phase which is not favourable for uptake. The inclusion of cholesterol led to the formation of a liquid ordered phase, which resulted in enhanced cellular uptake. Conversely, the addition of cholesterol to HSPC (T_M = 52 °C) liposomes modified the hard and faceted bilayer (solid-ordered phase) of this liposomes into a more rigid and rounder structure (liquid-ordered phase) consequently reducing cellular uptake (Abumanhal-Masarweh et al., 2019).

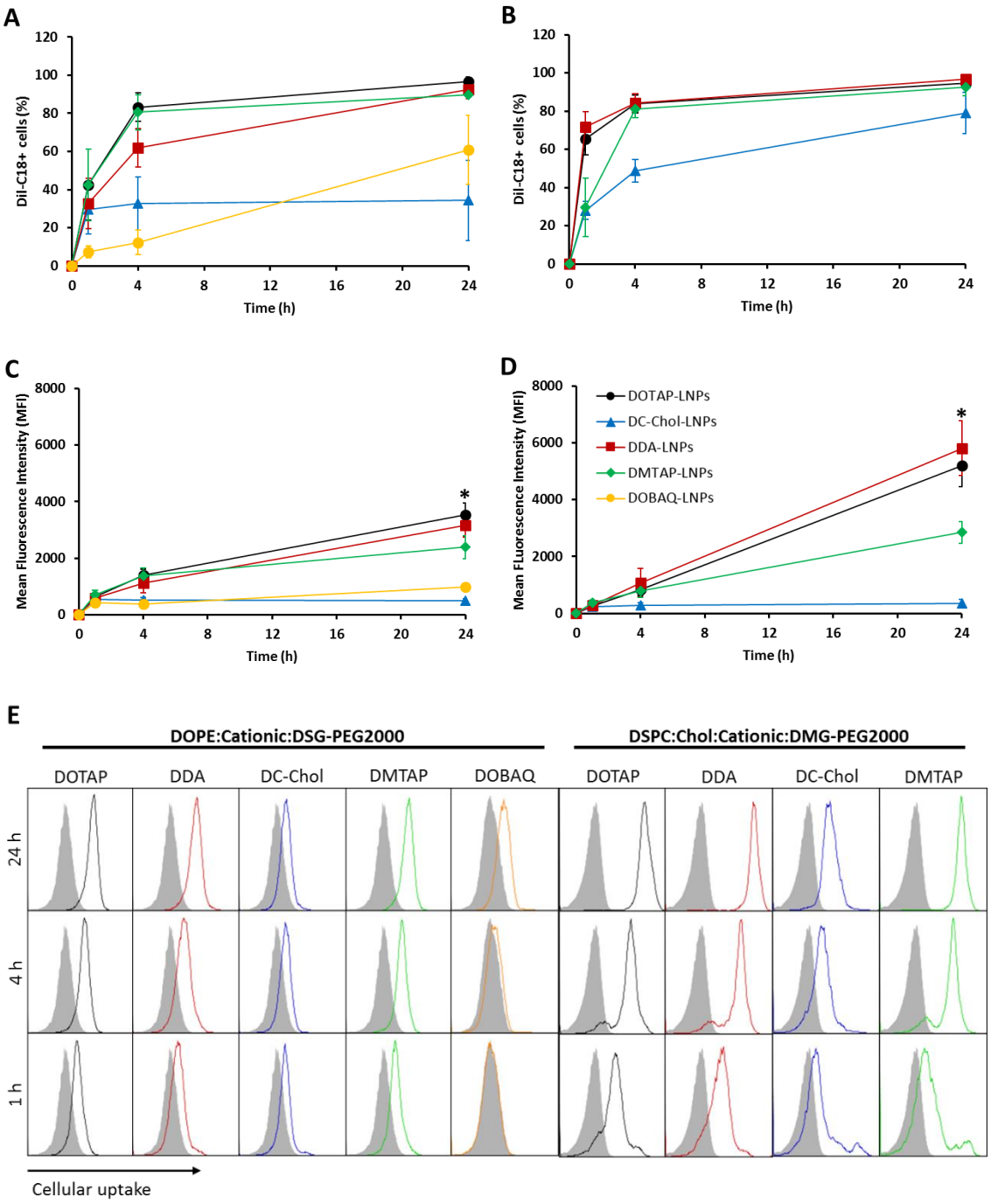

Figure 4.6. *In vitro* cellular uptake of GFP-SAM LNPs in BMDMs in DMEM (10 % FBS) in terms of percentage of DiI-C_{18}^{+} cells (internalised and surface-associated LNPs) **(A, B)** and Mean Fluorescence Intensity (MFI) **(C, D)**. **(C)** Representative flow cytometry plots of LNP uptake (colored) with respect to control cells (shaded grey). DOPE:Cationic:PEG-C18 **(A, C)**, DSPC:Chol:Cationic:PEG-C14 **(B, D)**. Cationic lipid: DOTAP (●), DDA (■), DC-Chol (▲), DMTAP (◆), DOBAQ (●). Results are represented as mean ± SD of 4 independent experiments. Statistical significances of DOTAP, DDA with respect to DMTAP, DC-Chol and DOBAQ-cLNPs. $p < 0.05$ (*).

4.4.2.2. BHK fibroblasts

Fibroblast cell lines (e.g. BHK, HEK293, COS-7) have been wide used as a model cell lines in transfection and lipofection studies (Dalby et al., 2004; Li et al., 2010; Regelin et al., 2000). Due to the lack of antigen expression observed in BMDMs, the fibroblast cell line BHK was chosen to investigate the *in vitro* potency of SAM-LNPs. As for BMDMs, the cellular uptake of SAM-cLNPs and GFP expression was investigated simultaneously. Moreover, an anti-dsRNA antibody was used to qualitatively quantify endosomal escape. cLNPs containing DOPE/PEG-C18, DOPE/PEG-C14 or DSPC/Chol/PEG-C14 and K-iLNPs were utilised.

After 24 hours, >98% of BHK were found in association with cLNPs regardless of cationic (DOTAP, DDA, DC-Chol, DMTAP, DOBAQ), structural (DOPE vs DSPC/Chol) or PEGylated lipid (PEG-C18 vs PEG-C14) and presence or absence of serum. Although complete cellular association (>99% positive cells) was achieved with K-iLNPs in presence of serum, its removal significantly reduced the ability of K-iLNPs to associate with BHK cells (55% positive cells, Fig. 4.7A and B).

All DOBAQ formulations had significantly lower MFI values compared to the other cLNP formulations. When co-formulated with DOPE/PEG-C18, DC-Chol-cLNPs were internalised in a lower extent than DOTAP, DDA and DMTAP-cLNPs both in presence and absence of serum. In contrast, they resulted in similar or even superior MFI values when co-formulated with DOPE/PEG-C14 or DSPC/Chol/PEG-C14 (Fig. 4.7C). Removal of serum resulted in reduced association (1.5-3-fold) of DOTAP and DDA-cLNPs containing DOPE/PEG-lipid (Fig 4.7D) but enhanced their potency as will be discussed below.

K-iLNPs had significantly lower MFI values compared to cLNPs (Fig. 4.7C). Furthermore, removal of serum resulted in 10-fold decrease in the MFI (Fig. 4.7C and D). iLNPs are mainly taken up in a ApoE-dependent manner by the low-density lipoprotein (LDL) receptor (LDLR) through a clathrin-mediated endocytosis process. Accordingly, while pre-incubation with ApoE results in enhanced internalisation, removal of serum (or ApoE) restrains their cell association and cellular uptake (Akinc et al., 2010). This effect was not observed on cLNPs due to the presence of cationic lipids. Indeed, although cLNPs exhibit an average neutral zeta-potential (<5 mV), they contain cationic lipids on their surface that enable cLNPs to interact with negatively charged cell membranes.

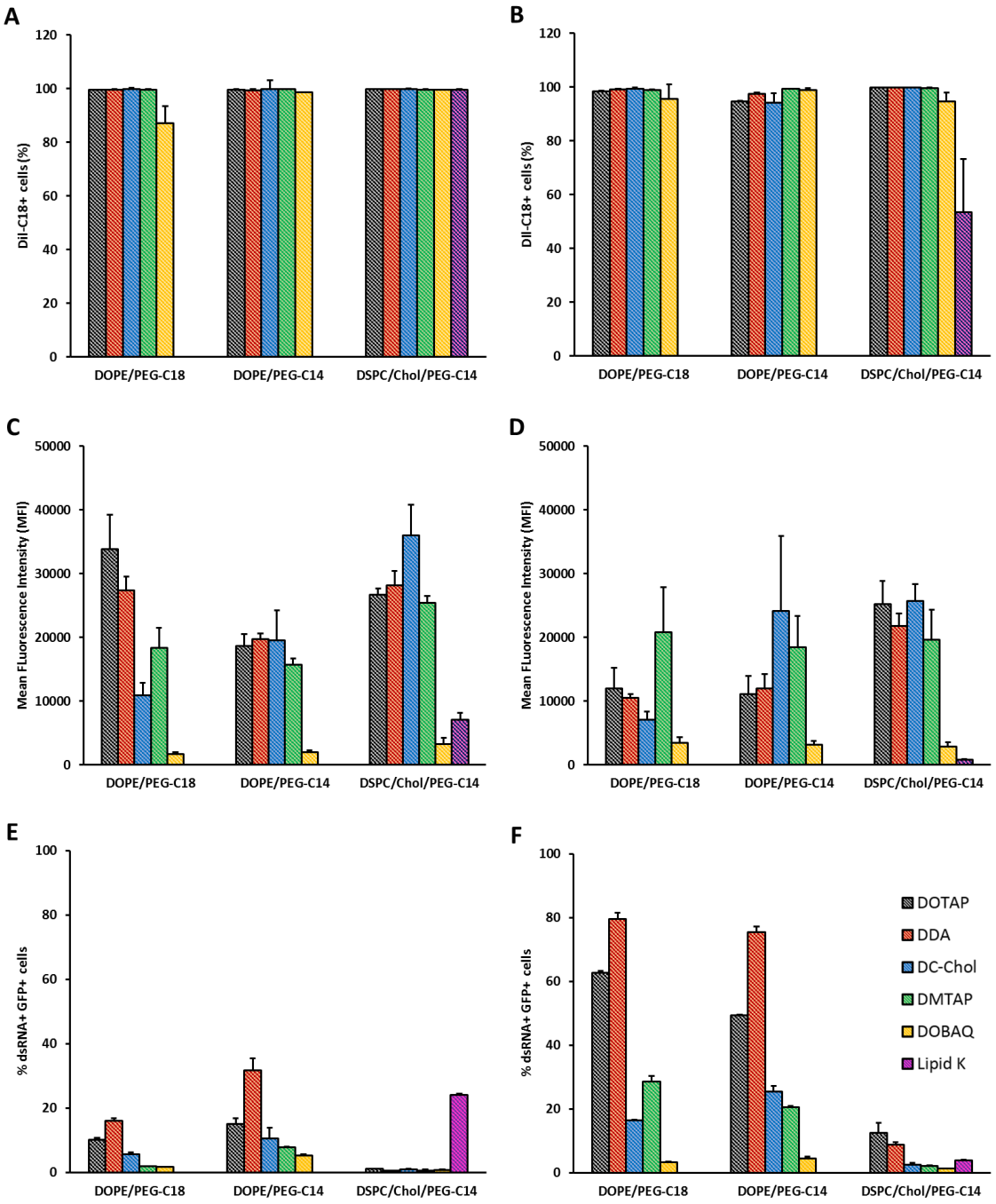

Figure 4.7. Effect of LNP formulation design on the *in vitro* cellular uptake **(A-D)**, endosomal escape of SAM and antigen expression **(E, F)** in BHK fibroblasts in presence (5 %) **(A, C, E)** and absence of serum **(B, D, F)** after 16 hours. Cells were treated with 200 ng SAM/well. Cellular uptake is represented in terms of LNP^+ cells and mean fluorescence intensity (MFI). Endosomal escape and antigen expression are represented as percentage of $dsRNA^+$ and GFP^+ cells respectively. Cationic lipid: DOTAP (▨), DDA (▨), DC-Chol (▨), DMTAP (▨), DOBAQ (▨) and Lipid K (▨). Results are represented as mean ± SD of 3 independent experiments.

Notably, the cellular uptake (in terms of MFI) did not correlate with endosomal escape (%dsRNA$^+$ cells) and antigen expression (%GFP$^+$ cells) (Fig. 4.7E and F). The combination of structural lipids and PEGylated lipid had a great impact. In presence of serum, the relative order of potency was ranked in the following order: DOPE/PEG-C14 > DOPE/PEG-C18 > DSPC/Chol/PEG-C14. Removal of serum resulted in enhanced potency of DOPE-containing cLNPs, with no significant differences between PEG-C18 and PEG-C14 cLNPs. Both DOPE/PEG-C18 and DOPE/PEG-C14 cLNPs were significantly more potent than DSPC/Chol/PEG-C14 cLNPs. For instance, the percentage of dsRNA$^+$ GFP$^+$ cells treated with DOPE:DDA:PEG-C14 cLNPs was 30 and 80% in presence and absence of FBS respectively. By contrast, significantly lower transfection efficiencies (<10%) were achieved with DSPC:Chol:DDA:PEG-C14 cLNPs even in absence of serum. (Fig. 4.7E and F). Accordingly, DSPC/Chol/PEG-C14 cLNPs were not investigated in following studies. These differences are likely attributed to the presence of DOPE, which tends to for inverted micelles and to destabilize the endosomal membrane (Farhood et al., 1995). DOPE is often incorporated in lipoplex formulations to increase transfection efficiency (Regelin et al., 2000).

The type cationic lipid was an important determinant on the ability of cLNPs to induce GFP expression. The relative transfection efficiencies of cationic lipids were DDA > DOTAP >> DC-Chol = DMTAP > DOBAQ, irrespective of presence or absence of serum. In 5% FBS, although iLNPs were taken up in a significantly lower extent ($p<0.05$) than DOPE/PEG-C14 DOTAP and DDA-cLNPs, they transfected a similar percentage of cells (24% vs 15% and 31%). As already expected, K-iLNPs induce negligible percentages of transfection (<5%, Fig. 4.7E and F) in absence of serum, due to impaired cellular uptake (Fig. 4.7D).

DOPE significantly increases transfection efficiencies of lipid-based formulations containing cationic lipids. Ionisable lipids have the intrinsic ability to form inverted micelles at acid pH. Therefore, the requirements for optimal iLNP formulations are different. For instance, the incorporation of unsaturated PC lipids such as 1-stearoyl-2-oleoyl-sn-glycero-3-phosphocholine (SOPC) and 1,2-dioleoyl-sn-glycero-3-phosphocholine (DOPC) resulted in enhanced transfection efficiencies in a variety of primary cells and immortal cell lines *in vitro*. This effect was attributed to an increased internalisation of PC-iLNPs compared to those formulations containing other structural lipids such as DOPE (Kulkarni et al., 2017).

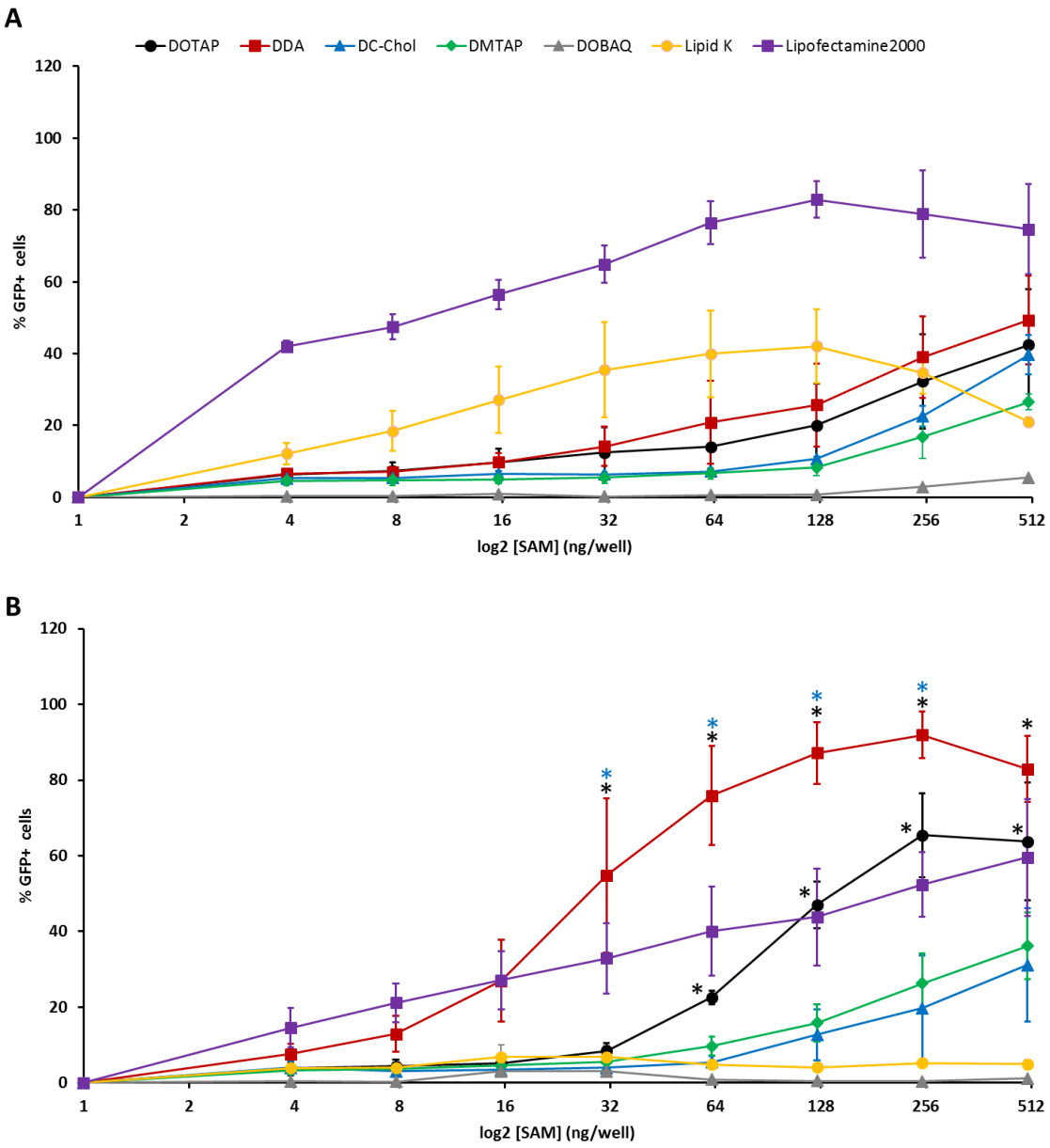

Figure 4.8. *In vitro* potency of GFP-SAM cLNPs and iLNPs in BHK cells in presence **(A)** and absence **(B)** of serum (5 %). GFP-SAM cLNPs were composed of DOPE, a cationic lipid and PEG-C18 (49:49:2 mole %), where cationic lipid was DOTAP (●), DDA (■), DC-Chol (▲), DMTAP (◆), DOBAQ (▲). ILNPs were composed of DSPC, Chol, lipid K and PEG-C14 (10:48:40:2 mole %) (●). Lipofectamine2000 (■) was used as a control. Results are represented as mean ± SD of 4 independent experiments. Statistical analysis was performed by one-way ANOVA followed by Tukey-test where appropriate. Statistical significances of DDA or DOTAP LNPs with respect to DC-Chol and DMTAP LNPs are shown in black, while those between DDA and DOTAP LNPs are represented in blue. $P < 0.05$ (*). *Please note that the representation of statistical significances with respect to DOBAQ-cLNPs, K-iLNPs and Lipofectamine2000 are not represented due to space limitations.*

When considering the effect of the alkyl chain of the PEGylated lipid, cLNPs containing PEG-C14 seemed to induce higher percentages of transfection compared to those prepared with PEG-C18. Herein, a low percentage (2%) of PEG2000-functionalised lipids (DSG and DMG) was incorporated in the LNP formulations. Such a % of PEGylation does not inhibit nanoparticle-cell interactions and subsequent internalisation. However, the ability of LNPs or lipoplexes to fuse with endosomal membrane and release their cargo into the cytosol is reduced in an alkyl-chain-length-dependent manner (Harvie et al., 2000; Song et al., 2002). PEG-lipids have been widely reported to transfer from lipid vesicles in a process known as de-PEGylation. Therefore, longer acyl chains are expected to provide stronger hydrophobic interactions within the lipid conformer and slower transfer rates. For instance, DLin-MC3-DMA iLNPs containing 1.5% of either PEG-C14, PEG-C16 or PEG-C18 had blood half-lives of approximately 0.6, 2.2 and 4.0 hours upon intravenous administration (Mui et al., 2013).

Because great differences in transfection efficiency were observed among LNP formulations, a range of SAM concentrations (up to 500 ng/well) was considered. The *in vitro* potency of cLNPs and iLNPs was first quantified with the GFP-SAM (Fig 4.8) before investigating the RVG-SAM vaccine (Figs. 4.9 and 4.10). Lipofectamine2000-transfected GFP-SAM induced high percentages of GFP^+ cells (up to 80%) irrespective of the presence or absence of serum proteins (Fig. 4.8A and B). For instance, 8 ng GFP-SAM were sufficient to transfect over 50% of the BHK cells in presence of serum proteins. Benchmark K-iLNPs were significantly more potent than cLNPs ($p<0.05$), with increasing amounts of SAM (15-125 ng/well) transfecting higher percentages of cells (25-40%). At higher SAM concentrations (250-500 ng/well), the efficiency of K-iLNPs plateaued and even dropped. DOTAP, DDA, DC-Chol and DMTAP-cLNPs transfected 25-50% of the BHK cells at 500 ng SAM/well, while DOBAQ-cLNPs failed to induce GFP expression (Fig 4.8A).

Again, removal of serum abolished the ability of K-iLNPs to induce antigen expression (<5% positive cells). However, the potency of cLNPs was enhanced in serum-free medium, with DOTAP and DDA-cLNPs inducing significantly higher levels of transfection (>70% positive cells, $p<0.05$) compared to DC-Chol, DMTAP or DOBAQ-cLNPs. At the same time, DDA-cLNPs were significantly more potent ($p<0.05$) than DOTAP-cLNPs. The calculated effective dose 50 (ED50), referred to as the concentration of SAM required to transfect 50% positive cells, was approximately 150 and 30 ng SAM/well for DOTAP and DDA-LNPs. Notably, DDA-cLNPs were more potent than

Lipofectamine2000 at SAM concentrations above 62.5 ng/well. For example, when transfected with 62.5 and 125 ng SAM respectively, DDA-cLNPs and Lipofectamine2000 yielded percentages of GFP^+ cells of 76% vs 40% and 87% vs 44% respectively (Fig. 4.8B).

The potency of DOTAP, DDA, DC-Chol, DMTAP-cLNPs and K-iLNPs was then investigated with a SAM encoding the rabies virus glycoprotein (RVG). This is the SAM vaccine with which immunisation studies will be performed (Chapters 5 and 6). Due to the reduced potency of DOBAQ-cLNPs, they were not further investigated. Importantly, results obtained with RVG-SAM followed a similar trend than those obtained with GFP-SAM. Lipofectamine2000 exhibited higher transfection efficiencies than cLNPs and iLNPs in presence of serum at concentrations of SAM from 8 to 250 ng/well. K-iLNPs and DDA-cLNPs induced similar percentages of positive cells at concentrations up 125 ng/well. At 250 ng SAM/well, however, DDA-cLNPs induced higher levels of antigen expression compared K-iLNPs (60% vs 34% RVG^+ cells). DDA-cLNPs were, at the same time, significantly more potent than DOTAP, DC-Chol and DMTAP-cLNPs, which were only able to induce up to 25% positive cells at 250 ng SAM/well (Fig 4.9A), as already seen on GFP-SAM.

Removal of serum restrained the ability of K-iLNPs to induce RVG expression but had no effect on cLNPs. DOTAP and DDA-cLNPs promoted high (>70%) levels of transfection in serum-free conditions as already observed with their GFP-SAM counterparts. Unlike GFP-SAM, the potency of DDA-cLNPs and Lipofectamine2000 in inducing RVG expression was comparable, with calculated ED50s of DOTAP and DDA-cLNPS being 50 and 15 ng SAM/well, respectively (Fig. 4.9B). It seems that RVG-SAM DOTAP and DDA-cLNPs were more potent (2-3-fold) than their GFP-SAM counterparts. It should be considered that antigen expression was evaluated by similar but different approaches. GFP is an intrinsically fluorescent protein and hence its expression was readily quantified by flow cytometry. In contrast, RVG is not a fluorescent protein and therefore its quantification required from a fluorescently labelled antibody. Hence, direct comparisons between GFP-SAM and RVG-SAM cannot be made. Nevertheless, the relative potency of SAM-cLNPs was the same regardless of the SAM construct (DDA > DOTAP > DMTAP = DC-Chol).

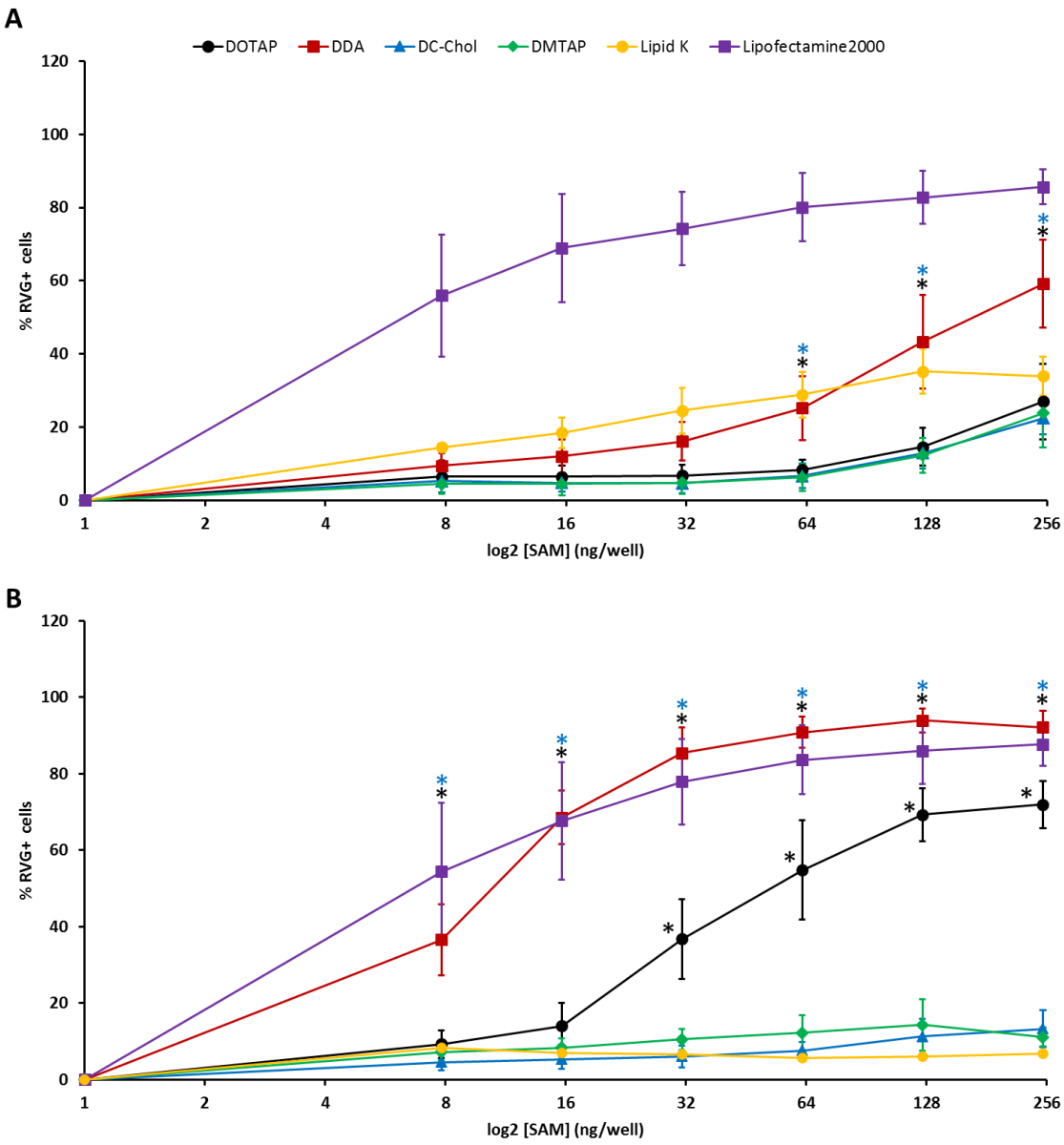

Figure 4.9. *In vitro* potency of RVG-SAM cLNPs and iLNPs in BHK cells in presence **(A)** and absence **(B)** of serum (5 %). RVG-SAM cLNPs were composed of DOPE, a cationic lipid and PEG-C18 (49:49:2 mole %), where cationic lipid was DOTAP (●), DDA (■), DC-Chol (▲), DMTAP (◆). ILNPs were composed of DSPC, Chol, lipid K and PEG-C14 (10:48:40:2 mole %) (●). Lipofectamine2000 (■) was used as a control. Results are represented as mean ± SD of 4 independent experiments. Statistical analysis was performed by one-way ANOVA followed by Tukey-test where appropriate. Statistical significances of DDA or DOTAP LNPs with respect to DC-Chol and DMTAP LNPs are shown in black, while those between DDA and DOTAP LNPs are represented in blue. $P < 0.05$ (*). *Please note that the representation of statistical significances with respect to K-iLNPs and Lipofectamine2000 are not represented due to space limitations.*

Results shown in Figs 4.7, 4.8 and 4.9 suggest that the potency of some cLNPs, especially the DDA formulation, is comparable to K-iLNPs *in vitro* likely to the increased internalisation of cationic LNPs compared to ionisable LNPs. Endosome recycling could be another reason for these observations. Tiffany and Szoka reported improved *in vitro* siRNA knockdown activity of DOTAP-cLNPs over DLin-DMA-iLNPs. The authors attributed this finding to an increased co-localisation of the DOTAP formulation with the protein Rab11a, a recycling endosomal marker, and proposed that Rab11a compartment could be acting as an intracellular reservoir for LNPs (Tiffany and Szoka, 2016)

As reported in Figure 4.7, the type of PEGylated lipid played a role in the transfection efficiency of SAM-cLNPs. Accordingly, the *in vitro* potency of RVG-SAM PEG-C18 and PEG-C14 cLNPs was compared In a head-to-head study. Notably, in presence of serum, PEG-C14/DOTAP and PEG-C14/DDA cLNPs induced significantly higher percentages of transfection ($p<0.05$) compared to their PEG-C18 cLNP counterparts at 50 and 100 ng SAM/well (Fig. 4.10A and C). For instance, the percentage of RVG^+ cells transfected with 100 ng SAM/well was 64% vs 19% for PEG-C14/DDA and PEG-C18/DDA cLNPs respectively. By contrast, the shorter PEGylated lipid did increase the potency of DC-Chol or DMTAP-LNPs in the range of concentrations investigated (Fig. 4.10E and G). The lower potency of these cLNPs (compared to DOTAP and DDA formulations) could explain why no enhancement in potency was observed. Hence, higher SAM concentrations would have been required to observe a PEG-lipid-dependent effect. Interestingly, the potency of cLNPs in absence of serum was not dependent on the choice of PEGylated lipid. Higher levels of transfection (>80%) were achieved with both DOTAP and DDA-cLNPs (Fig. 4.9B and D) compared to DC-Chol and DMTAP-cLNPs (<25%, Fig. 4.10F and H).

Negatively charged proteins of serum surround LNPs creating the so-called protein corona. This leads to cellular internalisation through receptor-mediated endocytosis (e.g. clathrin) and the co-localisation of LNPs in the endosomes (Akinc et al., 2010). Therefore, avoiding degradation in the endo-lysosomal compartment is a milestone in nucleic acid delivery. PEGylated lipids inhibit the interaction of LNPs with the endosomal membranes and hence result in impaired endosomal escape. Increasing the length of the alkyl chain of the PEGylated lipid results in stronger interactions with the endosomal membrane thereby impairing cargo release into the cytosol (Pozzi et al., 2014).

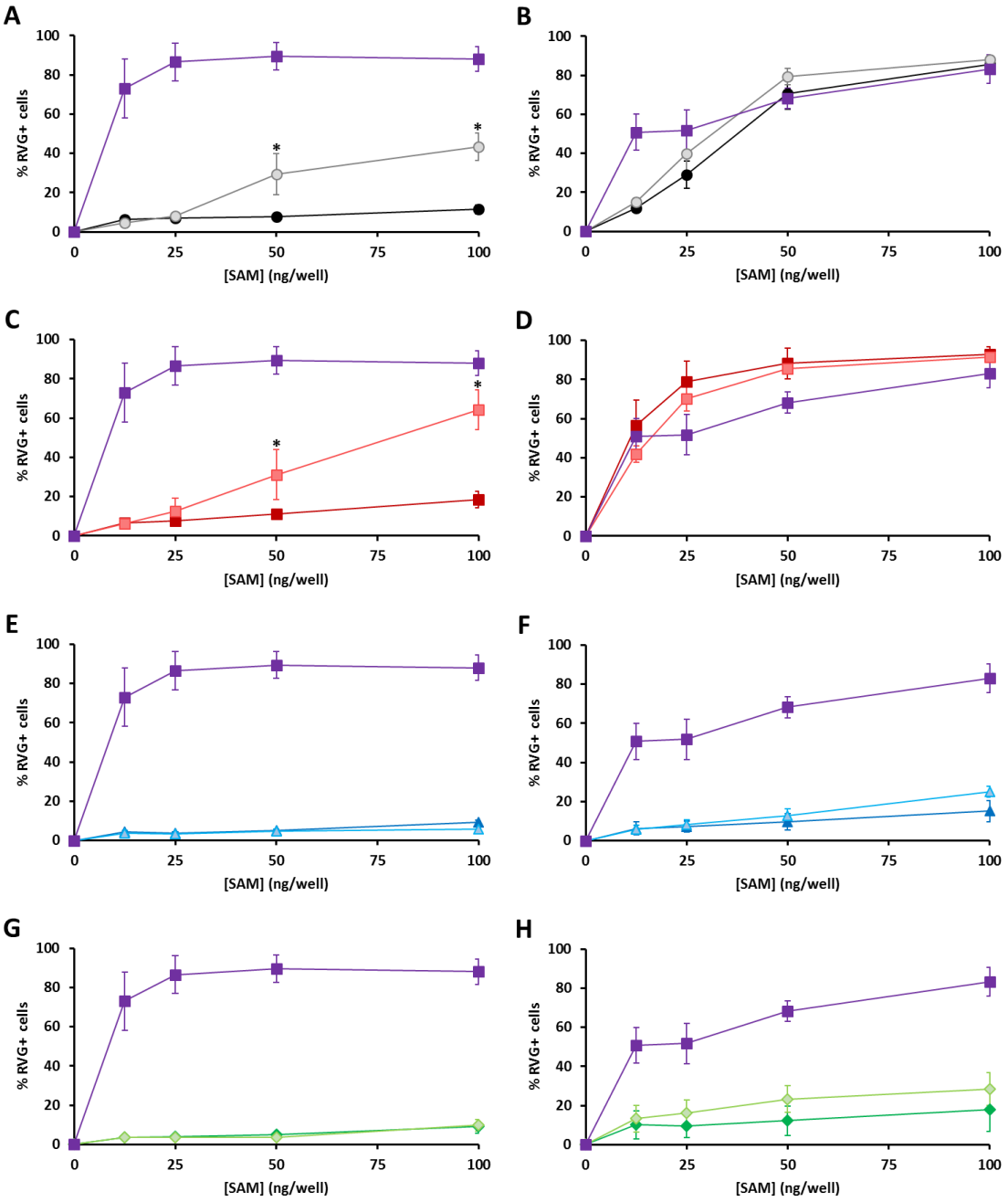

Figure 4.10. Effect of the PEGylated on the *in vitro* potency of RVG-SAM cLNPs in presence **(A, C, E, G)** and absence **(B, D, F, G)** of serum (5 %). cLNPs were composed of DOPE, a cationic lipid and a PEGylated lipid (PEG-C18 or PEG-C14) at 49:49:2 mole %. DOTAP/PEG-C18 (●) vs DOTAP/PEG-C14 (○) **(A, B)**, DDA/PEG-C18 (■) vs DDA/PEG-C14 (□) **(C, D)**, DC-Chol/PEG-C18 (▲) vs DC-Chol/PEG-C14 (△) **(E, F)**, DMTAP/PEG-C18 (◆) vs DMTAP/PEG-C14 (◇) **(G, H)**. Lipofectamine2000 (■) was used as a control. Results are represented as mean ± SD of 4 independent experiments. Statistical analysis was performed by one-way ANOVA comparing PEG-C18 cLNPs vs PEG-C14 cLNPs. $P < 0.05$ (*).

Conversely, in absence of serum, cationic lipid nanoparticles can directly interact with the negatively charged cell membrane, fuse and be released in the cytosol, in such a way that the length of the PEGylated lipid is not detrimental to the potency of LNPs. This may explains why the potency PEG-C18 and PEG-C14 LNPs was similar in serum-free conditions. Jian and co-workers (Jiang et al., 2015) reported direct delivery of siRNA using nanocapsules in absence of serum. In their studies, the use of nystatin, a drug which depletes cholesterol from plasma membrane impaired cellular uptake and knockdown activity of siRNA-nanocapsules. In contrast, nystatin had no effect on dextran, known to internalise via endocytic pathways. Due to their improved potency, DOPE:DOTAP:PEG-C14 and DOPE:DDA:PEG-C14 cLNPs were the selected candidates for *in vivo* studies.

4.5. CONCLUSIONS

A panel of cationic lipid nanoparticles (cLNPs) enclosing a self-amplifying RNA (SAM) vaccine have been designed and formulated by microfluidics. These cLNPs were composed of a cationic lipid (DOTAP, DDA, DC-Chol, DMTAP, DOBAQ), a fusogenic lipid (DOPE) and a PEGylated lipid (DSG-PEG2000 or DMG-PEG2000). In general, all SAM-cLNP formulations were sub-100 nm, with low polydispersity index (<0.2) and high SAM encapsulation efficiencies (>80 %). The ability of cLNPs to protect SAM from RNase degradation highly depended on the cationic lipid choice, with DDA conferring greater degree of protection than DOTAP, DMTAP and DC-Chol-cLNPs.

Lipid composition also played an important role on both *in vitro* cellular uptake and antigen expression. Although SAM-cLNPs were avidly taking up by murine bone marrow-derived macrophages (BMDMs), they failed to induce antigen expression. Moreover, no, antigen expression was observed in BMDMs even when transfected with Lipofectamine2000. However, SAM-cLNPs were able to induce high levels of antigen expression in BHK fibroblasts. Importantly, although cellular uptake was similar irrespective of the presence or absence of serum proteins, higher percentages of antigen-expressing cells were observed in serum-free conditions when transfected with SAM-cLNPs. In contrast, removal of serum inhibited cellular uptake of K-LNPs, and consequently, their ability to induce antigen expression.

The *in vitro* potency of SAM-cLNPs highly depended on LNP composition. DDA-cLNPs were significantly more potent than DOTAP-cLNPs, which, at the same time, were significantly more potent than DC-Chol, DMTAP and DOBAQ-cLNPs. Notably, the potency of DDA-cLNPs was comparable to Lipofectamine2000 in absence of serum. K-iLNPs were not significantly more potent than DOTAP or DDA-cLNPs, probably owing their reduced cellular uptake due to their neutral average surface charge.

The composition of cLNPs was optimised in terms of PEGylated lipid. Reducing the length of the alkyl chain of the PEGylated lipid from C18 (DSG-PEG2000) to C14 (DMG-PEG2000) resulted in improved potency of DOTAP and DDA-cLNPs, in the range of SAM concentration tested, in presence of serum. In absence of serum, however, no effect was observed. Considering these results, DOTAP and DDA-cLNPs containing the shorter PEGylated lipid (DMG-PEG, or PEG-C14) were selected as candidates for *in vivo* immunisation studies.

CHAPTER 5: IMMUNOGENICITY OF SAM VACCINES I: FORMULATION SCREENING AND DOSE TITRATION

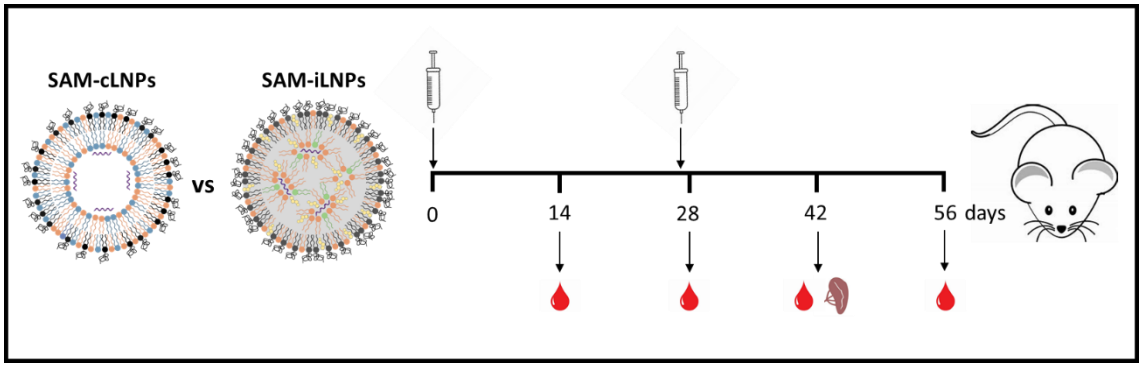

5.1. INTRODUCTION

The rabies virus causes over 50,000 human deaths annually, especially in developing countries of Africa and Asia (Sudarshan et al., 2007). Marketed vaccines such as Rabipur/RabAvert are based on inactivated cell culture-derived virus. Although they are efficacious, they must be administered several times for both pre- (days 0, 7, 21 and 28) and post-exposure prophylaxis (days 0, 3, 7, 14 and 30). In case of severe exposure, rabies virus-specific immunoglobulin (RIG) is also administered. Boosting is recommended at 2-5-year intervals for pre-exposure prophylaxis. Despite their efficacy, their high cost represents a great barrier for the developing countries (Hicks et al., 2012). Therefore, there is an unmet need for cheaper vaccines to confer long-term and sustained protection, ideally after a one single administration.

RNA-based vaccines have the potential for inexpensive, rapid and scalable production and promising alternative to current marketed vaccines (Pardi et al., 2018). The efficacy of RNA vaccines has been extensively demonstrated in animal models for rabies and other infectious diseases including respiratory syncytial virus (Geall et al., 2012), influenza (Liang et al., 2017), HIV (Bogers et al., 2015), zika virus (Richner et al., 2017) and ebola virus (Chahal et al., 2016) as well as for cancer (lung cancer, prostatic cancer and melanoma) (Pardi et al., 2018). The development of self-amplifying RNA (SAM) vaccines, based on viral replicons (usually an engineered alphavirus replicon) enable to induce local antigen expression and immune responses with lower doses compared to non-amplifying mRNA vaccines. Moreover, double-stranded RNA molecules formed in the replication process of SAM can engage toll-like receptor (TLRs) of innate cells potentially activating innate immunity, consequently resulting in broad immune responses (Iavarone et al., 2017).

The efficacy of SAM vaccines can be significantly enhanced by formulating them in delivery systems which not only protect SAM against RNase degradation but also facilitate the delivery into host cells. A range of formulations, including cationic lipid nanoparticles (Blakney et al., 2019b), ionisable lipid nanoparticles (Geall et al., 2012) and a cationic nanoemulsion (CNE) (Brito et al., 2014) has been investigated. By incorporating SAM in these delivery system robust immune responses can be induced. LNPs are being investigated in phase I/II clinical trials to deliver SAM vaccines to rabies (NCT03713086), zika (NCT04064905), influenza (NCT03345043).

5.2. AIM AND OBJECTIVES

SAM-cLNPs were extensively characterised in the previous chapter. Most promising candidates (DOTAP and DDA-cLNPs) were chosen according to their physicochemical properties (size, polydispersity index, SAM encapsulation efficiency), their ability to protect SAM from RNase degradation and their capacity to induce antigen expression *in vitro*. The aim of this chapter was to investigate the immunogenicity of a SAM vaccine, encoding the rabies virus glycoprotein (RVG), when formulated in DOTAP and DDA-cLNPs. To this end, the objectives were the following:

- To formulate SAM-LNPs and to ensure they fulfil a series of pre-requisites prior to vaccination (physicochemical characterisation, pH, osmolarity, endotoxin levels, bio-burden).
- To investigate the biodistribution of cLNPs and iLNPs in mice following intramuscular injection.
- To investigate humoral and cellular-mediated immune responses in mice following intramuscular injection.
- To compare their immunogenicity of these formulations to the commercial vaccine Rabipur and with well-established RNA delivery formulations as controls (K-iLNPs and CNE56).
- To select a SAM-cLNP candidate to probe alternative routes of administration.

5.3. MATERIALS AND METHODS

5.3.1. Materials

1,2-distearoyl-sn-glycero-3-phosphocholine (DSPC), 1,2-dioleoyl-sn-3-phosphoethanolamine (DOPE), 1,2-dioleoyl-3-trimethylammonium-propane (DOTAP), 1,2-dimyristoyl-sn-glycero-3-phosphoethanolamine-N-[methoxy(polyethylene glycol)-2000] (DMG-PEG2000) and dimethyldioctadecylammonium (DDA), were obtained from Avanti Polar Lipids. Penicillin-streptomycin, L-glutamine, cholesterol (Chol) and brefeldin A (BFA) were purchased from Sigma. Ribo Green RNA assay kit was obtained from Thermo Fisher. Live/dead fixable dead cell stain near-IR was purchased from Life Technologies. Low endotoxin foetal bovine serum (FBS) was obtained from HyClone. 100 mM citrate buffer pH 6.0 was purchased from Teknova. 10X

Perm/Wash buffer and Cytofix/Cytoperm buffer were obtained from BD Biosciences. Roswell Park Memorial Institute 1640 medium (RPMI-1640), Hank's Balance Salt Solution (HBSS) and DPBS were obtained from Gibco. Anti-mouse PE-CF594-conjugated CD8, V421-conjugated CD44, PE-conjugated TNF-α and BV786-conjugated IFN-γ and FITC-conjugated CD107a monoclonal antibodies and anti-mouse Ig, κ/negative control compensation particles set were obtained from BD Horizon. Anti-mouse BV510-conjugated CD4, APC-conjugated CD3 and PE-Cy5-conjugated IL-2 monoclonal antibodies and RBC lysis buffer were purchased from Biolegend. Anti-mouse PE-Cy7-conjugated IL-17, CD28 and CD3 monoclonal antibodies was purchased from ePharmingen. PLATELIA Rabies II Kit was obtained from Bio-Rad. The rabies peptide pool containing peptides of 15-mers with 11 amino acid overlap were obtained from Genescript. The ionisable lipid K and the vaccine Rabipur were kindly provided by GSK.

5.3.2. Self-amplifying RNA (SAM)

DNA plasmids encoding the self-amplifying RNA were constructed using standard molecular techniques. Plasmids were amplified in Escherichia coli and purified using Qiagen Plasmid Maxi kits (Qiagen). DNA was linearized immediately following the 3' end of the self-amplifying RNA sequence by restriction digest. Linearized DNA templates were transcribed into RNA using the MEGAscript T7 kit (Life Technologies) and purified by LiCl precipitation. RNA was then capped using the Vaccinia Capping system (New England BioLabs) and purified by LiCl precipitation before formulation (Quoted from (Geall et al., 2012)). A SAM encoding for the rabies virus glycoprotein (RVG) was used.

5.3.3. Formulation of SAM lipid nanoparticles (SAM-LNPs)

SAM-LNPs were produced in the Nanoassemblr Platform (Precision Nanosystems Inc.) in a Y-shaped staggered herringbone micromixer of 300 µm width and 130 µm height. Briefly, lipid mixtures composed of DOPE, a cationic lipid (DOTAP or DDA) and DMG-PEG2000 (49:49:2 molar ratio) or DSPC, Chol, lipid K and DMG-PEG2000 (10:48:40:2 molar ratio) were prepared in methanol. Then, the lipids and an aqueous phase containing SAM-RVG were injected simultaneously in the micromixer. SAM-LNPs were produced at 8 mg/mL lipid concentration, 3:1 aqueous:organic flow rate ratio (FRR), 5 mL/min total flow rate (TFR). SAM was injected in 100 mM citrate buffer pH 6.0 at a 8:1 N:P mole ratio (N in the cationic/ionisable lipid and P in SAM).

Newly formed SAM-LNPs (1mL) were dialysed against 100 mM TRIS 20 mM NaCl pH 7.4 (200 mL) for 1 hour under magnetic stirring.

5.3.4. Preparation of cationic nanoemulsion 56 (CNE56)

A cationic nanoemulsion (CNE56), designed and prepared by GSK group of companies, was used as a control for the *in vivo* immunisation studies. CNE56 was composed of DOTAP, squalene, Span 85 and Tween 80 at 0.4:4.3:0.5:0.5 weight percentage (Brito et al., 2014). Briefly, SAM-CNE56 complexation was performed by adding SAM (300 µg/mL) to the CNE56 at 1:1 v/v. Then, the mixture was vortexed for few seconds and incubated in ice for 30 seconds. SAM-CNE56 was further diluted to the desired concentration before injection.

5.3.5. Physicochemical characterisation of SAM-RVG nanoformulations

SAM formulations were characterised in terms of hydrodynamic size (Z-average), polydispersity index (PDI) and surface charge (zeta-potential) by dynamic light scattering (DLS) in a Zetasizer Nano ZS (Malvern, UK) at 0.1-0.2 mg/mL at 25 ˚C.

5.3.6. SAM encapsulation efficiency (SAM E.E.)

SAM E.E. was quantified by Ribo Green assay following manufacturer instructions. Because Ribo Green fluorescent dye is unable to penetrate the lipid membrane, samples were treated with 1 % Triton X-100 to release SAM from LNPs. Due to the interference of triton X-100 with Ribo Green quantification, calibration curves in presence and absence of 1% Triton X-100 were used. Fluorescence was measured at excitation and emission wavelength of 485 and 528 nm in a Synergy H1 microplate Reader (BioTek). Due to the inability of Ribo Green to penetrate the lipid membrane, SAM encapsulation efficiency was calculated as $(F_T - F_0)/F_T$ were F_T and F_0 are the amount of SAM quantified in presence and absence of 1 % Triton X-100.

5.3.7. *In vivo* biodistribution studies

All *in vivo* studies were conducted under the regulations of the Directive 2010/63/EU. All protocols were subjected to ethical review and were carried out in a designated establishment at the University of Strathclyde (Glasgow, UK). To track their biodistribution, cLNPs and iLNPs were co-formulated with the lipophilic fluorescent dye Di-OC_{18} (DiR). Groups of 5 6-8-week-old female balb/c mice were injected a total dose of LNPs of 25 µg (containing 1 µg of DiR dye)

intramuscularly in the right thigh (50 µL), Images were acquired at relevant time points (0, 0.17, 1, 2, 3, 6 and 10 days) in an IVIS spectrum *in vivo* imaging system (Perkin Elmer). Prior to each acquisition, mice were anaesthetised with isoflurane. The total flux (p/s) was calculated in the regions of interest (ROI) and normalised among formulations.

5.3.8. *In vivo* immunisation studies

Experiments were performed at the GSK Animal Facility in Siena, Italy, in compliance with the relevant guidelines (Italian Legislative Decree n. 26/14) and the institutional policies of GSK. The animal protocol was approved by the Animal Welfare Body of GSK Vaccines, Siena, Italy, and by the Italian Ministry of Health (Approval number "AWB 2015 01", CPR/2015/01). Groups of 10 7-weeks-old female BALB/c mice (Charles River) were immunised intramuscularly on days 0 and 28 in their right and left thigh (50 µL in total) with SAM-RVG nanoformulations (either with 1.5 or 0.15 µg SAM/dose). A group of mice was immunised with 50 µL of the commercial vaccine Rabipur (a trademark owned by GSK group of companies) corresponding to 1/20 of the human dose. Sera from individual mice was collected two and four weeks after each vaccination (days 14, 27, 42 and 56). Spleens from 3 randomly selected mice from each group were collected 2 weeks after the second immunisation to perform a T cell assay *in vitro*.

5.3.9. Total IgG titres

Total anti-RVG IgG titres were quantified with the PLATELIA RABIES II Kit *Ad Usum Veterinarium* (Bio-Rad) (Feyssaguet et al., 2007) following manufacturer instructions. First optimal pre-dilution for each formulation and time point were optimised. Then, total IgG titres were quantified in 5 pools of 2 animals per experimental group.

5.3.10. Antigen-specific T cell responses

Spleens from 3 randomly selected mice from each experimental group were taken on day 42 (2 weeks post-boost). Single cell suspensions were obtained as described elsewhere (Gallorini et al., 2014). Spleens were pushed, in cold HBSS, through 70 µm cell strainers and washed with HBSS. Samples were then incubated with RBC lysis buffer (2 mL) at 4 °C for 2 minutes. Subsequently, they were resuspended in complete RPMI (cRPMI) and passed again through cell strainers. Cells were counted in a Vi-CELL XR cell counter (Beckman Coulter). A total of $1.5 \cdot 10^6$ splenocytes were cultured per well in round-bottomed 96-well plates. Splenocytes were

stimulated with a RVGP-derived peptide pool library (2.5 µg/mL) consisting on 15-mers with 11 amino acid overlaps, anti-CD28 (2 µg/mL) and FITC-conjugated anti-CD107a (5 µg/mL) in presence of brefeldin A (5 µg/mL), for 4 hours at 37 °C. Cells were also stimulated with anti-CD3 (1 µg/mL) and anti-CD28 (2 µg/mL) or anti-CD28 alone as positive and negative controls respectively. Samples were then stained with a live/dead fixable near-IR dead cell stain kit, then fixed and permeabilised with Cytofix/Cytoperm and subsequently stained with the following antibodies in Perm/Wash Buffer: APC-conjugated anti-CD3, BV510-conjugated anti-CD4, PE-CF594-conjugated anti-CD8, BV785-conjugated anti-IFN-γ, PE-Cy5-conjugated anti-IL-2, anti-BV605-conjugated TNF-α and PE-Cy7-conjugated anti-IL-17. Samples were acquired in a LSR II flow cytometer (BD Biosciences) and analysed in FlowJo Software (Tree Star). Antigen-specific $CD4^+$ T cell subsets were identified based on the combination of secreted cytokines as follows: Th1 (IFN-γ^+ IL-2^+ TNF-α^+; IFN-γ^+ IL-2^+; IFN-γ^+ TNF-α^+; IFN-γ^+); Th0 (IL-2^+ TNF-α^+; IL-2^+; TNF-α^+). No $Th17^+$ cells were detected. The frequency of antigen-specific $CD8^+$ T cells were identified based on the combination of IFN-γ^+, IL-2^+ and TNF-α^+. The frequency of $CD8^+$ $CD107^+$ cells was calculated separately from $CD8^+$ cells.

5.3.11. Statistical analysis

Statistical analyses were performed in GraphPad Prism version 7 (GraphPad Software Inc., La Jolla, CA). The statistical significance of biodistribution studies was performed on the area under the curve (AUC) of each formulation by one-way analysis of variance (ANOVA) followed by Tukey's honest significance test. The statistical significance of total IgG titres was performed by Kruskal-Wallis test followed by Dunn's post-test. P-values below 0.05 were considered significant.

5.4. RESULTS AND DISCUSSION

5.4.1. *In vivo* biodistribution

All formulations were characterised physicochemically prior to administration. They had an average hydrodynamic size between 87 and 103 nm, low PDI (<0.2) and neutral zeta-potential (<5 mV, data not shown). All three formulations were well retained at the injection site upon intramuscular administration, with high radiances still being detected 10 days post injection (Fig. 5.1A). While the total flux of DOTAP-cLNPs and K-iLNPs decreased over time, that of DDA-cLNPs remained constant (Fig. 5.1B), suggesting that DDA-cLNPs create a stronger depot effect at the injection site. These differences were confirmed to be significant when comparing the area under the curve (AUC), with DDA-cLNPs, DOTAP-cLNPs and K-iLNPs having AUC (measured in corrected flux (p/s)·day) of $11 \cdot 10^{10}$, $7.3 \cdot 10^{10}$ and $7.2 \cdot 10^{10}$ respectively (Fig 5.1C).

Owing the neutral surface charge of K-iLNPs at physiological pH ($pKa_{(lipid\ K)} < 7$), K-iLNPs were expected to be cleared from the injection site faster than cLNPs, though K-iLNPs and DOTAP-cLNPs exhibited highly similar pharmacokinetic profiles. However, K-iLNPs are actively taken up by host cells by endogenous ligand-based mechanisms (ApoE) via scavenger receptors and the low-density lipoprotein (LDL) receptor (LDLR) (Akinc et al., 2010). LDLR is ubiquitously expressed in all nucleated cells, especially in liver cells (Goldstein and Brown, 2009), in such a way that such a targeting could compensate the neutral surface charge of this formulation.

These findings are in agreement with other investigations, in which cationic DDA:TDB liposomes and their associated antigen were retained significantly longer than DOTAP:TDB liposomes. Such a depot effect created by DDA-based liposomes resulted in more potent immune responses compared to the DOTAP formulation (Henriksen-Lacey et al., 2011a).

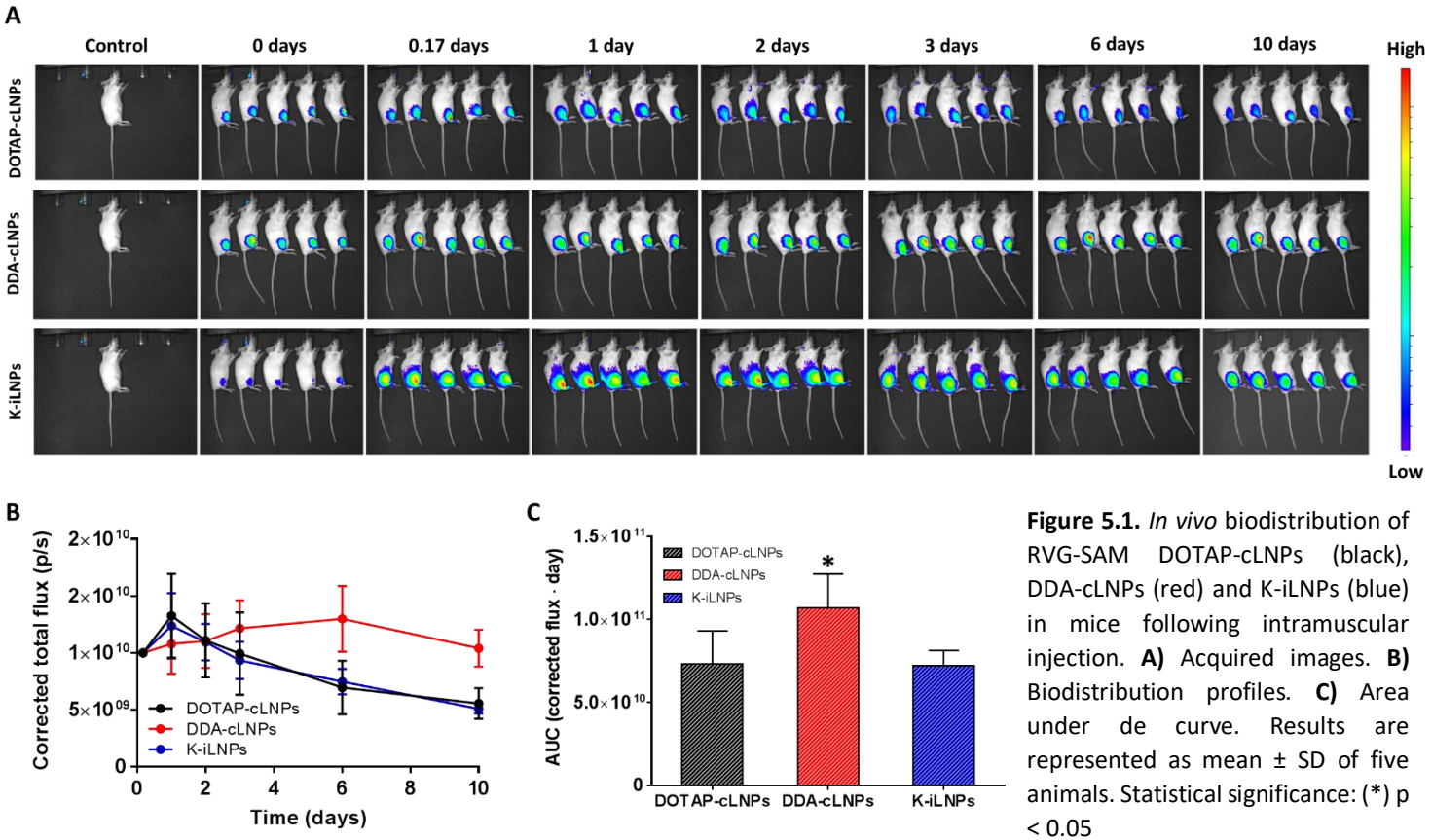

Figure 5.1. *In vivo* biodistribution of RVG-SAM DOTAP-cLNPs (black), DDA-cLNPs (red) and K-iLNPs (blue) in mice following intramuscular injection. **A)** Acquired images. **B)** Biodistribution profiles. **C)** Area under de curve. Results are represented as mean ± SD of five animals. Statistical significance: (*) $p < 0.05$

5.4.2. Humoral immune responses

Neutralising antibodies (NAs) confer full protection against rabies infection and therefore their production is critical (Xiang et al., 1995). Standard methods for quantifying NAs, developed several decades ago, include the rapid fluorescent focus inhibition assay (RFFIT) (Smith et al., 1973) and the fluorescent antibody virus neutralisation assay (FAVN) (Cliquet et al., 1998). However, these assays require the use of live rabies virus and therefore very well-trained technicians and certified laboratory facilities required. NA titres above 0.5 international units (IU), determined against an infectious reduction assay against a World Health Organisation (WHO) reference serum, are considered protective in mammals (Ertl, 2009). Herein, the commercial PLATELIA Rabies II Kit (Bio-Rad), based on an enzyme-linked immunosorbent assay (ELISA) assay, was used. By measuring total anti-RVG IgG titres (equivalent units/mL), it allows to indirectly quantify NAs. Remarkably, PLATELIA Rabies II Kit exhibited a strong correlation compared to the reference method of seroneutralisation (RFFIT) on >600 serum samples from naïve and vaccinate people (Feyssaguet et al., 2007).

All SAM-nanoformulations were characterised prior to administration. They had an average diameter size ranging from 80 to 160 nm and low PDI (<0.2). SAM cLNPs and iLNPs had a neutral zeta-potential (<5 mV) while SAM-CNE56 was slightly positive (15-20 mV). In addition, they had high SAM encapsulation efficiency (>95%) (Table 5.1). Furthermore, they had an osmolarity of 300 ± 60 mOsm/mL and a pH ranging from 7 to 7.4. In addition, no bioburden was detected after 24 hours when SAM-nanoformulations (10 µL) were incubated in agar plates at 37°C (data not shown).

Female 7-week-old BALB/c mice were immunised intramuscularly twice (prime and boost) four weeks apart with either 1.5 or 0.15 µg RVG-SAM formulated in DOTAP-cLNPs, DDA-cLNPs, K-iLNPs or CNE56. 1/20 of the human dose (HD) of the commercial vaccine Rabipur was used as a control. Sera was collected two and four weeks after first and second immunisation respectively and pooled in five pools of two sera per pool.

Table 5.1. Physicochemical properties of SAM-nanoformulations used for immunisation studies in mice. *SAM encapsulation efficiency (E.E.); zeta-potential (ZP)*. Size, PDI and zeta-potential values are represented as mean ± SD of three consecutive measurements. cLNPs were composed of DOPE, a cationic lipid (DOTAP or DDA) and DMG-PEG2000 at 49:49:2 mole %. K-iLNPs were composed of DSPC, Chol, lipid K and DMG-PEG2000 at 10.48:40:2 mole %.

Formulation	Dose	Size (d.nm)	PDI	ZP (mV)	SAM E.E. (%)
DOTAP-cLNPs	Prime	75.6 ± 0.7	0.19 ± 0.01	3.4 ± 0.7	98.9 ± 0.1
	Boost	74.4 ± 3.4	0.11 ± 0.02	2.6 ± 0.2	98.2 ± 0.1
DDA-cLNPs	Prime	78.5 ± 0.4	0.16 ± 0.01	3.1 ± 0.6	99.3 ± 0.1
	Boost	81.3 ± 0.6	0.18 ± 0.01	2.8 ± 0.4	99.0 ± 0.1
K-iLNPs	Prime	117 .2 ± 0.6	0.13 ± 0.01	-0.1 ± 0.3	96.8 ± 0.1
	Boost	155.4 ± 1.1	0.15 ± 0.02	1 ± 0.4	97.3 ± 0.1
CNE	Prime	136.5 ± 1.3	0.13 ± 0.02	19.3 ± 0.2	96.6 ± 0.1
	Boost	145.3 ± 1.4	0.12 ± 0.02	18.5 ± 0.4	96.4 ± 0.1

No anti-RVG IgGs were detected in non-immunised mice. The OD values of pre-immune sera were comparable to the blank (data not shown). When formulated in DOTAP or DDA-cLNPs, RVG-SAM elicited the production of anti-RVG IgGs above the protection threshold of 0.5 equivalent units/mL (EU/mL) two weeks after a single vaccination (prime) even with a dose as low as 0.15 µg, with no significant differences compared to CNE56-formulated SAM and Rabipur (5% HD, Fig 5.2A). With a dose of 0.15 µg of RVG-SAM, K-iLNPs elicited significantly higher antibody titres than cLNPs, CNE56 and Rabipur. Although a similar trend was observed for the higher (1.5 µg) dose, results were found to be non-significant. Interestingly, while a dose-dependent immune response was observed for both K-iLNPs and CNE56, no clear dose-response was observed for SAM-cLNP formulations (Fig 5.2A).

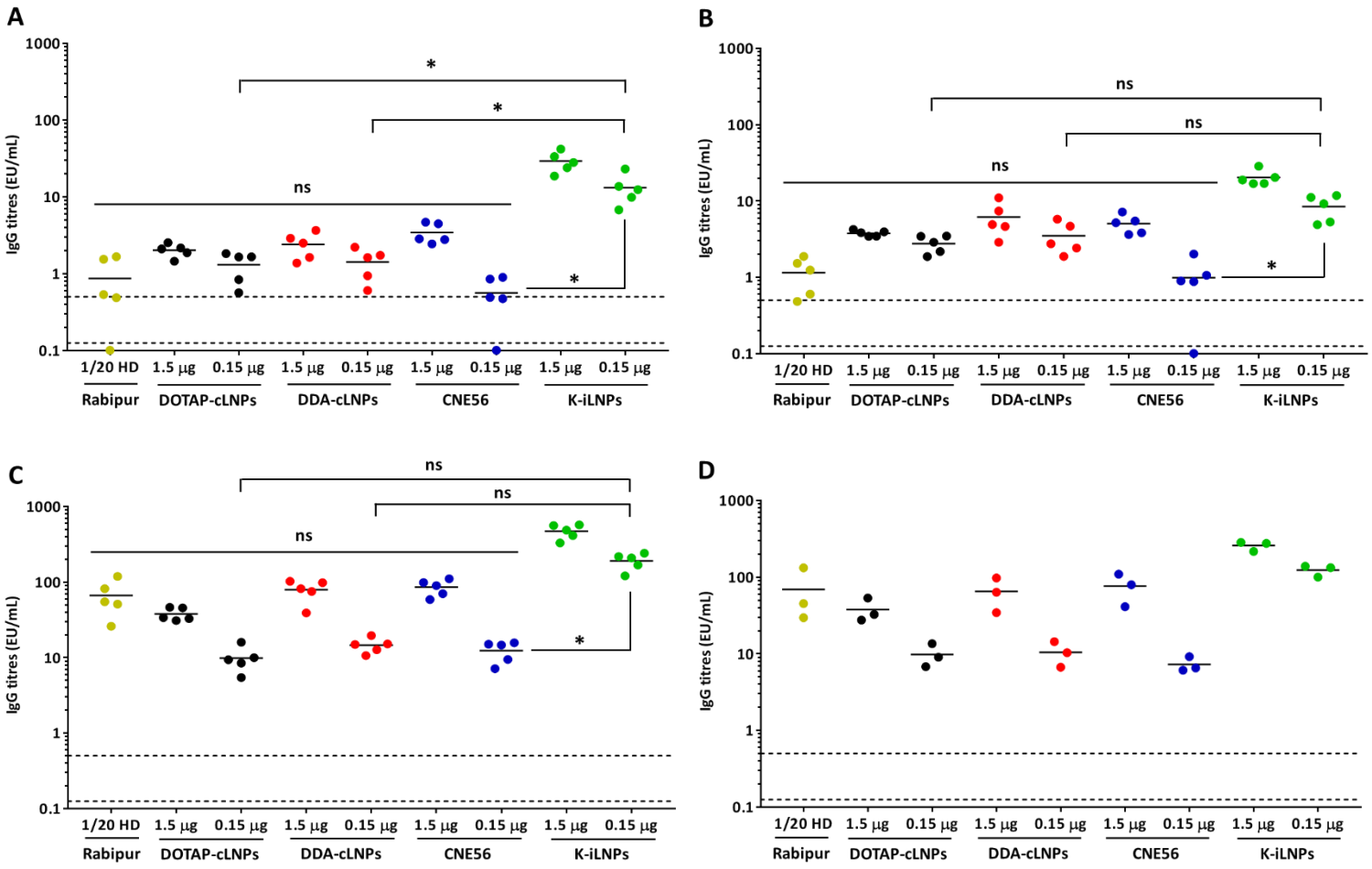

Figure 5.2. Total anti-RVG IgG titres in mice upon intramuscular injection of SAM formulations or Rabipur on days 0 and 28. Sera were collected after 14 **(A)**, 27 **(B)**, 42 **(C)** and 56 days **(D)** and total IgG titres were quantified using PLATELIA RABIES II KIT (Bio-Rad). Dots depict measurements from pools of 2 mice each. Solid lines represent the geometric mean of each group. Dotted lines at 0.5 and 0.125 EU/mL correspond to protection threshold and limit of quantification respectively. *HD (human dose*). The line represents the geometric mean titre (GMT) for the group. Statistical significance: (*) $p < 0.05$.

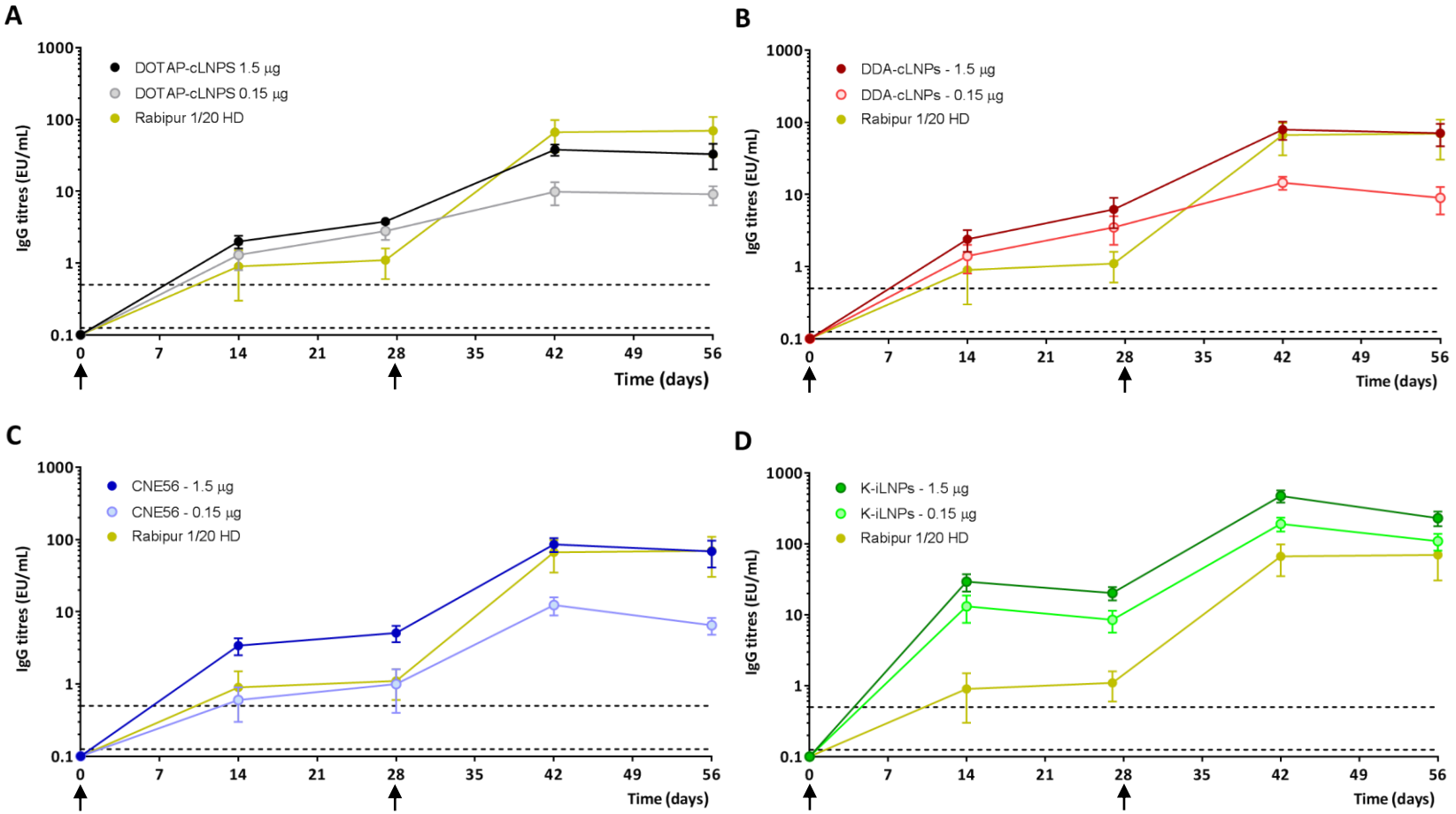

Figure 5.3. Time course of total anti-RVGP IgG titers in mice upon intramuscular injection of SAM formulations or Rabipur on days 0 and 28 (denoted by arrows). **A)** DOTAP-cLNPs, **B)** DDA-cLNPs, **C)** CNE56, **D)** K-iLNPs. Sera were collected after 14, 27, 42 and 56 days and total IgG titres were quantified using PLATELIA RABIES II KIT (Bio-Rad). Dotted lines at 0.5 and 0.125 EU/mL correspond to protection threshold (according to manufacturer) and limit of quantification respectively. *HD (Human dose*).

Four weeks after the first immunisation, protective levels of anti-RVG IgG titres were still maintained, with a similar trend in immunogenicity among all formulations (Fig 5.2B). For instance, vaccination with 1.5 μg of RVG-SAM formulated in DOTAP and DDA-cLNPs induced average titres of 3.8 ± 0.3 and 6.2 ± 2.8 EU/mL respectively. In contrast, a lower dose of RVG-SAM (0.15 μg) resulted in antibody titres of 2.8 ± 0.7 and 3.5 ± 1.5 EU/mL respectively. The immune responses elicited by cLNP-formulated RVG-SAM were not inferior to CNE56 and Rabipur. Similarly, although IgG titres elicited by K-iLNPs were higher than those elicited by cLNPs. RVG-SAM, especially when formulated in K-iLNPs, promoted a rapid production of antibodies above the protection threshold (0.5 EU/mL) thereby demonstrating the potential of SAM vaccines to elicit robust immune responses after one single injection, as previously reported (Brito et al., 2015).

Antibody titres increased up to 20-fold two weeks after a second vaccination (boost), with all SAM-nanoformulations inducing antibody titres above 10 EU/mL (Fig. 5.2C), and these titres were maintained for at least other two weeks (Fig. 5.2D). Notably, cLNP-formulated RVG-SAM was as immunogenic as the licensed vaccine Rabipur. After the second immunisation, a dose-dependent immune response was observed for DOTAP (38 vs 10 EU/mL) and DDA-cLNPs (80 vs 15 EU/mL, Fig. 5.2C). Although DDA-cLNPs were not significantly different to DOTAP-cLNPs. DDA-cLNPs induced greater antibody titres than DOTAP-cLNPs (80 EU/mL vs 38 EU/mL). These results are in agreement with recent investigations, where the antibody titres elicited by DDA:DOPE:Chol cLNPs (35:49:16 molar ratio), enclosing a SAM encoding for HIV gp140, were higher but not significantly superior than the DOTAP formulation (Blakney et al., 2019b). This effect is likely attributed to the adjuvating properties of DDA (Christensen et al., 2007).

Both cLNP formulations were as immunogenic as CNE56, a safe and efficient SAM delivery system in small animal models and non-human primates (Brito et al., 2014; Brito et al., 2015). Moreover, a RVG-SAM CNE56 vaccine candidate, designed and developed by GSK is currently being investigated in a phase I clinical trial in humans (NCT04062669, as of September 2019). The highest anti-RVG titres were achieved with K-iLNPs, with 474 and 191 EU/mL with doses of 1.5 and 0.15 μg SAM respectively. For the lower dose (0.15 μg), K-iLNPs were superior compared to cLNPs and CNE56 but comparable at a higher dose (1.5 μg). An illustrative time course of total anti-RVG IgG titres is shown for each of the formulations in Fig. 5.3. These findings are in

agreement with previous investigations on mRNA vaccines, where long-lived (up to 5 months) immune responses were reported (Brito et al., 2015; Lutz et al., 2017).

Few studies have compared the efficacy of cationic and ionisable LNPs to deliver therapeutic mRNAs. Akinc et al. compared the efficiency of cLNPs and iLNPs to deliver siRNA intravenously to knockdown FVII in hepatocytes. iLNPs were based on DLin-KC2-DMA, a less potent analogue of DLin-MC3-DMA, while cLNPs were prepared with the cationic lipidoid $98N_{12}$-5(I), cholesterol and DMG-PEG2000 (Akinc et al., 2009). Administration of 5 mg/Kg of cLNP-formulated siRNA resulted in 80% FVII knockdown, while only 0.2 mg siRNA/Kg were required to achieve the same effect when formulated in KC2-iLNPs (Akinc et al., 2010). In another study, DSPC:Chol:MC3:DMG-PEG2000 enclosing a SAM encoding the influenza hemagglutinin (HA) elicited robust production of antibodies. In contrast, no immunogenicity was observed for DOTAP-containing cLNPs (Hassett et al., 2019). However, it should be considered that DOTAP was co-formulated with DSPC, Chol and a DMG-PEG2000 for a direct comparison of DOTAP with MC3 and other ionisable lipids. Accordingly, the lack of immune responses was likely related to the absence of a fusogenic lipid such as DOPE, which enhances the capability of cLNPs to promote endosomal escape and induce antigen expression. Furthermore, the use of ionisable lipids does not necessarily guarantee more efficient delivery of mRNA and SAM vaccines. Indeed, in the investigations conducted by the same authors, some iLNPs containing other novel ionisable lipids did not elicit production of IgGs. Other comparisons between cationic and ionisable LNPs were carried out by Blakney et al. (Blakney et al., 2019b). In their studies, ionisable LNPs based on the lipid C12-200 (Love et al., 2010) elicited similar antibody titres than DOTAP and DDA-cLNPs.

5.4.3. T cell responses

Although cell-mediated immunity does not prevent initial viral infection, it plays a key role in virus clearance (Wiktor, 1978). On the other hand, $CD4^+$ T cells are pivotal in mounting robust immune responses through the production of NAs. Indeed, while mice vaccinated with RVG-mRNA (80 µg) conferred protection against lethal challenge, the depletion of $CD4^+$ T cells in mice resulted in loss of protection (Schnee et al., 2016). Accordingly, the production of cytokines by T cells was investigated.

Two weeks after the second immunisation, splenocytes from immunised mice were stimulated *in vitro* with a RVG-derived peptide pool and stained with a panel of antibodies to identify $CD4^+$ and $CD8^+$ T cells positive for selected cytokines (IFN-γ, TNF-α, IL-2 and IL-17). Finally, samples were analysed by flow cytometry to quantify and qualify antigen-specific (RVG-specific) T cells induced by vaccination. A representative example of the gating strategy used for the analysis of the flow cytometry data is shown in Fig. 5.4. SAM vaccines mimic a viral infection and hence are a suitable platform to induce potent T cell responses, particularly Th1 and cytotoxic T cells (CTLs).

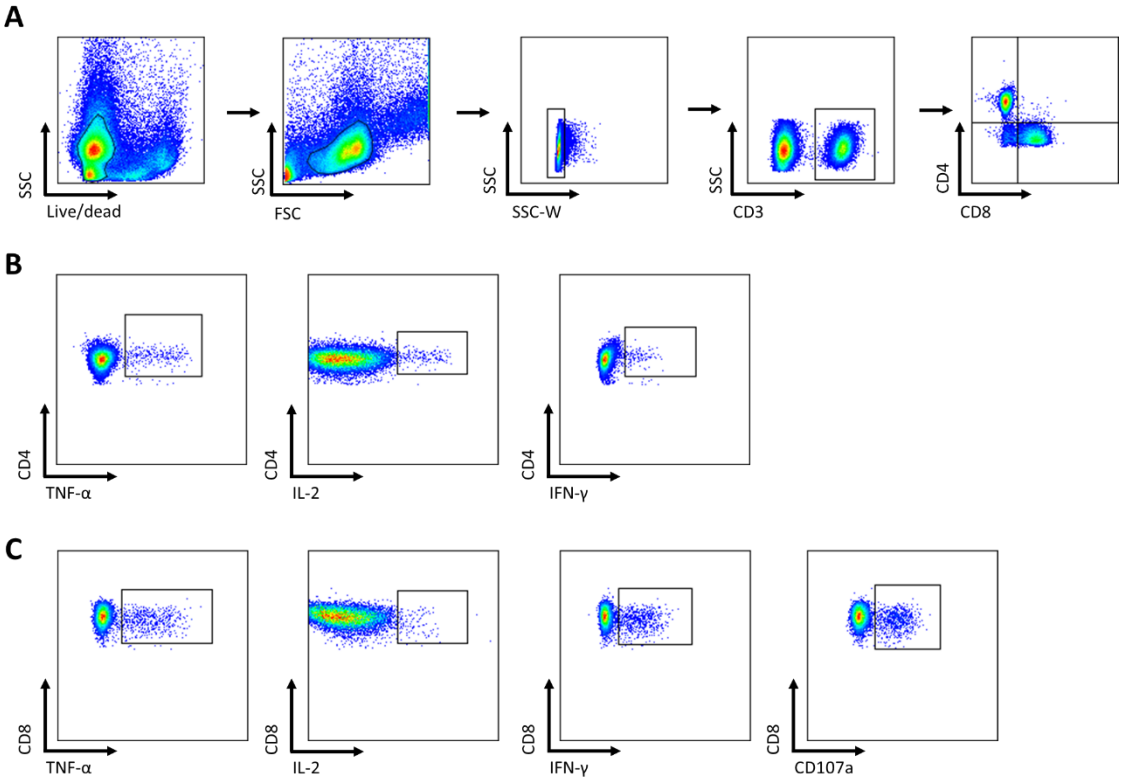

Figure 5.4. Gating strategy used for the identification of antigen-specific T cells upon restimulation. **A)** Gating on $CD4^+$ and $CD8^+$ T cells. **B)** $CD4^+$ T cell cytokines. **C)** $CD8^+$ T cell cytokines and CD107a. TNF-α^+, IL-2^+ and IFN-γ^+ cells were analysed in combination with Boolean gates. $CD107a^+$ cells were analysed separately.

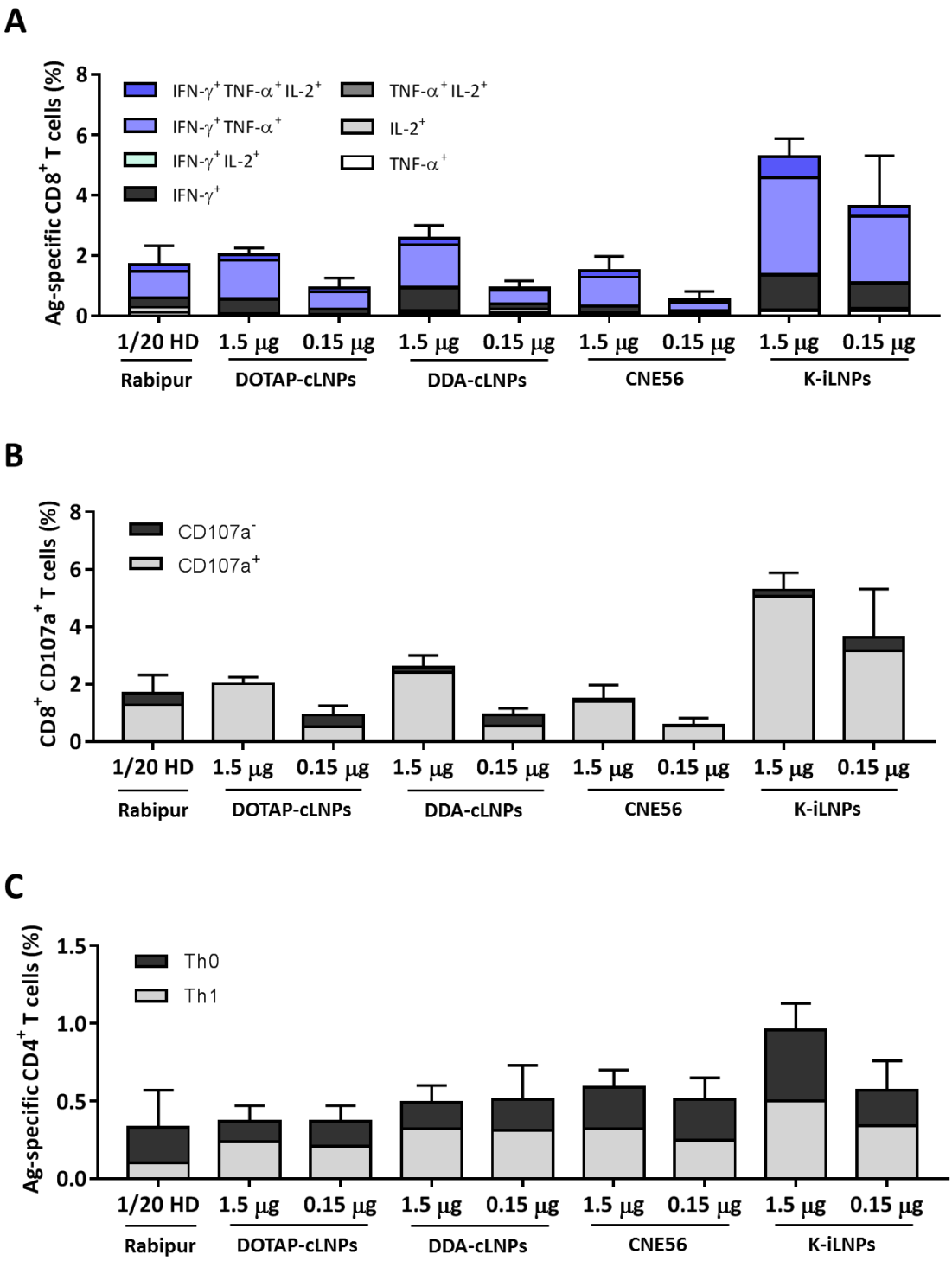

Figure 5.5. Frequencies of RVG Ag-specific T cells 2 after the second immunisation from splenocytes stimulated *in vitro* with a peptide pool spanning RVG. **A)** Cytokine-producing $CD8^+$ T cells **B)** $CD8^+$ $CD107^+$ T cells. **C)** Cytokine-producing $CD4^+$ Th0 and Th1 cells according to secreted cytokines. No $IL\text{-}17^+$ cells were detected. Results are represented as mean ± SD of three samples.

The greater *in vivo* potency of K-iLNPs observed on the production of antibodies was also reflected in higher frequencies of antigen-specific $CD8^+$ T cells compared to the rest of SAM-nanoformulations, with 5.3% and 3.6% for RVG-SAM doses of 1.5 and 0.15 μg respectively. Similar percentages of cytokine-producing $CD8^+$ T cells were observed among DOTAP-cLNPs, DDA-cLNPs and CNE56, with approximately 2% and 1% for 1.5 and 0.15 μg RVG-SAM respectively. Immunisation with Rabipur (5% HD), on the other hand, resulted in approximately 2.7% of antigen-specific $CD8^+$ T cells (Fig 5.5A). All formulations induced comparable cytokine profiles, with high frequency of polyfunctional $CD8^+$ T cells producing TNF-α and IFN-γ, typical of an effector phenotype. So as to quantify the cytotoxic potential of the induced $CD8^+$ T cells, the expression of CD107a, a degranulation marker that correlates with the cytotoxic activity of CTLs *in vivo*, was investigated (Fig. 5.5B) (Aktas et al., 2009; Zaritskaya et al., 2010). Most of antigen-specific $CD8^+$ T cells expressed this marker, meaning that all SAM-nanoformulations maintain the ability of SAM to induce functional cellular responses.

The immunisation with SAM-nanoformulations also promoted induction of antigen-specific $CD4^+$ T cells (Fig. 5.5C). $CD4^+$ T cells were qualified based on the combination of expressed cytokines. Th1 subset is represented by cells secreting IFN-γ alone or in combination with IL-2 and/or TNF-α; while the Th0 subset is defined by cells expressing TNF-α and/or IL-2. DOTAP and DDA-cLNPs induced similar frequencies (0.5%) at both doses tested. These frequencies were comparable to CNE56 and slightly lower compared to the high dose of SAM (1.5 μg) formulated in K-iLNPs (1% $CD4^+$ T cells). No IL-17 producing T cells were detected, as previously reported in other investigations with SAM-LNPs, where the production of IL-17 was negligible (Goswami et al., 2019). Previous investigations in mice have compared the cell-mediated immune responses of mRNA and SAM vaccines with Rabipur. In one study, vaccination with 80 μg of an unmodified RVG-mRNA resulted in similar percentages of TNF-α and IFN-γ producing $CD8^+$ T cells compared to Rabipur (10% HD). However, the RVG-mRNA vaccine elicited significantly higher percentages of antigen-specific $CD4^+$ T cells (Schnee et al., 2016). In the other study, 100 μg of a non-formulated RVG-SAM and Rabipur (10% HD) induced similar production of IL-2 and IFN-γ by T cells (Saxena et al., 2009). Whereas a relatively high dose of RVG-mRNA and RVG-SAM was needed to elicit immune responses comparable to Rabipur, the formulation of RNA vaccines in delivery systems allows to significantly reduce the therapeutic dose, as observed here, where

vaccination with 1.5 µg of RVG-SAM formulated in cLNPs or iLNPs resulted in similar immune responses compared to Rabipur (5% HD). Same observations were reported in the studies conducted by Brito et al., where immunisation with iLNP-formulated RVG-SAM (1.5 µg) resulted in higher cell-mediated immune responses (Brito et al., 2015).

Finally, no correlation was observed between biodistribution and immunogenicity (antibody production and T cell responses) of SAM-LNPs. The role of the depot effect is highly formulation dependent. For instance, the creation of a depot at the injection site is critical for the mechanism of action of the vaccine adjuvant CAF01, composed of DDA and TDB, while the emulsion-based adjuvant MF59 does not require the formation of a depot. Similarly, the immunogenicity of mRNA-iLNPs is thought to be unrelated to the persistence of LNPs at the injection site. Indeed, Hasset et al. investigated a panel of 30 iLNPs based on biodegradable ionisable lipids as to find that some of them were more potent than MC3-iLNPs despite they were cleared significantly faster (Hassett et al., 2019).

5.5. CONCLUSIONS

A self-amplifying RNA (SAM) vaccine encoding the rabies virus glycoprotein (RVG) elicited, in mice, robust production of IgGs above the protection threshold (0.5 EU/mL) when formulated in cationic lipid nanoparticles (cLNPs) based on DOTAP or DDA even after one single intramuscular injection; with DDA-cLNPs inducing slightly higher but not statistically significant antibody titres compared to the DOTAP formulation. Notably, DOTAP and DDA-cLNPs were not inferior to the commercial vaccine Rabipur (5% HD). Furthermore, antibody titres were comparable to the well-established CNE56, an effective SAM delivery system currently being investigated in a phase I clinical trial in humans. As expected, ionisable LNPs (iLNPs) were significantly more potent than the rest of the formulations. Moreover, antigen-specific $CD4^+$ and $CD8^+$ T cells, producing cytokines (TNF-α, IFN-γ and IL-2 or a combination thereof), were detected two weeks after the second vaccination. Again, highest frequencies of antigen-specific cells were observed with K-iLNPs, while no significant differences were observed among cLNPs, CNE and Rabipur. Biodistribution investigations suggested that DOTAP-cLNPs, DDA-cLNPs and K-iLNPs are well retained at the injection site when administered intramuscularly, tough no correlation with

immunogenicity was found. In summary, DOTAP and DDA-cLNPs were effective SAM delivery systems. When formulated in cLNPs, both humoral and cell-mediated immune responses were elicited. Considering that the quality of the immune response elicited by vaccines can be highly governed by the route of administration, following investigations were focused on probing alternative routes of administration (intradermal and intranasal) for selected SAM-nanoformulations.

CHAPTER 6: IMMUNOGENICITY OF SAM VACCINES II: ROUTE OF ADMINISTRATION

6.1. INTRODUCTION

The quality of the immune response can be strongly influenced by the route of administration, and optimal route of administration is highly influenced by the type of vaccine. Indeed, the physicochemical characteristics of each environment, as well as the types of cells found in them varies with the route of administration. Most vaccines are usually administered by intramuscular (IM) injection, though other routes of administration offer some advantages. For instance, intradermal (ID) vaccination allows to reduce the dose volume while maintaining the same profile of immunogenicity, thus allowing to reduce costs. On the other hand, the skin is highly populated by dendritic cells, which play a key role in innate-to-adaptive immune response transition. Indeed, their role in priming $CD8^+$ T cells upon vaccination with SAM has already been demonstrated (Lazzaro et al., 2015). Indeed, recent investigations have shown that functionalisation of ionisable lipid nanoparticles (iLNPs) with mannose-conjugated cholesterol results in improved immunogenicity of a SAM vaccine encoding the influenza hemagglutinin, especially after ID administration (Goswami et al., 2019).

The mucosa is the first barrier that many pathogens must interact with to initiate the infection. Mucosal immunity plays a pivotal role in preventing pathogen invasion through the secretion of IgA, the most abundant Ig isotype produced mucosal tissues. Accordingly, intranasal delivery benefits from the induction of local immunity in the mucosal associated lymphoid tissue (MALT). B and T cells activated in mucosal tissues are able to migrate through the common mucosal immune system (CMIS), thanks to the chemokines produced in the local microenvironment via mucosal tissue-specific receptors (e.g. integrins) on vascular endothelial cells. In addition, mucosal vaccination induces systemic production of IgGs such that it can be used for protecting against pathogens which infect the host by non-mucosal tissues. Finally, because intranasal vaccination a needle-free and non-invasive approach it can improve patient compliance and mitigate potential issues related to needle re-use. Some investigations have shown promising results on intranasally delivered nucleic acid-based vaccines, others have observed the opposite (Csaba et al., 2009). However, the IN delivery of SAM-LNP vaccines has not been explored to date.

6.2. AIM AND OBJECTIVES

Both DOTAP and DDA-cLNPs were efficient formulations to deliver RVG-SAM intramuscularly in mice. The *in vivo* immunisation studies conducted within this thesis fall within a research project were other SAM-nanoformulations (e.g. cationic polymeric nanoparticles or cationic solid-lipid nanoparticles) were investigated. Because these nanoformulations were based on DOTAP, DOTAP-cLNPs were investigated. The aim of this chapter was to investigate the immunogenicity of RVG-SAM DOTAP-cLNPs in mice via intramuscular, intradermal and intranasal administration. To this, the objectives were the following:

- To formulate RVG-SAM LNPs and to ensure they fulfil a series of pre-requisites prior to vaccination (physicochemical characterisation, pH, osmolarity, endotoxin levels, bio-burden).
- To investigate the biodistribution of DOTAP-cLNPs and K-iLNPs after intramuscular (IM), intradermal (ID) and intranasal (IN) administration.
- To investigate the immunogenicity of DOTAP-cLNPs following IM, ID and IN vaccination
- To compare the immunogenicity of DOTAP-cLNPs with the commercial vaccine Rabipur and K-iLNPs

6.3. MATERIALS AND METHODS

6.3.1. Materials

1,2-distearoyl-sn-glycero-3-phosphocholine (DSPC), 1,2-dioleoyl-sn-3-phosphoethanolamine (DOPE), 1,2-dioleoyl-3-trimethylammonium-propane (DOTAP) and 1,2-dimyristoyl-sn-glycero-3-phosphoethanolamine-N-[methoxy(polyethylene glycol)-2000] (DMG-PEG2000) were obtained from Avanti Polar Lipids. Penicillin-streptomycin, L-glutamine, cholesterol (Chol) and brefeldin A (BFA) were purchased from Sigma. Ribo Green RNA assay kit was obtained from Thermo Fisher. Live/dead fixable dead cell stain near-IR was purchased from Life Technologies. Low endotoxin foetal bovine serum (FBS) was obtained from HyClone. 100 mM citrate buffer pH 6.0 was purchased from Teknova. 10X Perm/Wash buffer and Cytofix/Cytoperm were obtained from BD Biosciences. Roswell Park Memorial Institute 1640 medium (RPMI-1640), Hank's Balance Salt

Solution (HBSS) and DPBS were obtained from Gibco. Anti-mouse PE-CF594-conjugated CD8, V421-conjugated CD44, PE-conjugated TNF-α and BV786-conjugated IFN-γ and FITC-conjugated CD107a monoclonal antibodies and anti-mouse Ig, κ/negative control compensation particles set were obtained from BD Horizon. Anti-mouse BV510-conjugated CD4, APC-conjugated CD3 and PE-Cy5-conjugated IL-2 monoclonal antibodies and RBC lysis buffer were purchased from Biolegend. Anti-mouse PE-Cy7-conjugated IL-17, CD28 and CD3 monoclonal antibodies was purchased from ePharmingen. PLATELIA Rabies II Kit was obtained from Bio-Rad. Collagenase D and DNAse I were purchased from Roche. The rabies peptide pool containing peptides of 15-mers with 11 amino acid overlap were obtained from Genescript. The ionisable lipid K and the vaccine Rabipur were kindly provided by GSK.

6.3.2. Self-amplifying RNA (SAM)

DNA plasmids encoding the self-amplifying RNA were constructed using standard molecular techniques. Plasmids were amplified in Escherichia coli and purified using Qiagen Plasmid Maxi kits (Qiagen). DNA was linearized immediately following the 3' end of the self-amplifying RNA sequence by restriction digest. Linearized DNA templates were transcribed into RNA using the MEGAscript T7 kit (Life Technologies) and purified by LiCl precipitation. RNA was then capped using the Vaccinia Capping system (New England BioLabs) and purified by LiCl precipitation before formulation (Quoted from (Geall et al., 2012)). A SAM encoding for the rabies virus glycoprotein (RVG) was used.

6.3.3. Formulation of SAM lipid nanoparticles (SAM-LNPs)

SAM-LNPs were produced in the Nanoassemblr Platform (Precision Nanosystems Inc.) in a Y-shaped staggered herringbone micromixer of 300 µm width and 130 µm height. Briefly, lipid mixtures composed of DOPE, DOTAP and DMG-PEG2000 (49:49:2 molar ratio) or DSPC, Chol, lipid K and DMG-PEG2000 (10:48:40:2 molar ratio) were prepared in methanol. Then, the lipids and an aqueous phase containing SAM-RVG were injected simultaneously in the micromixer. SAM-LNPs were produced at 8 mg/mL lipid concentration, 3:1 aqueous:organic flow rate ratio (FRR), 5 mL/min total flow rate (TFR). SAM was injected in 100 mM citrate buffer pH 6.0 at a 8:1 N:P mole ratio (N in the cationic/ionisable lipid and P in SAM). Newly formed SAM-LNPs (1mL) were dialysed against 100 mM TRIS 20 mM NaCl pH 7.4 (200 mL) for 1 hour under magnetic stirring.

6.3.4. Physicochemical characterisation of SAM-RVG nanoformulations

SAM formulations were characterised in terms of hydrodynamic size (Z-average), polydispersity index (PDI) and surface charge (zeta-potential) by dynamic light scattering (DLS) in a Zetasizer Nano ZS (Malvern, UK) at 0.1-0.2 mg/mL at 25 ˚C.

6.3.5. SAM encapsulation efficiency (SAM E.E.)

SAM E.E. was quantified by Ribo Green assay following manufacturer instructions. Because Ribo Green fluorescent dye is unable to penetrate the lipid membrane, samples were treated with 1 % triton X-100 to release SAM from LNPs. Due to the interference of triton X-100 with Ribo Green quantification, calibration curves in presence and absence of 1% triton X-100 were used. Fluorescence was measured at excitation and emission wavelength of 485 and 528 nm in a Synergy H1 microplate Reader (BioTek). Due to the inability of Ribo Green to penetrate the lipid membrane, SAM encapsulation efficiency was calculated as $(F_T - F_0)/F_T$ were F_T and F_0 are the amount of SAM quantified in presence and absence of 1 % triton X-100.

6.3.6. *In vivo* biodistribution studies

All *in vivo* studies were conducted under the regulations of the Directive 2010/63/EU. All protocols were subjected to ethical review and were carried out in a designated establishment at the University of Strathclyde (Glasgow, UK). To track their biodistribution, cLNPs and iLNPs were co-formulated with the lipophilic fluorescent dye Di-OC_{18} (DiR). Groups of 5 6-8-week-old female balb/c mice were injected a total dose of LNPs of 25 µg (containing 1 µg of DiR dye) intramuscularly in the right thigh (50 µL), intradermally in the *dorsum* (20 µL) or intranasally (5 µL per nostril). Images were acquired at relevant time points (0, 0.17, 1, 2, 3, 6 and 10 days) in an IVIS spectrum *in vivo* imaging system (Perkin Elmer). Prior to each acquisition, mice were anaesthetised with isoflurane. The total flux (p/s) was calculated in the regions of interest (ROI) and normalised among formulations.

6.3.7. *In vivo* vaccination studies

Experiments were performed at the GSK Animal Facility in Siena, Italy, in compliance with the relevant guidelines (Italian Legislative Decree n. 26/14) and the institutional policies of GSK. The animal protocol was approved by the Animal Welfare Body of GSK Vaccines, Siena, Italy, and by the Italian Ministry of Health (Approval number “AWB 2015 01”, CPR/2015/01). Groups of 10 7-

weeks-old female BALB/c mice (Charles River) were immunised intramuscularly (IM), intradermally (ID) or intranasally (IN) on days 0 and 28 with 0.15 µg (50 µL), 0.15 µg (20 µL) or 1.5 µg (50 µL) of RVG-SAM respectively. Other two groups of mice were immunised Rabipur (either 1/20 or 1/50 HD). Sera from individual mice was collected two and four weeks after the first immunisation (days 14 and 27) and two weeks after the second immunisation (day 42). Spleens from 3 randomly selected mice from each group were collected two weeks after the boost to perform a T cell assay *in vitro*. Lungs from 3 randomly selected mice from groups immunised intranasally and one group immunised intramuscularly (Rabipur 1/20 HD) were collected two weeks after the boost to perform a T cell assay.

6.3.8. Total IgG titres

Total anti-RVG IgG titres were quantified with the PLATELIA RABIES II Kit *Ad Usum Veterinarium* (Bio-Rad) (Feyssaguet et al., 2007) following manufacturer instructions. First, optimal pre-dilutions for each formulation and time point were optimised. Then, total IgG titres were quantified in 5 pools of 2 animals per experimental group.

6.3.9. Antigen-specific T cell responses in spleens

Spleens from 3 randomly selected mice from each experimental group were taken on day 42. Single cell suspensions were obtained as described elsewhere (Gallorini et al., 2014). Spleens were pushed, in cold HBSS, through 70 µm cell strainers and washed with HBSS. Samples were then incubated with RBC lysis buffer (2 mL) at 4 °C for 2 minutes. Subsequently, they were resuspended in complete RPMI (cRPMI) and passed again through cell strainers. Cells were counted in a Vi-CELL XR cell counter (Beckman Coulter). A total of $1.5 \cdot 10^6$ splenocytes were cultured per well in round-bottomed 96-well plates. Splenocytes were stimulated with a RVGP-derived peptide pool library (2.5 µg/mL) consisting on 15-mers with 11 amino acid overlaps, anti-CD28 (2 µg/mL) and FITC-conjugated anti-CD107a (5 µg/mL) in presence of brefeldin A (100 µg/mL), for 4 hours at 37 °C. Cells were also stimulated with anti-CD3 (1 µg/mL) and anti-CD28 (2 µg/mL) or anti-CD28 alone as positive and negative controls respectively. Samples were then stained with a live/dead fixable near-IR dead cell stain kit, then fixed and permeabilised with Cytofix/Cytoperm and subsequently stained with the following antibodies: APC-conjugated anti-CD3, BV510-conjugated anti-CD4, PE-CF594-conjugated anti-CD8, BV785-conjugated anti-IFN-γ, PE-Cy5-conjugated anti-IL-2, anti-BV605-conjugated TNF-α and PE-Cy7-conjugated anti-IL-17 in

Perm/Wash buffer. Samples were acquired in a LSR II flow cytometer (BD Biosciences) and analysed in FlowJo Software (Tree Star). Antigen-specific $CD4^+$ T cell subsets were identified based on the combination of secreted cytokines as follows: Th1 (IFN-γ^+ IL-2^+ TNF-α^+; IFN-γ^+ IL-2^+; IFN-γ^+ TNF-α^+; IFN-γ^+; Th0 (IL-2^+ TNF-α^+; IL-2^+; TNF-α^+). No $Th17^+$ cells were detected. The frequency of antigen-specific $CD8^+$ T cells were identified based on the combination of IFN-γ^+, IL-2^+ and TNF-α^+. The frequency of $CD8^+$ $CD107a^+$ cells was calculated separately from $CD8^+$ cells.

6.3.10. Antigen-specific T cell responses in lungs

Single cell suspensions from lungs were prepared as previously described (Magini et al., 2016). Briefly, samples were treated with 200 µL collagenase D (50 mg/mL) and 20 µL DNase I (10 mg/mL) and subsequently disrupted in a gentleMACS disruptor (Miltenyi Biotech). Then, they were washed (in PBS + 10 mM EDTA), filtered through 70 µm cell strainers and incubated with RBC lysis buffer for 3 minutes at room temperature. Finally, they were resuspended in cRPMI, filtered through 70 µm cell strainers and plated in round-bottomed 96-well plates. Stimulation, intracellular staining and sample acquisition by flow cytometry were performed following the protocol described for splenocyte samples.

6.3.11. Statistical analysis

Statistical analyses were performed in GraphPad Prism version 7 (GraphPad Software Inc., La Jolla, CA). The statistical significance of biodistribution studies was performed on the area under the curve (AUC) of each formulation by one-way analysis of variance (ANOVA) followed by Tukey's honest significance test. The statistical significance of total IgG titres was performed by Kruskal-Wallis test followed by Dunn's post-test. P-values below 0.05 were considered significant.

6.4. RESULTS AND DISCUSSION

6.4.1. *In vivo* biodistribution

The *in vivo* fate of particulate delivery systems is governed by their physicochemical attributes and the route of administration. Neutral liposomal formulations (e.g. DSPC:Chol) are rapidly cleared from the body when administered intramuscularly, subcutaneously or intradermally, while cationic liposomes (e.g. DOTAP or DDA-based liposomes) create a depot at the injection site. On the contrary, when administered intravenously, cationic liposomes are rapidly recognised by the mononuclear phagocytic system (MPS) thus resulting in rapid clearance, whereas neutral liposome formulations exhibit longer blood half-lives (Lou et al., 2019). The biodistribution of DOTAP-cLNPs and K-iLNPs was investigated in mice following intramuscular (IM), intradermal (ID) and intranasal (IN) administration and monitored over a period of 10 days by *in vivo* imaging. To this end, LNPs were co-formulated with the lipophilic fluorescent dye DiR. Both formulations were characterised prior to administration. DOTAP-cLNPs and K-iLNPs had an average hydrodynamic diameter of 97 and 103 nm respectively, low PDI (<0.2) and neutral zeta-potential (<5 mV, data not shown).

As discussed in chapter 5, K-iLNPs were expected to be cleared faster compared to DOTAP-cLNPs, though no significant differences were observed in their biodistribution profile after following IM, ID and IN administration. The lack of cationic surface charge of K-iLNPs at physiological pH ($pKa_{[lipid\ K]} < 7$) could be compensated by the efficient targeting of host cells (e.g. macrophages) by LDLR and scavenger receptors. Both DOTAP-cLNPs and K-iLNPs were well retained at the injection site when administered intramuscularly and intradermally. In contrast, a high percentage of the dose was observed in the gastrointestinal tract rapidly after intranasal administration (4 hours, Fig. 6.1). When looking at the AUCs, no significant differences were observed between cLNPs and iLNPs in none of the routes. Furthermore, the AUC of the IM and ID groups were comparable and significantly higher than the IN groups (Fig 6.2). The lack of muco-adhesive properties of cLNPs and iLNPs likely compromised their ability to interact with mucosal tissues thus resulting in rapid clearance compared to IM and ID, where the formation of a depot effect can be achieved. Indeed, particulate delivery systems are often tailored with muco-adhesive moieties to enhance retention in the mucosal tissue.

Figure 6.1. *In vivo* biodistribution of RVG-SAM DOTAP-cLNPs and K-iLNPs in mice following intramuscular, intradermal and intranasal administration.

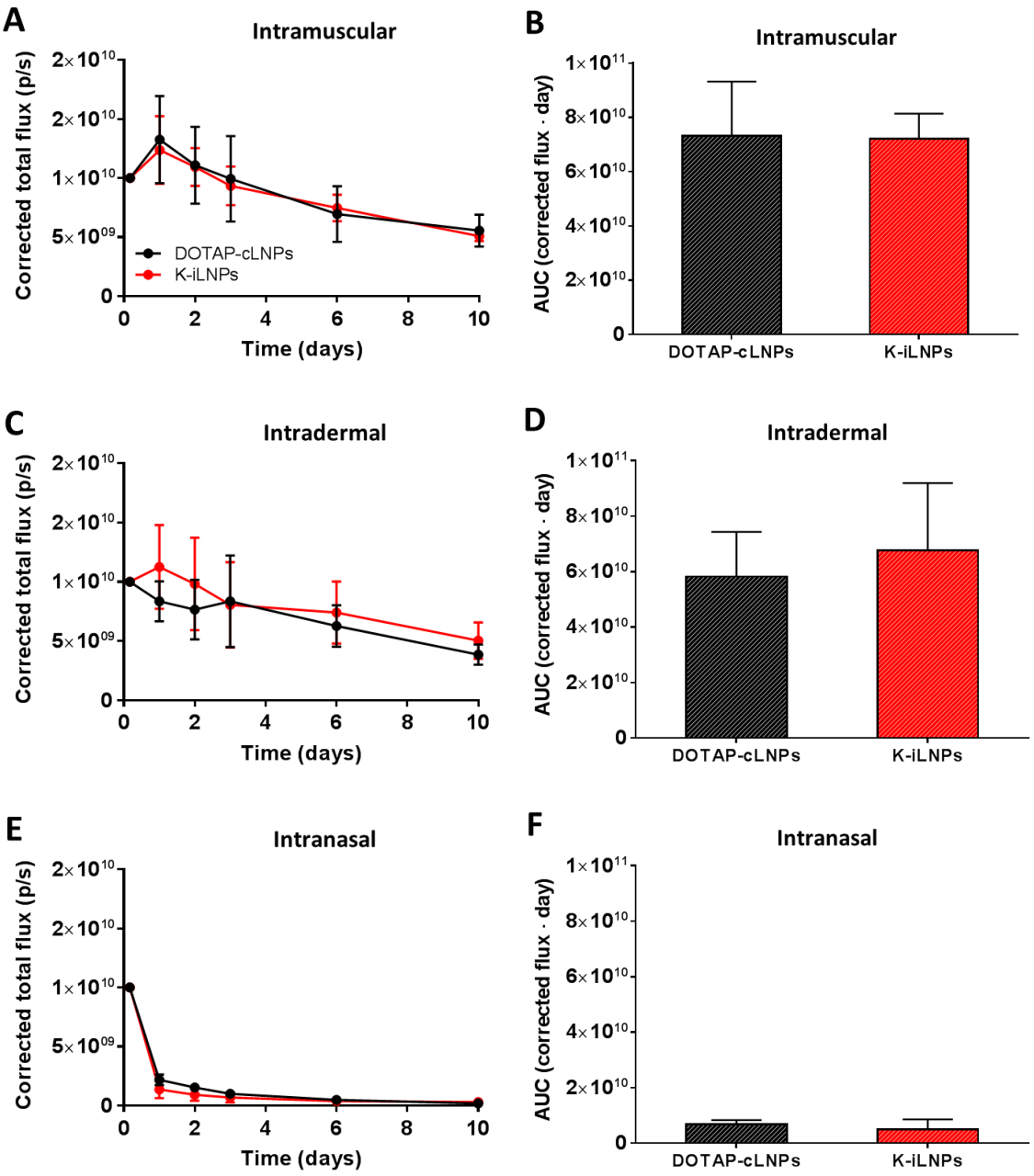

Figure 6.2. Biodistribution of DOTAP-cLNPs (black) and K-iLNPs (red) after intramuscular **(A, B)**, intradermal **(C, D)** and intranasal administration **(E, F)**. Biodistribution pharmacokinetics **(A, C, E)** and area under the curve (AUC), represented as corrected flux · day) for each of the formulations and routes tested **(B, D, F)**. Results are represented as mean ± SD of five animals per experimental group. The biodistribution data of the IM groups is the same as that represented in Fig. 5.1.

6.4.2. Humoral immune responses

The route of administration can highly influence the quality of the immune responses. The immunogenicity of RVG-SAM DOTAP-cLNPs and K-iLNPs after intramuscular (IM), intradermal (ID) and intranasal (IN) administration was investigated and compared to the commercial vaccine Rabipur. All formulations were characterised before injection. DOTAP-cLNPs and K-iLNPs formulations utilised for these studies exhibited the same physicochemical properties as those shown in chapter 5. Furthermore, "prime" and "boost" formulations had similar physicochemical attributes. DOTAP-cLNPs were slightly smaller in size (74 nm) in comparison to K-iLNPs (130 nm), though both formulations had low PDI (<0.1), neutral zeta-potential (<4 mV) and high SAM encapsulation efficiency (>97%) (Table 6.1). Moreover, they had an osmolarity of 300 ± 60 mOsm/mL and a pH ranging from 7 to 7.4 (data not shown). In addition, no bioburden was detected after 24 hours when DOTAP-cLNPs and K-iLNPs (10 µL) were incubated in agar plates at 37°C (data not shown).

Table 6.1. Physicochemical properties of SAM-nanoformulations used for immunisation studies in mice. *SAM encapsulation efficiency (E.E.); zeta-potential (ZP)*. Size, PDI and zeta-potential values are represented as mean ± SD of three consecutive measurements. DOTAP-cLNPs were composed of DOPE, DOTAP and DMG-PEG2000 at 49:49:2 mole %. K-iLNPs were composed of DSPC, Chol, lipid K and DMG-PEG2000 at 10.48:40:2 mole %.

Formulation	Dose	Size (d.nm)	PDI	ZP (mV)	SAM E.E. (%)
DOTAP-cLNPs	Prime	74.0 ± 0.4	0.10 ± 0.01	2.0 ± 0.8	97.9 ± 0.1
	Boost	73.0 ± 0.8	0..09 ± 0.01	3.7 ± 0.1	98.2 ± 0.1
K-iLNPs	Prime	131.9 ± 1.0	0.08 ± 0.01	0.3 ± 0.6	96.7 ± 0.1
	Boost	126.0 ± 0.8	0.09 ± 0.02	-1.0 ± 0.1	99.0 ± 0.0

Female 7-week-old BALB/c mice were immunised IM, ID or IN twice four weeks apart with 0.15, 0.15 and 1.5 µg RVG-SAM respectively either formulated in DOTAP-cLNPs or K-iLNPs. Mice were also vaccinated IM, ID and IN with 1/20, 1/50 and 1/20 of the human dose (HD) of Rabipur respectively. For a direct dose comparison between IM and ID, one group was also immunised IM with 1/50 HD Rabipur. Sera was collected two and four weeks after prime and two weeks after the boost respectively and pooled in five pools of two mice per experimental group. As

previously described, total anti-RVG IgG titres were quantified with the commercial PLATELIA Rabies II Kit (Bio-Rad), as it allows to indirectly correlate with neutralising antibody (NA) titres, a marker of protection. NA titres above 0.5 international units (IU), determined against an infectious reduction assay against a World Health Organisation (WHO) reference serum, are considered protective in mammals (Ertl, 2009).

No anti-RVG IgGs were detected in non-immunised mice. The OD values of pre-immune sera were comparable to the blank (data not shown). Humoral immune responses (in terms of total IgG titres) elicited by DOTAP-cLNPs (0.15 µg SAM), K-iLNPs (0.15 µg SAM) and Rabipur (1/20 HD) after IM administration were almost identical to those observed in the previous *in vivo* study shown in chapter 5 (Fig. 6.3). Indeed, when injected IM, K-iLNPs were significantly more potent compared to DOTAP-cLNPs and comparable to Rabipur (1/20 HD), (Fig. 6.3). Accordingly, the current chapter will be focused on comparisons among routes of administration (IM vs ID vs IN) and among formulations within ID and IN groups.

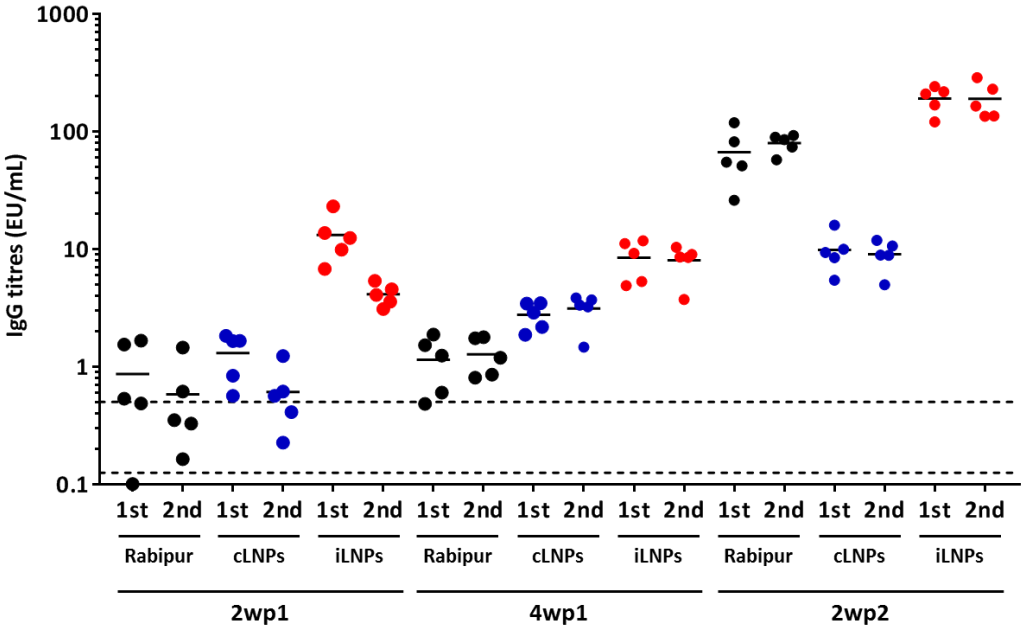

Figure 6.3. Comparison of total IgG titres of bridged groups from current Chapter (2nd) with the previous *in vivo* study shown in Chapter 5 (1st) two weeks after prime (*2wp1*), four weeks after prime (*4wp1*) and two after boost (*2wp2*) following IM administration. 1/20 HD Rabipur or 0.15 µg SAM formulated in either K-iLNPs (*iLNPs*) or DOTAP-cLNPs (*cLNPs*). Each dot represents the IgG titres of a pool of two animals. The line represents the geometric mean titre (GMT) for the group.

Regarding the ID administration, the immune responses elicited by K-iLNPs, DOTAP-cLNPs and Rabipur were comparable. Four weeks after the first immunisation, these vaccines elicited IgG titres of 6, <0.5 and <0.5 EU/mL respectively (Fig. 6.4). As also observed after IM injection, the onset of the immune response elicited by Rabipur injected ID was slower in comparison to SAM-formulations, with 0% and 60% responders two and four weeks after the first dose respectively. Two weeks after the boost dose, although K-iLNPs induced higher production of antibodies (31 ± 14 EU/mL) compared to DOTAP-cLNPs (6 ± 2 EU/mL) and Rabipur (8 ± 5 EU/mL), differences were found to be non-significant. Low percentages of responders were achieved after a single vaccination with cLNPs (0%), iLNPs (20%) and Rabipur (0%). The second vaccination with cLNPs and Rabipur did not boost the immune responses, while a modest response (80% responders, 3 ± 4 EU/mL) was achieved with a second vaccination of K-iLNPs (Fig 6.4).

When comparing IM and ID immunisations, the quality of the humoral immune response was formulation-dependent. IM vaccination with 1/20 HD and 1/50 HD Rabipur resulted mean titres of 80 and 40 EU/mL two weeks after the boost respectively. ID vaccination with 1/50 HD Rabipur induced lower (8 EU/mL) but non-inferior production of antibodies compared to the same dose given IM, though it was significantly lower compared to the higher dose (1/20 HD) injected IM. In humans, IM and ID vaccination with Rabipur in post-exposure prophylaxis result in similar NA titres. However, ID is slightly inferior compared to IM in pre-exposure prophylaxis (Giesen et al., 2015), in agreement with results shown in Fig. 6. Although IM injection is the standard route of administration of Rabipur, ID administration is an economic and antigen-saving alternative as it requires lower doses (0.1 mL) compared to IM (1 mL).

Similar anti-RVG IgG titres were observed after IM and ID vaccination with RVG-SAM DOTAP-cLNPs both before and after the boost dose (Fig 6.4). For K-iLNPs, although antibody titres two and four weeks after the first immunisation were similar between the IM and ID groups, subjects responded significantly better to the boost dose when vaccinated IM. Indeed, IgG titres after second ID vaccination with K-iLNPs was 6-fold lower compared to IM vaccination (191 EU/mL vs 31 EU/mL, $p<0.05$). IM injection of nucleic acid-based vaccines results in transfection of myocytes (Lazzaro et al., 2015), which act as a source of antigen to cross-prime dendritic cells to mount $CD8^+$ T cell responses.

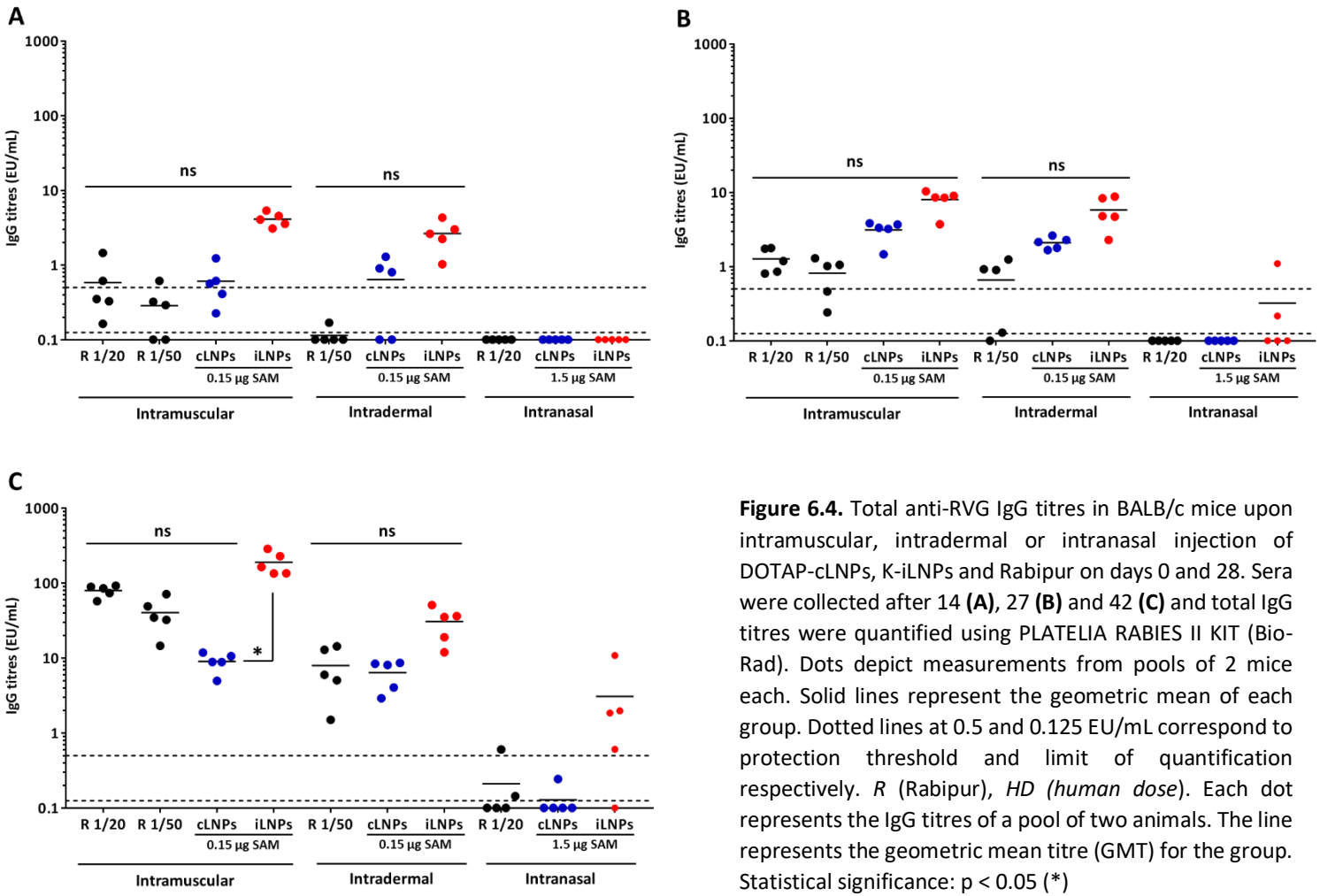

Figure 6.4. Total anti-RVG IgG titres in BALB/c mice upon intramuscular, intradermal or intranasal injection of DOTAP-cLNPs, K-iLNPs and Rabipur on days 0 and 28. Sera were collected after 14 **(A)**, 27 **(B)** and 42 **(C)** and total IgG titres were quantified using PLATELIA RABIES II KIT (Bio-Rad). Dots depict measurements from pools of 2 mice each. Solid lines represent the geometric mean of each group. Dotted lines at 0.5 and 0.125 EU/mL correspond to protection threshold and limit of quantification respectively. *R* (Rabipur), *HD (human dose*). Each dot represents the IgG titres of a pool of two animals. The line represents the geometric mean titre (GMT) for the group. Statistical significance: $p < 0.05$ (*)

Although direct transfection of dendritic cells is not a prerequisite to induce robust antigen-specific immune responses, direct transfection of these cells could potentially be achieved by ID injection, as the skin is highly populated with dendritic cells. In previous investigations, ID electroporation of DNA vaccines resulted in similar immunogenicity compared to IM electroporation (Kulkarni et al., 2013; Petkov et al., 2018). In another study, the ID administration of a pDNA vaccine encoding the hepatitis B virus surface antigen (HBsAg) formulated in cationic lipoplexes and injected ID elicited stronger production of IgGs compared to IM injection (Endmann et al., 2010).

An iLNP-formulated SAM vaccine encoding the RSV-F protein induced higher, but not significantly superior, anti-RSV-F IgG titres in mice after IM injection compared to ID injection (Geall et al., 2012). The same iLNP formulation was recently utilised to deliver a SAM vaccine encoding the influenza hemagglutinin (HA) both IM and ID in mice as to find comparable IgG and hemagglutinin titres. When iLNPs were functionalised with mannose (15% mole %), a ligand of C-type lectin receptors expressed in dendritic cells, a more rapid onset in the immune response was observed, especially after ID administration (Goswami et al., 2019).,Vaccination with a modified mRNA-HA vaccine formulated in a similar iLNP formulation resulted in a quicker onset of the immune response in rhesus macaques when administered ID compared to IM, but they equilibrated afterwards (Liang et al., 2017).

DOTAP-cLNPs and K-iLNPs were significantly less effective in inducing humoral immune responses after IN vaccination even after two doses. IN administration is an attractive route for vaccination as it allows to elicit both local and systemic immune responses. Some studies have shown enhanced production of IgGs with LNP vaccines. For instance, a single dose of a DDA-based cLNP formulation enclosing a DNA-hsp65 vaccine (25 µg) elicited robust cellular-mediated immune responses when administered IN and was significantly more potent than when administered IM (Rosada et al., 2008). In other studies, mice immunised with liposomal-adjuvanted subunit antigens showed high rates of survival when challenged with pathogens such as influenza and *Mycobacterium tuberculosis*. Conversely, other researchers have observed weaker immune responses compared to other routes of administration (Csaba et al., 2009). On the other hand, only few investigations have explored the IN administration of mRNA-LNP vaccines. A mRNA vaccine complexed with nanoparticles composed of a polymer and a

DOPC:DOTAP:DSG-PEG shell resulted in antigen-specific CTL responses against a lymphoma, delayed tumour onset and increased survival rates in prophylactic and therapeutic mouse models (Phua et al., 2014). However, the immunogenicity of SAM vaccines after IN vaccination has not been reported.

The poor retention of SAM-cLNPs and SAM-iLNPs at the administration site following IN administration (Fig 6.1 and Fig 6.2) could explain the lack of immunogenicity. Indeed, tailoring the composition of LNPs for IN delivery is also crucial to elicit robust immune responses. For instance, the use of muco-adhesive compounds, such as chitosan or polylactic acid (PLA) to improve the association to the epithelial tissue upon administration. The density of PEG-coating, on the other hand, can highly influence the efficiency of LNP delivery systems. High PEG density facilitates the interaction with the tissue and results in improved mucosal immunogenicity to subunit vaccines (Csaba et al., 2009). However, incorporation of high percentages of PEG is a double-edge weapon in RNA delivery: PEG-lipids impair the ability of LNPs to 1) associate with host cells and 2) disrupt endosomal membrane, the main barriers in RNA delivery (Pozzi et al., 2014).

6.4.2. T cell responses

T cells are essential for fighting rabies infection. Among them, $CD4^+$ T cells play a key role in mounting antiviral immune responses and their depletion has been shown to result in loss of protection against viral challenge (Schnee et al., 2016). Consequently, the effect of the route of administration of SAM-LNP vaccines on cellular-mediated immune responses was also investigated. Two weeks after the second immunisation, splenocytes from immunised mice were stimulated *in vitro* with a RVG-derived peptide pool and stained with a panel of antibodies to identify $CD4^+$ and $CD8^+$ T cells specific for selected cytokines (IFN-γ, TNF-α, IL-2 and IL-17). Finally, samples were analysed by flow cytometry to quantify and qualify antigen-specific (RVG-specific) T cells induced by vaccination. A representative example of the gating strategy used for the analysis of the flow cytometry data is shown in Fig. 6.5.

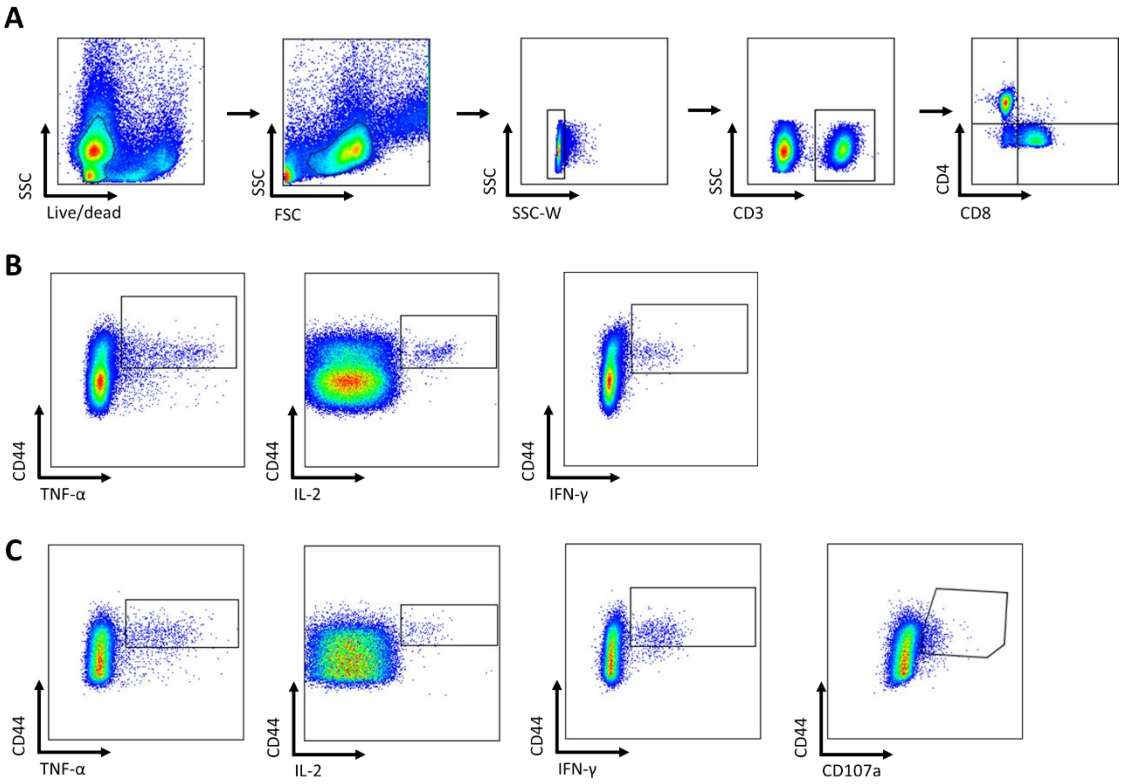

Figure 6.5. Gating strategy used for the identification of antigen-specific T cells upon restimulation as previously described (Goswami et al., 2019). **A)** Gating on $CD4^+$ and $CD8^+$ T cells. **B)** $CD4^+$ T cell cytokines. **C)** $CD8^+$ T cell cytokines and CD107a. TNF-α^+, IL-2^+ and IFN-γ^+ cells were analysed in combination with Boolean gates. $CD107a^+$ cells were analysed separately.

Multifunctional $CD8^+$ T cells (producing TNF-α, IFN-γ, IL-2 or combinations thereof) were detected after IM and ID vaccination with SAM formulated in DOTAP-cLNPs, with higher frequencies compared to Rabipur, especially after IM injection. As already observed in the previous study, SAM-K-iLNPs elicited the highest percentage of antigen-specific cytokine-producing $CD8^+$ T cells. However, lower frequencies of activated T cells were quantified (<0.2%) in mice vaccinated IN (Fig. 6.6A). The same trend was observed when looking at the degranulation marker CD107a, whose expression correlates with the cytotoxic activity of CTLs *in vivo (Aktas et al., 2009; Zaritskaya et al., 2010)*; with percentages of $CD8^+$ $CD107a^+$ T cells being ranked in the order K-iLNPs > DOTAP-cLNPs > Rabipur in IM and ID groups (Fig. 6.6B). The immunisation with SAM-nanoformulations also promoted induction of antigen-specific $CD4^+$ T cells (Fig. 6.6C). $CD4^+$ T cells were qualified based on the combination of expressed cytokines.

Th1 subset is represented by cells secreting IFN-γ alone or in combination with IL-2 and/or TNF-α; while the Th0 subset is defined by cells expressing TNF-α and/or IL-2. The percentages of antigen-specific $CD4^+$ T cells in the cLNP and iLNP groups after IM and ID vaccination were comparable. The effect of the route of administration on the percentage of activated $CD4^+$ T cells was less prominent compared to $CD8^+$ T cells. However, these differences were more evident when looking at the percentage of Th1 cells. Indeed, after IN vaccination, only 0.02-0.04% Th1 cells were quantified in cLNP and iLNP groups, while up to 0.16-0.33% Th1 were detected after IM or ID vaccination (Fig. 6.6C). Interestingly, the superiority of K-iLNPs over DOTAP-cLNPs in inducing cell-mediated immune responses was less evident after ID administration, as also observed on the humoral immune responses (Fig. 6.4). These findings further support that optimal LNP composition is highly influenced by the route of administration, as previously discussed in the previous chapter on LNPs for IV and IM delivery of RNA.

Similar findings were reported by Geall et al. (Geall et al., 2012) with RSV-F-SAM formulated in DLin-DMA-containing iLNPs. In their studies, similar percentages of Th1/Th0 $cytokine^+$ cells were detected upon IM and ID vaccination. However, the frequencies of antigen-specific $CD8^+$ T cells in the IM group were 2-fold higher (10%) compared to the ID group (5%). Similarly, the production of IFN-γ in murine splenocytes following IM vaccination with a iLNP-formulated mRNA-HA vaccine was higher, but not statistically superior, than ID vaccination (Bahl et al., 2017). The same formulation resulted in stronger production of IFN-γ by $CD4^+$ T cells in rhesus macaques when injected ID in comparison to IM. In this latter study the authors also suggested that antigen presentation to $CD4^+$ T cells was likely mediated by different dendritic cell subsets depending on the route of administration. Indeed, while IM administration targeted $CD11c^+$ and $CD1c^-$ $CD141^+$ dendritic cells, ID administration targeted $CD1a^+$ and $CD209^+$ dendritic cells (Liang et al., 2017). As discussed on the quality of the humoral immune responses, the lower frequencies of antigen-specific T cells in groups vaccinated IN were likely attributed to the LNP composition.

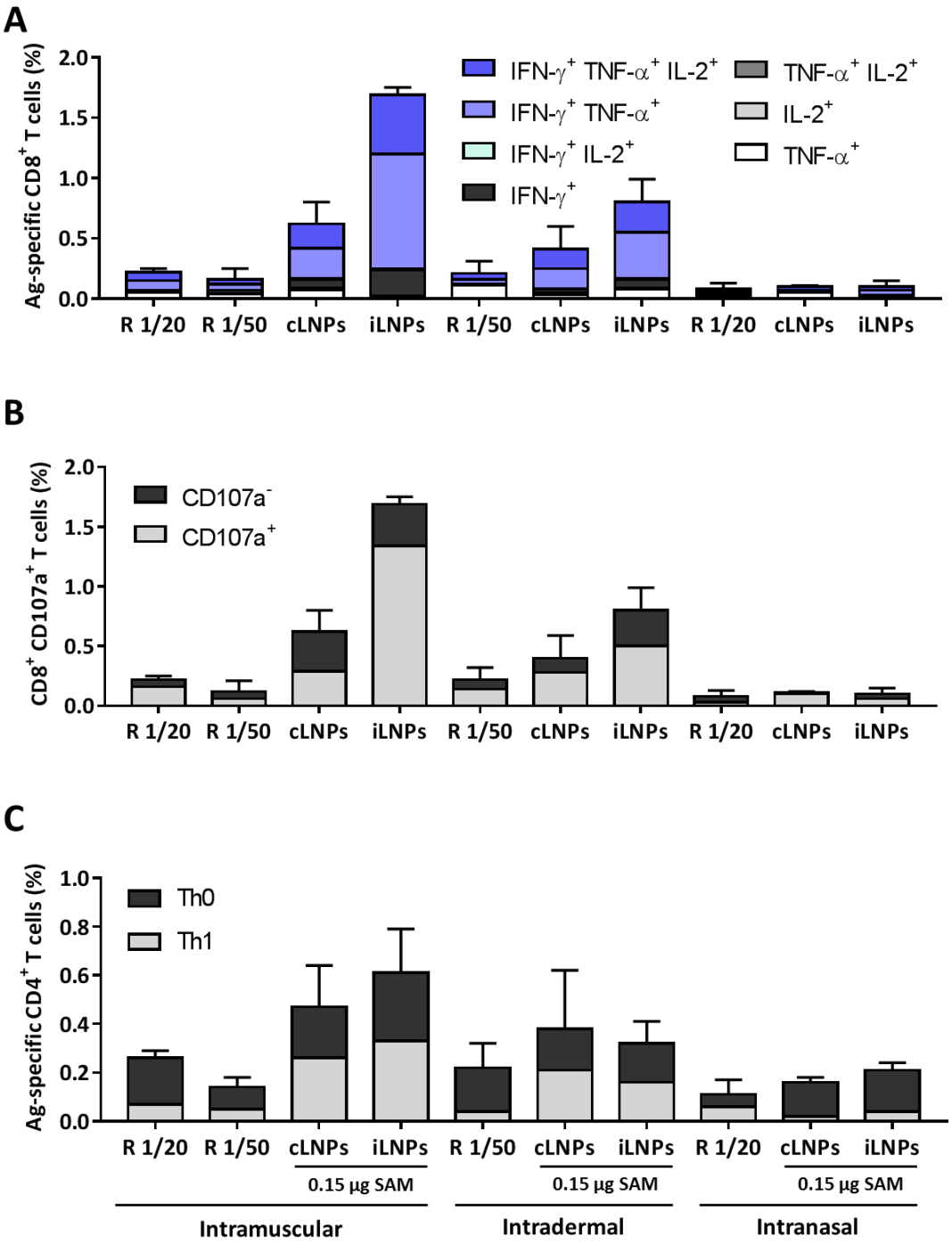

Figure 6.6. Frequencies of RVG Ag-specific T cells two weeks after boost from splenocytes stimulated *in vitro* with a peptide pool spanning RVG. **A)** Cytokine-producing $CD8^+$ T cells. **B)** $CD8^+$ $CD107a^+$ T cells. **C)** Cytokine-producing $CD4^+$ Th0 and Th1 cells according to secreted cytokines. No $IL\text{-}17^+$ cells were detected. *R (Rabipur).* Results are represented as mean ± SD of three samples.

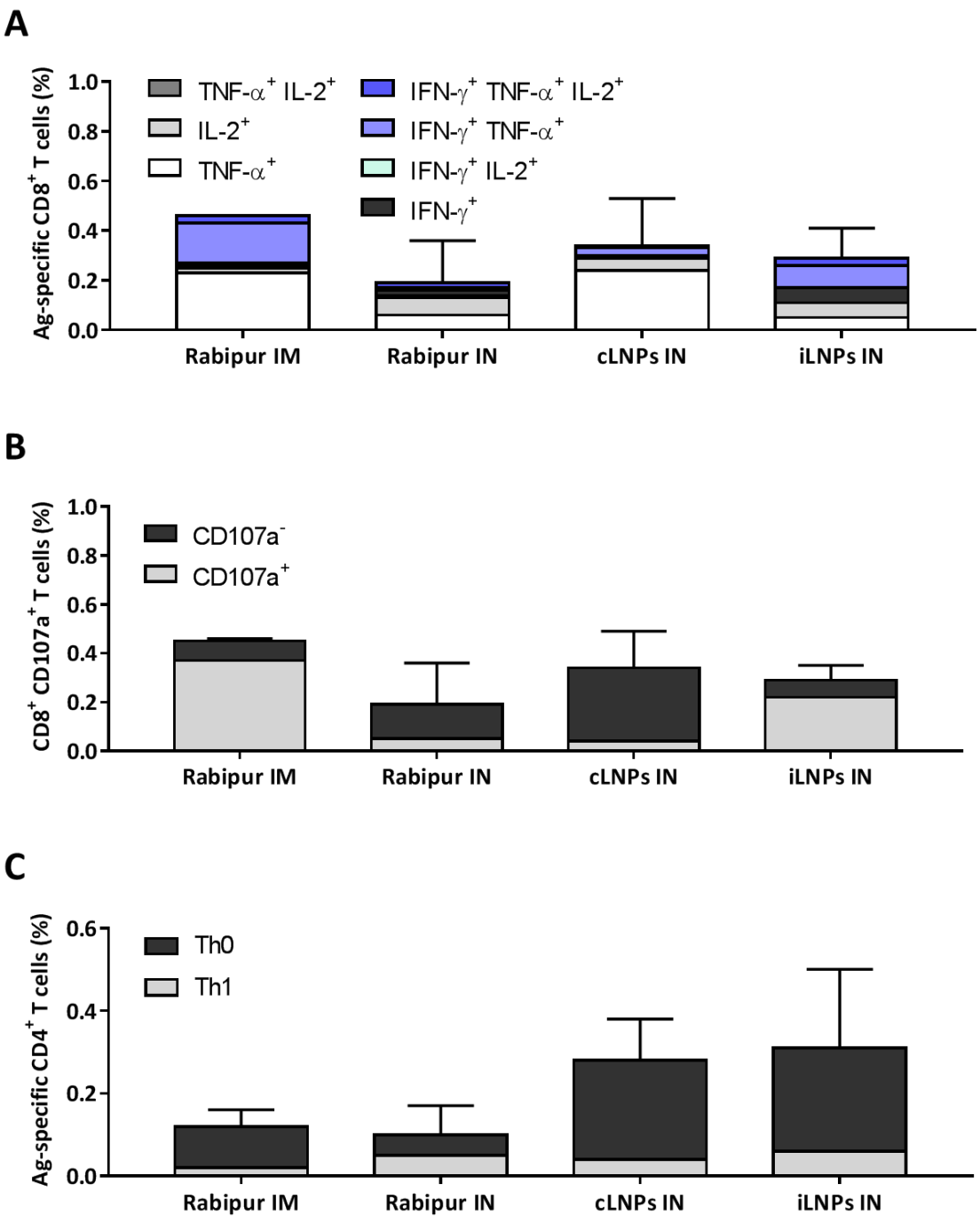

Figure 6.7. Frequencies of RVG Ag-specific T cells two weeks after boost from lung cells stimulated *in vitro* with a peptide pool spanning RVG. **A)** Cytokine-producing $CD8^+$ T cells. **B)** $CD8^+$ $CD107a^+$ T cells. **C)** Cytokine-producing $CD4^+$ Th0 and Th1 cells according to secreted cytokines. No IL-17^+ cells were detected. R (Rabipur). Results are represented as mean ± SD of three samples

When administered IN, vaccines can result in the generation of persistent lung effector T cells, which could significantly benefit host immunity against respiratory pathogens. Accordingly, a T cell assay was performed on lung cells from mice immunised IN. Mice immunised IM with 1/20 HD Rabipur were used as a control. This experiment was carried out simultaneously with the T cell assay in splenocytes. Consistent with the low immunogenicity of SAM-cLNPs and SAM-cLNPs, and Rabipur when administered IN, low frequencies of cytokine producing T cells were quantified in the lung cells (<0.4%). The percentages of cytokine$^+$ and CD107a$^+$ CD8$^+$ T cells detected in groups vaccinated IN were similar or slightly lower compared to the IM group (Fig. 6.7A and B). In contrast, the percentage of cytokine-producing CD4$^+$ T cells in the cLNP and iLNP group were slightly higher in comparison to the IM group. However, most of these CD4$^+$ T cells had a genotype Th0 (Fig 6.7C).

6.5. CONCLUSIONS

A self-amplifying RNA (SAM) vaccine encoding the rabies virus glycoprotein (RVG) elicited, in mice, robust production of IgGs above the protection threshold (0.5 EU/mL) when formulated in DOTAP-based cationic lipid nanoparticles (cLNPs) after IM and ID injection with a SAM dose as low as 0.15 µg RVG-SAM. DOTAP-cLNPs were inferior to K-ILNPs but comparable to Rabipur following IM vaccination. In contrast, all three vaccines were comparable after ID immunisation. SAM-cLNPs failed to induce protective levels of anti-RVG IgG titres following IN vaccination even after prime-boost immunisation with 1.5 µg RVG-SAM. Similarly, K-iLNPs were significantly less immunogenic when administered IN, as compared to IM and ID routes. Consistent with these observations, cell-mediated immune responses after IM and ID vaccination with DOTAP-cLNPs and K-iLNPs higher compared to IN immunisation. On the other hand, vaccination with DOTAP-cLNPs resulted in higher frequencies of CD4$^+$ and CD8$^+$ T cells compared to Rabipur both after IM and ID injection. Furthermore, DOTAP-cLNPs and K-iLNPs induced modest cellular-mediated immune responses in lung cells after IN administration, with no significant differences compared to groups vaccinated IM with Rabipur. The lack of immunogenicity of cLNPs and iLNPs upon IN immunisation was likely attributed to the lack of muco-adhesive properties, as evidenced by the rapid clearance of these formulations following IN administration. In contrast, both cLNPs and iLNPs were well retained at the injection site when administered IM and ID. Altogether, these

findings suggest that the efficiency of SAM vaccines is strongly dependent on both the formulation design and the route of administration.

CHAPTER 7: CONCLUDING REMARKS

In 1990, the intramuscular injection of *in vitro* transcribed mRNA was shown to induce protein expression, though such a discovery did not result in imminent development of RNA therapeutics, owing the poor stability of RNA *in vivo*. However, extensive research on optimising RNA delivery systems have enabled RNA vaccines to become a promising alternative to whole-cell and subunit vaccines. RNA vaccines have an acceptable safety profile and have the potential to be produce in an inexpensive, quick and scalable manner. Furthermore, they induce *in situ* antigen expression, mimicking a real viral infection, thus eliciting robust humoral and type-1 immune responses even after a single dose. They can be engineered to encode any antigen of interest on-demand and therefore represent a versatile tool to fight infectious diseases and emerging pathogens. Moreover, the antigen can be designed in a self-amplifying RNA (SAM) to enhance the immunogenicity and to reduce the therapeutic dose compared to conventional non-amplifying mRNA vaccines.

The encapsulation of RNA vaccines in delivery systems allows to protect them against biological degradation and to facilitate their delivery in host cells. Among them, lipid-based delivery systems and, more specifically, lipid nanoparticles (LNPs) have been proven to be an efficient delivery system for mRNA and SAM vaccines. The aim of this thesis was to design cationic lipid nanoparticles to probe alternative routes of administration for a SAM vaccine. The rabies virus was chosen as a model due to the existence of efficacious commercial vaccines (e.g. Rabipur) and a correlate of protection (neutralising antibodies). Moreover, marketed rabies vaccines require from several doses, such that patient compliance may be risked, while RNA-based vaccines have the potential to induce long-lived immune responses after a single dose, hence improving patience compliance. To this end, a SAM vaccine encoding the rabies virus glycoprotein (RVG), the only target for neutralising antibodies, was used. SAM-LNPs were prepared by microfluidics, a robust and scalable technology that allows the production of highly homogeneous LNPs with high encapsulation efficiencies compared to conventional methods, which has already been used to produce nanomedicines for human clinical trials and use (e.g. Onpattro)

Methods for producing empty cationic LNPs (cationic liposomes) of desired physicochemical properties were first developed. The total flow rate (TFR) was found to have little impact on the physicochemical attributes of LNPs in the range studied (5-20 mL/min). Indeed, while the TFR

has been shown to have an impact on the size of other particulate delivery systems such as polymeric (e.g. PLGA) nanoparticles, its effect on particles produced by flash nanoprecipitation (e.g. liposomes) has been reported to be negligible (Forbes et al., 2019). Nevertheless, it is important to consider that the ability to produce LNPs faster without jeopardizing their physicochemical attributes represents an important advantage for the high throughput production of LNPs.

Previous investigations using other micromixers have reported that liposome size increases with increasing lipid concentration and have attributed this effect to the increased availability of lipids in the aqueous-organic interface such that larger self-assemblies can form. Herein, increasing lipid concentration (in the range of 0.25 to 10 mg/mL) resulted in smaller particle sizes, dropping from >300 nm down to 40-60 nm (depending on the formulation). It should be considered, however, that micromixer characteristics such as inlet angles, materials and micromixer geometry (often neglected) strongly shape the effect of microfluidics operating parameters. For instance, Carugo et al. (Carugo et al., 2016) reported increasing liposome sizes with increasing FRRs with a given micromixer, while no effect was observed when a micromixer with different properties was used.

The impact of aqueous-to-organic flow rate ratio (FRR) on LNP size have a great influence on particle size. Because mixing time between aqueous and organic phase decreases with increasing FRR, lipid self-assemblies have less time to form and therefore smaller particles are expected (Kastner et al., 2014). At the same time, however, high FRR can induce turbulences and back flows thus promoting aggregation. This is what we observed with neutral DSPC:Chol liposomes, whose size and PDI increased and decreased respectively from 80 nm (PDI = 0.05) to 50 nm (PDI = 0.2) by increasing the FRR from 1:1 to 5:1. This effect was more evident on cLNPs composed of DOPE and a cationic lipid (DOTAP, DDA, DC-Chol), which had a size and a PDI of 40 nm and 0.2 respectively when produced at 1:1 FRR; while heterogeneous cLNPs (PDI>0.6) with poor batch-to-batch reproducibility were obtained when produced at higher FRRs.

Fine adjustments of conventional microfluidic operating parameters such as lipid concentration, TFR and FRR allow to obtain size-tuneable liposomes in the range of 30 to 300 nm. However, size increase usually comes along with increased polydispersity indexes. Remarkably, a novel approach to formulate size-tuneable cationic unilamellar liposomes was described. Previous

investigations have reported that high ionic strength can induce changes in size and shape (e.g. micelles, inverted micelles, etc.) to lipid self-assemblies containing charged lipids such as DDA and PS (Israelachvili et al., 1980). This effect is due to the electrostatic interactions between the salt and the head group of the charged lipid, which results in the formation of larger vesicles or alternative lipid-self assemblies (e.g. micelles) depending on the lipid composition and the concentration and type of ions. We hypothesized that increasing the ionic strength (i.e. buffer concentration) within the aqueous phase to be injected in the micromixer could allow to produce homogeneous size-tuneable cationic particles above 500 nm. While the size of neutral DSPC:Chol liposomes remained constant for the range of buffer concentrations tested (10-1000 mM TRIS buffer 7.4), the size of cationic DOPE:DOTAP and DOPE:DDA liposomes increased from 40 to above 500 nm. In contrast, formulations containing smaller lipids such as DMTAP and DC-Chol only increased in size up to 100-130 nm. Furthermore, all formulations produced with this approach were unilamellar, as demonstrated by cryo-TEM analysis, and had low PDI (<0.25). The increase in size was directly proportional to the molar ratio of cationic lipid within the formulation, as evidenced with neutral DSPC:Chol liposomes containing increasing molar ratios of DOTAP (up to 23%).

The ability of cLNPs to interact with cells was investigated in murine macrophages and dendritic cells with flow cytometry. At 4°C, only low percentages of cells (<15%) were found in association with cLNPs, while over 70% of the cells were positive at 37°C, thereby demonstrating that at 4°C cLNPs associated with cells with no further internalization. This effect was attributed to the inhibition of cellular endocytosis at 4°C, as widely reported in the literature. Future investigations could aim to analyse the cellular uptake by confocal microscopy in order to further support these findings. Furthermore, LNP size (<50 nm or >500 nm) influenced the ability of these cationic vesicles to associate with cells. Indeed, while no differences were observed in the cellular uptake of <50 nm (small) and >500 nm (large) DOPE:DOTAP and DOPE:DDA liposomes in terms of percentage of positive cells or mean fluorescence intensity, significant differences were noticed when the cellular uptake was represented in terms of relative number of liposomes and liposome volume. More specifically, a larger number of small cationic liposomes associated with cells in comparison to their larger counterparts, whereas their uptake was lower when represented as liposome volume. This is explained by the significantly higher surface-to-volume ratio of <50 nm

vesicles compared to >500 nm vesicles. These findings were not in line with some other investigations (Chono et al., 2006a; Chono et al., 2006b), in which large liposomes were reported to be taken up in a greater extent than smaller ones. However, the large vesicles used within these studies were multilamellar and the therefore the quantification of cellular association (measured by radio-counting of lipids labelled with isotopes) was biased by the lamellarity of liposomes. For instance, if we consider two liposome formulations of 500 nm with the exact same composition, one being unillamelar and the other one mulilamellar, we would expect higher uptake for the multilamellar vesicles, owing the higher number of radiolabelled lipids in the self-assembly as compared to the unilamellar formulation. This is exactly what was found by Hsu and Juliano (Hsu and Juliano, 1982), who reported a 2-fold uptake of 1000 nm multilamellar vesicles compared to 1000 nm oligolamellar vesicles.

When injected intramuscularly in mice, sub-50 nm DOPE:DOTAP and DOPE:DDA cLNPs were cleared significantly faster compared to their larger (>500 nm) counterparts and drained in a greater extent to the local lymph nodes likely due to a combination of free and cell-mediated transport; in agreement with previous investigations with polystyrene nanoparticles (Manolova et al., 2008) and cationic nanocapsules (Cordeiro et al., 2019), which suggest that 50-100 nm particles are able to reach the lymph nodes passively, while larger particles require from immune cells. This could explain why similar pharmacokinetics were observed for the vaccine adjuvant CAF01, composed of DDA and TDB, with particle sizes of 200-2000 nm when injected intramuscularly; with high percentages of PEG (25% molar ratio) being required to reduce the depot effect and enhance the lymphatic targeting (Henriksen-Lacey et al., 2011b; Kaur et al., 2012b).

Following investigations were focused on the design and optimisation of cLNPs enclosing the self-amplifying (SAM) vaccine. To this end, cLNPs were co-formulated with a PEGylated lipid (2 mole%) to avoid aggregation and uncontrolled particle growth during the production process. cLNPs were composed of a panel of cationic lipids (DOTAP, DDA, DC-Chol, DMTAP, DSTAP and DOBAQ) and helper lipids (DOPE/PEG-C18, DOPE-PEG-C14, DSPC/Chol-PEG14). As a control, benchmark ionizable LNPs (iLNPs) containing a cationic amino-lipid with a pKa value <7 (lipid K), a very efficient RNA delivery system (Kulkarni et al., 2018a), were used as a control. formulations had hydrodynamic sizes below 150 nm, low PDI (<0.2), neutral zeta-potential (<5 mV) and high

SAM encapsulation efficiency (>90%), with the exception of DSTAP-based cLNPs, which were significantly higher in size (>300 nm), polydisperse (>0.6) and had lower SAM encapsulation efficiency (<75%), as also reported elsewhere (Patel et al., 2019). Therefore, DSTAP-cLNPs were not considered for further investigations.

Despite all formulations were taken up by primary murine macrophages, they failed to induce antigen expression even in absence of serum proteins, conditions which favour cellular transfection (Zhang et al., 2010). Furthermore, a well-established commercial transfection reagent (Lipofectamine2000) also failed to transfect these cells in the same experimental conditions. These results were consistent with previous investigations, where SAM-LNPs were not able to transfect macrophages and dendritic cells in vitro (Lazzaro et al., 2015). This was likely attributed by the expression of the toll-like receptor 7 (TLR-7) by macrophages and dendritic cells, which can recognize RNA, thus resulting in its degradation (Kawai and Akira, 2009).

Subsequent experiments were therefore performed in baby hamster kidney (BHK) cells, a permissive fibroblast cell line. Within these experiments, Lipofectamine2000 was very efficient to transfect BHK cells. Lipofectamine2000 is composed of a multivalent cationic lipid and the fusogenic DOPE. Upon complexation with the nucleic acid to be transfected, it aggregates, thus facilitating cellular uptake, allowing to achieve high rates of transfection. Despite Lipofectamine2000 is a very useful positive control for in vitro experiments, it is not suitable for in vivo use owing its heterogeneity and aggregative nature. Consistent with results observed with primary cells, all LNP formulations were taken up by BHK cells, with cLNPs showing greater uptake than iLNPs. Moreover, K-iLNPs were not able to associate with cells in absence of serum proteins (foetal bovine serum [FBS]). Indeed, cLNPs contain constitutively charged cationic lipids that allow the interaction of cLNPs with negatively charged cellular membranes, such that they can be taken up by fusion, while iLNPs require from the apolipoprotein E to be internalised (Akinc et al., 2010). Importantly, the transfection efficiency of SAM-LNPs was highly influenced by type of cationic and helper lipids and the experimental conditions. While cLNPs were significantly more potent in absence of FBS, K-iLNPs completely failed to induce antigen expression due to the lack of cellular uptake. Despite cLNP formulations containing DSPC/Chol were taken up by BHK cells, they were significantly less potent than those containing DOPE. DOPE is a fusogenic properties of DOPE which undergoes a lamellar-to-hexagonal phase transition in the acidic

environment of the endosomes thus disrupting the endosomal membrane and promoting cargo release consequently enhancing the transfection efficiency of cationic LNPs (Mochizuki et al., 2013).

PEG-lipids have been widely reported to transfer from lipid vesicles in a process known as de-PEGylation. Therefore, longer acyl chains are expected to provide stronger hydrophobic interactions within the lipid conformer and slower transfer rates. For instance, DLin-MC3-DMA iLNPs containing 1.5% of either PEG-C14, PEG-C16 or PEG-C18 had blood half-lives of approximately 0.6, 2.2 and 4.0 hours upon intravenous administration (Mui et al., 2013). Similarly, PEG moieties impair the ability of LNPs to interact with endosomal membranes and therefore inhibit endosomal escape, such that formulations containing PEG-C14 are expected to be more potent that those containing PEG-C18 (Pozzi et al., 2014). Our SAM-cLNPs containing PEG-C14 had significantly higher transfection efficiencies than SAM-cLNP formulations having PEG-C18. When looking at the effect of the cationic lipid on the transfection efficiency, the potency of cLNPs was ranked in the order of DDA > DOTAP > DMTAP = DC-Chol > DOBAQ. Interestingly, DOPE:DOTAP:PEG-C14 and DOPE:DDA:PEG-C14 were more potent than K-iLNPs, largely owed to their enhanced cellular uptake compared to K-iLNPs, though these cLNPs were not expected to outperform K-iLNPs in vivo.

RNA is a labile molecule that can be degraded within seconds in presence of RNases and therefore its protection is a key challenge to achieve a potent therapeutic effect. Therefore, the ability of cLNPs to protect SAM against RNase degradation was investigated by agarose gel electrophoresis. Unformulated SAM was completely degraded when challenged with RNase A, while it was protected when formulated in cLNPs. DOTAP and especially DDA-cLNPs were particularly efficient in protecting SAM against degradation; and these findings could explain why formulations containing either DOTAP or DDA were more potent in vitro that those containing DMTAP, DC-Chol or DOBAQ.

Most promising candidates (DOPE:DOTAP:PEG-C14 and DOPE:DDA:PEG-C14 cLNPs, termed DOTAP and DDA-cLNPs from now now) were selected according to their physicochemical properties (size, size distribution, SAM encapsulation efficiency), ability to protect SAM from enzymatic degradation and their capacity to associate with cells and to induce antigen expression *in vitro*.

Inducing robust immune responses upon vaccinations requires to target the appropriate cell populations in the right place. The biodistribution pharmacokinetic of adjuvants have been tightly related to the quality the immune response (Schmidt et al., 2016). Accordingly, the biodistribution of LNPs was investigated in mice. DOTAP-cLNPs, DDA-cLNPs and K-iLNPs were well retained at the administration site over a period of 10 days following intramuscular (IM) and intradermal (ID) injection. In contrast, they were rapidly cleared when administered intranasally (IN), with only 25% of the total signal remaining at the administration site 4 hours after administration. DOTAP-cLNPs and K-iLNPs exhibited similar biodistribution pharmacokinetics by all three routes. When injected IM, these were cleared faster compared to DDA-cLNPs. The formation of a depot effect at the injection site has been shown to play a major role on the immunogenicity of liposome adjuvants and their associated subunit antigen (e.g. the adjuvant CAF01 in combination with the antigen Ag85B-ESAT-6). However, a long persistence of RNA-LNPs at the injection site has not been associated with enhanced immunogenicity. For instance, recent investigations have highlighted that biodegradable iLNPs can induced superior immunogenicity to iLNPs despite being cleared few hours after administration (Hassett et al., 2019).

The immunogenicity of DOTAP-cLNPs and DDA-cLNPs upon intramuscular injection was investigated in mice and compared to K-iLNPs, a DOTAP-based cationic nanoemulsion (CNE56), an efficient and well-established SAM delivery system which is currently being investigated in a phase I clinical trial (NCT04062669) and Rabipur, an inactivated tissue-culture vaccine. SAM-cLNP formulations elicited robust production of anti-RVG IgGs above the protection threshold (0.5 EU/mL) even after a single vaccination with a dose of RVG-SAM as low as 0.15 µg, with no significant differences between DOTAP and DDA formulations, despite the adjuvating properties of DDA. These results are in agreement with recent investigations, where the antibody titres elicited by DDA:DOPE:Chol cLNPs (35:49:16 molar ratio), enclosing a SAM encoding for HIV gp140, were higher but not significantly superior than the DOTAP formulation (Blakney et al., 2019b). Moreover, the immunogenicity of cLNP-formulated RVG-SAM was comparable to CNE56 and 5% of the human dose (HD) of Rabipur. As expected, K-iLNPs were significantly more potent than cLNPs and CNE56. Indeed, iLNP formulations have been extensively optimised over the past two decades to deliver RNA in vivo (Cullis and Hope, 2017).

Vaccination with nucleic acid-based vaccines results in situ endogenous antigen expression and the induction of Th1-type cellular-mediated immune responses. Both DOTAP-cLNPs and DDA-cLNPs induced antigen-specific polyfunctional T cell responses with effector phenotype two weeks after the second vaccination in splenocytes re-stimulated with a peptide pool library spanning the RVG. The frequency of cytokine producing $CD8^+$ and $CD4^+$ T cells (TNF-α, IL-2, IFN-γ and combinations thereof) achieved with DOTAP and DDA-cLNPs was comparable to CNE56 and Rabipur but inferior compared to K-ILNPs. Moreover, most (>80%) $CD8^+$ T cells were positive for the degranulation marker CD107, whose expression has been directly correlated to the cytotoxic activity of these cells in vivo (Aktas et al., 2009).

ID and IN are particularly attractive routes for administering vaccines. On the one hand, the dermis is very rich in skin-resident dendritic cells, which are pivotal in priming $CD8^+$ T cells following RNA vaccination. Moreover, ID vaccination has the potential to achieve equivalent immune responses compared to IM with lower doses (dose sparing). On the other hand, IN vaccination is a needle-free approach, particularly advantageous for developing countries, in which needle reuse represents an important issue. Moreover, IN vaccination not only allows to induce local immune responses in the mucosal tissue, the main entry of pathogens, but also systemic immune responses. Accordingly, the following *in vivo* vaccination study aimed to investigate the immunogenicity of DOTAP-cLNPs following intramuscular (IM), intradermal (ID) and intranasal (IN) administration. Some studies a have reported that SAM-LNP are more immunogenic IM compared to ID (Brito et al., 2015; Geall et al., 2012), while others have reported that, despite IM and ID routes are comparable, quicker onset of the immune response to SAM-LNP vaccines can be achieved when administered ID (Goswami et al., 2019; Liang et al., 2017). These discrepancies may arise from the different types of RNA molecules and LNP composition. Furthermore, it is important to point out that ID injection is particularly challenging in small animal models, where the dermis is barely 200 µm thick. In particular, these could be accidentally injected subcutaneously and, considering the great differences in the cellular environment between these tissues, completely different immune responses could be observed. Regarding this thesis, the humoral immune responses elicited by DOTAP-cLNPs (0.15 µg SAM) were inferior to K-iLNPs (0.15 µg SAM) and Rabipur when administered IM. In contrast, the immunogenicity of cLNPs, iLNPs and Rabipur was comparable when administered ID. Indeed,

while Rabipur and K-iLNPs were less potent after ID injection compared to their respective IM groups, the immunogenicity of DOTAP-cLNPs was similar in the IM and ID groups. These findings suggest that the use of iLNPs does not guarantee enhanced immunogenicity compared to cLNPs, as reported by Blakney and co-workers in their studies, where DOTAP and DDA-cLNPs were as immunogenic as iLNP formulation based on the ionisable lipid C12-200.

A similar trend was observed on the T cell responses, with frequencies of antigen-specific T cells being ranked in the order of IM = ID >> IN. As a proof of concept, a T cell assay was performed in lung cells from mice immunised IN. DOTAP-cLNPs and K-iLNPs seemed to elicit stronger cell-mediated immune responses in the lungs compared to Rabipur, especially by $CD4^+$ T cells, although differences were not significant. Such weak immune responses observed after IN administration could be explained by the rapid clearance of these formulations following IN administration. Altogether, these results suggest that DOTAP and DDA-cLNPs are efficient SAM delivery systems by IM and ID administration but also that the immunogenicity of SAM vaccines is highly influenced by the route of administration and the type of delivery system. Further investigations aiming to optimise the lipid composition of LNPs for IN delivery of RNA and SAM vaccines would be relevant.

REFERENCES

1. Abraham, S.A., Waterhouse, D.N., Mayer, L.D., Cullis, P.R., Madden, T.D., and Bally, M.B. (2005). The Liposomal Formulation of Doxorubicin. In Methods in Enzymology (Academic Press), pp. 71-97.
2. Abumanhal-Masarweh, H., da Silva, D., Poley, M., Zinger, A., Goldman, E., Krinsky, N., Kleiner, R., Shenbach, G., Schroeder, J.E., Shklover, J.*, et al.* (2019). Tailoring the lipid composition of nanoparticles modulates their cellular uptake and affects the viability of triple negative breast cancer cells. Journal of Controlled Release *307*, 331-341.
3. Akbarzadeh, A., Rezaei-Sadabady, R., Davaran, S., Joo, S.W., Zarghami, N., Hanifehpour, Y., Samiei, M., Kouhi, M., and Nejati-Koshki, K. (2013). Liposome: classification, preparation, and applications. Nanoscale Res Lett *8*, 102.
4. Akinc, A., Goldberg, M., Qin, J., Dorkin, J.R., Gamba-Vitalo, C., Maier, M., Jayaprakash, K.N., Jayaraman, M., Rajeev, K.G., Manoharan, M.*, et al.* (2009). Development of lipidoid-siRNA formulations for systemic delivery to the liver. Molecular therapy : the journal of the American Society of Gene Therapy *17*, 872-879.
5. Akinc, A., Querbes, W., De, S., Qin, J., Frank-Kamenetsky, M., Jayaprakash, K.N., Jayaraman, M., Rajeev, K.G., Cantley, W.L., Dorkin, J.R.*, et al.* (2010). Targeted delivery of RNAi therapeutics with endogenous and exogenous ligand-based mechanisms. Molecular therapy : the journal of the American Society of Gene Therapy *18*, 1357-1364.
6. Aktas, E., Kucuksezer, U.C., Bilgic, S., Erten, G., and Deniz, G. (2009). Relationship between CD107a expression and cytotoxic activity. Cellular Immunology *254*, 149-154.
7. Alam, M.M., Oka, T., Ohta, N., and Yamazaki, M. (2011). Kinetics of low pH-induced lamellar to bicontinuous cubic phase transition in dioleoylphosphatidylserine/monoolein. The Journal of Chemical Physics *134*, 145102.
8. Allen, T.M., Austin, G.A., Chonn, A., Lin, L., and Lee, K.C. (1991). Uptake of liposomes by cultured mouse bone marrow macrophages: influence of liposome composition and size. Biochimica et Biophysica Acta (BBA) - Biomembranes *1061*, 56-64.
9. Allen, T.M., and Cullis, P.R. (2013). Liposomal drug delivery systems: From concept to clinical applications. Advanced Drug Delivery Reviews *65*, 36-48.
10. Allen, T.M., and Everest, J.M. (1983). Effect of liposome size and drug release properties on pharmacokinetics of encapsulated drug in rats. J Pharmacol Exp Ther *226*, 539-544.
11. Andar, A.U., Hood, R.R., Vreeland, W.N., Devoe, D.L., and Swaan, P.W. (2014). Microfluidic preparation of liposomes to determine particle size influence on cellular uptake mechanisms. Pharm Res *31*, 401-413.
12. Angelova, M.I., and Dimitrov, D.S. (1986). Liposome electroformation. Faraday Discussions of the Chemical Society *81*, 303-311.
13. Attwood, A.T.F.a.D. (1998). Physicochemical Principles of Pharmacy (Palgrave, London).

14. Austyn, J.M., and Gordon, S. (1981). F4/80, a monoclonal antibody directed specifically against the mouse macrophage. Eur J Immunol *11*, 805-815.

15. Awad, T.S., Okamoto, Y., Masum, S.M., and Yamazaki, M. (2005). Formation of Cubic Phases from Large Unilamellar Vesicles of Dioleoylphosphatidylglycerol/Monoolein Membranes Induced by Low Concentrations of Ca2+. Langmuir *21*, 11556-11561.

16. Bachmann, D., Drechsler, M., and Bauer, K.H. (1990). Liposome Preparation by a New High Pressure Homogenizer Gaulin Micron Lab 40 AU - Brandl, M. Drug Development and Industrial Pharmacy *16*, 2167-2191.

17. Bachmann, M.F., and Jennings, G.T. (2010). Vaccine delivery: a matter of size, geometry, kinetics and molecular patterns. Nat Rev Immunol *10*, 787-796.

18. Badiee, A., Khamesipour, A., Samiei, A., Soroush, D., Shargh, V.H., Kheiri, M.T., Barkhordari, F., Robert Mc Master, W., Mahboudi, F., and Jaafari, M.R. (2012). The role of liposome size on the type of immune response induced in BALB/c mice against leishmaniasis: rgp63 as a model antigen. Exp Parasitol *132*, 403-409.

19. Bahl, K., Senn, J.J., Yuzhakov, O., Bulychev, A., Brito, L.A., Hassett, K.J., Laska, M.E., Smith, M., Almarsson, Ö., Thompson, J.*, et al.* (2017). Preclinical and Clinical Demonstration of Immunogenicity by mRNA Vaccines against H10N8 and H7N9 Influenza Viruses. Molecular Therapy *25*, 1316-1327.

20. Balazs, D.A., and Godbey, W. (2011). Liposomes for use in gene delivery. J Drug Deliv *2011*, 326497.

21. Balbino, T.A., Aoki, N.T., Gasperini, A.A.M., Oliveira, C.L.P., Azzoni, A.R., Cavalcanti, L.P., and de la Torre, L.G. (2013). Continuous flow production of cationic liposomes at high lipid concentration in microfluidic devices for gene delivery applications. Chemical Engineering Journal *226*, 423-433.

22. Bangham, A.D., and Horne, R.W. (1964). NEGATIVE STAINING OF PHOSPHOLIPIDS AND THEIR STRUCTURAL MODIFICATION BY SURFACE-ACTIVE AGENTS AS OBSERVED IN THE ELECTRON MICROSCOPE. J Mol Biol *8*, 660-668.

23. Bangham, A.D., Standish, M.M., and Watkins, J.C. (1965). Diffusion of univalent ions across the lamellae of swollen phospholipids. Journal of Molecular Biology *13*, 238-IN227.

24. Barnadas-Rodríguez, R., and Sabés, M. (2001). Factors involved in the production of liposomes with a high-pressure homogenizer. International Journal of Pharmaceutics *213*, 175-186.

25. Batzri, S., and Korn, E.D. (1973). Single bilayer liposomes prepared without sonication. Biochimica et Biophysica Acta (BBA) - Biomembranes *298*, 1015-1019.

26. Belliveau, N.M., Huft, J., Lin, P.J.C., Chen, S., Leung, A.K.K., Leaver, T.J., Wild, A.W., Lee, J.B., Taylor, R.J., Tam, Y.K.*, et al.* (2012). Microfluidic Synthesis of Highly Potent Limit-size Lipid Nanoparticles for In Vivo Delivery of siRNA. Mol Ther Nucleic Acids *1*, e37-.

27. Berger, N., Sachse, A., Bender, J., Schubert, R., and Brandl, M. (2001). Filter extrusion of liposomes using different devices: comparison of liposome size, encapsulation efficiency, and process characteristics. International Journal of Pharmaceutics *223*, 55-68.

28. Betageri, G.V., and Parsons, D.L. (1992). Drug encapsulation and release from multilamellar and unilamellar liposomes. International Journal of Pharmaceutics *81*, 235-241.

29. Blakney, A.K., McKay, P.F., Christensen, D., Yus, B.I., Aldon, Y., Follmann, F., and Shattock, R.J. (2019a). Effects of cationic adjuvant formulation particle type, fluidity and immunomodulators on delivery and immunogenicity of saRNA. Journal of Controlled Release *304*, 65-74.

30. Blakney, A.K., McKay, P.F., Yus, B.I., Aldon, Y., and Shattock, R.J. (2019b). Inside out: optimization of lipid nanoparticle formulations for exterior complexation and in vivo delivery of saRNA. Gene Therapy.

31. Bogers, W.M., Oostermeijer, H., Mooij, P., Koopman, G., Verschoor, E.J., Davis, D., Ulmer, J.B., Brito, L.A., Cu, Y., Banerjee, K.*, et al.* (2015). Potent immune responses in rhesus macaques induced by nonviral delivery of a self-amplifying RNA vaccine expressing HIV type 1 envelope with a cationic nanoemulsion. The Journal of infectious diseases *211*, 947-955.

32. Brewer, J.M., Pollock, K.G.J., Tetley, L., and Russell, D.G. (2004). Vesicle Size Influences the Trafficking, Processing, and Presentation of Antigens in Lipid Vesicles. The Journal of Immunology *173*, 6143.

33. Brewer, J.M., Tetley, L., Richmond, J., Liew, F.Y., and Alexander, J. (1998). Lipid vesicle size determines the Th1 or Th2 response to entrapped antigen. J Immunol *161*, 4000-4007.

34. Brito, L.A., Chan, M., Shaw, C.A., Hekele, A., Carsillo, T., Schaefer, M., Archer, J., Seubert, A., Otten, G.R., Beard, C.W.*, et al.* (2014). A Cationic Nanoemulsion for the Delivery of Next-generation RNA Vaccines. Molecular Therapy *22*, 2118-2129.

35. Brito, L.A., Kommareddy, S., Maione, D., Uematsu, Y., Giovani, C., Berlanda Scorza, F., Otten, G.R., Yu, D., Mandl, C.W., Mason, P.W.*, et al.* (2015). Chapter Seven - Self-Amplifying mRNA Vaccines. In Advances in Genetics, L. Huang, D. Liu, and E. Wagner, eds. (Academic Press), pp. 179-233.

36. Buboltz, J.T., and Feigenson, G.W. (1999). A novel strategy for the preparation of liposomes: rapid solvent exchange. Biochimica et Biophysica Acta (BBA) - Biomembranes *1417*, 232-245.

37. Calabro, S., Tortoli, M., Baudner, B.C., Pacitto, A., Cortese, M., O'Hagan, D.T., De Gregorio, E., Seubert, A., and Wack, A. (2011). Vaccine adjuvants alum and MF59 induce rapid recruitment of neutrophils and monocytes that participate in antigen transport to draining lymph nodes. Vaccine *29*, 1812-1823.

38. Capretto, L., Carugo, D., Mazzitelli, S., Nastruzzi, C., and Zhang, X. (2013). Microfluidic and lab-on-a-chip preparation routes for organic nanoparticles and vesicular systems for nanomedicine applications. Advanced Drug Delivery Reviews *65*, 1496-1532.

39. Carnie, S., Israelachvili, J.N., and Pailthorpe, B.A. (1979). Lipid packing and transbilayer asymmetries of mixed lipid vesicles. Biochimica et Biophysica Acta (BBA) - Biomembranes *554*, 340-357.

40. Carstens, M.G., Camps, M.G.M., Henriksen-Lacey, M., Franken, K., Ottenhoff, T.H.M., Perrie, Y., Bouwstra, J.A., Ossendorp, F., and Jiskoot, W. (2011). Effect of vesicle size on tissue localization and immunogenicity of liposomal DNA vaccines. Vaccine *29*, 4761-4770.

41. Carugo, D., Bottaro, E., Owen, J., Stride, E., and Nastruzzi, C. (2016). Liposome production by microfluidics: potential and limiting factors. *6*, 25876.

42. Chahal, J.S., Khan, O.F., Cooper, C.L., McPartlan, J.S., Tsosie, J.K., Tilley, L.D., Sidik, S.M., Lourido, S., Langer, R., Bavari, S.*, et al.* (2016). Dendrimer-RNA nanoparticles generate protective immunity against lethal Ebola, H1N1 influenza, and Toxoplasma gondii challenges with a single dose. Proceedings of the National Academy of Sciences *113*, E4133.

43. Charcosset, C., Juban, A., Valour, J.-P., Urbaniak, S., and Fessi, H. (2015). Preparation of liposomes at large scale using the ethanol injection method: Effect of scale-up and injection devices. Chemical Engineering Research and Design *94*, 508-515.

44. Cho, N.-J., Hwang, L.Y., Solandt, J.J., and Frank, C.W. (2013). Comparison of extruded and sonicated vesicles for planar bilayer self-assembly. Materials *6*, 3294-3308.

45. Chono, S., Tanino, T., Seki, T., and Morimoto, K. (2006a). Influence of particle size on drug delivery to rat alveolar macrophages following pulmonary administration of ciprofloxacin incorporated into liposomes. J Drug Target *14*, 557-566.

46. Chono, S., Tanino, T., Seki, T., and Morimoto, K. (2010). Uptake characteristics of liposomes by rat alveolar macrophages: influence of particle size and surface mannose modification. Journal of Pharmacy and Pharmacology *59*, 75-80.

47. Chono, S., Tauchi, Y., and Morimoto, K. (2006b). Influence of particle size on the distributions of liposomes to atherosclerotic lesions in mice. Drug Dev Ind Pharm *32*, 125-135.

48. Christensen, D., Henriksen-Lacey, M., Kamath, A.T., Lindenstrom, T., Korsholm, K.S., Christensen, J.P., Rochat, A.F., Lambert, P.H., Andersen, P., Siegrist, C.A.*, et al.* (2012). A cationic vaccine adjuvant based on a saturated quaternary ammonium lipid have different in vivo distribution kinetics and display a distinct CD4 T cell-inducing capacity compared to its unsaturated analog. J Control Release *160*, 468-476.

49. Christensen, D., Korsholm, K.S., Rosenkrands, I., Lindenstrøm, T., Andersen, P., and Agger, E.M. (2007). Cationic liposomes as vaccine adjuvants. Expert Review of Vaccines *6*, 785-796.

50. Chu, L.-Y., Utada, A.S., Shah, R.K., Kim, J.-W., and Weitz, D.A. (2007). Controllable Monodisperse Multiple Emulsions. Angewandte Chemie International Edition *46*, 8970-8974.

51. Cliquet, F., Aubert, M., and Sagné, L. (1998). Development of a fluorescent antibody virus neutralisation test (FAVN test) for the quantitation of rabies-neutralising antibody. Journal of Immunological Methods *212*, 79-87.

52. Cordeiro, A.S., Crecente-Campo, J., Bouzo, B.L., González, S.F., de la Fuente, M., and Alonso, M.J. (2019). Engineering polymeric nanocapsules for an efficient drainage and biodistribution in the lymphatic system. Journal of Drug Targeting, 1-13.

53. Cortesi, R. (1999). Preparation of liposomes by reverse-phase evaporation using alternative organic solvents. Journal of Microencapsulation *16*, 251-256.

54. Corti, D., and Lanzavecchia, A. (2013). Broadly Neutralizing Antiviral Antibodies. Annual Review of Immunology *31*, 705-742.

55. Cruz, C.C., Suthar, M.S., Montgomery, S.A., Shabman, R., Simmons, J., Johnston, R.E., Morrison, T.E., and Heise, M.T. (2010). Modulation of type I IFN induction by a virulence determinant within the alphavirus nsP1 protein. Virology *399*, 1-10.

56. Csaba, N., Garcia-Fuentes, M., and Alonso, M.J. (2009). Nanoparticles for nasal vaccination. Advanced Drug Delivery Reviews *61*, 140-157.

57. Cullis, P.R., and Hope, M.J. (2017). Lipid Nanoparticle Systems for Enabling Gene Therapies. Molecular Therapy *25*, 1467-1475.

58. Dabbas, S., Kaushik, R.R., Dandamudi, S., Kuesters, G.M., and Campbell, R.B. (2008). Importance of the Liposomal Cationic Lipid Content and Type in Tumor Vascular Targeting: Physicochemical Characterization and In Vitro Studies Using Human Primary and Transformed Endothelial Cells. Endothelium *15*, 189-201.

59. Daha, N.A., Banda, N.K., Roos, A., Beurskens, F.J., Bakker, J.M., Daha, M.R., and Trouw, L.A. (2011). Complement activation by (auto-) antibodies. Molecular Immunology *48*, 1656-1665.

60. Dalby, B., Cates, S., Harris, A., Ohki, E.C., Tilkins, M.L., Price, P.J., and Ciccarone, V.C. (2004). Advanced transfection with Lipofectamine 2000 reagent: primary neurons, siRNA, and high-throughput applications. Methods *33*, 95-103.

61. Danko, J.R., Kochel, T., Teneza-Mora, N., Luke, T.C., Raviprakash, K., Sun, P., Simmons, M., Moon, J.E., De La Barrera, R., Martinez, L.J*., et al.* (2018). Safety and Immunogenicity of a Tetravalent Dengue DNA Vaccine Administered with a Cationic Lipid-Based Adjuvant in a Phase 1 Clinical Trial. Am J Trop Med Hyg *98*, 849-856.

62. DeMello, A.J. (2006). Control and detection of chemical reactions in microfluidic systems. Nature *442*, 394-402.

63. Dietzschold, B., Wunner, W.H., Wiktor, T.J., Lopes, A.D., Lafon, M., Smith, C.L., and Koprowski, H. (1983). Characterization of an antigenic determinant of the glycoprotein that correlates with pathogenicity of rabies virus. Proceedings of the National Academy of Sciences of the United States of America *80*, 70-74.

64. DiStefano, D., Antonello, J.M., Bett, A.J., Medi, M.B., Casimiro, D.R., and ter Meulen, J. (2013). Immunogenicity of a reduced-dose whole killed rabies vaccine is significantly

enhanced by ISCOMATRIX™ adjuvant, Merck amorphous aluminum hydroxylphosphate sulfate (MAA) or a synthetic TLR9 agonist in rhesus macaques. Vaccine *31*, 4888-4893.

65. Dittrich, P.S., Heule, M., Renaud, P., and Manz, A. (2006). On-chip extrusion of lipid vesicles and tubes through microsized apertures. Lab on a Chip *6*, 488-493.

66. Edwards, K., Gustafsson, J., Almgren, M., and Karlsson, G. (1993). Solubilization of Lecithin Vesicles by a Cationic Surfactant: Intermediate Structures in the Vesicle-Micelle Transition Observed by Cryo-Transmission Electron Microscopy. Journal of Colloid and Interface Science *161*, 299-309.

67. Endmann, A., Baden, M., Weisermann, E., Kapp, K., Schroff, M., Kleuss, C., Wittig, B., and Juhls, C. (2010). Immune response induced by a linear DNA vector: Influence of dose, formulation and route of injection. Vaccine *28*, 3642-3649.

68. Epstein-Barash, H., Gutman, D., Markovsky, E., Mishan-Eisenberg, G., Koroukhov, N., Szebeni, J., and Golomb, G. (2010). Physicochemical parameters affecting liposomal bisphosphonates bioactivity for restenosis therapy: internalization, cell inhibition, activation of cytokines and complement, and mechanism of cell death. J Control Release *146*, 182-195.

69. Ertl, H.C.J. (2009). Novel vaccines to human rabies. PLoS neglected tropical diseases *3*, e515-e515.

70. Esnault-Dupuy, C., Chanussot, F., LaFont, H., Chabert, C., and Hauton, J. (1987). The relationship between HDL-, LDL-, liposomes-free cholesterol, biliary cholesterol and bile salts in the rat. Biochimie *69*, 45-52.

71. Etheridge, M.L., Campbell, S.A., Erdman, A.G., Haynes, C.L., Wolf, S.M., and McCullough, J. (2013). The big picture on nanomedicine: the state of investigational and approved nanomedicine products. Nanomedicine: Nanotechnology, Biology and Medicine *9*, 1-14.

72. Faber, M., Faber, M.-L., Papaneri, A., Bette, M., Weihe, E., Dietzschold, B., and Schnell, M.J. (2005). A single amino acid change in rabies virus glycoprotein increases virus spread and enhances virus pathogenicity. Journal of virology *79*, 14141-14148.

73. Farhood, H., Serbina, N., and Huang, L. (1995). The role of dioleoyl phosphatidylethanolamine in cationic liposome mediated gene transfer. Biochimica et Biophysica Acta (BBA) - Biomembranes *1235*, 289-295.

74. Felgner, P.L., Gadek, T.R., Holm, M., Roman, R., Chan, H.W., Wenz, M., Northrop, J.P., Ringold, G.M., and Danielsen, M. (1987). Lipofection: a highly efficient, lipid-mediated DNA-transfection procedure. Proc Natl Acad Sci U S A *84*, 7413-7417.

75. Ferraro, B., Morrow, M.P., Hutnick, N.A., Shin, T.H., Lucke, C.E., and Weiner, D.B. (2011). Clinical applications of DNA vaccines: current progress. Clinical infectious diseases : an official publication of the Infectious Diseases Society of America *53*, 296-302.

76. Feyssaguet, M., Dacheux, L., Audry, L., Compoint, A., Morize, J.L., Blanchard, I., and Bourhy, H. (2007). Multicenter comparative study of a new ELISA, PLATELIA™ RABIES II, for the detection and titration of anti-rabies glycoprotein antibodies and comparison

with the rapid fluorescent focus inhibition test (RFFIT) on human samples from vaccinated and non-vaccinated people. Vaccine *25*, 2244-2251.

77. Filion, M.C., and Phillips, N.C. (1997). Toxicity and immunomodulatory activity of liposomal vectors formulated with cationic lipids toward immune effector cells. Biochimica et Biophysica Acta (BBA) - Biomembranes *1329*, 345-356.

78. Forbes, N., Hussain, M.T., Briuglia, M.L., Edwards, D.P., Horst, J.H.t., Szita, N., and Perrie, Y. (2019). Rapid and scale-independent microfluidic manufacture of liposomes entrapping protein incorporating in-line purification and at-line size monitoring. International Journal of Pharmaceutics *556*, 68-81.

79. Gallorini, S., Taccone, M., Bonci, A., Nardelli, F., Casini, D., Bonificio, A., Kommareddy, S., Bertholet, S., O'Hagan, D.T., and Baudner, B.C. (2014). Sublingual immunization with a subunit influenza vaccine elicits comparable systemic immune response as intramuscular immunization, but also induces local IgA and TH17 responses. Vaccine *32*, 2382-2388.

80. Gaudinski, M.R., Houser, K.V., Morabito, K.M., Hu, Z., Yamshchikov, G., Rothwell, R.S., Berkowitz, N., Mendoza, F., Saunders, J.G., Novik, L.*, et al.* (2018). Safety, tolerability, and immunogenicity of two Zika virus DNA vaccine candidates in healthy adults: randomised, open-label, phase 1 clinical trials. Lancet *391*, 552-562.

81. Geall, A.J., Verma, A., Otten, G.R., Shaw, C.A., Hekele, A., Banerjee, K., Cu, Y., Beard, C.W., Brito, L.A., Krucker, T.*, et al.* (2012). Nonviral delivery of self-amplifying RNA vaccines. Proc Natl Acad Sci U S A *109*, 14604-14609.

82. Ghanekar, S.A., Nomura, L.E., Suni, M.A., Picker, L.J., Maecker, H.T., and Maino, V.C. (2001). Gamma Interferon Expression in CD8⁺ T Cells Is a Marker for Circulating Cytotoxic T Lymphocytes That Recognize an HLA A2-Restricted Epitope of Human Cytomegalovirus Phosphoprotein pp65. Clinical and Diagnostic Laboratory Immunology *8*, 628.

83. Giesen, A., Gniel, D., and Malerczyk, C. (2015). 30 years of rabies vaccination with Rabipur: a summary of clinical data and global experience. Expert Review of Vaccines *14*, 351-367.

84. Goldenthal, K.L., Pastan, I., and Willingham, M.C. (1984). Initial steps in receptor-mediated endocytosis. The influence of temperature on the shape and distribution of plasma membrane clathrin-coated pits in cultured mammalian cells. Exp Cell Res *152*, 558-564.

85. Goldstein, J.L., and Brown, M.S. (2009). The LDL receptor. Arteriosclerosis, thrombosis, and vascular biology *29*, 431-438.

86. Goswami, R., Chatzikleanthous, D., Lou, G., Giusti, F., Bonci, A., Taccone, M., Brazzoli, M., Gallorini, S., Ferlenghi, I., Berti, F.*, et al.* (2019). Mannosylation of LNP Results in Improved Potency for Self-Amplifying RNA (SAM) Vaccines. ACS Infectious Diseases.

87. Gregoriadis, G. (1976a). The carrier potential of liposomes in biology and medicine (first of two parts). N Engl J Med *295*, 704-710.

88. Gregoriadis, G. (1976b). The carrier potential of liposomes in biology and medicine (second of two parts). N Engl J Med *295*, 765-770.

89. Gregoriadis, G., Bacon, A., Caparros-Wanderley, W., and McCormack, B. (2002). A role for liposomes in genetic vaccination. Vaccine *20*, B1-B9.

90. Gregoriadis, G., da Silva, H., and Florence, A.T. (1990). A procedure for the efficient entrapment of drugs in dehydration-rehydration liposomes (DRVs). International Journal of Pharmaceutics *65*, 235-242.

91. Gregoriadis, G., Leathwood, P.D., and Ryman, B.E. (1971). Enzyme entrapment in liposomes. FEBS Lett *14*, 95-99.

92. Grunwald, T., and Ulbert, S. (2015). Improvement of DNA vaccination by adjuvants and sophisticated delivery devices: vaccine-platforms for the battle against infectious diseases. Clinical and experimental vaccine research *4*, 1-10.

93. Guimaraes Sa Correia, M., Briuglia, M.L., Niosi, F., and Lamprou, D.A. (2017). Microfluidic manufacturing of phospholipid nanoparticles: Stability, encapsulation efficacy, and drug release. Int J Pharm *516*, 91-99.

94. Gül, N., and van Egmond, M. (2015). Antibody-Dependent Phagocytosis of Tumor Cells by Macrophages: A Potent Effector Mechanism of Monoclonal Antibody Therapy of Cancer. Cancer Research *75*, 5008.

95. Gutcher, I., and Becher, B. (2007). APC-derived cytokines and T cell polarization in autoimmune inflammation. The Journal of clinical investigation *117*, 1119-1127.

96. Hamada, T., Miura, Y., Komatsu, Y., Kishimoto, Y., Vestergaard, M., and Takagi, M. (2008). Construction of asymmetric cell-sized lipid vesicles from lipid-coated water-in-oil microdroplets. J Phys Chem B *112*, 14678-14681.

97. Harding, C., Heuser, J., and Stahl, P. (1983). Receptor-mediated endocytosis of transferrin and recycling of the transferrin receptor in rat reticulocytes. J Cell Biol *97*, 329-339.

98. Harvie, P., Wong, F.M.P., and Bally, M.B. (2000). Use of Poly(ethylene glycol)–Lipid Conjugates to Regulate the Surface Attributes and Transfection Activity of Lipid–DNA Particles. Journal of Pharmaceutical Sciences *89*, 652-663.

99. Hassett, K.J., Benenato, K.E., Jacquinet, E., Lee, A., Woods, A., Yuzhakov, O., Himansu, S., Deterling, J., Geilich, B.M., Ketova, T.*, et al.* (2019). Optimization of Lipid Nanoparticles for Intramuscular Administration of mRNA Vaccines. Molecular Therapy - Nucleic Acids *15*, 1-11.

100. Hekele, A., Bertholet, S., Archer, J., Gibson, D.G., Palladino, G., Brito, L.A., Otten, G.R., Brazzoli, M., Buccato, S., Bonci, A.*, et al.* (2013). Rapidly produced SAM(®) vaccine against H7N9 influenza is immunogenic in mice. Emerg Microbes Infect *2*, e52-.

101. Helft, J., Böttcher, J., Chakravarty, P., Zelenay, S., Huotari, J., Schraml, Barbara U., Goubau, D., and Reis e Sousa, C. (2015). GM-CSF Mouse Bone Marrow Cultures Comprise a Heterogeneous Population of CD11c+MHCII+ Macrophages and Dendritic Cells. Immunity *42*, 1197-1211.

102. Henriksen-Lacey, M., Bramwell, V., and Perrie, Y. (2010a). Radiolabelling of Antigen and Liposomes for Vaccine Biodistribution Studies. Pharmaceutics *2*, 91.

103. Henriksen-Lacey, M., Bramwell, V.W., Christensen, D., Agger, E.-M., Andersen, P., and Perrie, Y. (2010b). Liposomes based on dimethyldioctadecylammonium promote a depot effect and enhance immunogenicity of soluble antigen. Journal of Controlled Release *142*, 180-186.

104. Henriksen-Lacey, M., Christensen, D., Bramwell, V.W., Lindenstrom, T., Agger, E.M., Andersen, P., and Perrie, Y. (2010c). Liposomal cationic charge and antigen adsorption are important properties for the efficient deposition of antigen at the injection site and ability of the vaccine to induce a CMI response. J Control Release *145*, 102-108.

105. Henriksen-Lacey, M., Christensen, D., Bramwell, V.W., Lindenstrom, T., Agger, E.M., Andersen, P., and Perrie, Y. (2011a). Comparison of the depot effect and immunogenicity of liposomes based on dimethyldioctadecylammonium (DDA), 3beta-[N-(N',N'-Dimethylaminoethane)carbomyl] cholesterol (DC-Chol), and 1,2-Dioleoyl-3-trimethylammonium propane (DOTAP): prolonged liposome retention mediates stronger Th1 responses. Mol Pharm *8*, 153-161.

106. Henriksen-Lacey, M., Devitt, A., and Perrie, Y. (2011b). The vesicle size of DDA:TDB liposomal adjuvants plays a role in the cell-mediated immune response but has no significant effect on antibody production. J Control Release *154*, 131-137.

107. Hicks, D.J., Fooks, A.R., and Johnson, N. (2012). Developments in rabies vaccines. Clinical and experimental immunology *169*, 199-204.

108. Hope, M.J., Bally, M.B., Webb, G., and Cullis, P.R. (1985). Production of large unilamellar vesicles by a rapid extrusion procedure. Characterization of size distribution, trapped volume and ability to maintain a membrane potential. Biochimica et Biophysica Acta (BBA) - Biomembranes *812*, 55-65.

109. Hsu, M.J., and Juliano, R.L. (1982). Interactions of liposomes with the reticuloendothelial system: II. Nonspecific and receptor-mediated uptake of liposomes by mouse peritoneal macrophages. Biochimica et Biophysica Acta (BBA) - Molecular Cell Research *720*, 411-419.

110. Iavarone, C., O'hagan, D.T., Yu, D., Delahaye, N.F., and Ulmer, J.B. (2017). Mechanism of action of mRNA-based vaccines. Expert Review of Vaccines *16*, 871-881.

111. Immordino, M.L., Dosio, F., and Cattel, L. (2006). Stealth liposomes: review of the basic science, rationale, and clinical applications, existing and potential. International Journal of Nanomedicine *1*, 297-315.

112. Inaba, K., Inaba, M., Romani, N., Aya, H., Deguchi, M., Ikehara, S., Muramatsu, S., and Steinman, R.M. (1992). Generation of large numbers of dendritic cells from mouse bone marrow cultures supplemented with granulocyte/macrophage colony-stimulating factor. J Exp Med *176*, 1693-1702.

113. Israelachvili, J.N. (1992). Intramolecular and Surface Forces (New York: Academic Press).

114. Israelachvili, J.N., Marcelja, S., and Horn, R.G. (1980). Physical principles of membrane organization. Q Rev Biophys *13*, 121-200.

115. Ivashkiv, L.B., and Donlin, L.T. (2014). Regulation of type I interferon responses. Nature reviews. Immunology *14*, 36-49.

116. Jahn, A., Stavis, S.M., Hong, J.S., Vreeland, W.N., DeVoe, D.L., and Gaitan, M. (2010). Microfluidic mixing and the formation of nanoscale lipid vesicles. ACS Nano *4*, 2077-2087.

117. Jahn, A., Vreeland, W.N., DeVoe, D.L., Locascio, L.E., and Gaitan, M. (2007). Microfluidic directed formation of liposomes of controlled size. Langmuir *23*, 6289-6293.

118. Jahn, A., Vreeland, W.N., Gaitan, M., and Locascio, L.E. (2004). Controlled vesicle self-assembly in microfluidic channels with hydrodynamic focusing. J Am Chem Soc *126*, 2674-2675.

119. Jeong, H.-H., Issadore, D., and Lee, D. (2016). Recent developments in scale-up of microfluidic emulsion generation via parallelization. Korean Journal of Chemical Engineering *33*, 1757-1766.

120. Jiang, Y., Tang, R., Duncan, B., Jiang, Z., Yan, B., Mout, R., and Rotello, V.M. (2015). Direct cytosolic delivery of siRNA using nanoparticle-stabilized nanocapsules. Angewandte Chemie (International ed. in English) *54*, 506-510.

121. Johnstone, S.A., Masin, D., Mayer, L., and Bally, M.B. (2001). Surface-associated serum proteins inhibit the uptake of phosphatidylserine and poly(ethylene glycol) liposomes by mouse macrophages. Biochimica et Biophysica Acta (BBA) - Biomembranes *1513*, 25-37.

122. Joshi, S., Hussain, M.T., Roces, C.B., Anderluzzi, G., Kastner, E., Salmaso, S., Kirby, D.J., and Perrie, Y. (2016). Microfluidics based manufacture of liposomes simultaneously entrapping hydrophilic and lipophilic drugs. Int J Pharm *514*, 160-168.

123. Kaczmarek, J.C., Kowalski, P.S., and Anderson, D.G. (2017). Advances in the delivery of RNA therapeutics: from concept to clinical reality. Genome Medicine *9*, 60.

124. Karikó, K., Muramatsu, H., Ludwig, J., and Weissman, D. (2011). Generating the optimal mRNA for therapy: HPLC purification eliminates immune activation and improves translation of nucleoside-modified, protein-encoding mRNA. Nucleic acids research *39*, e142-e142.

125. Karlsson, M., Davidson, M., Karlsson, R., Karlsson, A., Bergenholtz, J., Konkoli, Z., Jesorka, A., Lobovkina, T., Hurtig, J., Voinova, M., and Orwar, O. (2004). BIOMIMETIC NANOSCALE REACTORS AND NETWORKS. Annual Review of Physical Chemistry *55*, 613-649.

126. Kastner, E., Kaur, R., Lowry, D., Moghaddam, B., Wilkinson, A., and Perrie, Y. (2014). High-throughput manufacturing of size-tuned liposomes by a new microfluidics method using enhanced statistical tools for characterization. International Journal of Pharmaceutics *477*, 361-368.

127. Kastner, E., Verma, V., Lowry, D., and Perrie, Y. (2015). Microfluidic-controlled manufacture of liposomes for the solubilisation of a poorly water soluble drug. Int J Pharm *485*, 122-130.

128. Kaur, R., Bramwell, V.W., Kirby, D.J., and Perrie, Y. (2012a). Manipulation of the surface pegylation in combination with reduced vesicle size of cationic liposomal adjuvants modifies their clearance kinetics from the injection site, and the rate and type of T cell response. J Control Release *164*, 331-337.

129. Kaur, R., Bramwell, V.W., Kirby, D.J., and Perrie, Y. (2012b). Pegylation of DDA:TDB liposomal adjuvants reduces the vaccine depot effect and alters the Th1/Th2 immune responses. J Control Release *158*, 72-77.

130. Kaur, R., Henriksen-Lacey, M., Wilkhu, J., Devitt, A., Christensen, D., and Perrie, Y. (2014). Effect of Incorporating Cholesterol into DDA:TDB Liposomal Adjuvants on Bilayer Properties, Biodistribution, and Immune Responses. Molecular Pharmaceutics *11*, 197-207.

131. Kawai, T., and Akira, S. (2009). The roles of TLRs, RLRs and NLRs in pathogen recognition. International immunology *21*, 317-337.

132. Kedmi, R., Ben-Arie, N., and Peer, D. (2010). The systemic toxicity of positively charged lipid nanoparticles and the role of Toll-like receptor 4 in immune activation. Biomaterials *31*, 6867-6875.

133. Khadke, S., Stone, P., Rozhin, A., Kroonen, J., and Perrie, Y. (2018). Point of use production of liposomal solubilised products. International Journal of Pharmaceutics *537*, 1-8.

134. Khatri, N., Baradia, D., Vhora, I., Rathi, M., and Misra, A. (2014). Development and characterization of siRNA lipoplexes: Effect of different lipids, in vitro evaluation in cancerous cell lines and in vivo toxicity study. AAPS PharmSciTech *15*, 1630-1643.

135. Kim, B.K., Hwang, G.B., Seu, Y.B., Choi, J.S., Jin, K.S., and Doh, K.O. (2015). DOTAP/DOPE ratio and cell type determine transfection efficiency with DOTAP-liposomes. Biochim Biophys Acta *1848*, 1996-2001.

136. Kommareddy, S., Singh, M., and O'Hagan, D.T. (2017). Chapter 13 - MF59: A Safe and Potent Adjuvant for Human Use. In Immunopotentiators in Modern Vaccines (Second Edition), V.E.J.C. Schijns, and D.T. O'Hagan, eds. (Academic Press), pp. 249-263.

137. Kulkarni, J.A., Cullis, P.R., and van der Meel, R. (2018a). Lipid Nanoparticles Enabling Gene Therapies: From Concepts to Clinical Utility. Nucleic Acid Therapeutics *28*, 146-157.

138. Kulkarni, J.A., Darjuan, M.M., Mercer, J.E., Chen, S., van der Meel, R., Thewalt, J.L., Tam, Y.Y.C., and Cullis, P.R. (2018b). On the Formation and Morphology of Lipid Nanoparticles Containing Ionizable Cationic Lipids and siRNA. ACS Nano *12*, 4787-4795.

139. Kulkarni, J.A., Myhre, J.L., Chen, S., Tam, Y.Y.C., Danescu, A., Richman, J.M., and Cullis, P.R. (2017). Design of lipid nanoparticles for in vitro and in vivo delivery of plasmid DNA. Nanomedicine: Nanotechnology, Biology and Medicine *13*, 1377-1387.

140. Kulkarni, V., Rosati, M., Bear, J., Pilkington, G.R., Jalah, R., Bergamaschi, C., Singh, A.K., Alicea, C., Chowdhury, B., Zhang, G.-M.*, et al.* (2013). Comparison of intradermal and intramuscular delivery followed by in vivo electroporation of SIV Env DNA in macaques. Human vaccines & immunotherapeutics *9*, 2081-2094.

141. Kuribayashi, K., Tresset, G., Coquet, P., Fujita, H., and Takeuchi, S. (2006). Electroformation of giant liposomes in microfluidic channels. Measurement Science and Technology *17*, 3121-3126.

142. Lajunen, T., Hisazumi, K., Kanazawa, T., Okada, H., Seta, Y., Yliperttula, M., Urtti, A., and Takashima, Y. (2014). Topical drug delivery to retinal pigment epithelium with microfluidizer produced small liposomes. European Journal of Pharmaceutical Sciences *62*, 23-32.

143. Lasic, D.D. (1993). Kinetic and Thermodynamic Effects in the Formation of Amphiphilic Colloidal Particles. Journal of Liposome Research *3*, 257-273.

144. Latner, A.L. (1977). Isoelectric Focusing of Serum Proteins. In Biological and Biomedical Applications of Isoelectric Focusing, N. Catsimpoolas, and J. Drysdale, eds. (Boston, MA: Springer US), pp. 303-345.

145. Lazzaro, S., Giovani, C., Mangiavacchi, S., Magini, D., Maione, D., Baudner, B., Geall, A.J., De Gregorio, E., D'Oro, U., and Buonsanti, C. (2015). CD8 T-cell priming upon mRNA vaccination is restricted to bone-marrow-derived antigen-presenting cells and may involve antigen transfer from myocytes. Immunology *146*, 312-326.

146. Lee, C.-Y., Chang, C.-L., Wang, Y.-N., and Fu, L.-M. (2011). Microfluidic mixing: a review. International journal of molecular sciences *12*, 3263-3287.

147. Lesnik, E.A., and Freier, S.M. (1995). Relative thermodynamic stability of DNA, RNA, and DNA:RNA hybrid duplexes: relationship with base composition and structure. Biochemistry *34*, 10807-10815.

148. Leung, A.K.K., Hafez, I.M., Baoukina, S., Belliveau, N.M., Zhigaltsev, I.V., Afshinmanesh, E., Tieleman, D.P., Hansen, C.L., Hope, M.J., and Cullis, P.R. (2012). Lipid Nanoparticles Containing siRNA Synthesized by Microfluidic Mixing Exhibit an Electron-Dense Nanostructured Core. The Journal of Physical Chemistry C *116*, 18440-18450.

149. Li, D., Li, G., Li, P., Zhang, L., Liu, Z., Wang, J., and Wang, E. (2010). The enhancement of transfection efficiency of cationic liposomes by didodecyldimethylammonium bromide coated gold nanoparticles. Biomaterials *31*, 1850-1857.

150. Li, Y., Wang, J., Gao, Y., Zhu, J., Wientjes, M.G., and Au, J.L.S. (2011). Relationships between Liposome Properties, Cell Membrane Binding, Intracellular Processing, and Intracellular Bioavailability. The AAPS Journal *13*, 585-597.

151. Liang, F., Lindgren, G., Lin, A., Thompson, E.A., Ols, S., Röhss, J., John, S., Hassett, K., Yuzhakov, O., Bahl, K.*, et al.* (2017). Efficient Targeting and Activation of Antigen-Presenting Cells In Vivo after Modified mRNA Vaccine Administration in Rhesus Macaques. Molecular Therapy *25*, 2635-2647.

152. Liu, D.-Z., Chen, W.-Y., Tasi, L.-M., and Yang, S.-P. (2000). Microcalorimetric and shear studies on the effects of cholesterol on the physical stability of lipid vesicles. Colloids and Surfaces A: Physicochemical and Engineering Aspects *172*, 57-67.

153. Lobovkina, T., Jacobson, G.B., Gonzalez-Gonzalez, E., Hickerson, R.P., Leake, D., Kaspar, R.L., Contag, C.H., and Zare, R.N. (2011). In vivo sustained release of siRNA from solid lipid nanoparticles. ACS nano *5*, 9977-9983.

154. Lodmell, D.L., Parnell, M.J., Bailey, J.R., Ewalt, L.C., and Hanlon, C.A. (2002). Rabies DNA vaccination of non-human primates: post-exposure studies using gene gun methodology that accelerates induction of neutralizing antibody and enhances neutralizing antibody titers. Vaccine *20*, 2221-2228.

155. Lodmell, D.L., Ray, N.B., and Ewalt, L.C. (1998). Gene gun particle-mediated vaccination with plasmid DNA confers protective immunity against rabies virus infection. Vaccine *16*, 115-118.

156. Lonez, C., Vandenbranden, M., and Ruysschaert, J.M. (2012). Cationic lipids activate intracellular signaling pathways. Adv Drug Deliv Rev *64*, 1749-1758.

157. Loo, Y.-M., and Gale, M., Jr. (2011). Immune signaling by RIG-I-like receptors. Immunity *34*, 680-692.

158. Lou, G., Anderluzzi, G., Woods, S., Roberts, C.W., and Perrie, Y. (2019). A novel microfluidic-based approach to formulate size-tuneable large unilamellar cationic liposomes: Formulation, cellular uptake and biodistribution investigations. European Journal of Pharmaceutics and Biopharmaceutics *143*, 51-60.

159. Love, K.T., Mahon, K.P., Levins, C.G., Whitehead, K.A., Querbes, W., Dorkin, J.R., Qin, J., Cantley, W., Qin, L.L., Racie, T.*, et al.* (2010). Lipid-like materials for low-dose, in vivo gene silencing. Proc Natl Acad Sci U S A *107*, 1864-1869.

160. Lutz, J., Lazzaro, S., Habbeddine, M., Schmidt, K.E., Baumhof, P., Mui, B.L., Tam, Y.K., Madden, T.D., Hope, M.J., Heidenreich, R., and Fotin-Mleczek, M. (2017). Unmodified mRNA in LNPs constitutes a competitive technology for prophylactic vaccines. npj Vaccines *2*, 29.

161. Mackay, C.R. (2000). Follicular homing T helper (Th) cells and the Th1/Th2 paradigm. The Journal of experimental medicine *192*, F31-F34.

162. Mackett, M., Smith, G.L., and Moss, B. (1982). Vaccinia virus: a selectable eukaryotic cloning and expression vector. Proceedings of the National Academy of Sciences of the United States of America *79*, 7415-7419.

163. Maes, M., Song, C., Lin, A.-H., Bonaccorso, S., Kenis, G., De Jongh, R., Bosmans, E., and Scharpé, S. (1999). Negative Immunoregulatory Effects of Antidepressants: Inhibition of Interferon-γ and Stimulation of Interleukin-10 Secretion. Neuropsychopharmacology *20*, 370-379.

164. Magini, D., Giovani, C., Mangiavacchi, S., Maccari, S., Cecchi, R., Ulmer, J.B., De Gregorio, E., Geall, A.J., Brazzoli, M., and Bertholet, S. (2016). Self-Amplifying mRNA Vaccines Expressing Multiple Conserved Influenza Antigens Confer Protection against Homologous and Heterosubtypic Viral Challenge. PLoS One *11*.

165. Maitz, M.F., Sperling, C., Wongpinyochit, T., Herklotz, M., Werner, C., and Seib, F.P. (2017). Biocompatibility assessment of silk nanoparticles: hemocompatibility and

internalization by human blood cells. Nanomedicine: Nanotechnology, Biology and Medicine *13*, 2633-2642.

166. Manara, C., Brazzoli, M., Piccioli, D., Taccone, M., D'Oro, U., Maione, D., and Frigimelica, E. (2019). Co-administration of GM-CSF expressing RNA is a powerful tool to enhance potency of SAM-based vaccines. Vaccine *37*, 4204-4213.

167. Manolova, V., Flace, A., Bauer, M., Schwarz, K., Saudan, P., and Bachmann, M.F. (2008). Nanoparticles target distinct dendritic cell populations according to their size. Eur J Immunol *38*, 1404-1413.

168. Martinon, F., Krishnan, S., Lenzen, G., Magne, R., Gomard, E., Guillet, J.G., Levy, J.P., and Meulien, P. (1993). Induction of virus-specific cytotoxic T lymphocytes in vivo by liposome-entrapped mRNA. Eur J Immunol *23*, 1719-1722.

169. Maruggi, G., Shaw, C.A., Otten, G.R., Mason, P.W., and Beard, C.W. (2013). Engineered alphavirus replicon vaccines based on known attenuated viral mutants show limited effects on immunogenicity. Virology *447*, 254-264.

170. Maruggi, G., Zhang, C., Li, J., Ulmer, J.B., and Yu, D. (2019). mRNA as a Transformative Technology for Vaccine Development to Control Infectious Diseases. Molecular Therapy *27*, 757-772.

171. Masoud Rahman, S.L., Nancy Tawil, L'Hocine Yahia, Morteza Mahmoudi (2013). Protein-Nanoparticle Interactions Chapter 2., Vol 13.

172. Mayadas, T.N., Cullere, X., and Lowell, C.A. (2014). The multifaceted functions of neutrophils. Annual review of pathology *9*, 181-218.

173. McDonald, B., Pittman, K., Menezes, G.B., Hirota, S.A., Slaba, I., Waterhouse, C.C.M., Beck, P.L., Muruve, D.A., and Kubes, P. (2010). Intravascular Danger Signals Guide Neutrophils to Sites of Sterile Inflammation. Science *330*, 362.

174. McNab, F., Mayer-Barber, K., Sher, A., Wack, A., and O'Garra, A. (2015). Type I interferons in infectious disease. Nature Reviews Immunology *15*, 87.

175. Meyuhas, D., Bor, A., Pinchuk, I., Kaplun, A., Talmon, Y., Kozlov, M.M., and Lichtenberg, D. (1997). Effect of Ionic Strength on the Self-Assembly in Mixtures of Phosphatidylcholine and Sodium Cholate. Journal of Colloid and Interface Science *188*, 351-362.

176. Mijajlovic, M., Wright, D., Zivkovic, V., Bi, J.X., and Biggs, M.J. (2013). Microfluidic hydrodynamic focusing based synthesis of POPC liposomes for model biological systems. Colloids Surf B Biointerfaces *104*, 276-281.

177. Mochizuki, S., Kanegae, N., Nishina, K., Kamikawa, Y., Koiwai, K., Masunaga, H., and Sakurai, K. (2013). The role of the helper lipid dioleoylphosphatidylethanolamine (DOPE) for DNA transfection cooperating with a cationic lipid bearing ethylenediamine. Biochimica et Biophysica Acta (BBA) - Biomembranes *1828*, 412-418.

178. Moser, M., and Leo, O. (2010). Key concepts in immunology. Vaccine *28 Suppl 3*, C2-13.

179. Mozafari, M.R., Johnson, C., Hatziantoniou, S., and Demetzos, C. (2008). Nanoliposomes and their applications in food nanotechnology. J Liposome Res *18*, 309-327.

180. Mui, B., Chow, L., and Hope, M.J. (2003). Extrusion technique to generate liposomes of defined size. Methods Enzymol *367*, 3-14.

181. Mui, B.L., Tam, Y.K., Jayaraman, M., Ansell, S.M., Du, X., Tam, Y.Y.C., Lin, P.J.C., Chen, S., Narayanannair, J.K., Rajeev, K.G.*, et al.* (2013). Influence of Polyethylene Glycol Lipid Desorption Rates on Pharmacokinetics and Pharmacodynamics of siRNA Lipid Nanoparticles. Molecular Therapy - Nucleic Acids *2*, e139.

182. Muir, B.W., Zhen, G., Gunatillake, P., and Hartley, P.G. (2012). Salt Induced Lamellar to Bicontinuous Cubic Phase Transitions in Cationic Nanoparticles. The Journal of Physical Chemistry B *116*, 3551-3556.

183. Murthy, A.K., Li, W., Chaganty, B.K.R., Kamalakaran, S., Guentzel, M.N., Seshu, J., Forsthuber, T.G., Zhong, G., and Arulanandam, B.P. (2011). Tumor necrosis factor alpha production from CD8+ T cells mediates oviduct pathological sequelae following primary genital Chlamydia muridarum infection. Infection and immunity *79*, 2928-2935.

184. Muzio, M., Polentarutti, N., Bosisio, D., Prahladan, M.K.P., and Mantovani, A. (2000). Toll-like receptors: a growing family of immune receptors that are differentially expressed and regulated by different leukocytes. Journal of Leukocyte Biology *67*, 450-456.

185. Nagarajan, R. (2002). Molecular Packing Parameter and Surfactant Self-Assembly: The Neglected Role of the Surfactant Tail. Langmuir *18*, 31-38.

186. Nakayama, G.R., Caton, M.C., Nova, M.P., and Parandoosh, Z. (1997). Assessment of the Alamar Blue assay for cellular growth and viability in vitro. J Immunol Methods *204*, 205-208.

187. Nguyen, J., Walsh, C.L., Motion, J.P., Perttu, E.K., and Szoka, F. (2012). Controlled nucleation of lipid nanoparticles. Pharm Res *29*, 2236-2248.

188. Oka, T., Hasan, M., Islam, M.Z., Moniruzzaman, M., and Yamazaki, M. (2017). Low-pH-Induced Lamellar to Bicontinuous Primitive Cubic Phase Transition in Dioleoylphosphatidylserine/Monoolein Membranes. Langmuir *33*, 12487-12496.

189. Olson, F., Hunt, C.A., Szoka, F.C., Vail, W.J., and Papahadjopoulos, D. (1979). Preparation of liposomes of defined size distribution by extrusion through polycarbonate membranes. Biochimica et Biophysica Acta (BBA) - Biomembranes *557*, 9-23.

190. Osorio, J.E., Tomlinson, C.C., Frank, R.S., Haanes, E.J., Rushlow, K., Haynes, J.R., and Stinchcomb, D.T. (1999). Immunization of dogs and cats with a DNA vaccine against rabies virus. Vaccine *17*, 1109-1116.

191. Ota, S., Yoshizawa, S., and Takeuchi, S. (2009). Microfluidic Formation of Monodisperse, Cell-Sized, and Unilamellar Vesicles. Angewandte Chemie International Edition *48*, 6533-6537.

192. Özer, A.Y., Bloois, L.v., and Crommelin, D.J.A. (1989). The Size Reduction of Liposomes with a High Pressure Homogenizer (Microfluidizer™). Characterization of Prepared Dispersions and Comparison with Conventional Methods. AU - Talsma, H. Drug Development and Industrial Pharmacy *15*, 197-207.

193. Papahadjopoulos, D., and Miller, N. (1967). Phospholipid model membranes. I. Structural characteristics of hydrated liquid crystals. Biochimica et Biophysica Acta (BBA) - Biomembranes *135*, 624-638.

194. Pardi, N., Hogan, M.J., Porter, F.W., and Weissman, D. (2018). mRNA vaccines — a new era in vaccinology. Nature Reviews Drug Discovery *17*, 261.

195. Pardi, N., Tuyishime, S., Muramatsu, H., Kariko, K., Mui, B.L., Tam, Y.K., Madden, T.D., Hope, M.J., and Weissman, D. (2015). Expression kinetics of nucleoside-modified mRNA delivered in lipid nanoparticles to mice by various routes. Journal of Controlled Release *217*, 345-351.

196. Patel, S., Ryals, R.C., Weller, K.K., Pennesi, M.E., and Sahay, G. (2019). Lipid nanoparticles for delivery of messenger RNA to the back of the eye. Journal of Controlled Release *303*, 91-100.

197. Pautot, S., Frisken, B.J., and Weitz, D.A. (2003). Production of Unilamellar Vesicles Using an Inverted Emulsion. Langmuir *19*, 2870-2879.

198. Pepini, T., Pulichino, A.M., Carsillo, T., Carlson, A.L., Sari-Sarraf, F., Ramsauer, K., Debasitis, J.C., Maruggi, G., Otten, G.R., Geall, A.J.*, et al.* (2017). Induction of an IFN-Mediated Antiviral Response by a Self-Amplifying RNA Vaccine: Implications for Vaccine Design. J Immunol *198*, 4012-4024.

199. Perrie, Y., Frederik, P.M., and Gregoriadis, G. (2001). Liposome-mediated DNA vaccination: the effect of vesicle composition. Vaccine *19*, 3301-3310.

200. Petkov, S., Starodubova, E., Latanova, A., Kilpeläinen, A., Latyshev, O., Svirskis, S., Wahren, B., Chiodi, F., Gordeychuk, I., and Isaguliants, M. (2018). DNA immunization site determines the level of gene expression and the magnitude, but not the type of the induced immune response. PloS one *13*, e0197902-e0197902.

201. Phua, K.K.L., Staats, H.F., Leong, K.W., and Nair, S.K. (2014). Intranasal mRNA nanoparticle vaccination induces prophylactic and therapeutic anti-tumor immunity. Scientific reports *4*, 5128-5128.

202. Plotkin, S.A., and Plotkin, S.A. (2008). Correlates of Vaccine-Induced Immunity. Clinical Infectious Diseases *47*, 401-409.

203. Pollard, C., Rejman, J., De Haes, W., Verrier, B., Van Gulck, E., Naessens, T., De Smedt, S., Bogaert, P., Grooten, J., Vanham, G., and De Koker, S. (2013). Type I IFN counteracts the induction of antigen-specific immune responses by lipid-based delivery of mRNA vaccines. Molecular therapy : the journal of the American Society of Gene Therapy *21*, 251-259.

204. Pons, M., Foradada, M., and Estelrich, J. (1993). Liposomes obtained by the ethanol injection method. International Journal of Pharmaceutics *95*, 51-56.

205. Pozzi, D., Colapicchioni, V., Caracciolo, G., Piovesana, S., Capriotti, A.L., Palchetti, S., De Grossi, S., Riccioli, A., Amenitsch, H., and Lagana, A. (2014). Effect of polyethyleneglycol (PEG) chain length on the bio-nano-interactions between PEGylated lipid nanoparticles

and biological fluids: from nanostructure to uptake in cancer cells. Nanoscale *6*, 2782-2792.

206. Pozzi, D., Marchini, C., Cardarelli, F., Amenitsch, H., Garulli, C., Bifone, A., and Caracciolo, G. (2012). Transfection efficiency boost of cholesterol-containing lipoplexes. Biochimica et Biophysica Acta (BBA) - Biomembranes *1818*, 2335-2343.

207. Pradhan, P., Guan, J., Lu, D., Wang, P.G., Lee, L.J., and Lee, R.J. (2008). A facile microfluidic method for production of liposomes. Anticancer Res *28*, 943-947.

208. Probst, J., Brechtel, S., Scheel, B., Hoerr, I., Jung, G., Rammensee, H.-G., and Pascolo, S. (2006). Characterization of the ribonuclease activity on the skin surface. Genetic vaccines and therapy *4*, 4-4.

209. Pupo, E., Padrón, A., Santana, E., Sotolongo, J., Quintana, D., Dueñas, S., Duarte, C., de la Rosa, M.C., and Hardy, E. (2005). Preparation of plasmid DNA-containing liposomes using a high-pressure homogenization–extrusion technique. Journal of Controlled Release *104*, 379-396.

210. Rapp, B.E. (2017). Chapter 9 - Fluids. In Microfluidics: Modelling, Mechanics and Mathematics, B.E. Rapp, ed. (Oxford: Elsevier), pp. 243-263.

211. Reap, E.A., Morris, J., Dryga, S.A., Maughan, M., Talarico, T., Esch, R.E., Negri, S., Burnett, B., Graham, A., Olmsted, R.A., and Chulay, J.D. (2007). Development and preclinical evaluation of an alphavirus replicon particle vaccine for cytomegalovirus. Vaccine *25*, 7441-7449.

212. Regelin, A.E., Fankhaenel, S., Gürtesch, L., Prinz, C., von Kiedrowski, G., and Massing, U. (2000). Biophysical and lipofection studies of DOTAP analogs. Biochimica et Biophysica Acta (BBA) - Biomembranes *1464*, 151-164.

213. Reichmuth, A.M., Oberli, M.A., Jaklenec, A., Langer, R., and Blankschtein, D. (2016). mRNA vaccine delivery using lipid nanoparticles. Therapeutic Delivery *7*, 319-334.

214. Richner, J.M., Himansu, S., Dowd, K.A., Butler, S.L., Salazar, V., Fox, J.M., Julander, J.G., Tang, W.W., Shresta, S., Pierson, T.C.*, et al.* (2017). Modified mRNA Vaccines Protect against Zika Virus Infection. Cell *168*, 1114-1125.e1110.

215. Roces, C.B., Khadke, S., Christensen, D., and Perrie, Y. (2019). Scale-independent microfluidic production of cationic liposomal adjuvants and development of enhanced lymphatic targeting strategies. Molecular Pharmaceutics.

216. Rock, K.L., and Clark, K. (1996). Analysis of the role of MHC class II presentation in the stimulation of cytotoxic T lymphocytes by antigens targeted into the exogenous antigen-MHC class I presentation pathway. J Immunol *156*, 3721-3726.

217. Rosada, R.S., de la Torre, L.G., Frantz, F.G., Trombone, A.P.F., Zárate-Bladés, C.R., Fonseca, D.M., Souza, P.R.M., Brandão, I.T., Masson, A.P., Soares, E.G.*, et al.* (2008). Protection against tuberculosis by a single intranasal administration of DNA-hsp65 vaccine complexed with cationic liposomes. BMC immunology *9*, 38-38.

218. Sardesai, N.Y., and Weiner, D.B. (2011). Electroporation delivery of DNA vaccines: prospects for success. Current opinion in immunology *23*, 421-429.

219. Saxena, S., Sonwane, A.A., Dahiya, S.S., Patel, C.L., Saini, M., Rai, A., and Gupta, P.K. (2009). Induction of immune responses and protection in mice against rabies using a self-replicating RNA vaccine encoding rabies virus glycoprotein. Veterinary Microbiology *136*, 36-44.

220. Schlake, T., Thess, A., Fotin-Mleczek, M., and Kallen, K.-J. (2012). Developing mRNA-vaccine technologies. RNA Biology *9*, 1319-1330.

221. Schmidt, S.T., Khadke, S., Korsholm, K.S., Perrie, Y., Rades, T., Andersen, P., Foged, C., and Christensen, D. (2016). The administration route is decisive for the ability of the vaccine adjuvant CAF09 to induce antigen-specific CD8+ T-cell responses: The immunological consequences of the biodistribution profile. Journal of Controlled Release *239*, 107-117.

222. Schnee, M., Vogel, A.B., Voss, D., Petsch, B., Baumhof, P., Kramps, T., and Stitz, L. (2016). An mRNA Vaccine Encoding Rabies Virus Glycoprotein Induces Protection against Lethal Infection in Mice and Correlates of Protection in Adult and Newborn Pigs. PLoS neglected tropical diseases *10*, e0004746-e0004746.

223. Schwendener, R.A. (2014). Liposomes as vaccine delivery systems: a review of the recent advances. Ther Adv Vaccines *2*, 159-182.

224. Schwendener, R.A., Lagocki, P.A., and Rahman, Y.E. (1984). The effects of charge and size on the interaction of unilamellar liposomes with macrophages. Biochim Biophys Acta *772*, 93-101.

225. Semple, S.C., Akinc, A., Chen, J., Sandhu, A.P., Mui, B.L., Cho, C.K., Sah, D.W., Stebbing, D., Crosley, E.J., Yaworski, E.*, et al.* (2010). Rational design of cationic lipids for siRNA delivery. Nat Biotechnol *28*, 172-176.

226. Shi, W., Kou, Y., Xiao, J., Zhang, L., Gao, F., Kong, W., Su, W., Jiang, C., and Zhang, Y. (2018). Comparison of immunogenicity, efficacy and transcriptome changes of inactivated rabies virus vaccine with different adjuvants. Vaccine *36*, 5020-5029.

227. Smith, J.S., Yager, P.A., and Baer, G.M. (1973). A rapid reproducible test for determining rabies neutralizing antibody. Bulletin of the World Health Organization *48*, 535-541.

228. Song, L.Y., Ahkong, Q.F., Rong, Q., Wang, Z., Ansell, S., Hope, M.J., and Mui, B. (2002). Characterization of the inhibitory effect of PEG-lipid conjugates on the intracellular delivery of plasmid and antisense DNA mediated by cationic lipid liposomes. Biochimica et Biophysica Acta (BBA) - Biomembranes *1558*, 1-13.

229. Squier, M.K.T., and John Cohen, J. (1994). Cell-mediated cytotoxic mechanisms. Current Opinion in Immunology *6*, 447-452.

230. Stachowiak, J.C., Richmond, D.L., Li, T.H., Liu, A.P., Parekh, S.H., and Fletcher, D.A. (2008). Unilamellar vesicle formation and encapsulation by microfluidic jetting. Proceedings of the National Academy of Sciences *105*, 4697.

231. Stepto, R.F.T. (2010). Dispersity in polymer science (IUPAC Recommendation 2009). Polymer International *59*, 23-24.

232. Stroock, A.D., Dertinger, S.K.W., Ajdari, A., Mezić, I., Stone, H.A., and Whitesides, G.M. (2002). Chaotic Mixer for Microchannels. Science *295*, 647.

233. Sudarshan, M.K., Madhusudana, S.N., Mahendra, B.J., Rao, N.S.N., Ashwath Narayana, D.H., Abdul Rahman, S., Meslin, F.X., Lobo, D., Ravikumar, K., and Gangaboraiah (2007). Assessing the burden of human rabies in India: results of a national multi-center epidemiological survey. International Journal of Infectious Diseases *11*, 29-35.

234. Sugiura, S., Kuroiwa, T., Kagota, T., Nakajima, M., Sato, S., Mukataka, S., Walde, P., and Ichikawa, S. (2008). Novel Method for Obtaining Homogeneous Giant Vesicles from a Monodisperse Water-in-Oil Emulsion Prepared with a Microfluidic Device. Langmuir *24*, 4581-4588.

235. Szoka, F., and Papahadjopoulos, D. (1978). Procedure for preparation of liposomes with large internal aqueous space and high capture by reverse-phase evaporation. Proc Natl Acad Sci U S A *75*, 4194-4198.

236. Takano, S., Aramaki, Y., and Tsuchiya, S. (2003). Physicochemical Properties of Liposomes Affecting Apoptosis Induced by Cationic Liposomes in Macrophages. Pharmaceutical Research *20*, 962-968.

237. Takeda, K., and Akira, S. (2005). Toll-like receptors in innate immunity. International Immunology *17*, 1-14.

238. Tam, Y.Y.C., Chen, S., and Cullis, P.R. (2013). Advances in Lipid Nanoparticles for siRNA Delivery. Pharmaceutics *5*, 498-507.

239. Tan, Y.-C., Cristini, V., and Lee, A.P. (2006). Monodispersed microfluidic droplet generation by shear focusing microfluidic device. Sensors and Actuators B: Chemical *114*, 350-356.

240. Tang, D., Kang, R., Coyne, C.B., Zeh, H.J., and Lotze, M.T. (2012). PAMPs and DAMPs: signal 0s that spur autophagy and immunity. Immunological reviews *249*, 158-175.

241. Tang, D.C., DeVit, M., and Johnston, S.A. (1992). Genetic immunization is a simple method for eliciting an immune response. Nature *356*, 152-154.

242. Tatematsu, M., Funami, K., Seya, T., and Matsumoto, M. (2018). Extracellular RNA Sensing by Pattern Recognition Receptors. Journal of Innate Immunity *10*, 398-406.

243. Tesmer, L.A., Lundy, S.K., Sarkar, S., and Fox, D.A. (2008). Th17 cells in human disease. Immunological reviews *223*, 87-113.

244. Tiffany, M., and Szoka, F.C. (2016). Co-localization of fluorescent labeled lipid nanoparticles with specifically tagged subcellular compartments by single particle tracking at low nanoparticle to cell ratios. Journal of Drug Targeting *24*, 857-864.

245. Toh, M.-R., and Chiu, G.N.C. (2013). Liposomes as sterile preparations and limitations of sterilisation techniques in liposomal manufacturing. Asian Journal of Pharmaceutical Sciences *8*, 88-95.

246. Tordo, N., Poch, O., Ermine, A., Keith, G., and Rougeon, F. (1988). Completion of the rabies virus genome sequence determination: Highly conserved domains among the L

(polymerase) proteins of unsegmented negative-strand RNA viruses. Virology *165*, 565-576.

247. Ulmer, J.B., Mason, P.W., Geall, A., and Mandl, C.W. (2012). RNA-based vaccines. Vaccine *30*, 4414-4418.

248. Ushikubo, F.Y., Birribilli, F.S., Oliveira, D.R.B., and Cunha, R.L. (2014). Y- and T-junction microfluidic devices: effect of fluids and interface properties and operating conditions. Microfluidics and Nanofluidics *17*, 711-720.

249. Van Lint, S., Goyvaerts, C., Maenhout, S., Goethals, L., Disy, A., Benteyn, D., Pen, J., Bonehill, A., Heirman, C., Breckpot, K., and Thielemans, K. (2012). Preclinical evaluation of TriMix and antigen mRNA-based antitumor therapy. Cancer Res *72*, 1661-1671.

250. van Swaay, D., and deMello, A. (2013). Microfluidic methods for forming liposomes. Lab Chip *13*, 752-767.

251. Vangasseri, D.P., Cui, Z., Chen, W., Hokey, D.A., Falo, L.D., Jr., and Huang, L. (2006). Immunostimulation of dendritic cells by cationic liposomes. Mol Membr Biol *23*, 385-395.

252. Vogel, A.B., Lambert, L., Kinnear, E., Busse, D., Erbar, S., Reuter, K.C., Wicke, L., Perkovic, M., Beissert, T., Haas, H.*, et al.* (2018). Self-Amplifying RNA Vaccines Give Equivalent Protection against Influenza to mRNA Vaccines but at Much Lower Doses. Molecular Therapy *26*, 446-455.

253. Weiner, N., Lieb, L., Niemiec, S., Ramachandran, C., Hu, Z., and Egbaria, K. (1994). Liposomes: a novel topical delivery system for pharmaceutical and cosmetic applications. J Drug Target *2*, 405-410.

254. Wiktor, T.J. (1978). Cell-mediated immunity and postexposure protection from rabies by inactivated vaccines of tissue culture origin. Dev Biol Stand *40*, 255-264.

255. Wolff, J.A., Malone, R.W., Williams, P., Chong, W., Acsadi, G., Jani, A., and Felgner, P.L. (1990). Direct gene transfer into mouse muscle in vivo. Science *247*, 1465-1468.

256. Wu, X., and Brewer, G. (2012). The regulation of mRNA stability in mammalian cells: 2.0. Gene *500*, 10-21.

257. Xiang, Z.Q., Knowles, B.B., McCarrick, J.W., and Ertl, H.C.J. (1995). Immune Effector Mechanisms Required for Protection to Rabies Virus. Virology *214*, 398-404.

258. Xu, L., Wempe, M.F., and Anchordoquy, T.J. (2011). The effect of cholesterol domains on PEGylated liposomal gene delivery in vitro. Therapeutic delivery *2*, 451-460.

259. Xu, Y., and Szoka, F.C. (1996). Mechanism of DNA Release from Cationic Liposome/DNA Complexes Used in Cell Transfection. Biochemistry *35*, 5616-5623.

260. Xue, H.Y., Guo, P., Wen, W.C., and Wong, H.L. (2015). Lipid-Based Nanocarriers for RNA Delivery. Curr Pharm Des *21*, 3140-3147.

261. Yu, C.-D., Wangsatorntanakun, V., and Roosdorp, N. (1990). Large-Scale Production of Liposomes by A Microfluidizer AU - Vemuri, Sriram. Drug Development and Industrial Pharmacy *16*, 2243-2256.

262. Zaritskaya, L., Shurin, M.R., Sayers, T.J., and Malyguine, A.M. (2010). New flow cytometric assays for monitoring cell-mediated cytotoxicity. Expert Rev Vaccines *9*, 601-616.

263. Zhang, Y., Li, H., Sun, J., Gao, J., Liu, W., Li, B., Guo, Y., and Chen, J. (2010). DC-Chol/DOPE cationic liposomes: a comparative study of the influence factors on plasmid pDNA and siRNA gene delivery. Int J Pharm *390*, 198-207.

264. Zook, J.M., and Vreeland, W.N. (2010). Effects of temperature, acyl chain length, and flow-rate ratio on liposome formation and size in a microfluidic hydrodynamic focusing device. Soft Matter *6*, 1352-1360.